

Diss. ETH NO. 19398

**Structure Property Relations of
Coupled Squaraine Dyes**

A dissertation submitted to

ETH ZURICH

for the degree of

Doctor of Sciences

presented by

SIMON KUSTER

Master of Science ETH in Chemie and dipl. Chemiker FH

born on the 24th of December 1980

citizen of Diepoldsau (SG) - Switzerland

accepted on the recommendation of

Prof. Dr. A. Dieter Schlüter, examiner

Dr. Thomas Geiger, co-examiner

Prof. Dr. Paul Smith, co-examiner

Prof. Dr. Peter Walde, co-examiner

2010

"spricht der HERR; Denn so hoch der Himmel über der Erde ist,
so weit reichen meine Gedanken über alles hinaus, was ihr euch denkt,
und meine Möglichkeiten über alles, was für euch machbar ist." *Jesaja 55, 9.*

or

"What we know is a drop, what we don't know is an ocean." *Isaac Newton*

Summary

The investigation of different structure-property relations of some squaraines dyes was the objective of this thesis. The synthesized squaraines consisted of one, two or three chromophore units. For all the dyes the indole end grouped squaraine dye (4-((3,3-dimethyl-1-octyl-3*H*-indolium-2-yl)methylene)-2-((3,3-dimethyl-1-octylindolin-2-ylidene)methyl)-3-oxocyclobut-1-enolate) was chosen as a reference system. This Monosquaraine (MSQ) was chemically modified with one and two phenyl or benzo[*e*]indole, respectively, in order to determine their influence on the properties of the chromophore. The unsymmetrical introduction of a single modification thereof were made according to the synthesis method of Terpetschnig et al. (*Analytica Chimica Acta*, 282(3):633–641, 1993). The symmetric implementation was performed according to Treibs and Jacob (*Justus Liebig's Annalen der Chemie*, 712:123–137, 1968). The value of the absorption maximum (λ_{max}), measured in chloroform, could thereby be shifted from 637.5 nm of the reference MSQs to 665.5 nm of the double benzo[*e*]indole modification. The molar absorption coefficient of the MSQs remained practically unchangeably giant at about 350000 L·mol⁻¹·cm⁻¹. A linear structure-property relation was found: for each additional π -electron pair outside the chromophore unit the λ_{max} value is bathochromically shifted by 7 nm.

For a better understanding of the interaction of two squaraine chromophores in one molecule, the dye units were linked together over various conjugated aromatic bridges. These bridges were selected in a way that the distance dependence (phenylene versus fluorene; naphthalene vs. anthracene), the donor or acceptor properties (phenylene vs. alkoxy-phenylene vs. perfluoro-phenylene) and the torsion angular dependence of the bridge relative to the dye system could be correlated with the optical and electrochemical properties. In order to synthesize the said Bissquaraines (BSQs) individually, the synthesis strategy of Terpetschnig et al. was adopted. As a result of the dye-dye interaction the λ_{max} values of these BSQs were red shifted and they were in the range of 670 to 730 nm.

Some Trissquaraine (TSQs) were synthesized upon polymerization with the same bridges as the BSQs (phenylene, fluorene, alkoxy-phenylene and perfluoro-phenylene). Those λ_{max} values were in the range of 674–688 nm, which was a few nano meters further red shifted than the absorption of the BSQs. However, the naphthalene bridged TSQ was synthesized regio-selectively to the trimer, which showed a λ_{max} value of 760

nm in chloroform which corresponded to a 100 nm shift compared with the MSQ and a 30 nm shift compared with the BSQ.

The λ_{max} values were then related with the number of repeat units in a plot from which the bridge-dependent saturation curves were developed. Depending on the kind of the bridge, the saturation of the λ_{max} value will be reached after five to eight repeating units which is in the range between 700 and 800 nm. This data was used to describe a multi dimensional saturation formula to determine the absorption maximum of any structurally related dye. The parameters for this formula were given by the molecular structure of the dye. For this formula, the torsion angle between the dye system and the bridge, the distance between the individual chromophores and the number of π -electron pairs in conjugation were balanced. Thus, the influence of the donor or acceptor properties of the bridges on the λ_{max} value is negligible. Furthermore, the therewith calculated absorption maximum had an accuracy of a few nanometers.

The electrochemical properties of the squaraine dyes were effect by their molecular structure in similar way as the optical ones. Concluding, a linear relation between the optical band gap (ΔE_{opt}) and the first electrochemical oxidation or reduction potential (E_{ox}^1 and E_{red}^1 , respectively) was found. The developed structure-property relations from the optical and the electrochemical measurements were confirmed with molecular modeling. The geometry optimized molecular structures and the picture of the frontier orbitals were calculated using Density Functional Theory (DFT) with B3LYP functional and 6-31G* as basis set. The molecular modeling additionally showed that an unsymmetrically constructed, naphthalene bridged dimeric squaraine dye shows a directional charge transfer during optical excitation. This unsymmetric BSQ was synthesized, immobilized on titanium dioxide nano-particles and to get a proof-of-concept a first dye sensitized solar cell (DSC) was made therewith having an energy conversion efficiency (η) of 1.3%.

In addition to all the indole-based dyes, a 1,5-diaza anthrazene bridge was synthesized over a double Doebner-Miller-Reaction wherewith then the corresponding BSQ was synthesized. This BSQ shows a λ_{max} value of 805 nm in chloroform which was unexpectedly far red shifted. According to molecular modeling, the two squaraine dye units were fused together, which exceeds the chromophore-chromophore interactions of the other BSQs.

Zusammenfassung

Die Untersuchung verschiedener Struktur-Eigenschafts-Beziehungen von einigen Squaraine Farbstoffen sind die Zielsetzungen dieser Dissertation. Die dafür synthetisierten Squaraine bestehen aus einer, zwei oder drei Chromophor-Einheiten. Als Referenzsystem wurde der Indol-Endgruppen-Squaraine-Farbstoff gewählt (4-((3,3-Dimethyl-1-octyl-3*H*-indolium-2-yl)methylen)-2-((3,3-dimethyl-1-octylindolin-2-yliden)methyl)-3-oxocyclobut-1-enolat). Dieses Monosquaraine (MSQ) wurde mit einer bzw. zwei Phenylsubstituenten oder Benzo[*e*]indolsysteme modifiziert, um deren Einfluss auf die Chromophor-Eigenschaften zu bestimmen. Die unsymmetrische, also einfache Einführung dieser Modifikationen erfolgte gemäss der Synthesemethode von Terpetschnig et al. (*Analytica Chimica Acta*, 282(3):633–641, 1993). Die symmetrische, also zweifache Einführung wurde gemäss Treibs und Jacob (*Justus Liebig's Annalen der Chemie*, 712:123–137, 1968) durchgeführt. Das Absorptionsmaximum (λ_{max}), gemessen in Chloroform, konnte dabei von 637.5 nm des Referenz MSQs bis 665.5 nm mit der zweifachen Benzo[*e*]indole Modifikation verschoben werden. Der molare Absorptionskoeffizient der MSQs blieb dabei praktisch unverändert riesig bei etwa $350000 \text{ L}\cdot\text{mol}^{-1}\cdot\text{cm}^{-1}$. Eine lineare Struktur-Eigenschafts-Beziehung wurde gefunden, welche für jedes weitere Elektronenpaar ausserhalb der Chromophoreinheit das λ_{max} um 7 nm bathochromisch verschiebt.

Um das Zusammenspiel zweier squaraine Chromophore in einem Molekül besser zu verstehen, wurden diese Systeme über verschiedene konjugierte aromatische Brücken miteinander verbunden. Diese Brücken wurden so gewählt, dass die Distanzabhängigkeit (Phenylen versus Fluoren; Naphthalen vs. Anthrazen), die Donor oder Akzeptor Eigenschaften (Phenylen vs. Alkoxy-phenylen vs. Perfluoro-phenylen) und die Torsionswinkelabhängigkeit der Brücke relativ zum Farbstoffsystem mit den optischen und elektrochemischen Eigenschaften in Korrelation gebracht werden konnten. Um die jeweiligen Bissquaraine (BSQs) individuell zu synthetisieren, wurde die Synthesestrategie von Terpetschnig et al. angewendet. Als Resultat der Farbstoff-Farbstoff-Wechselwirkung sind die λ_{max} Werte dieser BSQs rot-verschoben und liegen im Bereich zwischen 670 und 730 nm.

Einige Trissquaraine (TSQs) wurden durch Polymerisation mit den gleichen Brücken wie die BSQs synthetisiert (Phenylen, Fluorene, Alkoxy-phenylen und Perfluoro-phenylen). Die λ_{max} Werte dieser TSQs lagen im Bereich von 674 bis 688 nm, was

im Vergleich mit den BSQs nur ein paar Nanometer weiter rot verschoben ist. Im Gegensatz dazu steht das Naphthalen verbrückte TSQ, welches über regioselektive Synthese zum Trimer aufgebaut wurde und ein λ_{max} Wert von 760 nm in Chloroform aufwies. Dieser Wert ist im Vergleich zum entsprechenden MSQ um 100 nm und zum BSQ um 30 nm rot verschoben.

Die λ_{max} -Werte wurden dann als Funktion von der Anzahl Wiederholungseinheiten in einem Graphen korreliert, aus welchem die brückenabhängige Sättigungskurven entwickelt werden konnten. Je nach Art der Brücke wird die Sättigung von λ_{max} nach fünf bis acht Wiederholungseinheiten erreicht und liegt im Bereich zwischen 700 und 800 nm. Mit diesen Daten konnte eine multidimensionale Sättigungsformel zur Bestimmung des Absorptionsmaximums eines beliebigen strukturverwandten Farbstoffes beschrieben werden, dessen Parameter durch die molekulare Struktur des Farbstoffes gegeben sind. Für diese Formel wurden der Torsionswinkel zwischen Farbstoffsystem und der Brücke, die Distanz zwischen den einzelnen Chromophoren und die Anzahl an in Konjugation stehenden π -Elektronenpaare miteinander gewichtet. Somit kann der Einfluss auf den λ_{max} Wert der Donor- oder Akzeptorgruppen an der Brücken vernachlässigt werden. Des Weiteren, stimmten die damit berechneten Absorptionsmaxima bis auf wenige Nanometer mit den gemessenen überein.

Die elektrochemischen Eigenschaften der Squaraine-Farbstoffe werden durch deren molekulare Struktur gleichermassen wie die optischen beeinflusst. Daraus ergab sich ein linearer Zusammenhang zwischen der optischen Bandlücke (ΔE_{opt}) und dem ersten elektrochemischen Oxidationspotenzial (E_{ox}^1); sowie dem ersten elektrochemischen Reduktionspotenzial (E_{red}^1). Die mittels optischen und elektrochemischen Messungen hergeleiteten Struktur-Eigenschafts-Beziehungen konnten mit Molekular Modelling bestätigt werden. Sowohl die geometrie-optimierte Molekülstruktur als auch die Bilder der Grenzorbitale wurden mit Density Functional Theory (DFT) mit B3LYP Functional und 6-31G* als Basis Set berechnet. Des weiteren zeigte das Molekular Modelling, dass ein unsymmetrisch aufgebautes, naphthalen verbrücktes Squarain Dimer eine gerichtete Ladungsverschiebung während der optischen Anregung zeigt. Dieses BSQ wurde synthetisiert, auf Titandioxid-Nanopartikeln immobilisiert und als proof-of-concept wurde damit eine Hybridsolarzelle (dye sensitized solar cell, DSC) hergestellt, welche einen Wirkungsgrad der Energieübertragung (η) von 1.3% aufwies.

Zusätzlich zu diesen Indol-basierten Farbstoffen wurde eine 1,5-Diazaanthrazene-Brücke über eine doppelte Doebner-Miller-Reaktion synthetisiert, mit welchem dann ein BSQ Farbstoff aufgebaut wurde. Dieser BSQ zeigte in Chloroform ein λ_{max}

Wert von 805 nm. Diese unerwartet grosse Rotverschiebung stammt gemäss Molekular Modelling von einer Fusion der Farbstoffsysteme, was über die Chromophor-Chromophor Interaktionen der anderen BSQs hinausgeht.

Contents

Summary	IV
Zusammenfassung	VI
Contents	X
1 Introduction	1
1.1 Interaction of matter with light	1
1.2 Molecular structure in relation to the absorption	4
1.3 Squaraine Dyes	11
1.4 Targets and Approach	13
2 Results and discussions	19
2.1 Synthesis	19
2.1.1 Synthesis of squaraines with one dye unit	19
2.1.2 Synthesis of squaraines with two dye units	25
2.1.3 Synthesis of squaraines with more than two dye units	38
2.2 Analysis and Characterization	43
2.2.1 Optical Properties	43
2.2.2 Solvatochromy	63
2.2.3 Electrochemical Properties	67
2.2.4 Analysis of the dye structure - molecular modeling	73

2.2.5 Proof-of-concept in DSC	79
3 Conclusions and outlook	85
3.1 Conclusions	85
3.2 Outlook	87
4 Experimental Descriptions	89
4.1 General Information and Procedures	89
4.2 Synthesis: Prescription and Characterization	94
References	177
Acknowledgments	187
Curriculum Vitae	188

Chapter 1

Introduction

If a compound possesses the ability to absorb or emit light in the visible (vis) range (400–700 nm [1]), it is called a colourant [2]. Colourants can be of inorganic or organic nature and they were classified as being either soluble *dyes* or insoluble *pigments* with many subordinated hierarchy elements [2].

The first few thoughts, when talking about dyes and pigments, are the colouring and dyeing of hair, textiles, paper, leather goods, plastics, walls, paintings and also their use in varnish, in CDs, DVDs and BDs, as bio markers, in TV screens and as food colourant [3]. Many of those dyes and pigments are of organic nature. The here presented work deals with *organic dyes* and focuses on organic molecules with more than one dye unit. The influences of the molecular structure on properties of the dye systems and the intra molecular dye-dye interactions were studied.

1.1 Interaction of matter with light

From the structural point of view, organic dyes are in general polarised aromatic compounds. The chromophoric part of the molecule consists of a conjugated π -electron system in between a π -electron donor (*D*) and a π -electron acceptor (*A*). According to the valence bond theory the organic dyes are represented by several contributing structures which either show charge separation or are neutral. The changing between these canonical forms is known as the delocalized π -system. With the help of the charge separated contributing structures the polarization is substantiated. However,

the interaction of a dye with light is described using quantum mechanics. Light as electromagnetic waves is formulated by the adapted Maxwell's differential equations 1.1 to 1.4 [1], here stated with the Nabla operator (∇). Where the space and time dependent electric field $\vec{E}(\vec{r}, t)$ is defined by a function of the space and time dependent magnetic field $\vec{B}(\vec{r}, t)$ and visa versa. For μ_0 and ϵ_0 in equation 1.4 refer to the magnetic field constant and the electric field constant, respectively.

$$\nabla \cdot \vec{E}(\vec{r}, t) = 0 \quad (1.1)$$

$$\nabla \cdot \vec{B}(\vec{r}, t) = 0 \quad (1.2)$$

$$\nabla \times \vec{E}(\vec{r}, t) = -\frac{\partial \vec{B}(\vec{r}, t)}{\partial t} \quad (1.3)$$

$$\nabla \times \vec{B}(\vec{r}, t) = +\mu_0 \cdot \epsilon_0 \cdot \frac{\partial \vec{E}(\vec{r}, t)}{\partial t} \quad (1.4)$$

In order to disentangle this equation system one normally introduces the vector potential $\vec{A}(\vec{r}, t)$ and the scalar potential $\phi(\vec{r}, t)$ resulting in equation 1.5 and 1.6 [1, 4, 5, 6, 7].

$$\vec{E}(\vec{r}, t) = -\nabla \cdot \phi(\vec{r}, t) - \frac{\partial \vec{A}(\vec{r}, t)}{\partial t} \quad (1.5)$$

$$\vec{B}(\vec{r}, t) = \nabla \times \vec{A}(\vec{r}, t) \quad (1.6)$$

With the help of the vector potential $\vec{A}(\vec{r}, t)$ and the scalar potential $\phi(\vec{r}, t)$ the time dependent Hamiltonian for a *single* free particle of mass m , momentum p and charge q in an electromagnetic field takes the form 1.7 [4, 5, 6, 7].

$$H(t) = \frac{1}{2 \cdot m} \left(p - q \cdot \vec{A}(\vec{r}, t) \right)^2 + q \cdot \phi(\vec{r}, t) \quad (1.7)$$

However, a dye is not a single particle and therefore the Hamiltonian becomes accordingly more complex. To answer the question which molecular properties interact with the electromagnetic irradiation during a finite measurement, e.g. recording an UV/vis spectrum of a dye, the time dependent Hamilton operator $\hat{H}(t)$ of the dye is calculated. $\hat{H}(t)$ is given by the sum of the the time independent Hamilton operator

\hat{H}_0 and the time dependent Hamilton operator $\hat{V}(t)$ (Equation 1.8 [4, 5, 6, 7]). \hat{H}_0 represents the equilibrium state of the molecular system and $\hat{V}(t)$ represents an external perturbation as the electromagnetic field of the light beam.

$$\hat{H}(t) = \hat{H}_0 + \hat{V}(t) \quad (1.8)$$

$\hat{V}(t)$ is the negative sum of all products of a molecule property based interaction operator and a time dependent experimental stimuli. The dipole approximation was used as an approach for this equation 1.8 when only the main interactions were accounted [4]. Since the experimental stimuli is a light beam, $\hat{V}(t)$ is split into an electric and a magnetic part. So those operators act on $\vec{E}(\vec{r}, t)$ and $\vec{B}(\vec{r}, t)$. Without going into the details, the molecule property based interaction operators are the electric dipole operator $\hat{\mu}_{el}$ and the magnetic dipole operator $\hat{\mu}_{mag}$ [4]. So the time dependent perturbation is described by the formula 1.9 [4].

$$\hat{V}(t) = - \left(\hat{V}_{el}(t) + \hat{V}_{mag}(t) \right) = - \left(\hat{\mu}_{el} \cdot \vec{E}(t) + \hat{\mu}_{mag} \cdot \vec{B}(t) \right) \quad (1.9)$$

In UV/vis spectroscopy as well as in infrared (IR) and microwave spectroscopy the *electric* dipole dominates the measurable interaction with the light, whereas in nuclear magnetic resonance (NMR) and electron paramagnetic resonance (EPR) spectroscopy the *magnetic* dipole interaction with the experimental electromagnetic wave is determined. Therefore, considering an electronic transition in the UV/vis range of a chromophore, the measurable response after the perturbation with a light pulse is the electric transition dipole moment \vec{M}_{ge} (g for ground state $|g\rangle$ and e for excited state $|e\rangle$). One can determine \vec{M}_{if} by solving the Dirac Bra-ket notation $\langle f | \hat{\mu}_{el} | i \rangle$ (i for initial and f for final state) with the harmonic oscillator approximation but this is only valid for the same energy state; so it is used for IR and microwave spectroscopy [4, 8, 9]. For an electron transition the absolute value $|\vec{M}_{ge}|$ can be approximated as linear combination of the norm of the static electric dipole moments of each electronic state ($\mu_{el,g}$ and $\mu_{el,e}$) as shown in equation 1.10, where the sum of the coefficients a_g and a_e is unity.

$$|\vec{M}_{ge}| = a_g \cdot |\vec{\mu}_{el,g}| + a_e \cdot |\vec{\mu}_{el,e}| = a_g \cdot \mu_{el,g} + a_e \cdot \mu_{el,e} \quad (1.10)$$

Except for the linear combination coefficients all three values can be estimated from a series of UV/vis and fluorescence spectra. The experimental determination of those

values is included in section 2.2.

1.2 Molecular structure in relation to the absorption

After defining the general physical property for the absorption phenomenon, the structural aspects in respect to their absorption were discussed with the help of the following examples of the azo dye class [2] as representatives for most of the organic dyes [2, 10, 11] (Figure 1.1): (*E*)-azobenzene (**1**), 4-(*N,N*-dimethylamino)-azobenzene (**2**) and 4-(*N,N*-dimethylamino)-4'-nitro-azobenzene (**3**). When molecule **1** is excited by light the absorption maximum (λ_{max}^{abs}) is 450 nm and one quantity of the strength of the transition is the molar absorption coefficient ($\epsilon(\lambda_{max}^{abs})$). The value of $\epsilon(\lambda_{max}^{abs})$ for molecule **1** is very low $463 \text{ M}^{-1}\text{cm}^{-1}$ [2]. Understandably, molecule **1** is not a dye, because it only contains two aromatic π -systems with one π -electron accepting group *A*, namely the azo group. In accordance with the valence bond theory no canonical form with charge separation fulfilling the octet rule can be drawn for molecule **1**, because it does not possess a π -electron donating group *D*. Therefore, also no static electric dipole moment is dominant in this molecule. However, when formally a donor group *D* in form of a *N,N*-dimethylamino group at the 4-position is added to the structure of molecule **1**, the azo dye 4-(*N,N*-dimethylamino)-azobenzene (**2**) is created (Figure 1.1). As shown in this figure, charge separation occurs in one of the canonical formulas of dye **2**. From this resonance structure a reasonable static electric dipole moment for the ground state $\mu_{el,g}$ and presumably also for the excited state $\mu_{el,e}$ can be derived. The bigger the value of the transition moment and the more probable the charge separated canonical formulas are, the more intensive the absorptivity of the electronic transition is. Consequently, a 60-fold higher value of $\epsilon(\lambda_{max}^{abs})$ for dye **2** ($27500 \text{ M}^{-1}\text{cm}^{-1}$ at $\lambda_{max}^{abs} = 408 \text{ nm}$, [2]) than that of molecule **1** underlines the theory from a structure property relation of a *D*- π -*A* dye system.

In order to answer the question about the properties of multi dye unit molecules, extended *D*- π -*A* systems were investigated. When an additional *A* in form of a nitro group was formally added to dye **2**, then dye **3** (4-(*N,N*-dimethylamino)-4'-nitro-azobenzene, Figure 1.1) was formed. Dye **3** represents a *D*- π -*A*- π -*A* system and possesses two canonical formulas with charge separation of which one is uniform with the one of dye **2** (Figure 1.1). This resonance structure is symbolized by $\overrightarrow{D-\pi-\dot{A}}-\pi-A$. The second canonical formula with charge separation showed a resonance system through the hole

molecule ($\overrightarrow{D-\pi-A-\pi-A}$). These arrows were suggested as representatives for the static electric dipole moments (Figure 1.1). These two vectors of the extended dye system in dye **3** are linearly dependent because they have the same origin and the same direction. Linearly depending vectors could be linearly combined but cannot be coupled.

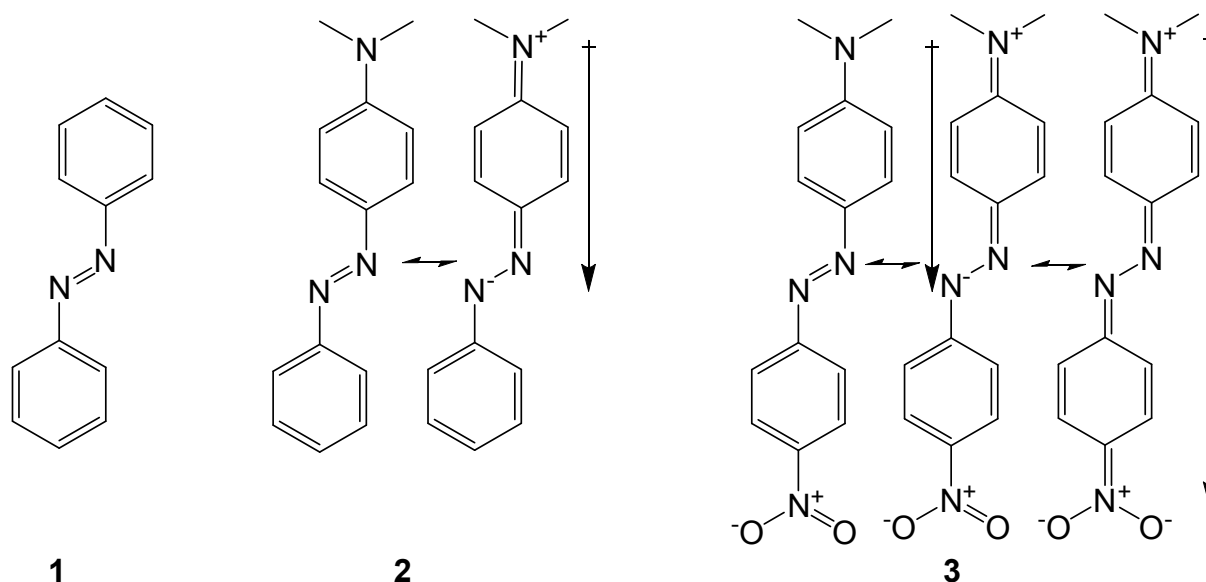


Figure 1.1: (*E*)-azobenzene (**1**), 4-(*N,N*-dimethylamino)-azobenzene (**2**) and 4-(*N,N*-dimethylamino)-4'-nitro-azobenzene (**3**) and their canonical formulas.

As a result, \vec{M}_{ge} of dye **3** is a linear combination of the dipole moments from the two resonance structures and therefore its value is larger than the value of \vec{M}_{ge} of dye **2**. With this theoretical ansatz the further increased value of $\epsilon(\lambda_{max}^{abs})$ to $33100 \text{ M}^{-1} \cdot \text{cm}^{-1}$ of dye **3** is easily explained. In addition to the hyperchromic shift, λ_{max}^{abs} is bathochromically shifted to 478 nm because of the enlargement of the π -system.

Furthermore, many different concepts to elongate the π -system in combination with *A* and *D* were realized, for example: $(D-\pi-A)_n$, $D-(\pi)_n-A$, $D-(\pi-A)_n$ and $(D-\pi)_n-A$, where *n* refers to the number of repeating units. These concepts were applied in several dye families: azo dyes, the carbonyl dyes (hydroquinone, anthraquinone and perylene derivatives), arylmethane dyes and polymethine dyes to yield a diversity of hundreds of thousands of dyes [3, 2, 10, 11].

The influence on λ_{max}^{abs} and $\epsilon(\lambda_{max}^{abs})$ upon elongation of the dye system led to the question if these values are further increased when one or more additional "- π -A-" units are introduced. If yes, is it a linear increase or does it follow a function? In addition it is

of interest whether the values of λ_{max}^{abs} can decrease and if any exceptional or special compounds exist. Meier dealt with these questions and summarized his results in a review [12, 13]. He discussed the relation of the number of repeating units n with the optical properties with the help of several examples of the polyene dye class (dyes with $D-(\pi)_n-A$ as general structure) polythiophene dyes, merocyanine dyes and some other dye classes [12]. Here, the dye system $D-(\pi)_n-A$ was chosen to explain the context. Therefore, a series of phenylene vinylene dye systems **4a-e** were displayed in figure 1.2. The donor of the dyes **4a-e** was a tertiary amine function and the A was varied as shown by the different R's being a hydrogen (**4a**), a cyano group (**4b**), a formyl function (**4c**), a nitro group (**4d**) or a dicyanovinylene moiety (**4e**). For each series the number of repeating units n was varied from one to four. The series **4a-c** showed a monotonic growth of the λ_{max}^{abs} value with increasing number of repeating units n . Which was explained with the expansion of the π -system [12] comparable with the elongation of the one dimensional box length in the electron-in-the-box model [14]. In contrast, the values of $\lambda_{max}^{abs}(n)$ for the two other series **4d,e** run in the opposite direction (Figure 1.2). Particularly, because of the very strong A (nitro group and dicyanovinylene moiety) in comparison with the amine donor in respect to the Lewis acid-base theory. According to Meier, the smaller the distance in the molecule inbetween A and D was and the stronger A was, the more populated the canonical structure with charge separation was, resulting in a more red shifted spectra due to the intra molecular charge transition (ICT) [12]. The resulting monotonic hypsochromic shift is a contrary tendency to the bathochromic shift upon π -electron framework elongation. If the ICT dominated over the bathochromic effect by enlarging the π -system, the λ_{max}^{abs} was hypsochromically shifted, else bathochromic. However, in any case the value of λ_{max}^{abs} reached a limit – so called λ_{∞} – after a certain number of repeating units n (Figure 1.2, [12]). λ_{∞} corresponded to λ_{max}^{abs} of a poly phenylene vinylene [15]. The progress of $\lambda_{max}(n)$ was described with an exponential growth function (Equation 1.11 [15, 12]) which was fitted to the data set, where λ_1 was equal to λ_{max}^{abs} of the initial compound ($n=1$) and b represents the only parameter in this equation!

$$\lambda_{max}(n) = \lambda_{\infty} - (\lambda_{\infty} - \lambda_1)e^{-b(n-1)} \quad (1.11)$$

In general the limit of the optical properties was approximatively reached after 5 to 10 repeating units. This point was called effective conjugation length (n_{eff} , [15, 12]) and it represented the canonical formula with the furthestmost charge separation. n_{eff} was

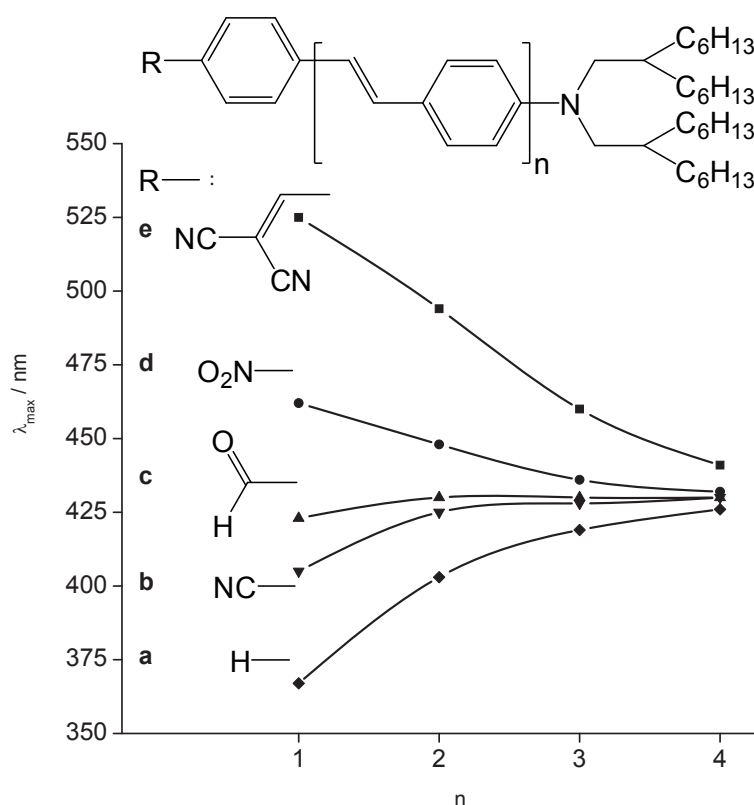


Figure 1.2: Comparison of λ_{max}^{abs} of phenylene vinylene dye system series **4a-e** with various different R 's as acceptors being a hydrogen (**4a**), a cyano group (**4b**), a formyl function (**4c**), a nitro group (**4d**) or a dicyanovinylene moiety (**4e**); $n = 1$ to 4 [12].

calculated using the same parameters as in equation 1.11 from equation 1.12 [15, 12].

$$n_{eff} = 1 + \frac{\ln(\lambda_{\infty} - \lambda_1)}{b} \quad (1.12)$$

Meier stated, that equation 1.11 was true for all conjugated oligomeric dyes, except for the cyanine dye class [12] which made them more interesting for further investigation. The cyanine dye class is part of the polymethine dye family [11]. In order to see the special behavior of the cyanine dye class, their function $\lambda_{max}^{abs}(n)$ was plotted with other dye classes of the polymethine dye family in figure 1.3: polyene oligomers (magenta) [16], poly(triacetylene) oligomers (red) [17], poly(phenylene vinylene) oligomers (light green) [15], merocyanine dyes (blue) [18], oxonol dyes (cyan) [18] and cyanine dyes (black) [18]. In all these cases the values of $\lambda_{max}^{abs}(n)$ showed a monotonic increase with mostly a decreasing slope, resulting in a limitation, except for the oxonol dyes and the cyanine dyes; or at least no proven convergence up to now. Because of the linear

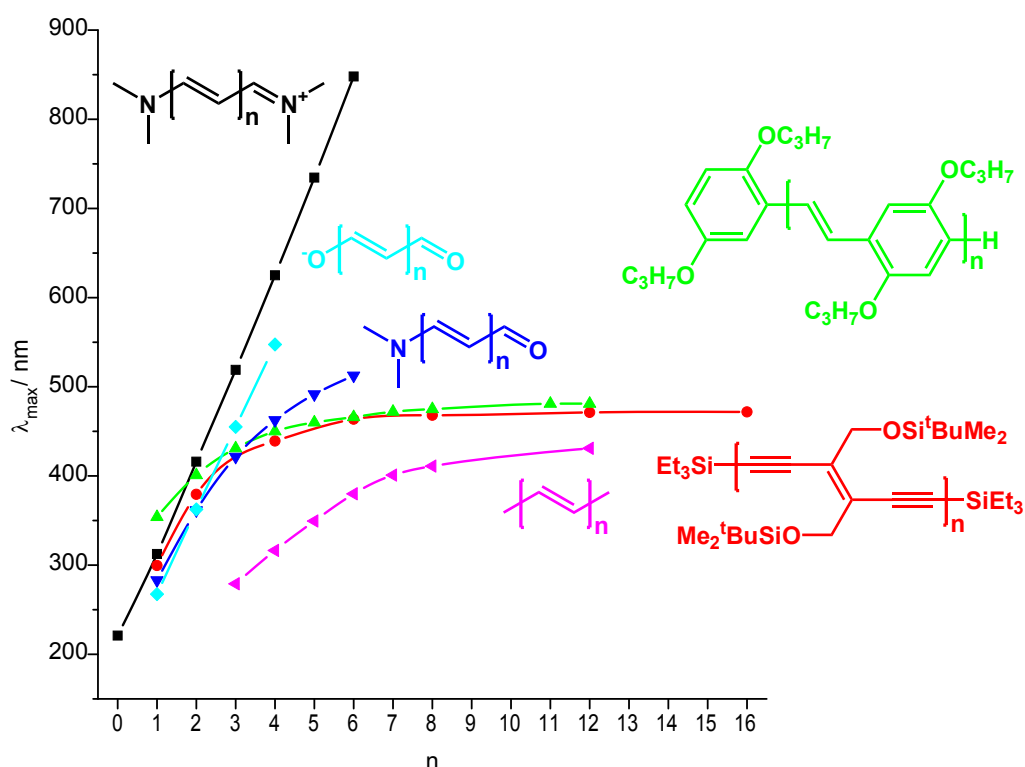


Figure 1.3: Some groups of the polymethine dye class: polyene oligomers (magenta) [16], poly(triacetylene) oligomers (red) [17], poly(phenylene vinylene) oligomers (green) [15], merocyanine dyes (blue) [18], oxonol dyes (cyan) [18] and cyanine dyes (black) [18].

behaviour of the function $\lambda_{max}^{abs}(n)$ for these two dye classes the cyanine dyes (Equation 1.13) and the oxonole dyes (Equation 1.14) it is suggested, that no limitation of the optical properties exist.

$$\lambda_{max}(n) = 105 \cdot n + 211 \quad [nm] \quad \text{with } R^2 : 0.999. \quad (1.13)$$

$$\lambda_{max}(n) = 93 \cdot n + 175 \quad [nm] \quad \text{with } R^2 : 1.000. \quad (1.14)$$

It is not yet clearly known why the behavior of the oxonol dyes and cyanine dyes is fundamentally different from the analogue merocyanine dyes and polyenes. Obviously, from the structural point the two latter are basically neutral structures. They therefore have one or several canonical formulas where charge separated occurs which is similar to the above mentioned canonical formulas of azo dyes **2** and **3**. However, oxonol dyes and cyanine dyes have a permanently charged conjugated and therefore delocalized

π -system with two mirror-inverted contributing structures which fulfill the octet-rule (Figure 1.4). Thus, one can set n_{eff} equal to n for the reported data of the oxonol dyes and cyanine dyes. And according to Shalhoub et al. the cyanine dyes were "real world" examples for the electron-in-the-box model [11, 14]. So no limiting effective conjugation length (n_{eff}) exists than the real length of the resonance system. Because the probability to find oxonol and cyanine dyes in the canonical form with charge separation is 100%, these dyes have a bigger $|\vec{M}_{ge}|$ value in respect to the one for the merocyanine dyes and the polyenes. The static electric dipole moment for each canonical form of the cyanine and the oxonol dyes was also drawn in figure 1.4. In the conversion from one

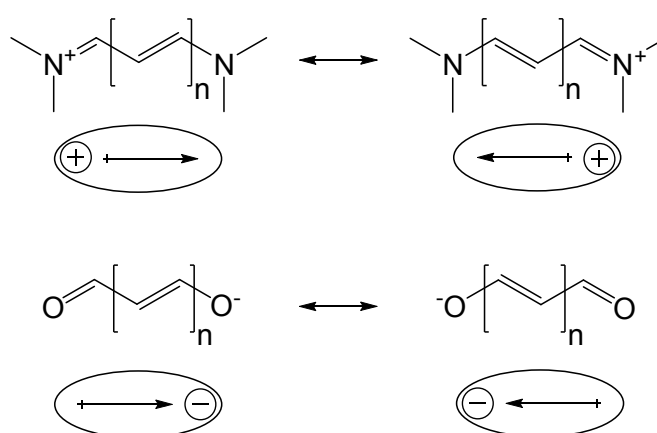


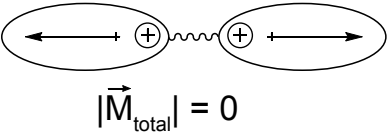
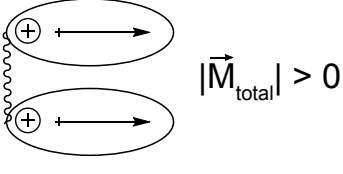
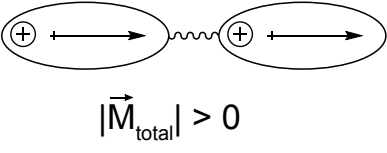
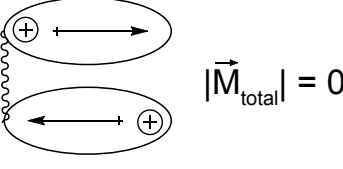
Figure 1.4: The two mirror-inverted canonical forms from cyanine dyes (top) and oxonol dyes (bottom) with their static electric dipole moment approximated as schematic representation (always below the structure).

form into the other the charge also moves, entailing an oscillation of $|\vec{M}_{ge}|$ since the two canonical forms have an opposite vectorial orientation. Thus it is to mention, that these dye systems cannot be elongated from the side meaning the chromophore synthon of these dyes starts and ends with the heteroatoms, but neighbouring groups have a strong influence on the chromophoric part of the dye [11].

The above mentioned concept to connect several D - π - A units together was also applied to the cyanine dye class. This ansatz led to the interesting questions whether the connection influences the optical properties and whether the optical properties show a linear behaviour or if they follow a saturating growth function. Kiprianov dealt with these questions and studied the interference of two covalently connected cyanine dyes [19]. He found, that the total transition dipole moment $|\vec{M}_{total}|$ of dimeric cyanine dyes is a result of a coupling of the individual transition dipole moment $|\vec{M}_{ge}|$ of each chromophore

unit and not a linear combination. By comparing a series of dimeric cyanine dyes he also found a dependency of the relative angle (φ) of the two connected chromophores. In the two extreme cases, where φ is 0° or 180° , the connection is either serial or parallel as indicated in table 1.1. In this table the schematic representation of the cyanine dyes of figure 1.4 with suggested dipole moments were used to illustrate the theory of Kiprianov. In both cases the two individual dipole moments of each chromophore unit can be drawn rectified or antipodal. When both chromophores in such a compound were the same, then the sum of the individual dipole moments in the antipodal combination is zero and consequently $|\vec{M}_{total}|$ is also zero. In terms of the previously mentioned quantum mechanic description, if the time dependent perturbation operator $\hat{V}(t)$ (equation 1.9) acts on zero, the time dependency vanishes. Concluding, the state with the antipodal combination of the dipole moments does not interact with light. Furthermore, Kiprianov defined that the state where charge repulsion occurs as the high energy state. For the serial connection of the chromophores the antipodal combination of the theoretically individual dipole moments is the high energy state and for the parallel connection it is the rectified combination [19] (table 1.1). According to him this led to the following result for a dimeric cyanine dye [19]: in respect

Table 1.1: Comparison of serial and parallel connected cyanine dyes by the schematic representation from figure 1.4 with the individual dipole moments and the overall transition moment $|\vec{M}_{total}|$ [19].

	serial connection	parallel connection
High energy state	 $ \vec{M}_{total} = 0$	 $ \vec{M}_{total} > 0$
Low energy state	 $ \vec{M}_{total} > 0$	 $ \vec{M}_{total} = 0$

to the absorption band of the corresponding single cyanine dye the absorption band is bathochromically shifted when serially connected, because the measurable optical transition (rectified dipole moment combination) is in the lower energy state. For the

absorption band of the parallel connected compound the absorption band is therefore hypsochromically shifted.

The correlation of Kiprianov paved the way for the preparation of new dyestuffs. With his serial approach, oligomeric and polymeric cyanine dyes could be synthesized which absorb in the far near infra red (NIR) region, but up to now only a few have been reported. The first oligomeric cyanine dye (n : 4–6) was described by Pailer and Renner-Kuhn [20], Kiprianov reported a cyanine dye trimer [19], Kossmehl et al. proclaimed polymeric cyanine dyes [21, 22] and Geiger et al. recently synthesized polymeric cyanine dyes with n : 30–60 [23]. They all used an eight π -electron resonance system as dye, a so called trimethine cyanine dye, however with some different connecting groups. The measured bathochromic shifts between the trimethine monomer ($\lambda_{max}^{abs} \approx 550$ nm [22, 23]) and the polymers (λ_{max}^{abs} : 680–710 nm [22, 23]) were 130–160 nm. Since the polydispersity of the polymeric material from Geiger et al. [23] was broad and its published absorption spectrum did not show an absorption curve with several discrete absorption maxima it is assumed that $\lambda_{max}^{abs}(n)$ of serially coupled cyanine dye systems connected over the reported conjugated bridges will show a limitation. Geiger et al. also introduced a twelve π -electron resonance system (heptamethine cyanine dye) into a polymer and observed the same bathochromic shift of 160 nm (λ_{max}^{abs} (monomer): 831 nm, λ_{max}^{abs} (polymer): 990 nm) [23]. Since only little was reported in this area the field of oligomeric and polymeric cyanine dyes is still undiscovered. Nevertheless, new questions arose. Whether the structure of the connected conjugated bridge influences the coupling and therefore the optical properties and if the reported bathochromic shift of 160 nm is the maximal achievable one. To these questions it is referred in section 1.4 after the introduction into the main dye class for this thesis.

1.3 Squaraine Dyes

If an oxonol dye is formally integrated into a cyanine dye then it can be done in such a way that the charges are still permanently separated but leading to an overall electronically neutral species. One of these special species are the so called *squaraine dyes*, or just *squaraines*. They were named according to their synthetic equivalent: squaric acid (3,4-dihydroxy-3-cyclobuten-1,2-dion). Here, squaraine **5** was formally made from a pentamethin cyanine dye **6** and a monomethin oxonol dye **7** as shown in figure 1.5. Since it is a combination of two polymethine dye systems their dipoles

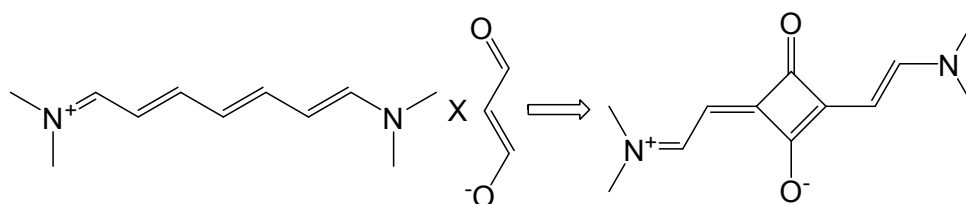


Figure 1.5: Artificial combination of a pentamethin cyanine dye **6** and a monomethin oxonol dye **7** to a squaraine **5**.

were also combined. When all four resonance structures were drawn side by side as in figure 1.6, one could almost think that squaraines have rather an electronic quadrupole than a dipole. Indeed, squaraines have a not-negligible quadrupole which interacts in solution with the permanent dipole of the solvent [24]. Also the quadrupole tensors were calculated by Xu et al. [25]. A quadrupole is also a condition for non-linear optics (NLO) and those effects were surprisingly big for squaraines [26, 27, 28]. However, some of

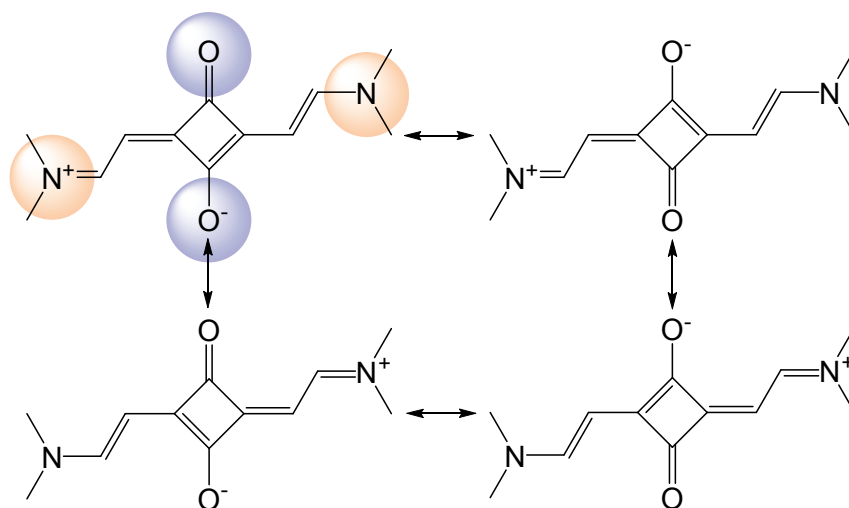


Figure 1.6: The four resonance structures of squaraine **5** with its controversial quadrupole (drawing).

these NLO effects were later diminished by Ashwell et al. [29].

Squaraines were not only used for NLO applications but also in solar cells, due to their good ability to absorb light and transfer the energy of the absorbed light efficiently which is an essential property for this application [30]. Unsymmetric squaraine dyes were used as sensitizer in dye sensitized solar cells (DSC's) where they achieved an *Incident-Photon-to-electron Conversion Efficiency* (IPCE) of over 80%, which is quite unique in this area [30,31,32]. However the "energy conversion efficiency" (η) was only

around 5%, because squaraines similar to cyanine dyes have an intense but narrow absorption band. Efforts were made to broaden the absorption band but the dye showed a diminished η of about 1% presumably due to an unoptimised cell preparation [33].

Also polymeric squaraine dyes were prepared [34, 35, 36], but since they were barely soluble they were not characterized very well. Their optical band gap (ΔE_{opt}) of 0.8 eV was extrapolated from a diluted sulfuric acid solution. This very low value of ΔE_{opt} gave an input to theoreticians which calculated some polymeric squaraines with *ab initio* methods and predicted semiconducting properties for this dye class [37]. As a result several chemists synthesized polymeric squaraines and measured their conductivity [38, 39], which was poor (10^{-7} to 10^{-4} S·cm⁻¹ [38]). Although lots of oligomeric and polymeric squaraines were reported there is less known about the interaction of the chromophores over the conjugated bridge than for the cyanine dyes.

Additionally, the optophysical property of squaraines to absorb light and transfer the energy was also used in cancer treatment by Devi et al. [40]. He used bis(3,5-diiodo-2,4,6-trihydroxyphenyl)squaraine as an anti skin cancer agent [40]. They used cancerogenic mice and medicated them with this squaraine dye under full sun light treatment. Basically, the dye acted as a photo energy absorber which interacted after excitation with oxygen and produced singlet oxygen. This reactive compound "burnt" the tumors. It was also found, that this treatment reactivated the apoptosis (programmed cell death, which is arrested during cancer progression [40]). Both properties led to a destruction of the cancer. Indeed, the reduction of the mean tumor burden on mice was 88%.

1.4 Targets and Approach

As previously indicated, the knowledge about squaraines with more than one chromophore is poor. In order to increase it, the targeted questions concentrate on the structure property relations of coupled squaraines. The main questions were: How differently conjugated bridges influence the coupling of two squaraines? And whether one can predict the optophysical properties from the nature of the coupling or not. In order to prove a coupling inbetween two squaraine chromophore units, the structural influence of the aromatic surrounding on the optophysical properties of squaraines were investigated by model compounds. As a reference dye, the unmodified 3H-

indole squaraine **8** (Figure 1.9) was chosen because of the following four reasons: Firstly, the indole side group is synthetically readily available, offers several synthetic modification possibilities and orthogonal derivatization. Secondly, the used *3H*-indole offers possibilities for derivatization at the aromatic synthon, nitrogen side group as well as at the *3H*-dimethyl groups. Thirdly, the incident solubility of these dyes increases in respect to other aromatic end groups as quinolines, oxazolines, thiazolins [11] due to the latter methyl groups. Fourthly, the *3H*-indoles are also a common end group for cyanine dyes [11] which facilitates the comparison with literature.

The model compounds were mono squaraines (MSQs) with an additional aromatic ring system connected to the *3H*-indole end group. On the one hand, the additional aromatic ring system was connected at the 5-position of one (MSQ **9**) or on both (MSQ **10**) *3H*-indoles as phenyl substituent as shown in figure 1.7. On the other hand, the additional

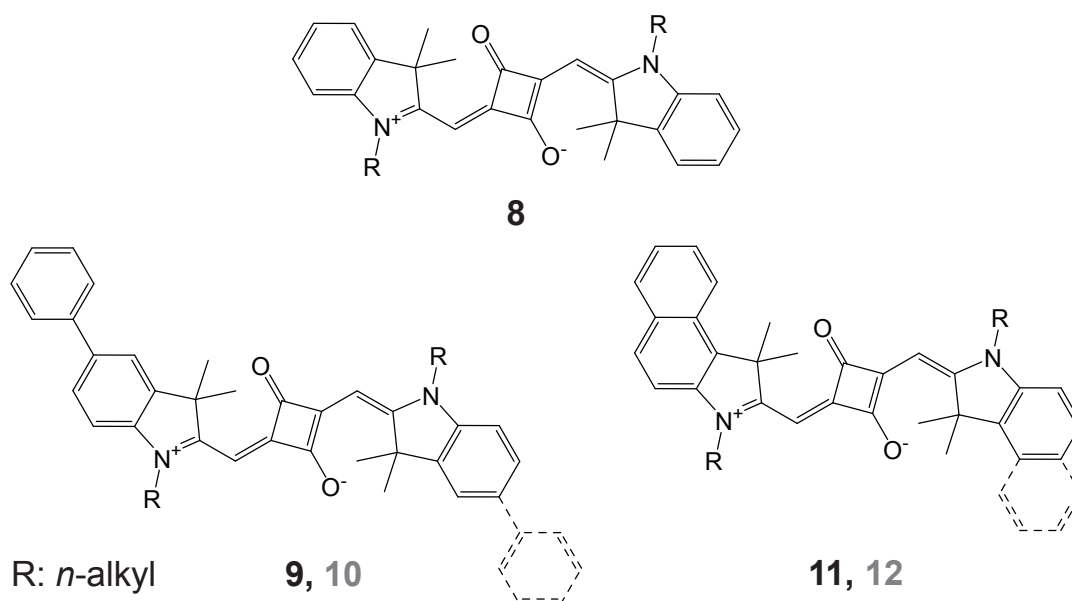


Figure 1.7: Targeted mono squaraines (MSQs) used to study the influence of the aromatic end groups on the optophysical properties of the chromophore.

aromatic ring system was condensed to the [e] bond of the *3H*-indoles resulting in MSQ **11** and MSQ **12** with one and two *1H*-benzo[e]indole end groups, respectively (Figure 1.7). Please also note the changed numeration of indoles and benzo[e]indole according to the IUPAC nomenclature.

The basic principle to explore the structure property relation of squaraines with two chromophore units connected over a conjugated bridging synthon was to prepare

defined bis squaraine (BSQ) dyes with 1*H*-benzo[*e*]indole end groups where only the bridging synthon was varied. Furthermore, it was decided to aim at solely serially connected dyes because in this relative constitution only one allowed transition occurs leading to a bathochromic shift of the absorption band according to Kiprianov (table 1.1).

The interesting questions concerning the bridging synthon were whether the torsion angle (ϕ) between the π -system of the chromophore and the π -system of the conjugated bridge is a factor influencing the dye-dye interaction. Whether the distance inbetween the two chromophores plays an important role. And whether the interaction is effected by a different electrostatic environment of the bridge. As an approach for the study of the influence of ϕ the tilted phenylene bridging synthon and the planar naphthalene bridging synthon were introduced resulting in the bis squaraines (BSQs) **13** and **14**, respectively, as shown in figure 1.8. To determine the distance dependency in the bridging synthons of the BSQs **13** and **14**, an additional phenyl system was inserted, resulting in the fluorenylene bridged BSQ **15** and the anthracene bridged BSQ **16** (Figure 1.8). The influence of the aromatic end groups on squaraines with two chromophores was analysed using the naphthalene bridge. Thereto both end groups were changed to 3*H*-indoles in BSQ **17** (Figure 1.9). Kiprianov also investigated the combination of different chromophores [19], however, only squaraines were used as chromophores in this work. To study this possibility, two different end groups were introduced in a naphthalene bridged BSQ **18** resulting in two slightly different chromophores.

To study the effect of the electronic environment of the bridge, the phenylene synthon was modified. To create a higher π -electron density on the bridge an alkoxy phenylene synthon was used and the opposite, a poorer π -electron density, a tetrafluoro phenylene bridge was used. These two bridges were introduced in the target molecules BSQ **19** and BSQ **20**, respectively (Figure 1.9).

The next interesting question was whether the Meier's equation could be adapted to the squaraines with more than one dye unit connected over the before mentioned bridging synthons. For this, oligomeric squaraines were targeted with the phenylene bridged dye **21**, the fluorenylene bridged dye **22**, the bis-alkoxy-phenylene bridged dye **23**, tetrafluoro phenylene bridged dye **24** and in addition to investigate on the distance dependency another oligomeric squaraine (dye **25**) was synthesized. Dye **25** is the homo oligomer of the reference dye **8** connected over a single bond at the 5-position of the indole system. Alongside the naphthalene bridged oligomeric dye **26** was synthesized.

Next to the torsion angle also the planarity of bridge might have an influence on the coupling. Consequently, the out-of-plane elements in the five membered ring system of the 3*H*-indoles on the bridging synthons were replaced by a six membered aromatic system. The 1,5-diaza anthracene derivative was introduced as a bridging synthetic equivalent into BSQ **27** (Figure 1.8).

In order to analyse the above named structure based impact, the optical properties of the target molecules were studied. It was investigated whether the structure have a similar or different influence on the absorption maximum λ_{max}^{abs} , the molar absorption coefficient $\epsilon(\lambda_{max}^{abs})$, the emission maximum λ_{max}^{abs} , the Einstein coefficients ($A_{g,e}$ and $B_{g,e}$), the static electronic dipole moments of the ground state and excited state ($\mu_{el,g}$ and $\mu_{el,e}$) and the optical band gap (ΔE_{opt}). Additionally, the question was asked whether the predicted bathochromic shift correlates with the transition moment $|\vec{M}_{ge}|$ of the dye as the theory of Kiprianov predicted. Thereto, $|\vec{M}_{ge}|$ was calculated on the one hand by the integral of the absorbance of a UV/vis spectrum (see section 2.2.1) and on the other hand with the help of the Lippert parameter which was determined by the solvatochromy of the dyes (see section 2.2.2).

In addition, the structure was related to the electrochemical properties. Those were determined by cyclic voltammetry measurements to give evidence whether the redox potentials, the electronic band gap (ΔE_{el}) or the number of involved electrons were influenced by the molecular structure of the target molecules. Furthermore, the question shall be answered whether the optical property correlates with the electrochemical ones.

The structural influence of the bridge in the BSQs on the spacial frontier orbital cloud distributions was investigated by molecular modeling using the reported parameters by Geiger et al. [32] on the Ipazia cluster [41].

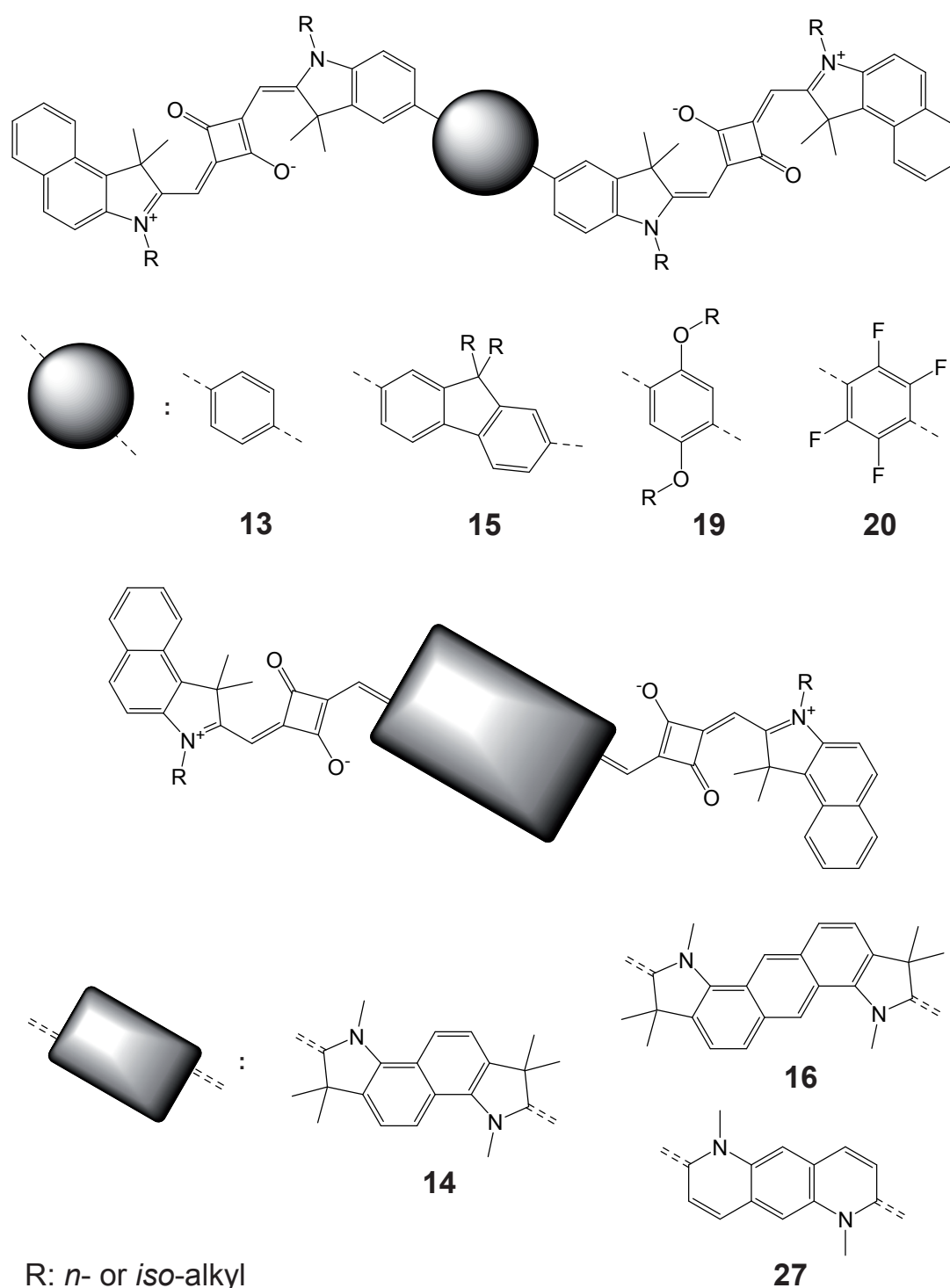


Figure 1.8: Targeted bis squaraines (BSQs) used to study the influence of different bridging synthons on squaraines with two chromophores. The circle represents the phenylene, the fluorenylene, the bis alkoxy phenylene and the tetra fluoro phenylene bridging synthon. The rectangle represents the naphthalene, the anthracene and the diaza-anthracene bridging synthon.

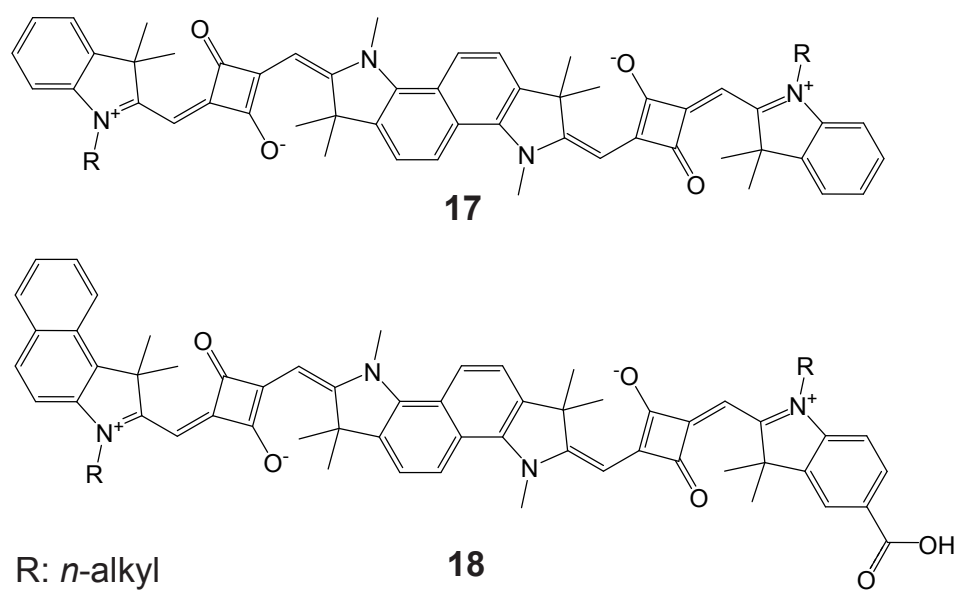


Figure 1.9: Special targeted bis squaraines (BSQs) used to study the influence of the aromatic end groups on squaraines with two chromophores.

Chapter 2

Results and discussions

2.1 Synthesis

2.1.1 Synthesis of squaraines with one dye unit

The synthesis towards the reference mono squaraine (MSQ) dye **8** started with an octylation of 1,1,2-trimethyl-1*H*-indole to yield imminium ion **28** as shown in figure 2.1 (details on page 126). In the literature, indole derivatives are normally alkylated in acetonitril with a yield of 46–59% within 72 h [42, 31, 43, 44]. In the present case, the reaction was performed in 1-butanol which yielded 68% in half the time. Further correction of the reported "standard" procedure had to be made, namely an anion exchange from the *in situ* generated imminium iodide **28** to the imminium perchlorate. This was necessary because the iodide was a honey-like resin and the exchange lead to a crystalline powder. The final reaction step to obtain MSQ **8** was a double Knoevenagel type condensation (page 94). Thereto, the imminium perchlorate **28** was deprotonated *in situ* by quinoline to the homologous Emil-Fischer base which then reacted as the reactive nucleophilic species with the electrophilic squaric acid. Interestingly, the reported homologue product with *N*-methyl instead of *N*-octyl groups has a decomposition point at about 300°C [45, 46]. However, MSQ **8** and also its dibromo derivative **29** (Figure 2.4) have a melting point of 155–160°C and 205–215°C, respectively. Furthermore, MSQ **8** can be sublimated which is an outstanding property for a permanently charged organic dye, especially for a possible further use of this compound in thin-film photovoltaic applications.

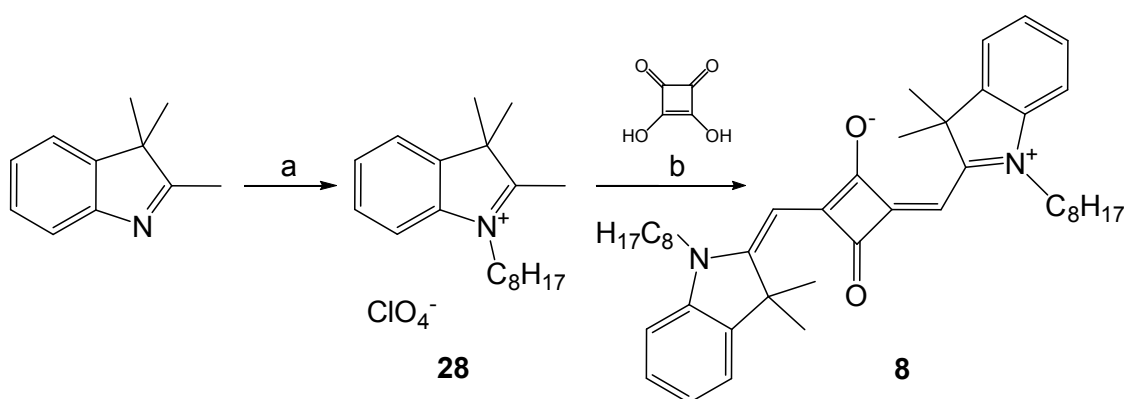


Figure 2.1: **a)** Synthesis of imminium perchlorate **28** from 1,1,2-trimethyl-1H-indole, details described on page 126; **b)** synthesis of MSQ **8** (page 94).

The route to obtain unsymmetrical squaraines with one dye unit was developed by Terpetschnig et al. [47, 48]. Their route was followed to produce the mono phenyl extended MSQ **9** (Figure 2.3). For this, squaric acid diethyl ester (**30**) (Figure 2.2) and bromo indolium compound **31** (Figure 2.2) had to be synthesized first. The diester **30** was synthesized according to Liu et al. [49] with necessary changes in the isolation procedure (page 130). Liu et al. prepared the diester **30** as yellow oil after column chromatography with 91% yield. Here, it was distilled twice to get a colourless transparent liquid with a similar yield of 86%. The other intermediate, the bromo indolium derivative **31**, was synthesized starting with a Fischer-Indole-Synthesis according to the described method by Kim et al. [43] from 4-bromophenylhydrazine hydrochloride to the bromo indole derivative **32** [50] in 49% yield (page 132). Followed by an ethylation reaction of intermediate **32** in 1-butanol yielded bromo indole derivative **31** [50] (page 131). The next reaction step towards the unsymmetrical MSQ **9** (Figure 2.3) was the coupling of one indole synthetic equivalent to the squaric acid derivative. So imminium perchlorate **28** was deprotonated with triethylamine to the homologue Emil-Fischer base which then reacted as a nucleophilic en-amine with the electrophilic vinylogue carboxylic acid ester synthon in squaric acid diethyl ester **30** which yielded in ester **33** (Figure 2.3; details on page 133) after elimination of ethanol. Next, the ester group in the ester **33** was cleaved in alkaline conditions to obtain the acid sodium salt of **34** [48] which was then acidified in aqueous solution to yield the free, water insoluble acid **34** (page 135). With the isolated acid **34** the pH could be controlled easier in the following reaction than with the sodium salt, because the latter contained a not negligible amount of inseparable sodium hydroxide. The subsequent condensation

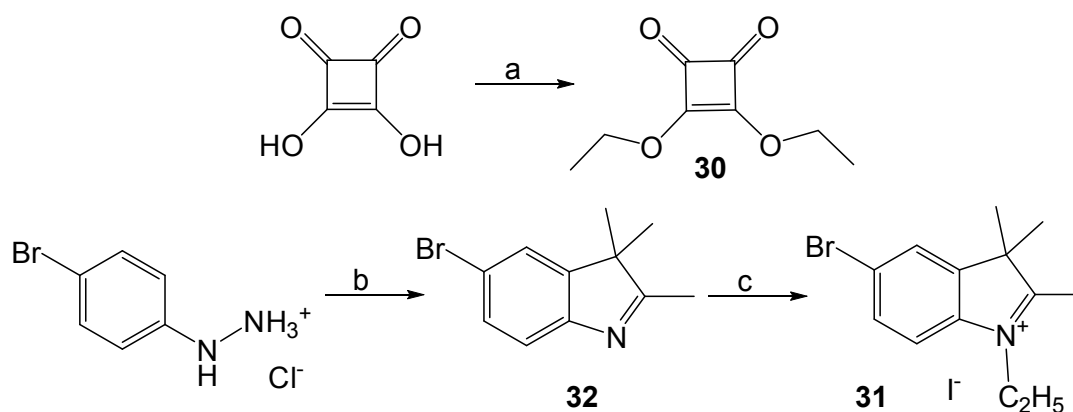


Figure 2.2: *a)* Synthesis of squaric acid diethyl ester **30** from squaric acid (page 130); *b)* synthesis of bromo indole derivative **32** from 4-bromophenylhydrazine hydrochloride (page 132); *c)* synthesis of bromo indolium compound **31** (page 131).

reaction of acid **34** with the previously produced bromo indolium derivative **31** according to literature [47, 48] yielded an unsymmetrical squaraine dye **35** (page 136). Via the

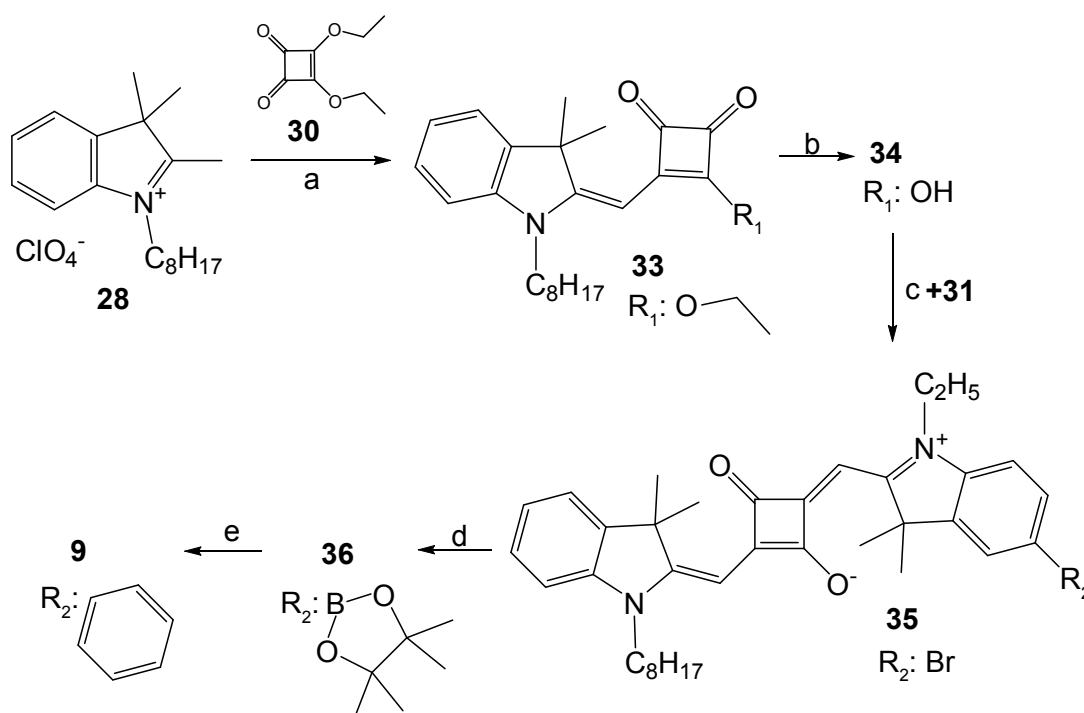


Figure 2.3: *a)* Synthesis of ester **33** from imminium perchlorate **28** and diester **30** (page 133); *b)* synthesis of acid **34** (page 135); *c)* synthesis of bromo dye **35** also by bromo indolium derivative **31** (page 136); *d)* synthesis of boron dye **36** (page 138); *e)* synthesis of unsymmetrical MSQ **9** (page 95).

Miyaura-Borylation-Reaction [51] with the protocol described by Sauter et al. [52, 53] the aryl bromide in dye **35** was transformed into a boronic acid ester to yield borone dye **36** (page 138). By following the patent protocol [52] MSQ **9** was yielded by the Suzuki coupling of boron dye **36** with bromobenzene (page 95).

The synthesis to the symmetric MSQ **10** is illustrated in figure 2.4 and started with the octylation of bromo indole derivative **32** in 1-butanol to bromo imminium iodide **37** (page 139), followed by a double Knoevenagel type condensation with squaric acid to the meltable squaraine dye **29** analogue to the method in [43] with necessary changes (page 128). Dye **29** was purified by column chromatography where an interesting major

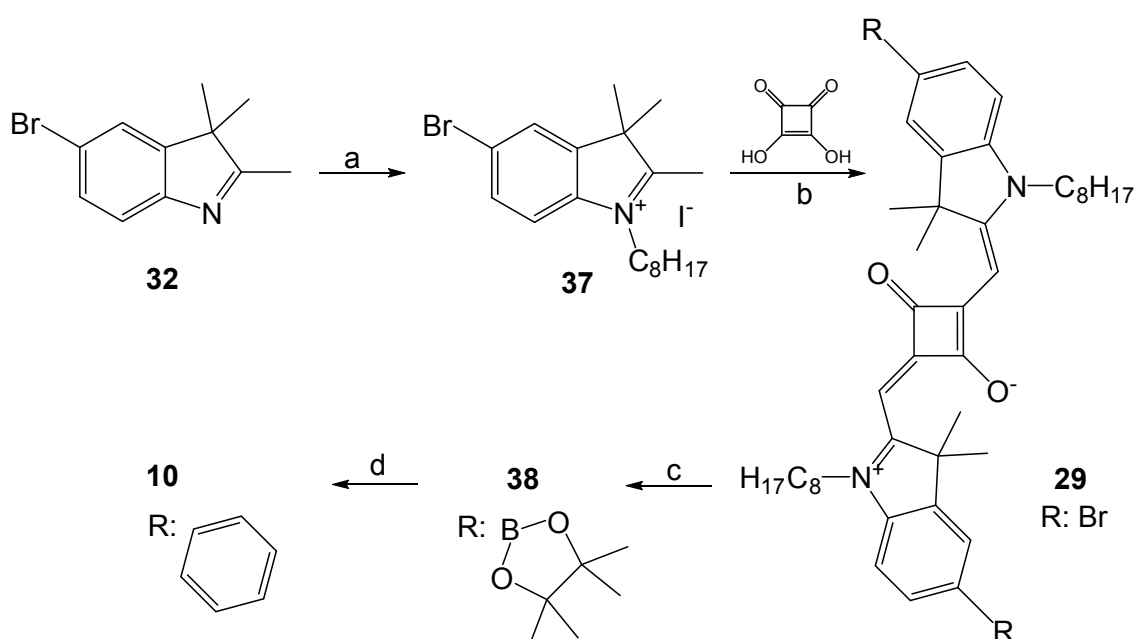


Figure 2.4: **a)** Synthesis of bromo imminium iodide **37** from bromo indole derivative **32** (page 139); **b)** synthesis of dibromo dye **29** (page 128); **c)** synthesis of diboron dye **38** (page 140); **d)** synthesis of symmetric MSQ **10** (page 96).

side product was separated (3–5% yield) which was an unsymmetric squaraine dye with a similar structure to dye **29** according to NMR analysis but with two different *N*-alkyl chains: one a *N*-octyl and the other *N*-butyl (data not shown). It is suggested that the butyl chain originated from 1-butanol in the previous octylation from an undesired side reaction. Thereby, the nitrogen atom in indole **32** attacks the electrophilic carbon of protonated 1-butanol in a $\text{S}_{\text{N}}2$ reaction which is caused by traces of water. Even the crystallization step in order to purify the alkylated indolium derivative was insufficient for

the removal of this major side product.

The next reaction step in the route towards MSQ **10** was a double Miyaura-Borylation-Reaction with dibromo dye **29** according to the prescription of Sauter et al. [52], but with an adjusted isolation method of the diboron dye **38** (page 140). The thereby produced intermediate and product react with the starting material under the applied conditions in an undesirable poly Suzuki cross coupling reaction. Therefore, a low concentration of starting material in the reaction mixture (~13 mM) and a 100% excess of bis(pinacolato)diboron was used. Thus, no dimeric or oligomeric side products were detected by UV/vis spectroscopy and NMR analysis in the isolated product. Finally, the desirable Suzuki coupling of the diboron dye **38** with bromobenzene yielded MSQ **10** ([52], details on page 96).

For the production of the unsymmetrical MSQ **11** the Terpetschnig ansatz was adapted (Figure 2.5). The two different end groups were synthesised separately. One end group was prepared by starting with an ethylation reaction of 2,3,3-trimethyl-3*H*-indole to indolium iodide **39** as reported by Pardal [42] with the following adjustments: 1-butanol was used instead of acetonitril, only 2 equivalents of ethyl iodide in respect to 3–5 equivalents were inserted and the concentration of the starting material in the reaction mixture was increased from 0.04 M to 2.3 M. All these modifications yielded one third more product in half the time (page 141). The other end group was synthesised as already published elsewhere [33]. Hereunto, 1,1,2-trimethyl-1*H*-benzo[*e*]indole was ethylated in 1-butanol to the benzo[*e*]indole derivative **40** (page 142) which was then condensed with squaric acid diethyl ester **30** in a Knoevenagel type condensation to ester **41** (page 143). Subsequent alkaline ester cleavage of ester **41** followed by acidification yielded the free acid **42** (page 145). Both end groups, indolium iodide **39** and acid **42** were then combined by another Knoevenagel condensation to yield MSQ **11** (page 98).

The double benzo extended MSQ **12** was produced in a one step synthesis from benzo[*e*]indole derivative **40** with squaric acid by a double Knoevenagel type condensation (Figure 2.6) according to Kim et al. [43]. During the optimization of the isolation method of MSQ **12** two differently coloured crystals were obtained. Copper coloured crystals appeared when MSQ **12** was recrystallized from chloroform and they were golden-green when methanol was used for the recrystallization. According to differential scanning calorimetry (DSC) and NMR analysis the former showed solvent incorporation and the latter not. Details thereof are reported in the experimental description on page 99.

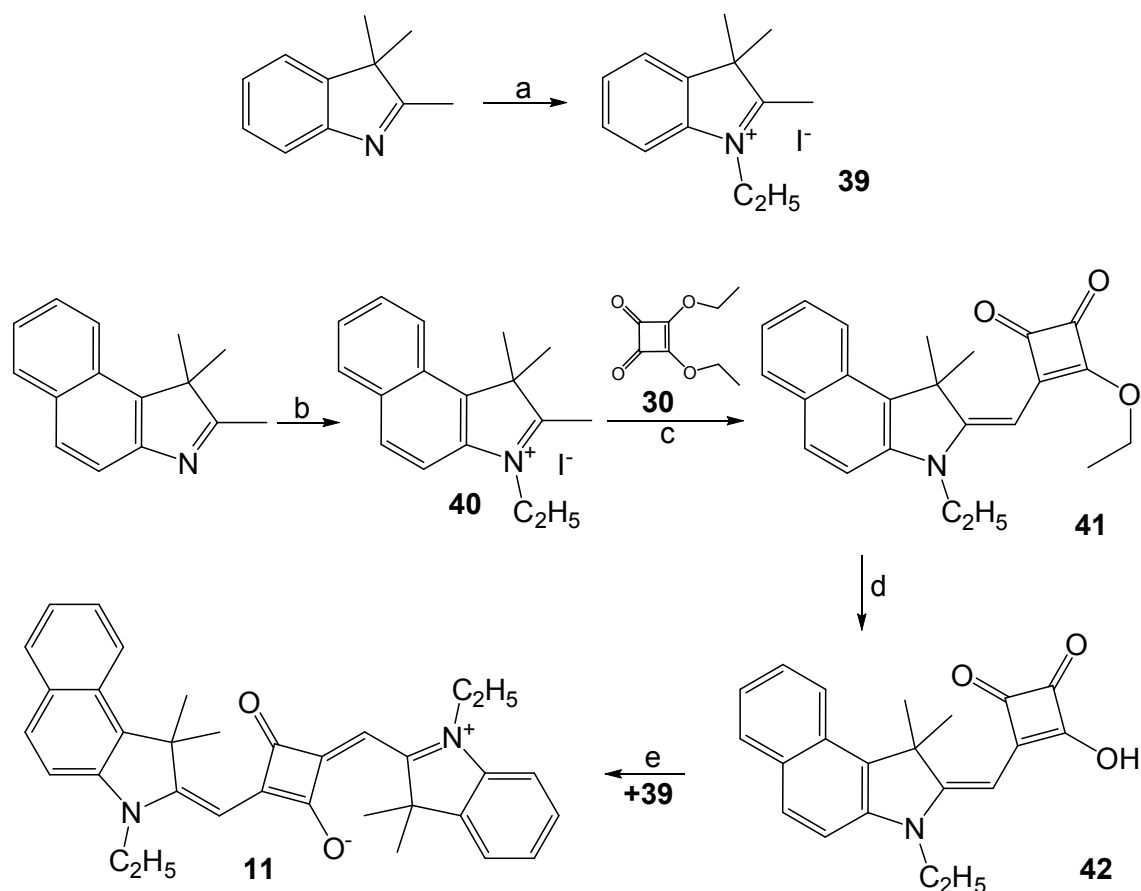


Figure 2.5: **a)** Synthesis of indolium iodide **39** from 2,3,3-trimethyl-3H-indole (page 141); **b)** synthesis of benzo[e]indole derivative **40** from 1,1,2-trimethyl-1H-benzo[e]indole (page 142); **c)** synthesis of ester **41** also with diester **30** (page 143); **d)** synthesis of acid **42** (page 145); **e)** synthesis of unsymmetric MSQ **11** also with indolium iodide **39** (page 98).

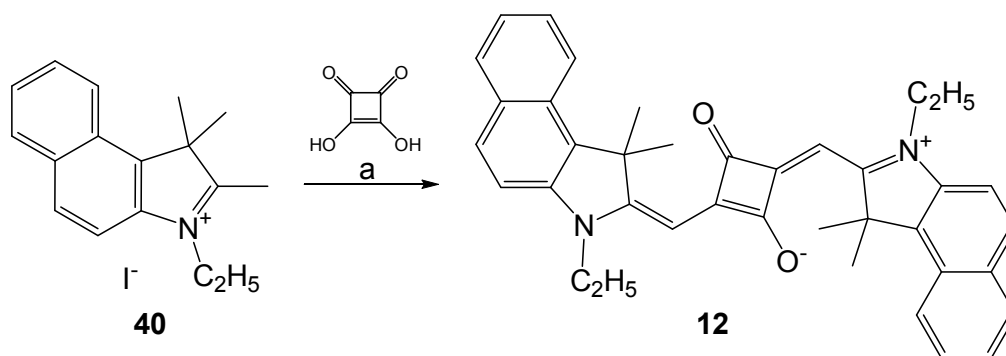


Figure 2.6: **a)** Synthesis of symmetric MSQ **12** (page 99).

2.1.2 Synthesis of squaraines with two dye units

The retrosynthetic analysis of bis squaraine dyes (BSQ's) followed an enhanced method from the Terpetschnig ansatz. Thereby, any BSQ was split into two squaraine containing synthetic equivalents like the previously described acid **42** (Figure 2.5) and the bridge with two alkylated 3*H*-indolium synthons. To improve the solubility of the BSQ's their benzo[*e*]indole end group was alkylated with an octyl chain. Therefore, the homologue acid **43** (Figure 2.7) from the published one **42** [32, 33] was prepared as follows: First,

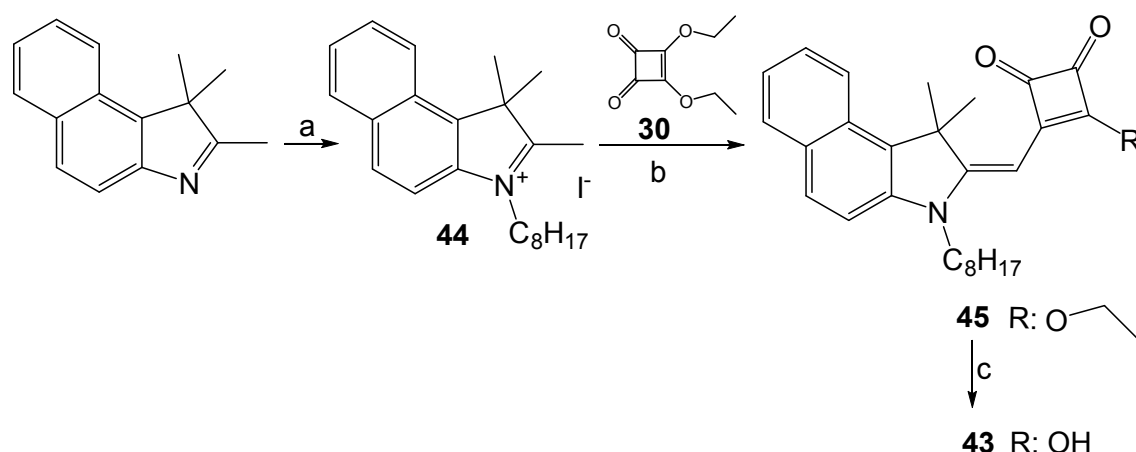


Figure 2.7: **a**) Synthesis of imminium ion **44** from 1,1,2-trimethyl-1*H*-benzo[*e*]indole (page 147); **b**) synthesis of ester **45** (page 148); **c**) synthesis of acid **43** (page 146).

1,1,2-trimethyl-1*H*-benzo[*e*]indole was octylated in 1-butanol to imminium ion **44** (page 147). Second, Knoevenagel condensation of imminium ion **44** with squaric acid diethyl ester **30** to ester **45** (page 148). Ester **45** was purified by column chromatography to separate the side product with the *N*-butyl synthon before it was incorporated into the dye. Finally, basic ester cleavage of compound **45** with subsequent aqueous acidification yielded acid **43** (page 146). This acid was used in most of the BSQ productions.

The synthesis path of phenyl bridged BSQ **13** is displayed in figure 2.8. The first step, a double Suzuki coupling with bromo indole derivative **32** and benzene-1,4-diboronic acid catalysed by tetrakis(triphenylphosphin)palladium(0) yielded bis-indole

derivative **46** (page 149). Followed by a double methylation reaction of this bis-indole derivative **46** with methyl *p*-toluenesulfonate the bis-imminium ion **47** (page 151) was obtained. Finally, two acids **43** were condensed to the bridging synthetic equivalent **47** in a Knoevenagel type condensation which resulted in the phenyl linked BSQ **13** (page 102). In this last reaction procedure, the first condensation was very fast and proceeded as expected whereas the second was very slow. It is suggested that some volatile acid condensed with water in the Dean-Stark trap which changed the pH value of the reaction mixture during the reaction. For the product isolation, quinoline had to be removed because it would disturb the phase separation in the extraction, reduce the separation ability of the column and hinder the crystallization. Therefore, a precipitation in aqueous citric acid was selected to remove the quinoline. A further task was to increase the critical solubility of the BSQs by replacing the two *N*-methyl groups at the bridge with longer alkyl chains. Accordingly, the bis alkylation was performed with butyl iodide and octyl iodide, respectively, in chloroform, dimethylsulfoxide or in substance, but no corresponding bis alkylated product was obtained. So the longer alkyl chains were introduced in the previous reaction step of the synthetic pathway. Thus, an alkylated bromo indole derivative like **37** was used in the Suzuki-Reaktion with benzene-1,4-diboronic acid. Different catalysts ($\text{Pd}(\text{PPh}_3)_4$ and $\text{Pd}[\text{P}(p\text{-tol})_3]_3$) and bases (NaHCO_3 and K_2CO_3) were tested, but without success. This can be explained as follows: After oxidative addition of the palladium(0) species at the aryl bromide, charge repulsion occurs with the positive imminium ion which might hinder the catalytic cycle. When a stronger base was used the imminium ion was deprotonated to the Emil-Fischer base derivative. Thus the palladium(0) species preferred to coordinate to the en-amine in lieu of starting the catalytic cycle by an oxidative addition.

The synthesis of the next target molecule, the fluorenylene bridged BSQ **15** started from commercial available 2,7-dibromo-9,9-bis-(2-ethyl-hexyl)-9*H*-fluorene. However for the Suzuki coupling a boronic acid derivative was needed. For this reason, the bromo indole derivative **32** was derivatized by a Miyaura-Borylation-Reaction according to the patent description [52] to the boron indole intermediate **48** with a 81% yield after column chromatography and sublimation (Figure 2.9, prescription on p. 152). The said boron compound **48** and 2,7-dibromo-9,9-bis-(2-ethyl-hexyl)-9*H*-fluorene reacted in a double Suzuki coupling to the fluorene bridged bis indole derivative **49** (page 153) which was then double methylated by methyl *p*-toluenesulfonate to the fluorenylene bridged bis indolium **50** (page 155). The condensation of the end group acid **43** to the fluorenylene bridged bis indolium **50** was not performed with quinoline as the previous ones because

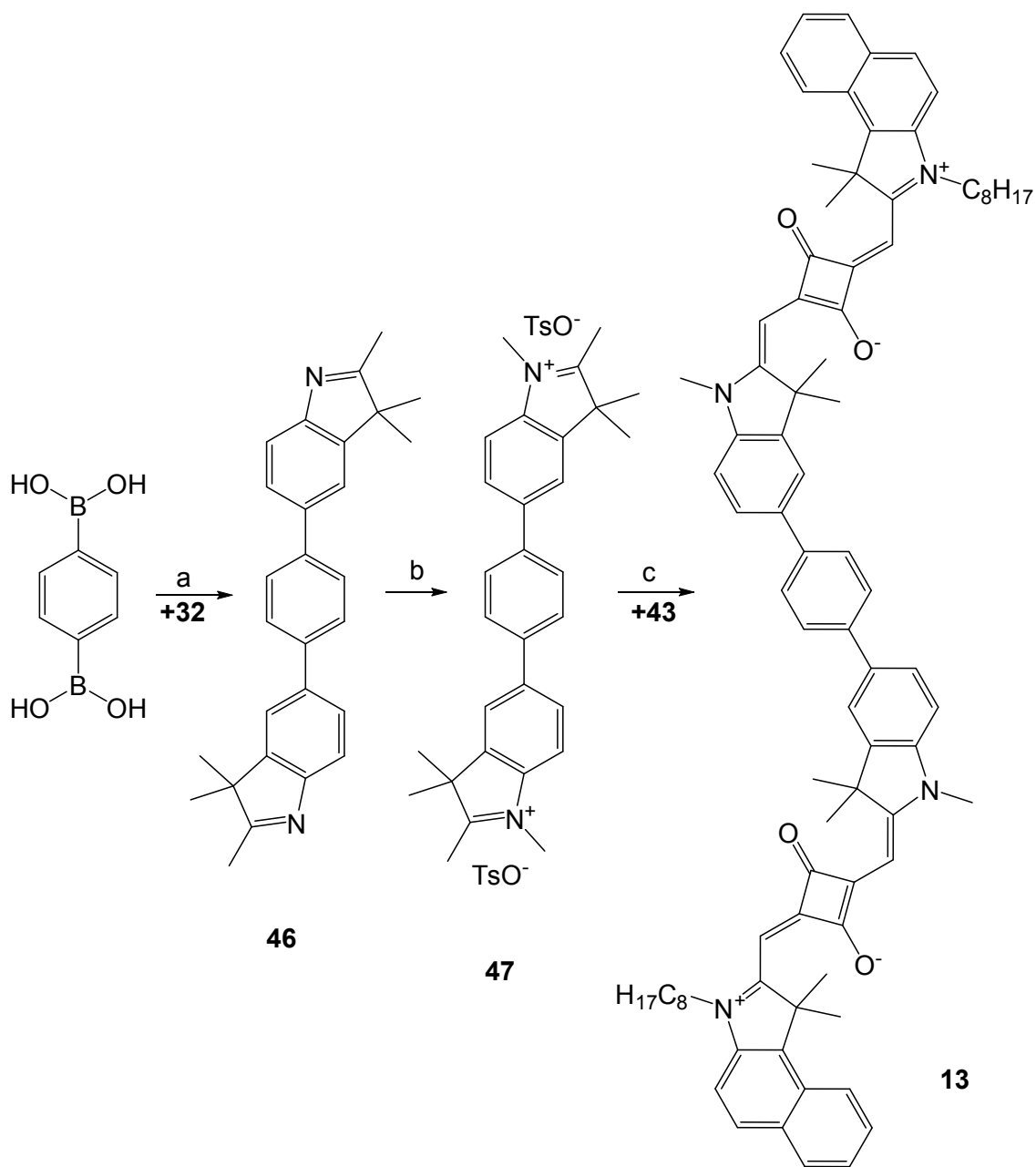


Figure 2.8: a) Synthesis of bis-indole derivative **46** from benzene-1,4-diboronic acid and bromo indole derivative **32** (page 149); b) synthesis of bis-imminium ion **47** (page 151); c) synthesis of phenyl linked BSQ **13** (page 102).

of the above mentioned problems in the isolation of the product. For solubility reasons, 1-methyl-2-pyrrolidinone was added to the solvent mixture of toluene and 1-butanol. With these conditions BSQ **15** was yielded in 82% after two days (page 106).

In order to synthesize BSQ **19** which has an electron rich center, the bis-iso-

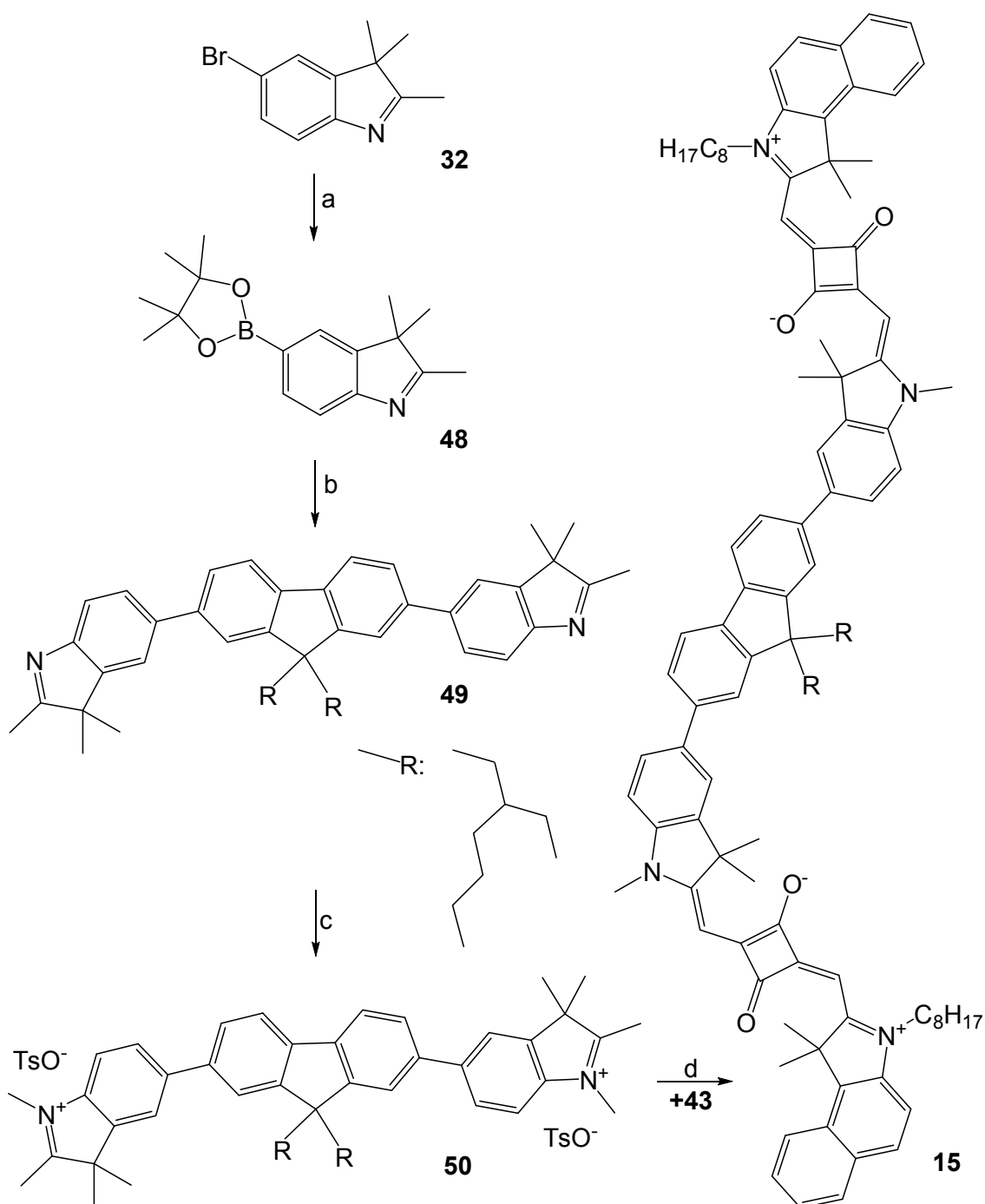


Figure 2.9: a) Synthesis of boron indole derivative **48** from bromo indole derivative **32** (page 152); b) synthesis of fluorenylene bridged bis indole **49** from boron indole derivative **48** and 2,7-dibromo-9,9-bis-(2-ethyl-hexyl)-9H-fluorene (page 153); c) synthesis of fluorenylene bridged bis indolium **50** (page 155); d) synthesis of fluorenylene bridged MSQ **15** (page 106).

octyloxy bridge had to be prepared in advance. The whole synthetic pathway is illustrated in figure 2.10. Thus, hydroquinone was transformed in a Williamson-Ether synthesis as reported by Aubert et al. [54] into diether **51** (page 156). Subsequently, electrophilic aromatic substitution of diether **51** with *N*-bromosuccinimide yielded the dibromo derivative **52** [54] (page 157). A double Suzuki coupling of dibromo derivative **52** with boron indole derivative **48** followed which resulted in bis-indole derivative **53**; performed according to Sauter et al. [52] with some necessary modifications (page 158). Double methylation of this bis-*iso*-octyloxy bridged bis-indole derivative **53** with methyl *p*-toluenesulfonate followed by anion exchange from the tosylates to the perchlorates, yielded bis-indolium ion **54** (page 160). This exchange was a purification step but it also made the product thermo sensitive. Bis-indolium ion **54** as perchlorate decomposes spontaneously at 286 °C! The final step to BSQ **19** was via the Knoevenagel condensation and was performed similarly to the one for BSQ **15**. However, this reaction paused after the first condensation of end group acid **43** to the bis-indolium ion **54**. This was because the pH changed during the reaction which will be explained later. After adjusting the pH with a small amount of aqueous hydrochloric acid the reaction continued as expected and yielded BSQ **19** (page 113).

BSQ **20** with the tetra fluorinated bridge (Figure 2.11) was prepared in a similar way as the previous one, whereas the preparation of the center part was not as complicated. The boron compound **48** was reacted with commercially available 1,4-dibromotetrafluorobenzene under Suzuki coupling conditions following the description in the patent [52] to the bis indole derivative **55** (page 161). After the double methylation of bis indole derivative **55** with methyl *p*-toluenesulfonate the anion was exchanged to perchlorate for purification reasons to result in the center unit **56** which was also thermolabile. In the final reaction of this synthetic path (Figure 2.11), the center unit **56** was condensed to the two end groups **43** in a Knoevenagel type condensation using toluene, 1-butanol and 1-methyl-2-pyrrolidinone as solvents. As observed in the analogue reaction to BSQ **19**, also this reaction paused after the first condensation step, due to a change in the pH. After adjusting the pH with aqueous hydrochloric acid, the reaction continued and BSQ **20** was formed. The correct pH value is crucial for the Knoevenagel-Reaction because it is an acid *and* base catalysed reaction. In the general accepted reaction mechanism [55] the catalytic base deprotonates the "*C-H*"-acid compound to generate a *C*-nucleophile. Here, the positive charged indolium ion was deprotonated to the nucleophilic en-amine. The catalytic acid increases the electrophilic character of the vinylogue carboxylic acid synthon. In this particular case,

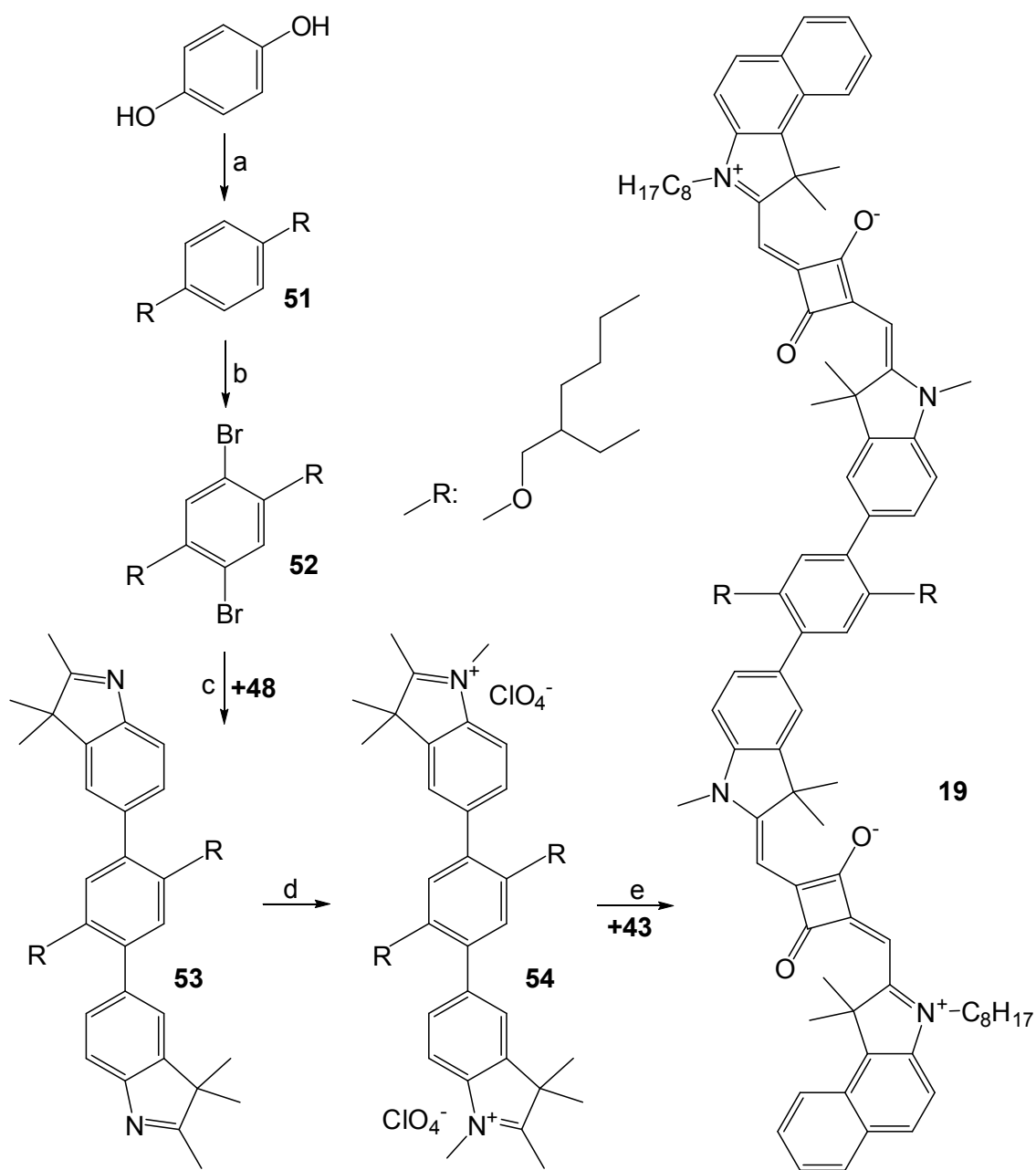


Figure 2.10: **a)** Synthesis of diether **51** from hydroquinone (page 156); **b)** synthesis of dibromo derivative **52** (page 157); **c)** synthesis of bis-indole derivative **53** also with boron compound **48** (page 158); **d)** synthesis of bis-iso-octyloxy bridged bis-indolium ion **54** (page 160); **e)** synthesis of MSQ **19** (page 113).

it protonated the squaric acid unit of the end group **43**. Furthermore, acid is important for the elimination of water which is the "psydo"-irreversible step in the Knoevenagel condensation mechanism because the water is removed from the reaction mixture

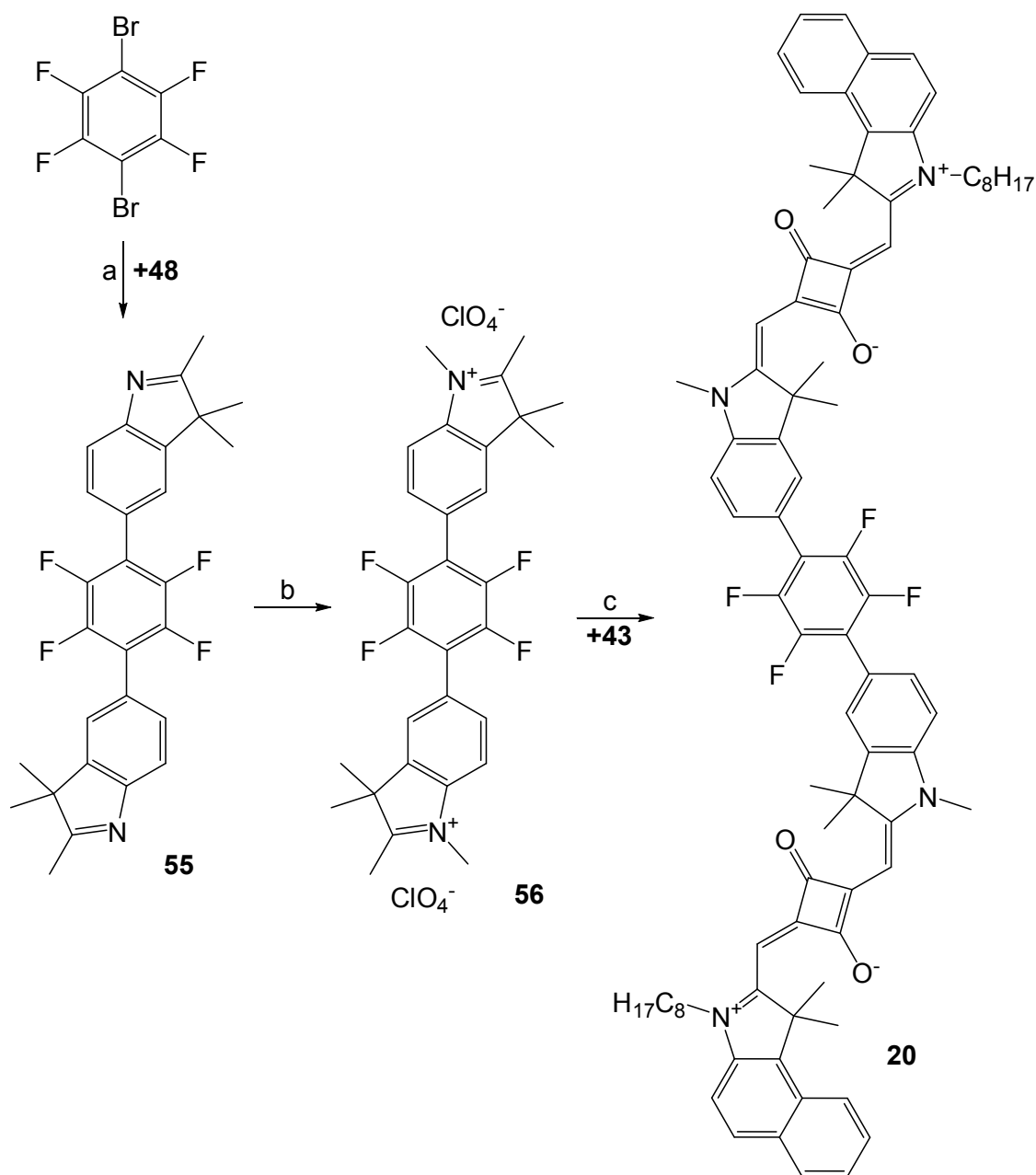


Figure 2.11: **a)** Synthesis of bis indole derivative **55** from 1,4-dibromotetrafluorobenzene and boron compound **48** (page 161); **b)** synthesis of center unit **56** (page 162); **c)** synthesis of tetra fluoro phenylene bridged BSQ **20** (page 115).

by azeotropic distillation into the Dean-Stark trap. So a buffering system consisting of a weak base and its corresponding acid is the preferable catalyst for this reaction. These additional requirements are needed for the base: non nucleophilic character, soluble in the used organic solvent, stable during the reaction and less volatile than

water. Quinoline fulfills these parameters and so it is normally used in the Knoevenagel condensation, however it causes problems in the isolation and purification of the product. Therefore, the last three reactions were performed without this base which lead to the prior described uncontrollable pH during the reaction. Nevertheless, it was decided to use quinoline as catalyst since the advantages overruled the disadvantages. The big disadvantage is that quinoline has to be removed in a laborious and messy way – precipitation of the reaction concentrate in aqueous citric acid – before the "real" isolation of the product could start. In all following condensations quinoline was chosen as catalyst.

The planar naphthalene bridged BSQ **14** (Figure 2.12) was prepared according to the reported conditions of Kim et al. [43] in a double Knoevenagel type condensation of the benzo[e]indole end group **43** (Figure 2.7) with the naphthalene bridge **57** which was obtained by Geiger et al. [32] (page 104). After reaction, quinoline was removed by an acidic precipitation in water and the excess of end group derivative **43** was washed out with water after alkali treatment. BSQ **14** was purified by column chromatography. Fortunately, the intermediate mono condensation product MSQ **58** was thereby also isolated in one of the earlier fractions, which was used in the preparation of the tris squaraine (TSQ) **26** (Figure 2.20, details on page 123).

In the series of the flat bridged squaraines with two chromophore units BSQ **16** had an anthracene derivative as its linker. The bis indolium synthetic equivalent of the said bridge had to be synthesized *ab ovo*. The synthetic strategy as illustrated in figure 2.13 followed the path suggested by Geiger et al. [23] for the preparation of the naphthalene bridge **57**. Because anthracene derivatives are generally light sensitive, the entire preparation of BSQ **16** was performed under exclusion of light. Since 1,5-diaminoanthracene (**59**) was not commercially available it was produced by a modified Clemmensen-Reduction from 1,5-diaminoanthraquinone following the general description of Martin [56] with a changed isolation and purification procedure (page 163). The amino groups in diamine **59** were derivatisated to an intermediate with two diazonium groups which were directly reduced *in situ* with tin(II)chloride to hydrazine functional groups yielding the compound bis hydrazine **60**. For the success of the reaction the controlling of the temperature was essential (page 165). The subsequent Fischer-Indole-Synthesis was performed stepwise. Bis hydrazone **61** was produced from bis hydrazine **60** and 3-methyl-2-butanone (page 166), which was directly used in the final Fischer-Indole synthesis reaction step. The thereby obtained bis indole derivative **62** (page 167) was methylated by methyl *p*-toluenesulfonate and subsequent

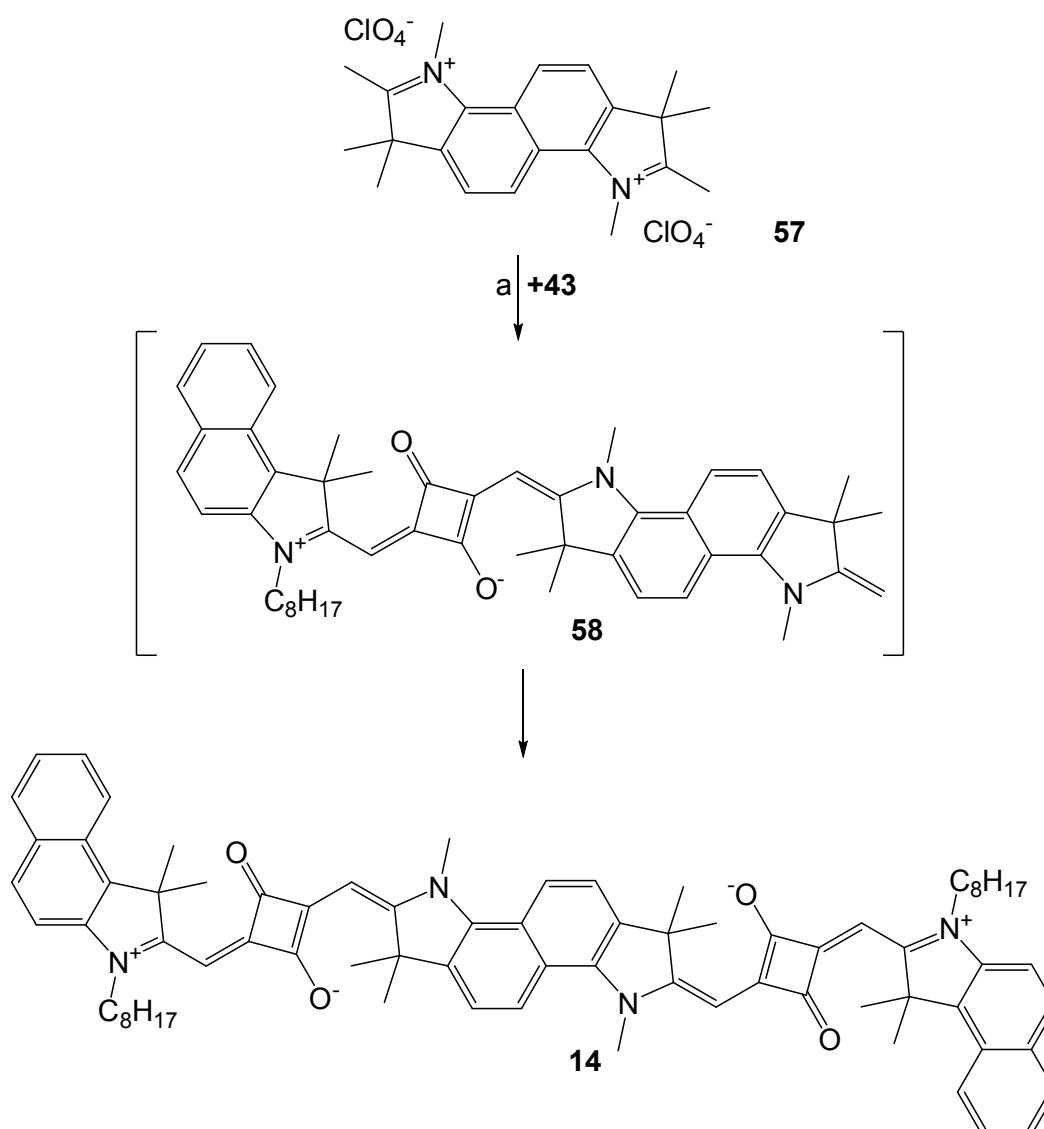


Figure 2.12: a) Synthesis of intermediate MSQ **58** and BSQ **14** from naphthalene bridge **57** and acid **43** (page 104).

anion exchange from tosylate to perchlorate yielded the anthracene linker **63** which was purified by elutriation with boiling water (page 168). BSQ **16** was finally obtained by a Knoevenagel condensation of the end group acid **43** and the anthracene linker **63** (page 107).

The second BSQ with a naphthalene bridge, BSQ **17** was synthesized as shown in figure 2.14. So the indole acid **34** (in figure 2.3) was condensed to the naphthalene bridge **57**, which was obtained by Geiger et al. [32] in a similar way as it was described for BSQ **14**. The washing of the precipitation after the quinoline removal increased the

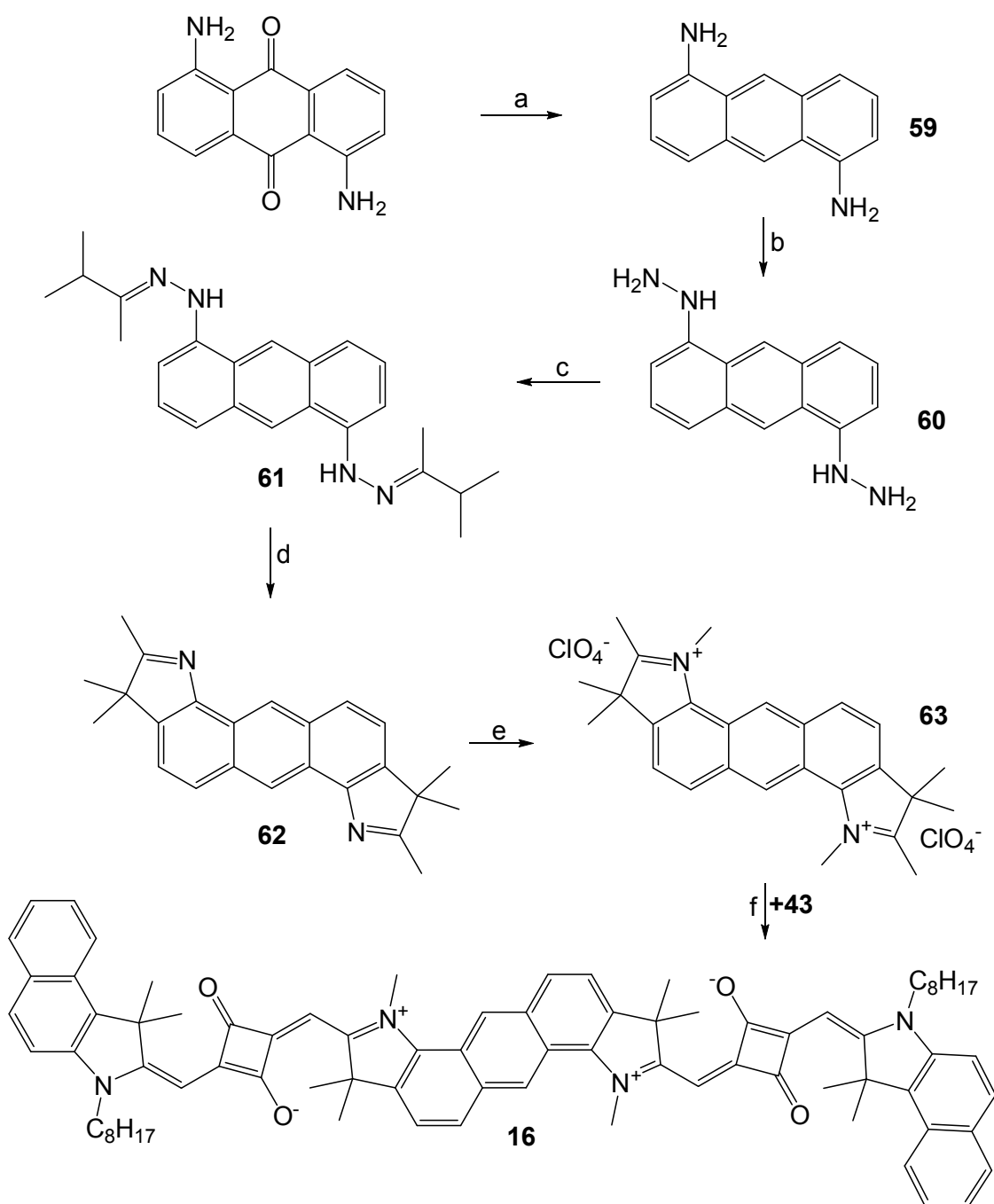


Figure 2.13: **a)** Synthesis of 1,5-diaminoanthracene **59** from 1,5-diaminoanthraquinone (page 163); **b)** synthesis of bis hydrazine **60** (page 165); **c)** synthesis of bis hydrazone **61** (page 166); **d)** synthesis of bis indole derivative **62** (page 167); **e)** synthesis of anthracene linker **63** (page 168); **f)** synthesis of anthracene bridged BSQ **16** also with acid **43** (page 107).

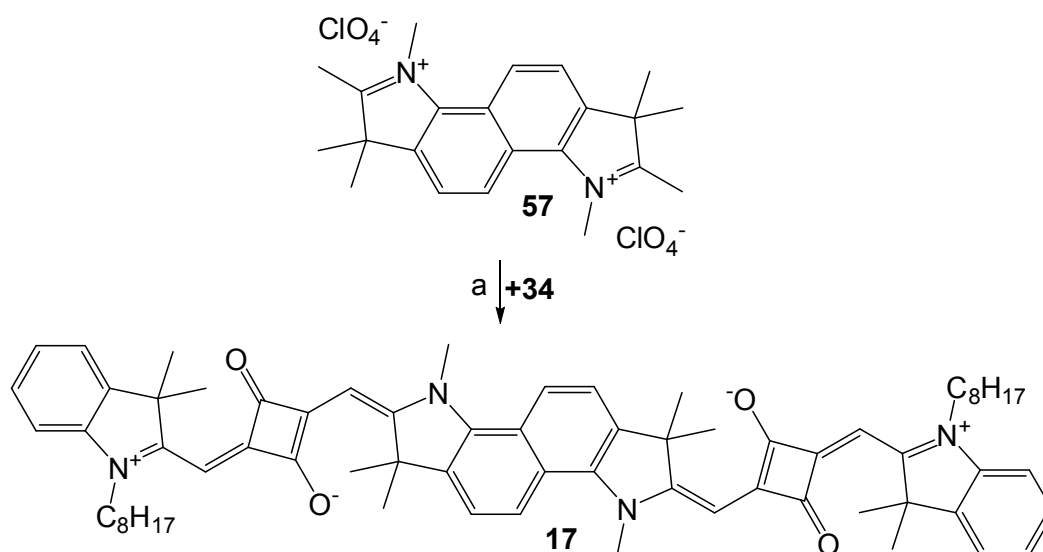


Figure 2.14: a) Synthesis of BSQ **17** from naphthalene bridge **57** and acid **34** (page 109).

separation performance on the silica column which led to the improved yield (page 109).

For the investigation of the coupling of two slightly different dye units, the third BSQ dye with a naphthalene bridge **18** was created which had two different end groups as reported elsewhere [33]. One was a benzo[*e*]indole derivative where acid **42** was used as synthetic equivalent. And for the other one, an indole derivative with a carboxylic acid function (diacid **64**) was prepared. The synthetic strategy to obtain BSQ **18** followed the path of the Terpetschnig route to prepare the carboxylic acid functionalized end group (Figure 2.15) and then the stepwise condensation of the two different end groups to the linker (Figure 2.16). The synthetic path started with the octylation reaction of 2,3,3-trimethyl-3*H*-indole-5-carboxylic acid according to literature [31] with some essential modifications in the isolation procedure to yield carboxy indole derivative **65** (page 170). Subsequently, squaric acid diethyl ester **30** was condensed to carboxy indole derivative **65** to yield ester **66** (page 171). Alkaline ester cleavage of ester **66** followed by acidification yielded diacid **64** (Figure 2.15; details on page 169). The key step in the synthesis of unsymmetric BSQ **18** was the condensation of a single end group synthetic equivalent (acid **42**) to the naphthalene linker of derivative **57**. Although it was found that the reaction pauses after the first condensation when no quinoline was used in the preparation of BSQ **19** and **20**, it could not be adapted to the naphthalene bridge **57**. Furthermore, any trials using the barely soluble **57** directly resulted in very low (~5%)

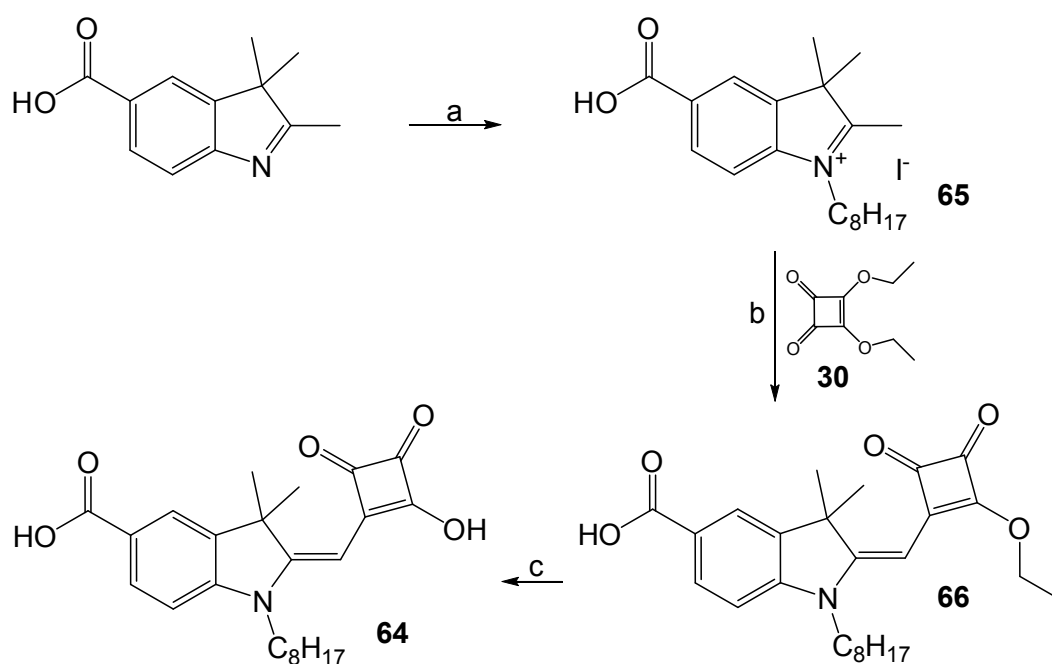


Figure 2.15: **a)** Synthesis of carboxy indole derivative **65** from 2,3,3-trimethyl-3H-indole-5-carboxylic acid (page 170); **b)** synthesis of ester **66** also with squaric acid diethyl ester **30** (page 171); **c)** synthesis of diacid **64** (page 169).

yields of **68**, because the basicity of quinoline is too low to deprotonate both imminium ions in the linker **57**. Thereunto the naphthalene derivative **57** was deprotonated in a two layer mixture of toluene and aqueous sodium hydroxide solution (40%). The resulting highly reactive, well soluble bis enamine intermediate **67** reacted with one acid **42** in a kinetically controlled Knoevenagel type condensation to MSQ **68** (Figure 2.16; details on page 172). Finally, the diacid end group **64** was condensed to MSQ **68** to yield the unsymmetric BSQ **18** (page 110).

The last target molecule with two squaraine dye units, BSQ **27**, had a flat linker. The bridge was not an indole derivative with a five membered heterocycle, but a six membered aromatic ring system. The two six membered heterocycles were part of a 1,5-diaza-anthracene system, which was chosen because the starting materials were commercially available and the synthetic rout towards BSQ **27** (Figure 4.2) was straight forward. First, the flat bridge was produced starting with a double Doebner-Miller-Reaction, a variation of the Skraup-Quinoline-Synthesis, of 1,4-benzene diamine with crotonaldehyde to yield 2,6-dimethyl-1,5-diaza-anthracene **69** (page 173). This intermediate was subsequently bis methylated by methyl *p*-toluenesulfonate and yielded bridging synthetic equivalent **70** after anion exchange from tosylate

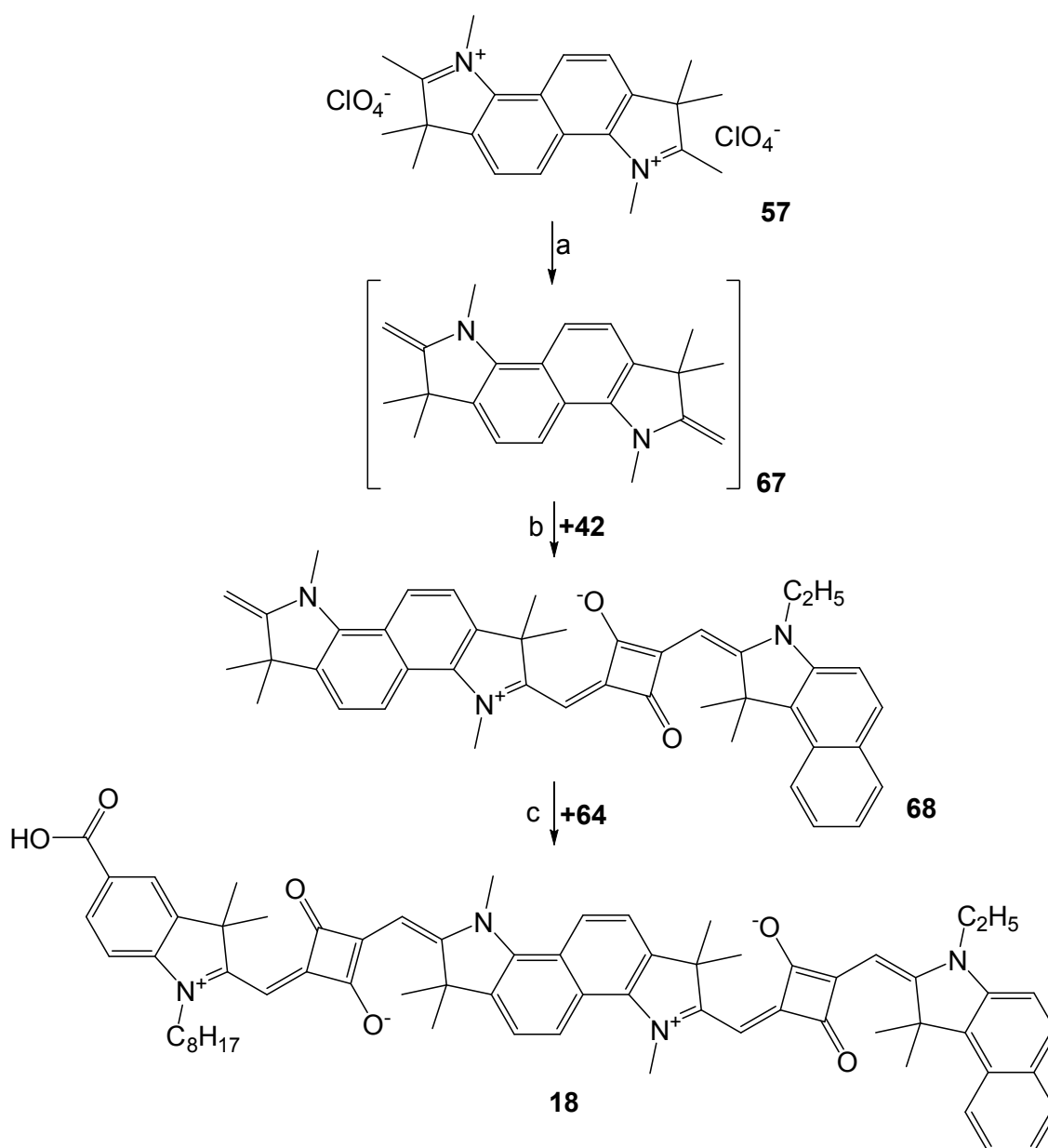


Figure 2.16: a) Synthesis without isolation of bis enamine intermediate **67** from naphthalene linker derivative **57** (page 172); b) synthesis of MSQ **68** also with acid **42** (page 172); c) synthesis of unsymmetric BSQ **18** also with diacid **64** (page 110).

to perchlorate (page 174). This double methylation took longer than any other bis-methylation so far. The first nitrogen atom was methylated within hours but the second one took two and a half days. Presumably the generated positive charge on the nitrogen atom after the first methylation step reduced the nucleophilic character of the second nitrogen atom in the fully conjugated aromatic system. The rate of the second

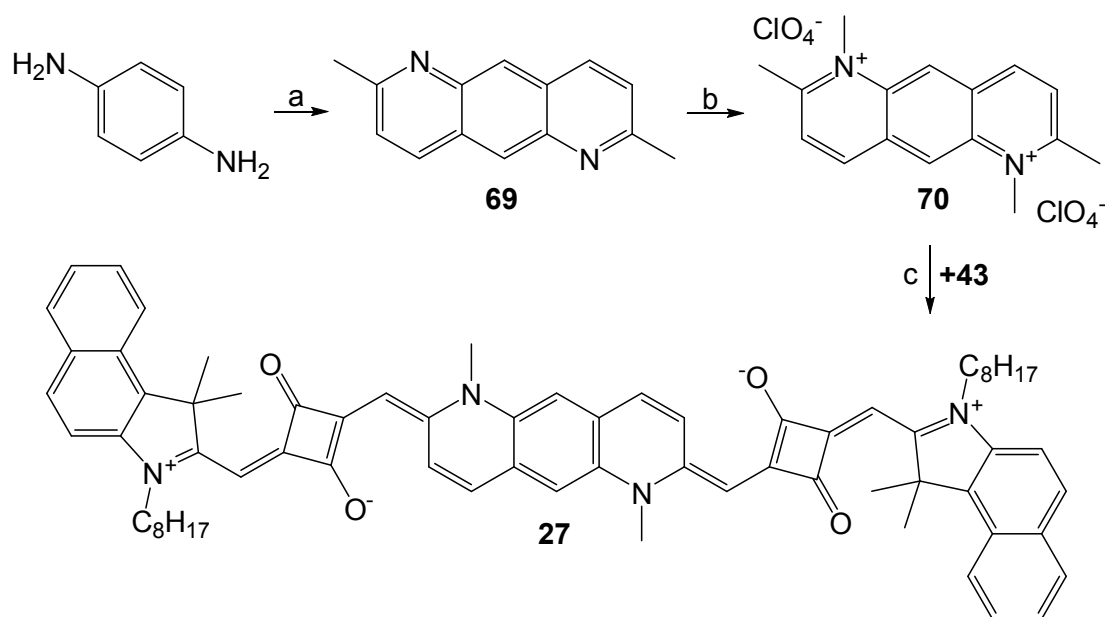


Figure 2.17: **a)** Synthesis of 2,6-dimethyl-1,5-diaza-anthracene **69** from 1,4-benzene diamine and crotonaldehyde (page 173); **b)** synthesis of the bridging synthetic equivalent **70** (page 174); **c)** synthesis of super flat bridged BSQ **27** also with acid **43** (page 125).

methylation was estimated to be about 100 times slower than the first one. Finally, BSQ **27** was obtained by a doubled Knoevenagel type condensation of two end group synthetic equivalents in the form of acid **43** to the bridging moiety **70** using the reported method [43] with the isolation method developed in this work (page 125).

2.1.3 Synthesis of squaraines with more than two dye units

Oligomeric dyes were prepared in order to determine the possible limitation of the optical properties as it was correlated by Meier for the $D-\pi-A$ dyes [12]. The synthetic ansatz for the preparation of the four phenylene derivative bridged (dye **21**, dye **22**, dye **23** and dye **24**) and the direct linked oligomeric dyes (dye **25**) was an AA/BB type poly Suzuki cross coupling reaction. For the synthesis of the phenylene bridged oligomeric squaraine **21** (Figure 2.18) diboronic acid ester **37** was prepared from benzene-1,4-diboronic acid (page 139) according to Kandre et al. [57]. Also their reaction conditions for the poly Suzuki coupling were adopted [57]. So dibromo MSQ **29**, diboronic acid ester **37** and catalyst **71** were mixed in a mixture of tetrahydrofuran and 1-methyl-2-

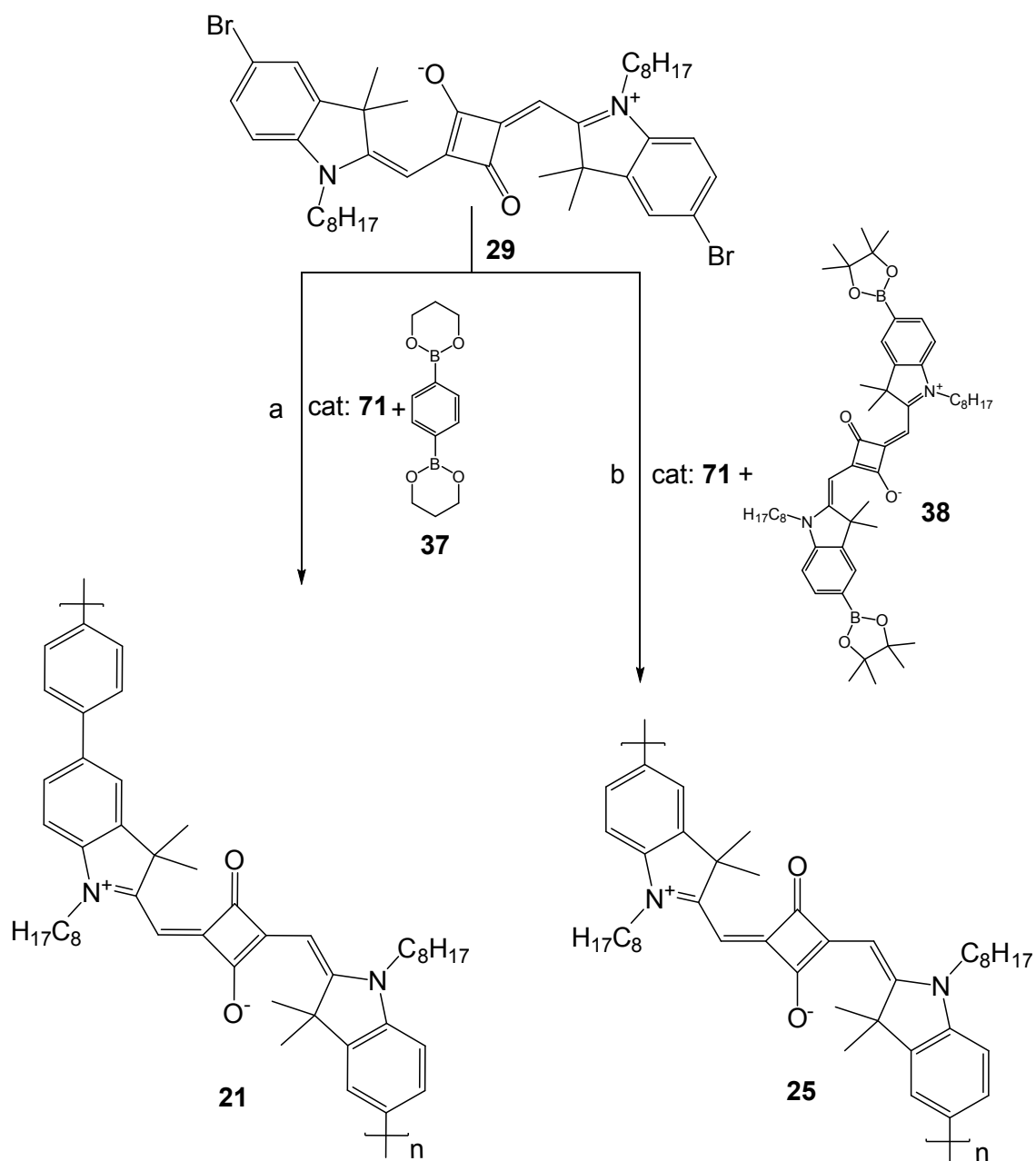


Figure 2.18: **a**) Synthesis of phenylene bridged TSQ **21** from dibromo dye **29**, diboronic acid ester **37** and catalyst **71** (page 116); **b**) synthesis of TSQ **25** from dibromo dye **29**, diboron dye **38** and catalyst **71** (page 122).

pyrrolidinone (page 116). The latter solvent was added to increase the solubility of the starting materials as well as the products. Unfortunately, chloroform could not be used as solvent during the reaction due to its intolerance with the used catalyst [58]. Although the solvent mixture was optimised oligomeric material precipitated during the reaction.

Therefore, a product precipitation was performed in the isolation procedure. According to the UV/vis analysis the λ_{max}^{abs} value of the filtrate quite well matched with the one of the corresponding BSQ **13**. But λ_{max} of a dissolved aliquot of the filtration residue was more bathochromically shifted which indicated that this precipitation method separated some of the lower molecular weight materials. The averaged number of repeating units \bar{X}_n in the filtration residue of the oligomeric materials was determined by three methods: $\bar{X}_n^{Carother}$ by the Carother's equation (eq. 4.1, page 90), $\bar{X}_n^{MALDI-TOF}$ by the medial allegation of the MALDI-TOF measurement (eq. 4.2, page 90) and \bar{X}_n^{NMR} by the end group determination by NMR (eq. 4.3, page 90). \bar{X}_n for product **21** was determined by Carother's and by MALDI-TOF to be three and by NMR to be five to six (table 2.1). Dyes **22**, **23**, **24**, **25** were prepared according to the production method of dye **21**. Their averaged number of repeating units were also calculated and summarized in table 2.1. Since all these products showed \bar{X}_n values which are typical for trimeric to tetrameric squaraines, they were abbreviated as TSQs. TSQ **22**, the one with the fluorenylene bridge, was synthesized from diboron dye **38**, specially purified 2,7-dibromo-9,9-bis-(2-ethyl-hexyl)-9H-fluorene and freshly prepared catalyst **71** following the developed route of TSQ **21** (Figure 2.19, details on page 118). Although TSQ **22** had additional long and branched side chains, the degree of polymerization was not noticeably different from the one of TSQ **21**. Thus, even two *iso*-octyl side chains were too small for these rod like, flat molecules.

Also TSQ **23** had two *iso*-octyl side chains but connected to the linker as two ethers. TSQ **23** was synthesized as the previous TSQ **21** starting with diboron dye **38**, the already prepared 1,4-dibromo-2,5-bis(2-ethylhexyloxy)benzene (**52**) and catalyst **71** (Figure 2.19, details on page 119).

Also starting from diboron dye **38** the tetrafluoro phenylene bridged TSQ **24** was prepared. Additionally, freshly sublimed 1,4-dibromotetrafluorobenzene and freshly

Entry	$\bar{X}_n^{Carother}$	$\bar{X}_n^{MALDI-TOF}$	\bar{X}_n^{NMR}
TSQ 21	3	3	5
TSQ 22	3	3	4–5
TSQ 23	2	4	4–6
TSQ 24	2	3	n.d.
TSQ 25	3	3	5–6

Table 2.1: Comparison of the averaged number of repeating units (\bar{X}_n) determined by the Carothers equation, the medial allegation of the MALDI-TOF measurement and the end group determination by NMR.

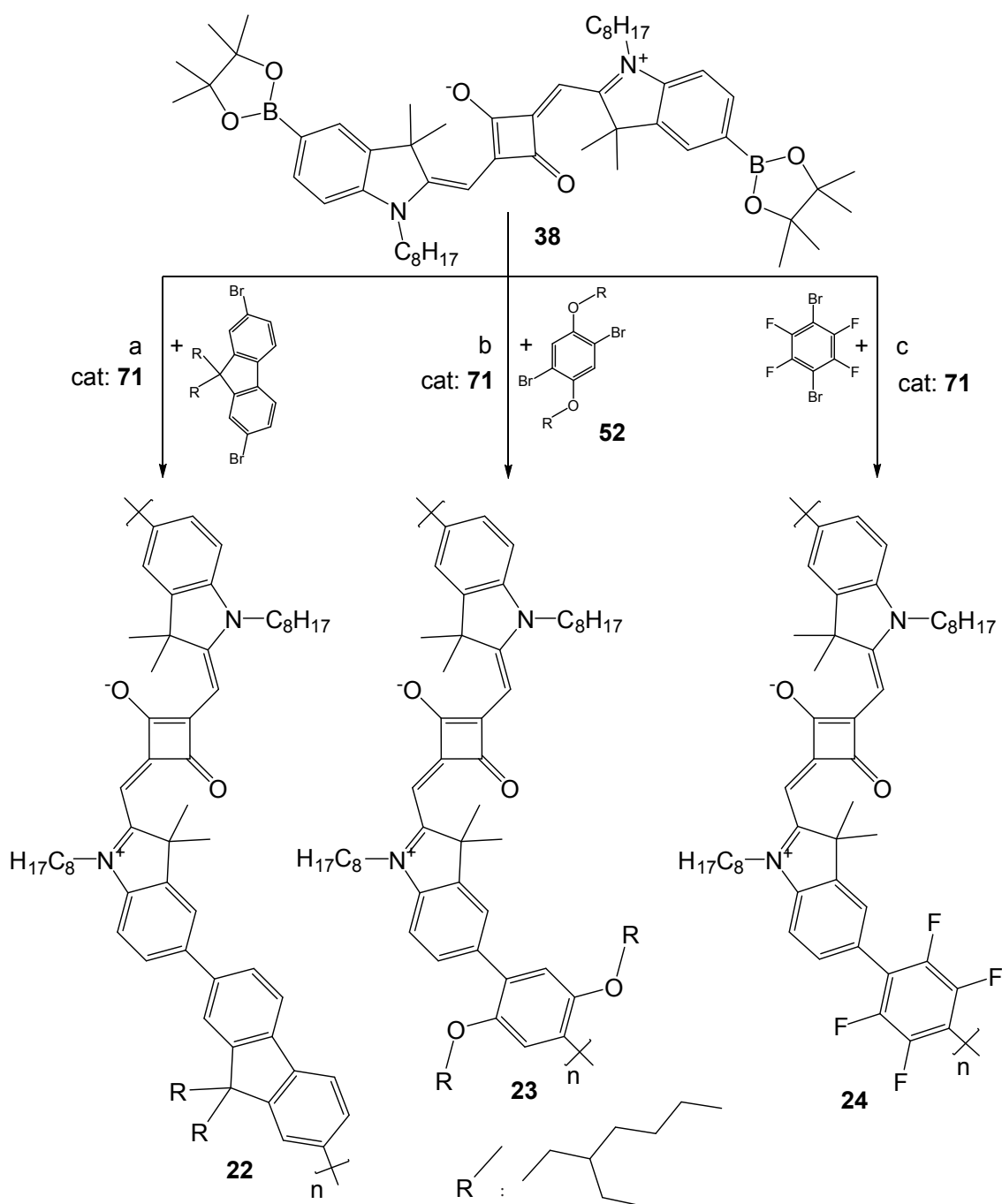


Figure 2.19: **a**) Synthesis of fluorenylene bridged TSQ **22** from diboron dye **38**, 2,7-dibromo-9,9-bis-(2-ethyl-hexyl)-9H-fluorene and catalyst **71** (page 118); **b**) synthesis of bis iso-octyloxy phenylene bridged TSQ **23** from diboron dye **38**, 1,4-dibromo-2,5-bis-(2-ethylhexyloxy)benzene **52** and catalyst **71** (page 119); **c**) synthesis of tetrafluoro phenylene linked TSQ **24** from diboron dye **38**, 1,4-dibromotetrafluorobenzene and catalyst **71** (page 119).

prepared catalyst **71** were added following the here developed standard procedure (page 121). But several problems appeared, especially in the analysis of TSQ **24**. Not only did it have the lowest yield of all TSQ productions, but also the MALDI-TOF was very noisy and the end groups could not be resolved by NMR. These observations led to the assumption, that some not negligible side reaction occurred. Although the *C-F* bond is known for its chemical stability, unfortunately, perfluorinated aromatic systems can undergo nucleophilic substitution under the applied conditions according to Sandford et al. [59]. This suggests that the palladium(0) species did not only react as nucleophile with the *C-Br* bond in 1,4-dibromotetrafluorobenzene, but also with the *C-F* bond which led to cross linking, bends in the linear structure and ligand scrambling.

The direct dye-dye connection in TSQ **25** (Figure 2.18) was also formed in a poly Suzuki coupling using dibromo dye **29** and diboron dye **38** as monomers. This homo trimer was prepared and analysed according to the same procedure as for the previous four TSQs, meaning TSQ **25** also precipitated during the reaction in the tetrahydrofuran / 1-methyl-2-pyrrolidinone solvent mixture (page 122). Simultaneously to this preparation, Voelker et al. synthesized and published a structure homologue of TSQ **25** with hexadecyl instead of octyl side chains by a nickel catalyzed Yamamoto coupling from its dibromo precursor [60]. But their polymerised dye had about 40 repeating units. This large degree of polymerization was enabled because of the better solubility of the product in their dimethyl formamide and toluene solvent mixture due to the longer side chains [60]. In the here presented work, the shorter octyl synthon was introduced, because it was a compromise between chain length and price per mol of the synthetic equivalent 1-iodooctane.

To also investigate the promising optophysical properties of multi chromophoric squaraine dyes with the said naphthalene bridge a poly Knoevenagel condensation of naphthalene linker **57** and squaric acid were performed. The condensation stopped automatically after the formation of the trimeric species, which could be measured by UV/vis spectroscopy when dissolved in hot 1-methyl-2-pyrrolidinone. In order to increase the solubility, a defined dye (TSQ **26**, Figure 2.20) with three squaraine chromophores and two octyl side chains was prepared as already mentioned in the preparation of MSQ intermediate **58** (Figure 2.12 on page 33) and squaric acid in a Knoevenagel type condensation (page 123).

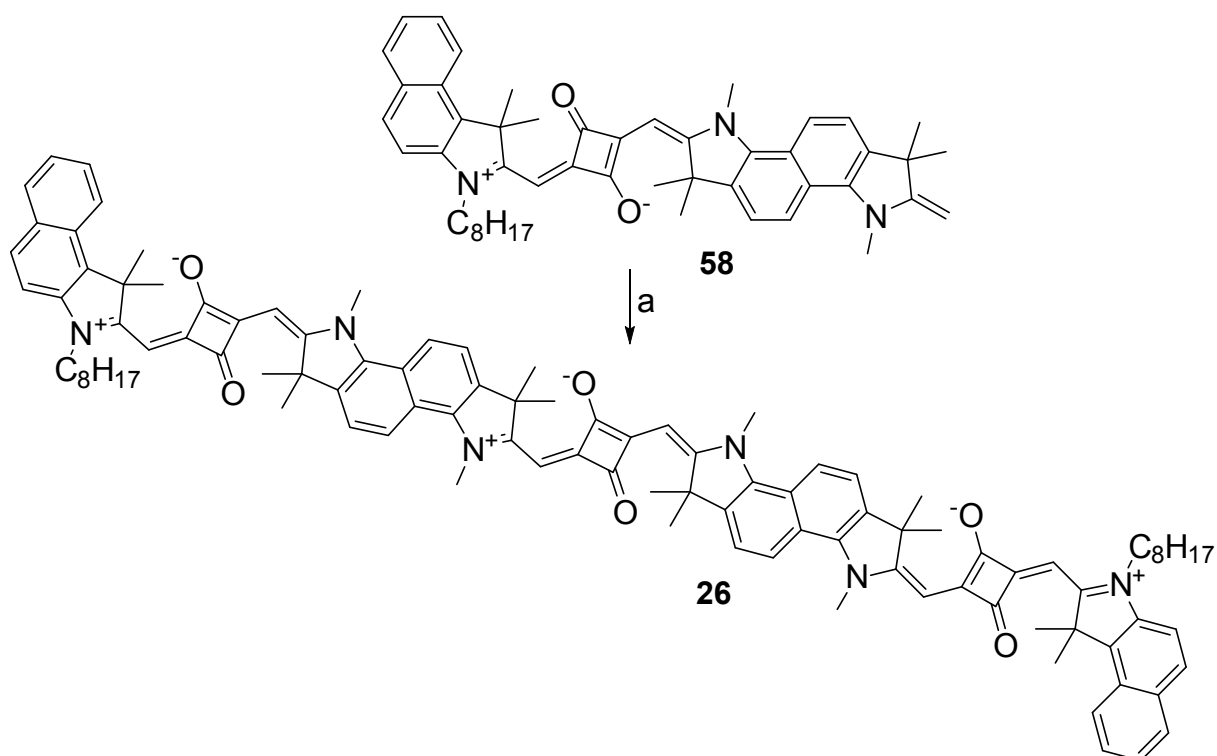


Figure 2.20: a) Synthesis of naphthalene bridged TSQ 26 from MSQ 58 (page 123).

2.2 Analysis and Characterization

2.2.1 Optical Properties

UV/vis and fluorescence spectra of all target molecules were recorded in chloroform. The analysis procedure of the optical spectra was explicitly explained by using reference dye MSQ 8. A solution of MSQ 8 ($2.8 \mu\text{mol}\cdot\text{dm}^{-3}$; 4.3 mg in 5.00 mL chloroform with an additional dilution by factor 500) was used for recording the UV/vis spectrum and a 1:10 dilution thereof was used for the fluorescence spectrum ($0.28 \mu\text{mol}\cdot\text{dm}^{-3}$). Both normalized and base line corrected spectra [61] of MSQ 8 are shown in figure 2.21. From the baseline corrected absorption spectra [61] of MSQ 8 the $\lambda_{\text{max}}^{\text{abs}}$ value was determined to be 637.5 nm (literature [62]: 636.5 nm) and the molar extinction coefficient $\epsilon(\lambda_{\text{max}}^{\text{abs}})$ of $350000 \text{ dm}^3\cdot\text{mol}^{-1}\cdot\text{cm}^{-1}$ was calculated with the Lambert-Beer equation 2.1:

$$\epsilon(\lambda_{\text{max}}^{\text{em}}) = \frac{A(\lambda_{\text{max}}^{\text{em}})}{c_{\text{mol}} \cdot L} \left[\frac{\text{dm}^3}{\text{mol} \cdot \text{cm}} \right] \quad (2.1)$$

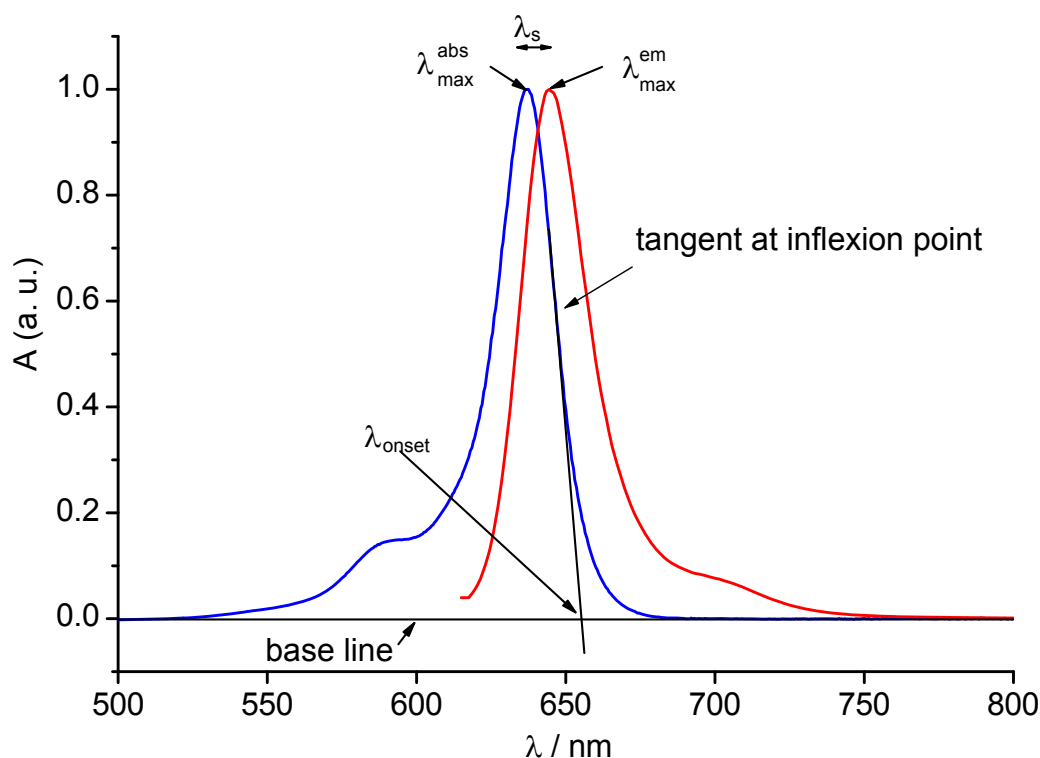


Figure 2.21: Normalized and baseline corrected absorption (—) and fluorescence (—) spectra of MSQ **8** in chloroform as a function of absorption A vs. wavelength λ .

where the unitless absorbance $A(\lambda_{max}^{abs})$ is the maximum peak height, c_{mol} is the used molar concentration in $[\text{mol}/\text{dm}^3]$ and L is the width of the cuvette in $[\text{cm}]$. The very narrow absorption band is a characteristic for squaraines. Since the chromophore of squaraines does not have diffuse aromatic ring systems nor multiple path between the donor group D to the acceptor group A , it behaves more like a two dimensional box with confined length and resonance frequency resulting in the small half-width of 23.5 nm of MSQ **8** and the strong absorbance. The appearing shoulder in the UV/vis spectrum is a contradicting argument to this demonstration but it is known as vibronic shoulder which is similar to the one in cyanine dyes [11]. The optical band gap (ΔE_{ge}^{opt}), an important value for the comparison with the electrochemical analysis, was calculated from the onset wavelength (λ_{onset}) of the absorption. λ_{onset} is defined as the intersection of the tangent at the inflexion point of the absorption curve and its baseline (Figure 2.21). From this follows equation 2.2 for the determination ΔE_{ge}^{opt} with the Planck's constant h , the speed of light c and the energy transition frequency ν_{ge} . Since λ_{onset} of MSQ **8** was

645.5 nm, its ΔE_{ge}^{opt} was 1.921 eV.

$$\Delta E_{ge}^{opt} = h\nu_{ge} = \frac{h \cdot c}{\lambda_{onset}} \quad (2.2)$$

The maximal emission wavelength (λ_{max}^{em}) was taken from the fluorescence spectrum (λ_{max}^{em} (**8**): 644.0 nm; literature [62]: 647 nm). The shape of the fluorescence spectrum is almost the mirror image of the absorption spectrum with a small variation of the vibronic shoulder intensity (Figure 2.21). The Stock's shift (λ_s) was calculated from the difference of λ_{max}^{em} and λ_{max}^{abs} . For MSQ **8**, λ_s is 6.5 nm which implies that the minima of the potential curve in the ground state $|g\rangle$ is approximately exactly below the minima of the excited state $|e\rangle$. And this again gave reason to assume that the geometric orientation of the excited state is the same as in the ground state. Furthermore, this observation verified the previously made "dipole approximation" on page 3. Especially, it validates the splitting of the Hamilton operator in equation 1.8 in a time-independent operator \hat{H}_0 (containing the geometric orientation of the molecule) and the time-dependent perturbation $\hat{V}(t)$ which only acts on the electromagnetic transition moments $|\vec{M}_{ge}|$ of the molecule. $|\vec{M}_{ge}|$ was calculated from an absorption spectrum as it was mentioned in the explanation to equation 1.10 on page 3. Therefore, the wavelength axis and the absorbance axis had to be transformed. Each data point of the wavelength λ axis in [nm] was transformed to frequency ν in [s^{-1}] by the formula 2.3:

$$\nu_i = \frac{c}{\lambda_i} \quad [s^{-1}] \quad (2.3)$$

The transformation of the absorbance axis starts with the Lambert-Beer law (eq. 2.4), in which the absorbance $A(\lambda_{max})$ is defined by the logarithm of the relation of the intensity of the light beam before (I_0) and after (I) the sample.

$$A(\lambda_{max}) = \log\left(\frac{I_0}{I}\right) = \epsilon(\lambda_{max}) \cdot c_{mol} \cdot L \quad [-] \quad (2.4)$$

In order to transform the axis, the Lambert-Beer law was rewritten using the Napierian absorbance $\ln\left(\frac{I_0}{I}\right)$ as shown in equation 2.5 with the absorption cross section $\sigma_{ge}(\nu)$ for a specific transition in [m^2], concentration $c_{particle}$ of absorbing particles [m^{-3}] and the width of the cuvette L in [m].

$$A(\lambda_{max}) = \frac{1}{\ln(10)} \cdot \ln\left(\frac{I_0}{I}\right) = \frac{\sigma_{ge}(\nu_{max}) \cdot c_{particle} \cdot L}{\ln(10)} \quad [-] \quad (2.5)$$

$\sigma_{ge}(\nu_{max})$ is given by equation 2.6 as a result of the combination of equation 2.5 and the relation of c_{mol} with $c_{particle}$ by the Avogadro constant N_A .

$$\sigma_{ge}(\nu) = \frac{\ln(10) \cdot A(\lambda_{max})}{c_{mol} \cdot N_A \cdot L} \quad [m^2] \quad (2.6)$$

For the reference dye MSQ **8** $\sigma_{ge}(\nu)$ was calculated to be $1.34 \cdot 10^{-19} \text{ m}^2$. For the transformation the value of the absorbance axis $A(\lambda_{max})$ was scaled by $\sigma_{ge}(\nu)$ and then each data point was divided by its frequency value. So the new axis $\frac{\sigma_{ge}(\nu)}{\nu}$ was plotted versus ν as shown in figure 2.22 for the reference dye **8**. The area under this

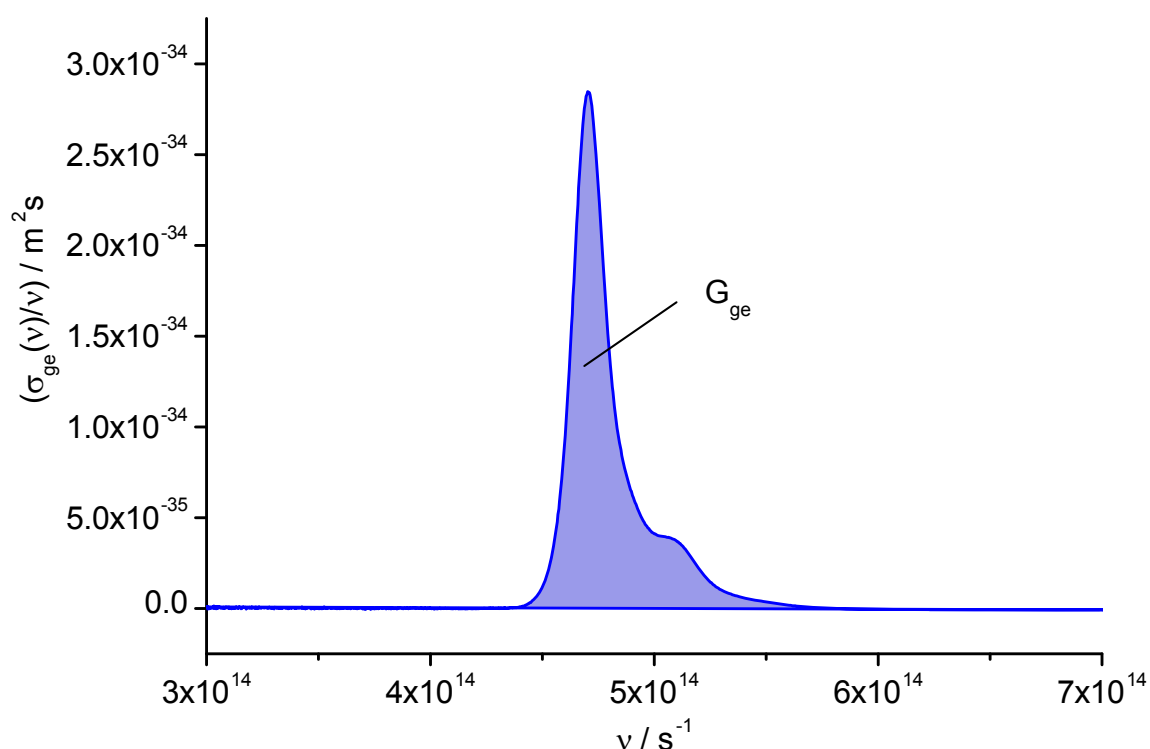


Figure 2.22: Transformed UV/vis absorption spectrum of MSQ **8** in chloroform as a function of $\frac{\sigma_{ge}(\nu)}{\nu}$ vs. ν . The area under the curve is equal to the integral absorption cross section (G_{ge}).

particular curve is called integral absorption cross section (G_{ge}) and was calculated with the program Origin [61]. For dye **8** G_{ge} was $6.92 \cdot 10^{-21} \text{ m}^2$ (eq. 2.7).

$$G_{ge} = \int \frac{\sigma_{ge}(\nu)}{\nu} d\nu \quad [m^2] \quad (2.7)$$

G_{ge} is the value to calculate the Einstein coefficients A_{ge} for the spontaneous emission (eq. 2.8 [4]) and B_{eg} for the absorption (eq. 2.9 [4]). The energy density of the monochromatic light source during the UV/vis measurement was assumed to be low and therefore, the excited state $|e\rangle$ is not populated significantly. Because the third Einstein coefficient B_{ge} for the stimulated emission relies on the product of the energy density and the population of $|e\rangle$, B_{ge} was neglected. The value of A_{ge} for the reference dye was $1.94 \cdot 10^{+08} \text{ s}^{-1}$ according to equation 2.8 and the one of B_{eg} was $3.13 \cdot 10^{+21} \text{ m} \cdot \text{kg}^{-1}$ according to equation 2.9.

$$A_{ge} = \frac{8 \cdot \pi \cdot \nu_{ge}^3}{c^2} \cdot G_{ge} \quad [\text{s}^{-1}] \quad (2.8)$$

$$B_{eg} = \frac{c}{h} \cdot G_{ge} \quad [\text{m} \cdot \text{kg}^{-1}] \quad (2.9)$$

For the comparison of dyes from this work with each other and the theory the relation of G_{ge} to $|\vec{M}_{ge}|$ in $[\text{C} \cdot \text{m}]$ (eq. 2.10 [4]) is more useful than the Einstein coefficients. Additionally, the unitless oscillator strength f_{ge} (eq. 2.11 [4]) was calculated from G_{ge} which gives an indication for the number of electrons involved in the transition. For the above mentioned equations the following constants were used: the vacuum permittivity ϵ_0 in $[\text{C}^2 \cdot \text{N}^{-1} \cdot \text{m}^{-2}]$, the mass of an electron m_e in $[\text{kg}]$ and the charge of an electron e in $[\text{C}]$.

$$|\vec{M}_{ge}| = \sqrt{\frac{3 \cdot h \cdot \epsilon_0 \cdot c}{2 \cdot \pi^2}} \cdot G_{ge} \quad [\text{C} \cdot \text{m}] \quad (2.10)$$

$$f_{ge} = \frac{4 \cdot \epsilon_0 \cdot m_e}{e^2} \cdot \frac{\nu_{ge}}{c} \cdot G_{ge} \quad [-] \quad (2.11)$$

Since $|\vec{M}_{ge}|$ is normally given in Debye and not in an SI unit equation 2.10 was reformulated to

$$|\vec{M}_{ge}| / [\text{Debye}] = \sqrt{\frac{G_{ge}}{41.624}} / [\text{pm}^2] \quad (2.12)$$

The transition moment of the reference dye **8** was determined to be 13 D (lit. [63]: 12.2 D). The comparison of $|\vec{M}_{ge}|$ of the target molecules is discussed later in this section. The calculated f_{ge} value of 1.2 of the reference dye gives evidence that one electron interacts with light in the absorption process. f_{ge} will be relevant in the comparison of the optical and electrochemical properties of the squaraines.

After the detailed analysis of the optical properties of the reference dye **8** the structure-

property relation of the MSQ dyes will be discussed. The normalized UV/vis spectra of all five MSQ dyes are shown in figure 2.23. Strikingly, all curves have the same shape but are just bathochromically shifted in respect to the reference dye MSQ **8** (black line). In chloroform the mono phenylene extended MSQ **9** (cyan line) had a λ_{max}^{abs} value of 646.5 nm (compare table 2.2) and the double phenylene extended MSQ **10** (blue line) one of 658.5 nm. For the benzo extended MSQ series (**11** in red, **12** in green) the following basic rule can be applied: the more enlarged the aromatic system the more increased the bathochromic shift of λ_{max}^{abs} is. This was already known for the cyanine dyes [11]. Also the emission maximum λ_{max}^{em} and the optical band gap ΔE_{opt} followed this trend. No such tendency was observed for the values of $\epsilon(\lambda_{max}^{abs})$. A slightly larger λ_s was calculated for the phenyl extended MSQs (**9** and **10**) then for the benzo extended MSQs, presumably due to the additional degree of freedom in the rotation. Finally, all of the

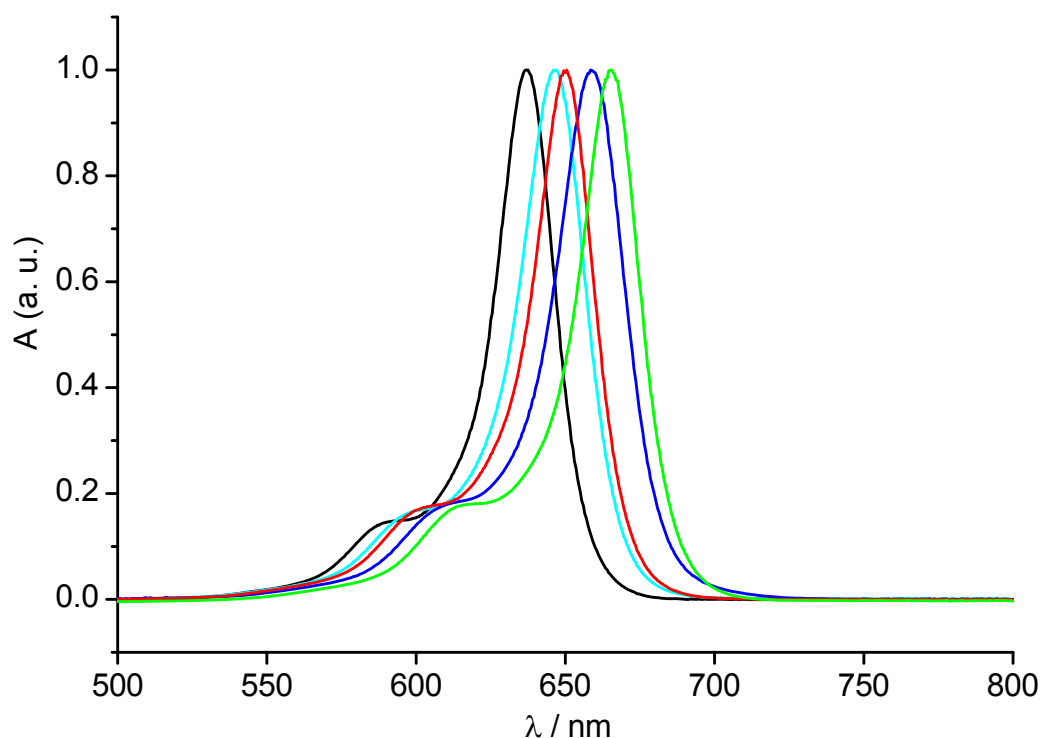


Figure 2.23: Normalized UV/vis spectra of MSQ **8** (—), MSQ **9** (—), MSQ **10** (—), MSQ **11** (—) and MSQ **12** (—) in chloroform.

optical properties were related to the structure of the dyes. Although, the π -system of the phenyl extended dyes is more extended than the benzo π -system, the λ_{max}^{abs} values of the former are lower than those of the latter. However, one should also take into account,

Table 2.2: Photophysical properties of MSQs in homogeneous chloroform solution and the structure related corrected number of π -electron pairs outside the chromophore unit (#EP).

entry	λ_{max}^{abs} [nm]	$\log(\epsilon(\lambda_{max}^{abs}))$ [-]	λ_{onset} [nm]	ΔE_{opt} [eV]	λ_{max}^{em} [nm]	λ_s [nm]	#EP
MSQ 8	637.5	5.54	645.5	1.921	644.0	6.5	6.0
MSQ 9	646.5	5.47	665.5	1.863	656.0	9.5	7.5
MSQ 10	658.5	5.60	680.0	1.824	667.5	9.0	9.1
MSQ 11	650.0	5.53	668.5	1.855	657.5	7.5	8.0
MSQ 12	665.5	5.52	684.0	1.813	672.0	6.5	10.0

that the phenyl substituents were tilted whereas the benzo extensions lay in plane. These observations led to the question how one could merge the optical properties of these five dyes. The information of the structure were the number of π -electron pairs at the end groups outside the chromophore unit and their relative angle to the π -system of the chromophore. So the sum of the π -electron pairs corrected with a \cos^2 function of their torsion angle (ϕ) contains all information of the structure. This sum is called the actual number of π -electron pairs (#EP) and this was then correlated to the absorption maximum value. The \cos^2 function was used because Vonlanthen et al. reported the structure property relation of ϕ with the conductivity in single molecules and they used the $\cos^2(\phi)$ function for the correlation [64]. For this work the function was adapted to $\cos^{2 \cdot m}(\phi)$ with m as the number of tilts inbetween the π -systems. Furthermore, it was assumed that in the MSQs 9 and 10 ϕ was the same as the equilibrium ϕ in a bisphenyl molecule (44.4° [65]).

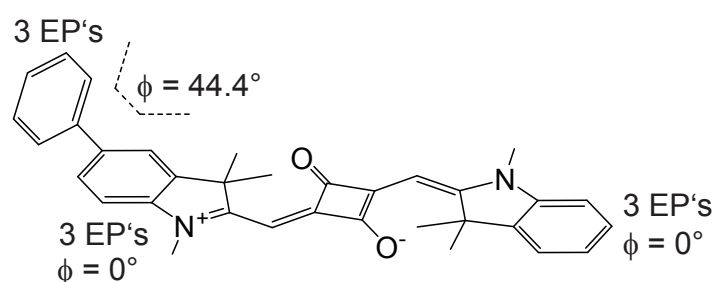


Figure 2.24: Projection of MSQ 9 with the number of π -electron pairs (EP's) and their torsion angle (ϕ) relative to the π -electron system of the chromophore.

For example MSQ 9 has 6 EP's with $\phi = 0^\circ$ and 3 EP's with $\phi = 44.4^\circ$ (Figure 2.24). So

#EP is about 7.5 (see table 2.2) according to equation 2.13.

$$\#EP = \sum_{i=1}^j EP_i \cdot \cos^{2 \cdot m}(\phi) \quad [-] \quad (2.13)$$

The plot of #EP of the MSQs versus their λ_{max}^{abs} value showed a linear correlation with R^2 : 0.994 (Figure 2.25). The formula 2.14 which described the linear fit is as follows:

$$\lambda_{max}^{abs} = 7 \cdot \#EP + 595 \quad [nm] \quad (2.14)$$

This equation 2.14 indicated that per additional π -electron pair lying in the chromophore π -system plain the value of λ_{max}^{abs} was increased by 7 nm. This structure property relation

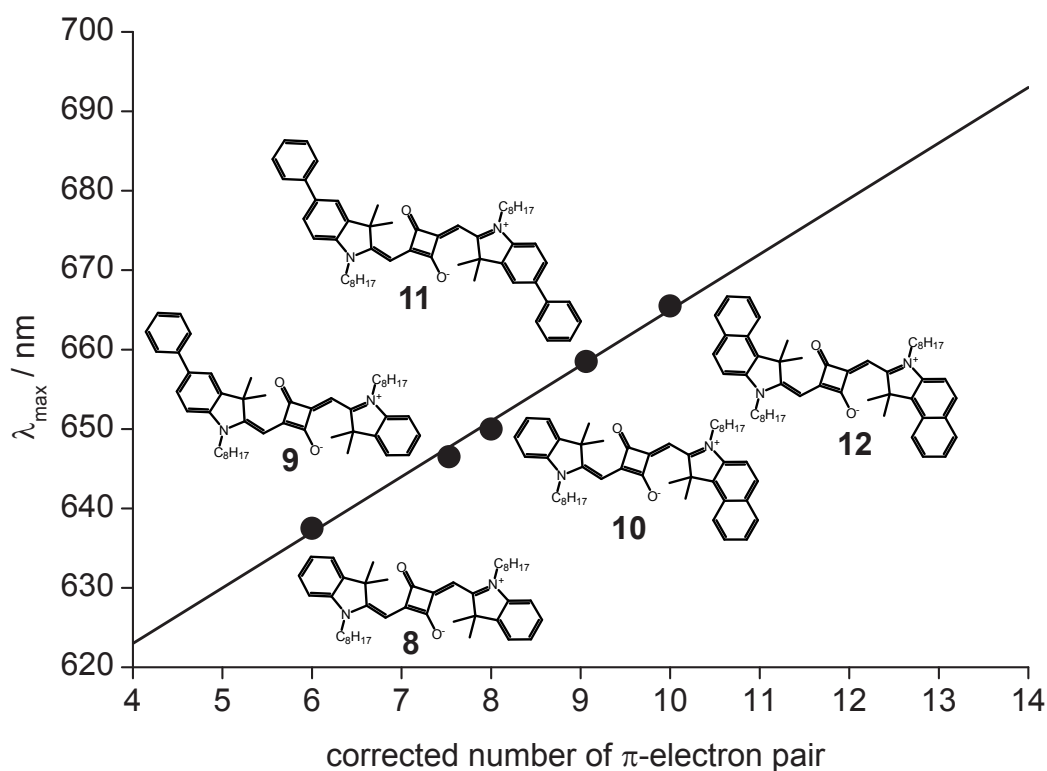


Figure 2.25: The plot of λ_{max}^{abs} versus the effective number of planar π -electron pairs outside the chromophore unit (#EP) of the MSQs **8**, **9**, **10**, **11** and **12** with the correlation displayed in equation 2.14 with $R^2 = 0.994$.

was used to estimate the influence of the aromatic system in the phenylene bridged BSQ **13** in order to answer the question whether a dye-dye interaction occurs in this

BSQ or not. Thus, #EP for BSQ **13** was calculated from its structure (Figure 2.26) by the equation 2.13. #EP was calculated by the sum of $5 \cdot \cos^0(0^\circ)$ of the benzo end group plus $3 \cdot \cos^0(0^\circ)$ from the indole at the bridge plus $3 \cdot \cos^2(44.4^\circ)$ from the phenylene bridge plus $3 \cdot \cos^4(44.4^\circ)$ from the indol of the second chromophore which resulted in 10.3.

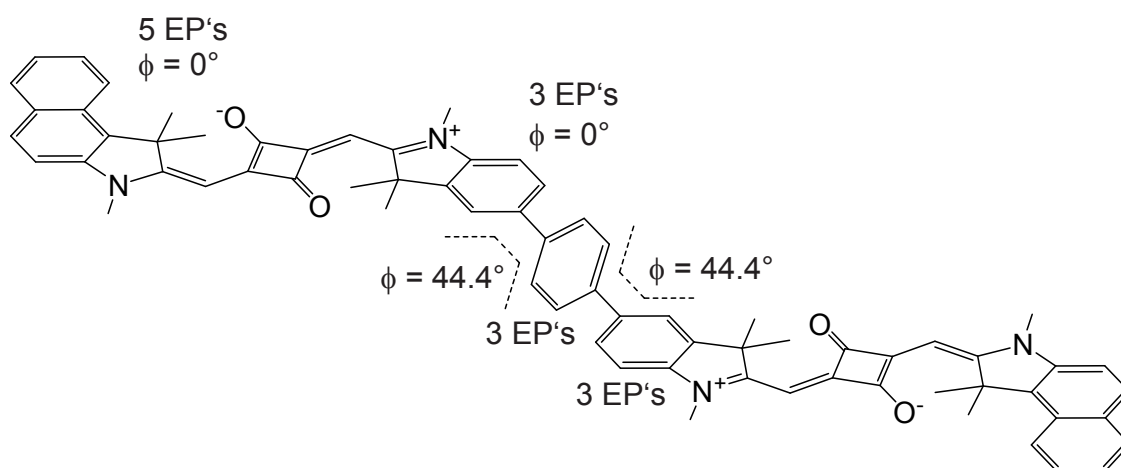


Figure 2.26: Projeccion of BSQ **13** with the number of π -electron pairs (EP's) and their torsion angle (ϕ) relative to the π -electron system of the chromophore.

Therefore, the aromatic surroundings of the chromophore shifted the λ_{max}^{abs} value to 667 nm (Equation 2.14). Anything further red shifted than this value derives from the dye-dye interaction. In deed, BSQ **13** showed a λ_{max}^{abs} value of 678.0 nm in chloroform which is a bathoromic shift of about 11 nm compared to the solely aromatic influenced calculation. After the proof of existence of the dye-dye interaction, the influence of the electron density of the bridge on this interaction was investigated. Therefore, the normalized and base line corrected UV/vis spectra of the discussed phenylene bridged BSQ **13** (Figure 2.8), the fluorenylene bridged BSQ **15** (Figure 2.9), BSQ **19** with a high electron density (Figure 2.10) and BSQ **20** (Figure 2.11) with a low electron density on the bridge were plotted in figure 2.27 and their analysed photophysical properties were listed in table 2.3. On the one hand the four BSQ spectra were not uniform indicating that different effects influence the system and on the other hand it was not possible to determine a correlation of λ_{max}^{abs} with their electron density property of the bridging synthon. Obviously, all three BSQs (**15**, **19** and **20**) with electronically modified bridges have a hypsochromic shifted λ_{max}^{abs} value compared to the phenylene

bridged BSQ **13**. Neither λ_{max}^{abs} nor $\epsilon(\lambda_{max}^{abs})$, nor ΔE_{opt} gave a reasonable correlation

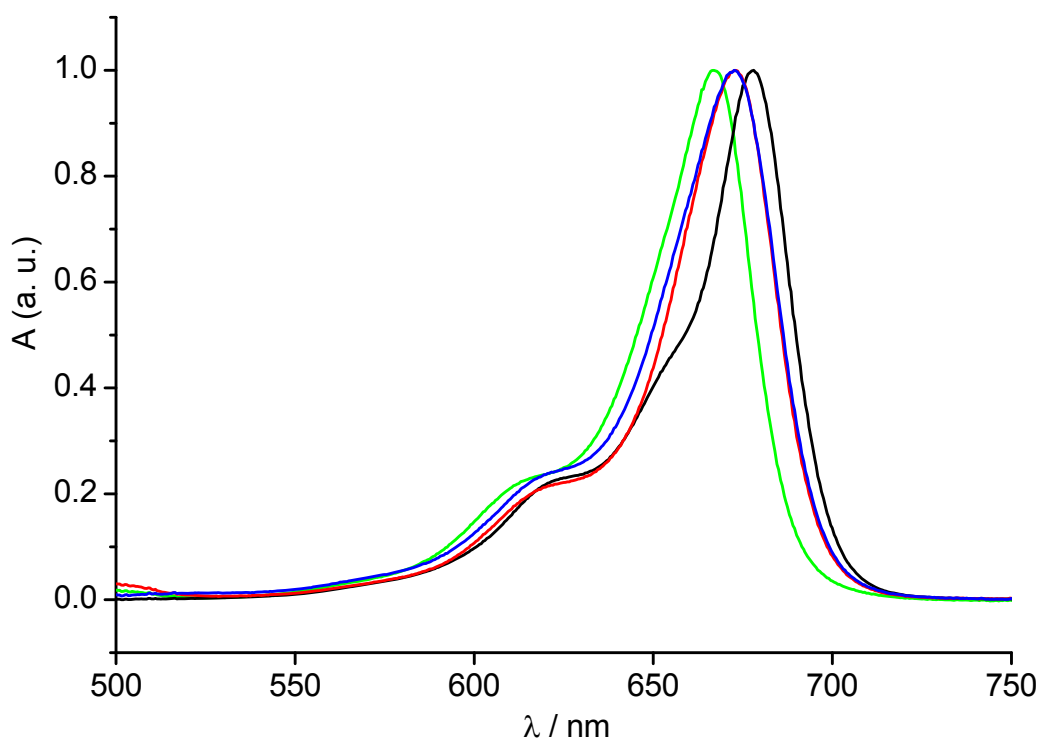


Figure 2.27: Normalized absorption spectra of BSQ **13** (—), BSQ **15** (—), BSQ **19** (—) and BSQ **20** (—) measured in chloroform.

with the electronic density. Only the λ_s values were in the same range for all four BSQ with tilted bridges presumably due to the same degree of freedom (data in table 2.3). Consequently, it was suggested that another influence dominates the dye-dye interaction. Using the developed formula 2.14 to determine #EP the influence of the planar bridges on the optical properties of the BSQ was calculated. #EP of BSQ **17**, structure in figure 2.14, was 8. Therefore, the aromatic bridge shifted the λ_{max}^{abs} value

Table 2.3: Photophysical properties of BSQs with tilted bridges in homogeneous chloroform solution.

entry	λ_{max}^{abs} [nm]	$\log(\epsilon(\lambda_{max}^{abs}))$ [—]	λ_{onset} [nm]	ΔE_{opt} [eV]	λ_{max}^{em} [nm]	λ_s [nm]	#EP [—]
BSQ 13	678.0	5.68	697.5	1.778	688.5	10.5	10.3
BSQ 15	673.0	5.65	695.0	1.784	684.0	11.0	11.8
BSQ 20	667.0	5.62	686.0	1.808	676.0	9.0	10.3
BSQ 19	672.5	5.67	694.5	1.785	682.0	9.5	10.3

to 651 nm and anything further red shifted originated from the dye-dye interaction. Due to this interaction λ_{max}^{abs} of BSQ **17** was shifted by 64 nm to 715 nm in chloroform (normalized and base line corrected UV/vis spectrum in figure 2.28 and data in table 2.4). This amazing shift was also observed in BSQ **14** (structure in figure 2.12) where

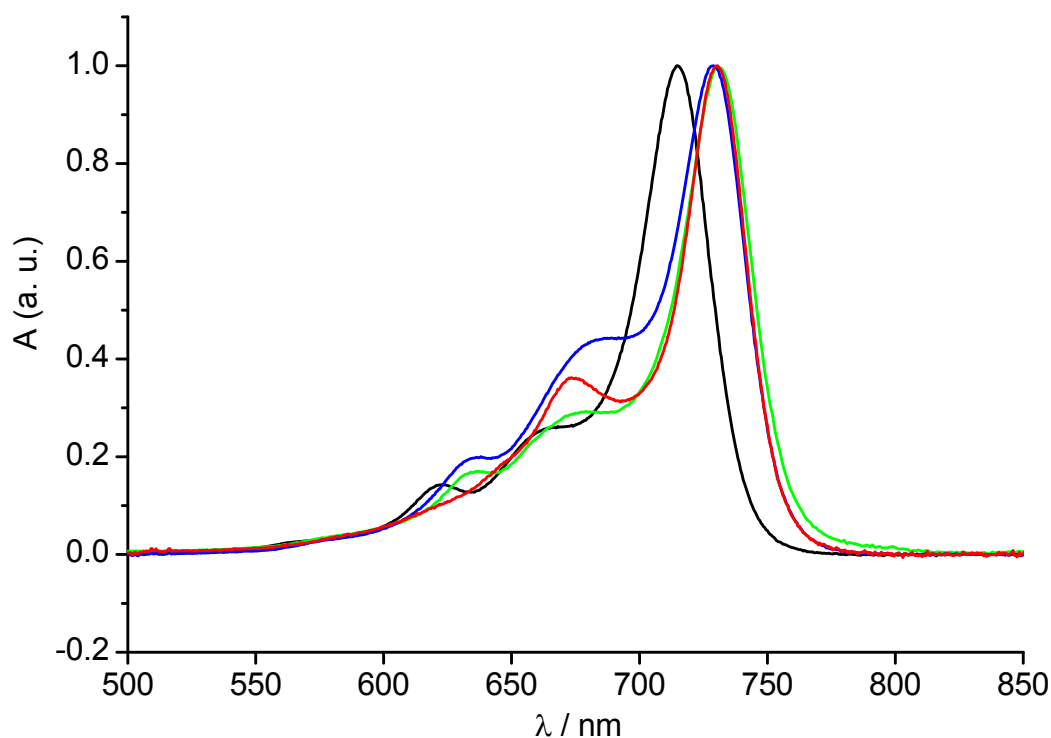


Figure 2.28: Normalized absorption spectra of BSQ **17** (—), BSQ **14** (—), BSQ **18** (—) and BSQ **16** (—) measured in chloroform.

the aromatic surroundings shifted λ_{max}^{abs} to 665 nm and the dye-dye interaction further to 728.5 nm (+63.5 nm). Also the unsymmetrical BSQ **18**, which had a comparable #EP to the symmetrical naphthalene linked BSQ **14**, had a λ_{max}^{abs} of 727 nm in chloroform. The maximal absorption wavelength of BSQ **16** (Figure 2.13) was 730.5 nm in chloroform which is about the same as the naphthalene bridged BSQ **14** which is contradictive since #EP of BSQ **16** is larger than that of BSQ **14**. This was interpreted as the decreasing influence of the dye-dye interaction when enlarging the distance inbetween. By coincidence this reduction of 14 nm was about as large as the reduction caused by the enlarged π -system (Equation 2.14). Consequently, the distance between the two chromophores should also be considered in the formula to relate the structure with the optical property.

Table 2.4: Optical properties of planar naphthalene and anthracene linked BSQ dyes in homogeneous chloroform solution.

entry	λ_{max}^{abs} [nm]	$\log(\epsilon(\lambda_{max}^{abs}))$ [-]	λ_{onset} [nm]	ΔE_{opt} [eV]	λ_{max}^{em} [nm]	λ_s [nm]	#EP [-]
BSQ 17	715.0	5.61	738.5	1.679	726.5	11.5	8
BSQ 14	728.5	5.51	754.0	1.645	739.5	11.0	10
BSQ 16	730.5	5.69	753.0	1.647	738.0	7.5	12
BSQ 18	727.0	5.63	753.0	1.647	743.0	16.0	10

Before continuing with the discussion about the structure-property relation, the shape of the displayed UV/vis spectra in figure 2.28 of the naphthalene and anthracene linked BSQs shall be explained. Each main transition band of these BSQs showed more than one shoulder. Additional shoulders could appear due to aggregate formation or can be explained according to the theory of Kiprianov that the antipodal superimposed transition moment of serial connected BSQs is practically not zero (see table 1.1). Since the shape of aggregate spectra would change with the concentration, the former argument was verified by taking UV/vis spectra of every order of magnitude in the range of $3 \cdot 10^{-5}$ to $3 \cdot 10^{-10}$ mol/L as shown in figure 2.29 with BSQ 14. Indeed, the shape of the spectra did not change in this concentration range, indicating that the spectra was recorded of nicely solvated single molecules. Therefore, the additional shoulders originated from the non-zero antipodal superimposed transition moments. These cannot origin from the coupled antipodal *dipole* moments because of the serial connection (see Table 1.1 and [19]). Consequently, it is assumed that the non-zero contribution to the transition moment derived from higher order coupling, for example quadrupole coupling, which were not zero [24]. In other words the small additional shoulders might be evidence of the presence of "not negligible quadrupole interactions" [24] in squaraine dyes according to Laia et al. [24].

The spectra were normalized and base line corrected with the help of the program Origin [61]. The corrected spectra of the synthesized oligomeric squaraines are shown in figure 2.30 and the corresponding analysed optical data are reported in table 2.5. λ_{max}^{abs} value of the phenylene linked TSQ 21 was 687.5 nm. Thus, the additional coupling with a third chromophore shifted the λ_{max}^{abs} value bathochromically by "only" about 10 nm in respect to λ_{max}^{abs} of BSQ 13. A similar small additional red shift was also observed for the fluorenylene bridged TSQ 22, the bis alkoxy phenylene bridged TSQ 23 and the tetra fluoro phenylene linked TSQ 24. The direct linked homo oligomere of a squaraine dye, TSQ 25, showed an absorption maximum of 718.0 nm. This relatively high λ_{max}^{abs} is

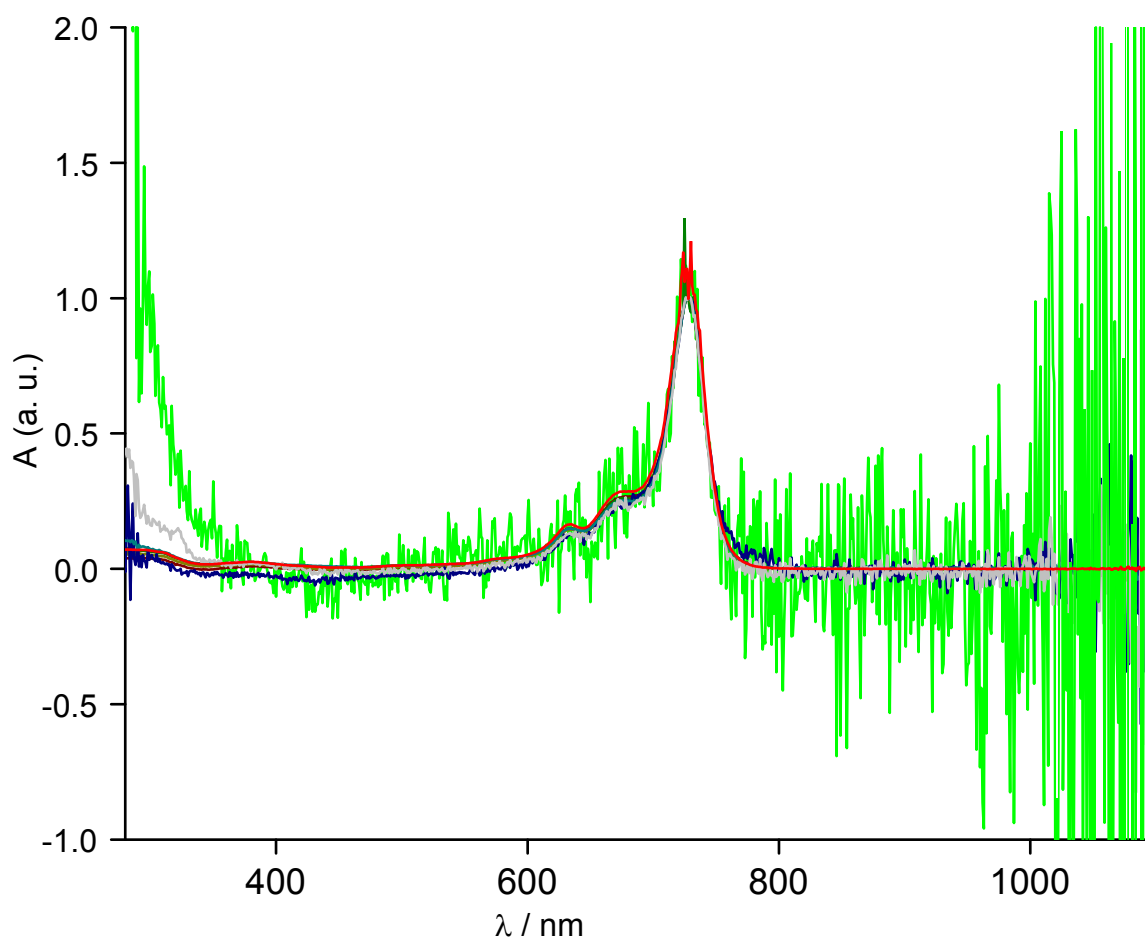


Figure 2.29: UV/vis spectra of BSQ **14** of every order of magnitude from $3 \cdot 10^{-5}$ to $3 \cdot 10^{-10}$ mol/L in chloroform were normalized and put on top of each other. The two most concentrated spectra were recorded in a 1 mm cell, the lowest two in a 100 mm cell and the rest in a 10 mm cell.

explained with the shorter distance between the two chromophores and the fact, that the structure of TSQ **25** contains one tilted single bond between the chromophores whereas the just mentioned TSQs contain two of them. As mentioned earlier, Voelker et al. [60] also synthesized the structure homologue of TSQ **25** with a value of λ_{max}^{abs} of 738 nm measured as ~ 40 -mer in chloroform which is henceforth considered as λ_{∞} in the Meier's equation (eq. 1.11 at page 6) for the series of the direct linked squaraine dyes. The value of λ_{max}^{abs} of the defined naphthalene trimer **26** (Figure 2.30) was red shifted by 31 nm in respect to the corresponding dimeric BSQ **14**. This bathochromic shift was about half as big as the one from MSQ **12** to BSQ **14**, which implied that the used linker in combination with squaraine dyes led to a limitation of the λ_{max}^{abs} .

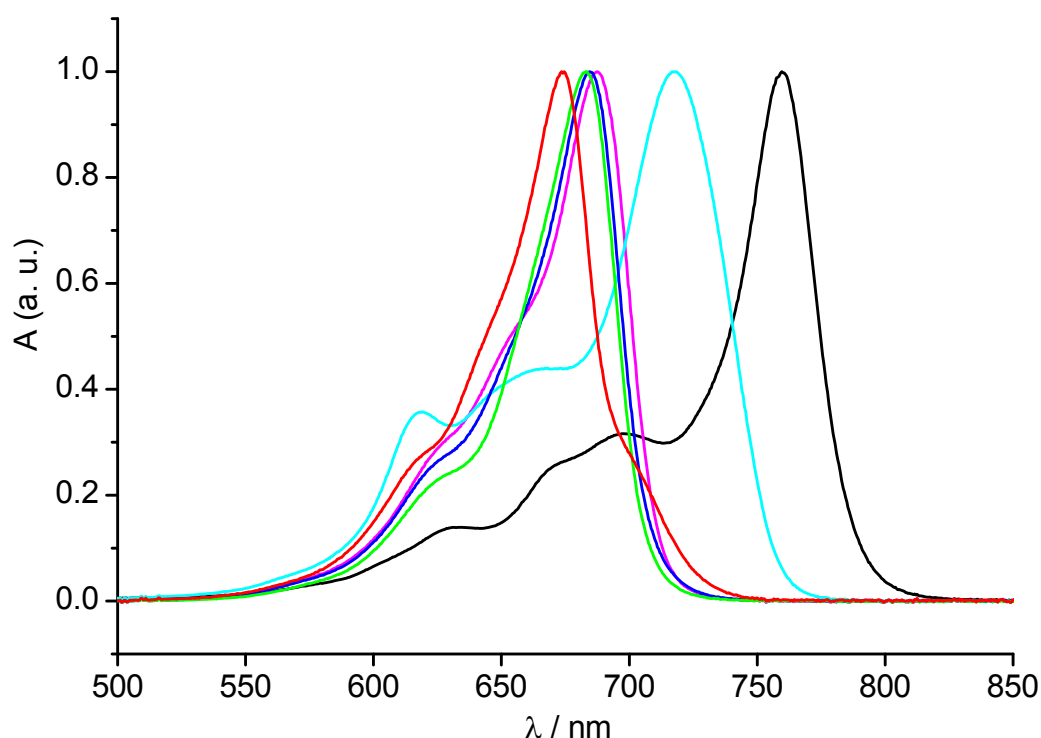


Figure 2.30: Normalized and base line corrected absorption spectra [61] of phenylene bridged TSQ **21** (—), fluorenylene bridged TSQ **22** (—), alkoxy phenylene bridged TSQ **23** (—), tetrafluoro phenylene bridged TSQ **24** (—), directly linked TSQ **25** (—) and the naphthalene bridged TSQ **26** (—) measured in chloroform.

The theory of Meier [12] was adopted in order to correlate the optical properties of the TSQs to the corresponding BSQs and MSQs. Therefore, the photophysical properties of the dye series, consisting of a MSQ, a BSQ, a TSQ and a ∞ -SQ as a real polymer with the same bridge, were compared within one series and with each other series. Because of the different electron density of the linker synthon the bis-alkoxy-phenylene and the tetrafluorophenylene bridged dye series were left aside, since they could not be compared with the pure hydrocarbon linked dyes. So three known data points in the hydrocarbon linked dye series were used to calculate the three parameters in the Meier equation (eq. 1.11). Therefore, λ_{max}^{abs} of MSQ **12** was chosen as λ_1 for the naphthalene linked dye series (DS1), because MSQ **12** had the most structural similarity with the repeating unit of the DS1. For direct linked DS2 and the phenylene linked DS3 λ_{max}^{abs} of MSQ **10** was defined as λ_1 . As a result the Meier equation for DS1 (eq. 2.15), DS2 (eq. 2.16) and DS3 (eq. 2.17) were reported here and the curves were shown in the main

Table 2.5: Photophysical properties of the TSQs, parameters of the Meier's equations 2.15, 2.16 and 2.17 and the estimated length of the linking synthon from the geometry optimized molecular structure.

entry	λ_{max}^{abs} [nm]	$\log(\epsilon(\lambda_{max}^{abs}))$ [-]	λ_{onset} [nm]	ΔE_{opt} [eV]	λ_{max}^{em} [nm]	λ_s [nm]	λ_∞ [nm]	$-b$ [-]	d [nm]
TSQ 21	687.5	5.82	711.0	1.744	697.0	9.5	696.5	-0.720	1.418
TSQ 22	683.5	5.96	704.0	1.761	692.0	8.5	-	-	-
TSQ 23	684.5	6.09	706.0	1.756	691.0	6.5	-	-	-
TSQ 24	674.0	5.26	697.0	1.779	681.0	7.0	-	-	-
TSQ 25	718.0	5.77	754.5	1.644	-	-	738	-0.692	0.984
TSQ 26	759.5	5.81	785.5	1.579	771.0	11.5	789.5	-0.709	0.632

part of figure 2.31. The calculated parameters were also summarized in table 2.5.

$$DS1 : \lambda_{max}^{abs}(n) = 789.5 - (789.5 - 665.5) \cdot e^{-0.709 \cdot (n-1)} \quad (2.15)$$

$$DS2 : \lambda_{max}^{abs}(n) = 738.0 - (738.0 - 658.5) \cdot e^{-0.692 \cdot (n-1)} \quad (2.16)$$

$$DS3 : \lambda_{max}^{abs}(n) = 696.5 - (696.5 - 658.5) \cdot e^{-0.720 \cdot (n-1)} \quad (2.17)$$

Because no structure analogue MSQ was prepared for the fluorenylene linked DS4 the Meier equation for the fluorenylene dye series DS4 was not calculated for now by the known data set.

To answer the initial question about which dye class shows a bigger bathochromic shift, DS1 was compared with the reported maximal red shift of the polymeric cyanine dyes [23]. The naphthalene bridge in combination with squaraines showed a maximal red shift of 124 nm whereas in combination with a cyanine chromophore a red shift of 159 nm occurs [23]. The reduced coupling strength is explained by the presence of the quadrupole in the squaraines. This interaction is estimated to be smaller than the coupling of a pure dipole in the cyanine dyes.

In order to get a three dimensional plot with one axis related to the structural input, the second axis being the number of repeating units and third the absorption maximum. Therefore, the two individual parameters in the Meier's equation, the exponential decay coefficient $-b$ and the limiting absorption maximum λ_∞ , must be correlated. According to the Meier's equation the $-b$ value defines the decay of interaction which is mainly

influenced by the nature of the linking synthon. So the #EP value was correlated with the experimental based $-b$ values as it was done for the MSQs (see insert in figure 2.31). The #EP for one bridge was inserted into equation 2.18 to give $-b$ as a function of EP_i , ϕ and m with $R^2 = 1.00$:

$$-b(EP_i, \phi, m) = -\frac{14.47 + \sum_{i=1}^j EP_i \cdot \cos^{2 \cdot m}(\phi)}{27.46} \quad (2.18)$$

For the determination of the second individual parameter λ_∞ the following ansatz was chosen. λ_∞ is an indicator for the maximal coupling of the chromophores. The closer

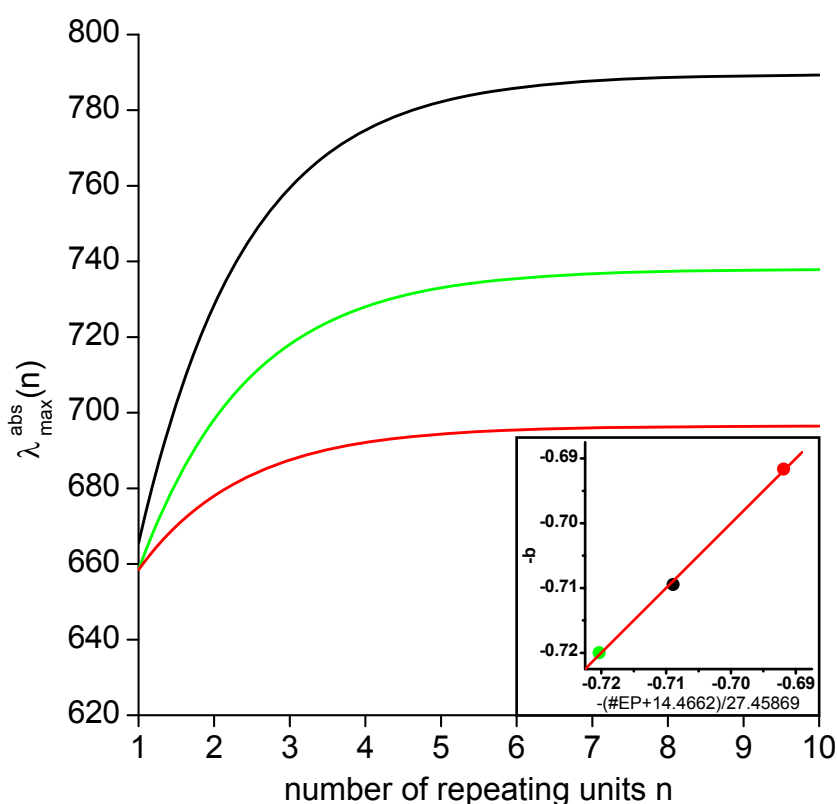


Figure 2.31: graph: Calculated Meier's equation for DS1 (—, eq. 2.15), for DS2 (—, eq. 2.16) and for DS3 (—, eq. 2.17); insert: linear correlation of Meier's exponential decay coefficient $-b$ with the empiric formula with the torsion angle ϕ and the distance square d^2 as parameters, $R^2 = 1.00$.

the chromophores the more intense is the coupling. The distance (d) was defined as the measurable length from one nitrogen atom to the other nitrogen atom over the conjugated bridge in the geometry optimized molecular structure. According to the

radiation law the $1/d^2$ function was used to correlate the distance with the optical property. However, this distance does not have any influence on the coupling if the torsion angle is 90° . Therefore, a fraction of the pure cosine function and the distance square $\left(\frac{\cos^{2\cdot m}(\phi)}{d^2}\right)$ was used as the x-axis in a plot versus the calculated λ_∞ from equation 2.15, 2.16 and 2.17. These d values were also reported in the table 2.5. The empirical fit for the three data points was a natural logarithm. As a result of that λ_∞ was defined by empirical equation 2.19 as a function of ϕ , m and d .

$$\lambda_\infty(\phi, m, d) = 34.30 \cdot \ln \left(0.03937 + \frac{\cos^{2\cdot m}(\phi)}{d^2} \right) + 757.5 \quad (2.19)$$

For a proof of concept the above stated equation for $\lambda_\infty(\phi, m, d)$ was probed by inserting two limiting conditions. Firstly, if ϕ is 90° , then $\lambda_\infty(\phi, m, d)$ is 646.5 nm, which is very similar to a single squaraine dye. Secondly, if two nitrogen were as close as possible like in hydrazine (0.146 nm), so the linker inbetween the two chromophores is only one single bond and it is assumed that ϕ is 0° , then $\lambda_\infty(\phi, m, d)$ is 889.5 nm. These are reasonable values for serial connected squaraines with indole type end groups if no other influence is present.

Finally, the simple $\lambda_{max}^{abs}(n)$ of the Meier's equation was developed to a multi dimensional structure related $\lambda_{max}^{abs}(n, EP_i, d, \phi, m)$ (eq. 2.20) for the characterization of the structural dependent influence on the optical property.

$$\lambda_{max}^{abs}(n, EP_i, d, \phi, m) = \lambda_\infty(\phi, m, d) - (\lambda_\infty(\phi, m, d) - \lambda_1) \cdot e^{-b(EP_i, \phi, m) \cdot (n-1)} \quad (2.20)$$

To verify the corrected Meier's equation and to show that with this equation the absorption maximum of any similar dye can be calculated, the λ_{max}^{abs} of the fluorenylene bridged dyes BSQ **15** and TSQ **22** were calculated using 1.809 nm for d , 44.4° for ϕ , 2 for m , the assumed value of 658.5 nm for λ_1 and the calculated #EP of 11.8 with $n = 2$ for BSQ **15** and #EP of 13.6 with $n = 3$ for TSQ **22** (Figure 2.32). With these settings $\lambda_{max}^{abs}(2)$ resulted in 674 nm and $\lambda_{max}^{abs}(3)$ in 681 nm which was pretty close to the measured values of λ_{max}^{abs} of 673 nm and 683.5 nm, respectively. The example with the fluorenylene bridged dyes proved the validity of the found structure-property relations in squaraines within certain parameter ranges.

Unfortunately, the developed equation 2.20 could not predict λ_{max}^{abs} for the flat bridged BSQ **27** correctly. The prediction proclaimed 727.5 nm (#EP: 3, ϕ : 0° , d : 0.565 nm) but in reality a λ_{max}^{abs} of 804.5 nm was measured in chloroform. One would have to use

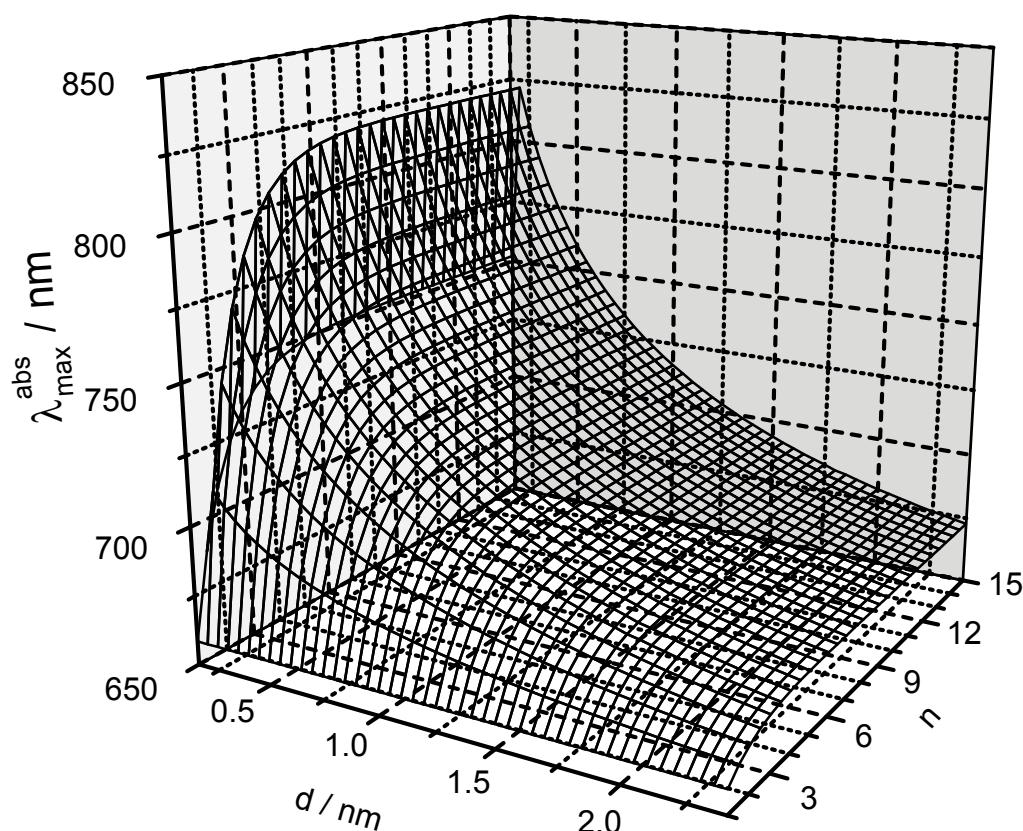


Figure 2.32: $\lambda_{max}^{abs}(n, EP_i, d, \phi, m)$ calculated for the fluorenylene bridged dye series based on the oligomeric structure of TSQ **22** with #EP of 13.6, ϕ of 44.4° , m was 2 and λ_1 was assumed to be 658.5 nm.

a d value of 0.05 nm in the corrected Meier's equation to obtain the found absorption maximum, but such a small d value is unnatural. Also the unexpected giant red shift of 139 nm even exceeded the λ_∞ value of the naphthalene dye series. As a result BSQ **27** was treated as a speciality and was therefore excluded from the comparison so far. The photophysical properties of BSQ **27** were tabulated in an extra table 2.6.

Up to now the analysis of the structure-property relation was based on the geometric orientation of the molecules. Thus, the nature of the dye-dye interaction should also be studied. Specially, the determination whether the coupling is dominated by the dipole-

Table 2.6: Photophysical properties of the BSQ **27** and the distance d between the middler two nitrogen atoms.

entry	λ_{max}^{abs} [nm]	$\log(\epsilon(\lambda_{max}^{abs}))$ [-]	λ_{onset} [nm]	ΔE_{opt} [eV]	λ_{max}^{em} [nm]	λ_s [nm]	d [nm]
BSQ 27	804.5	5.36	838	1.480	818	13.5	0.565

dipole coupling or if it is influenced otherwise. Therefore, in the following the electronic structure represented by the absolute value of the transition moment $|\vec{M}_{ge}|$ is compared with the optical properties. According to the theory of Kiprianov when two chromophores are serially connected and they show a dipole-dipole coupling, then due to the reduction of the band gap the bathochromic shift of λ_{max}^{abs} occurs and the overall $|\vec{M}_{ge}|$ is larger than each individual one. In fact this relation can be visualized by plotting the λ_{max}^{abs} of the dyes versus their $|\vec{M}_{ge}|$. The calculation of $|\vec{M}_{ge}|$ was mentioned at the beginning of this section with the help of the reference dye MSQ **8**. In table 2.7 the spectroscopic quantities of all targeted molecules were listed: the integral absorption cross section G_{ge} , the first and second Einstein coefficient A_{ge} and B_{eg} , the oscillator strength f_{ge} and the absolute value of the transition moment $|\vec{M}_{ge}|$. In figure 2.33 $|\vec{M}_{ge}|$ of the dyes versus their λ_{max}^{abs} was plotted. Although the pattern is quite weird, some generalities were found. In average the MSQs (●) and the BSQs (■) were about on the same level. Whereas the TSQs (▼) have the highest $|\vec{M}_{ge}|$ values. However MSQs, all tilted bridged

Table 2.7: Summary of the optical properties of all targeted molecules measured in chloroform.

entry	G_{ge} [m ²]	A_{ge} [s ⁻¹]	B_{eg} [m·kg ⁻¹]	f_{ge} [-]	$ \vec{M}_{ge} $ [Debey]
MSQ 8	$6.92 \cdot 10^{-21}$	$1.94 \cdot 10^{+08}$	$3.13 \cdot 10^{+21}$	1.2	13
MSQ 9	$5.45 \cdot 10^{-21}$	$1.39 \cdot 10^{+08}$	$2.46 \cdot 10^{+21}$	0.9	11
MSQ 10	$1.20 \cdot 10^{-20}$	$2.87 \cdot 10^{+08}$	$5.42 \cdot 10^{+21}$	2.0	17
MSQ 11	$8.43 \cdot 10^{-21}$	$2.13 \cdot 10^{+08}$	$3.81 \cdot 10^{+21}$	1.4	14
MSQ 12	$1.01 \cdot 10^{-20}$	$2.37 \cdot 10^{+08}$	$4.55 \cdot 10^{+21}$	1.7	16
BSQ 13	$1.64 \cdot 10^{-20}$	$3.63 \cdot 10^{+08}$	$7.40 \cdot 10^{+21}$	2.7	20
BSQ 15	$7.52 \cdot 10^{-21}$	$1.69 \cdot 10^{+08}$	$3.40 \cdot 10^{+21}$	1.2	13
BSQ 20	$7.21 \cdot 10^{-21}$	$1.68 \cdot 10^{+08}$	$3.26 \cdot 10^{+21}$	1.2	13
BSQ 19	$8.39 \cdot 10^{-21}$	$1.89 \cdot 10^{+08}$	$3.80 \cdot 10^{+21}$	1.4	14
BSQ 17	$7.71 \cdot 10^{-21}$	$1.44 \cdot 10^{+08}$	$3.49 \cdot 10^{+21}$	1.2	14
BSQ 14	$6.58 \cdot 10^{-21}$	$1.16 \cdot 10^{+08}$	$2.98 \cdot 10^{+21}$	1.0	13
BSQ 16	$3.88 \cdot 10^{-21}$	$6.85 \cdot 10^{+07}$	$1.76 \cdot 10^{+21}$	0.6	10
BSQ 18	$1.39 \cdot 10^{-20}$	$2.46 \cdot 10^{+08}$	$6.30 \cdot 10^{+21}$	2.1	18
BSQ 27	$3.64 \cdot 10^{-21}$	$4.66 \cdot 10^{+07}$	$1.65 \cdot 10^{+21}$	0.5	9
TSQ 21	$1.27 \cdot 10^{-20}$	$2.66 \cdot 10^{+08}$	$5.73 \cdot 10^{+21}$	2.0	17
TSQ 22	$1.62 \cdot 10^{-20}$	$3.50 \cdot 10^{+08}$	$7.33 \cdot 10^{+21}$	2.6	20
TSQ 23	$2.16 \cdot 10^{-20}$	$4.64 \cdot 10^{+08}$	$9.79 \cdot 10^{+21}$	3.5	23
TSQ 24	$2.65 \cdot 10^{-21}$	$5.89 \cdot 10^{+07}$	$1.20 \cdot 10^{+21}$	0.4	8
TSQ 25	$1.73 \cdot 10^{-20}$	$3.04 \cdot 10^{+08}$	$7.84 \cdot 10^{+21}$	2.6	20
TSQ 26	$1.56 \cdot 10^{-20}$	$2.42 \cdot 10^{+08}$	$7.04 \cdot 10^{+21}$	2.2	19

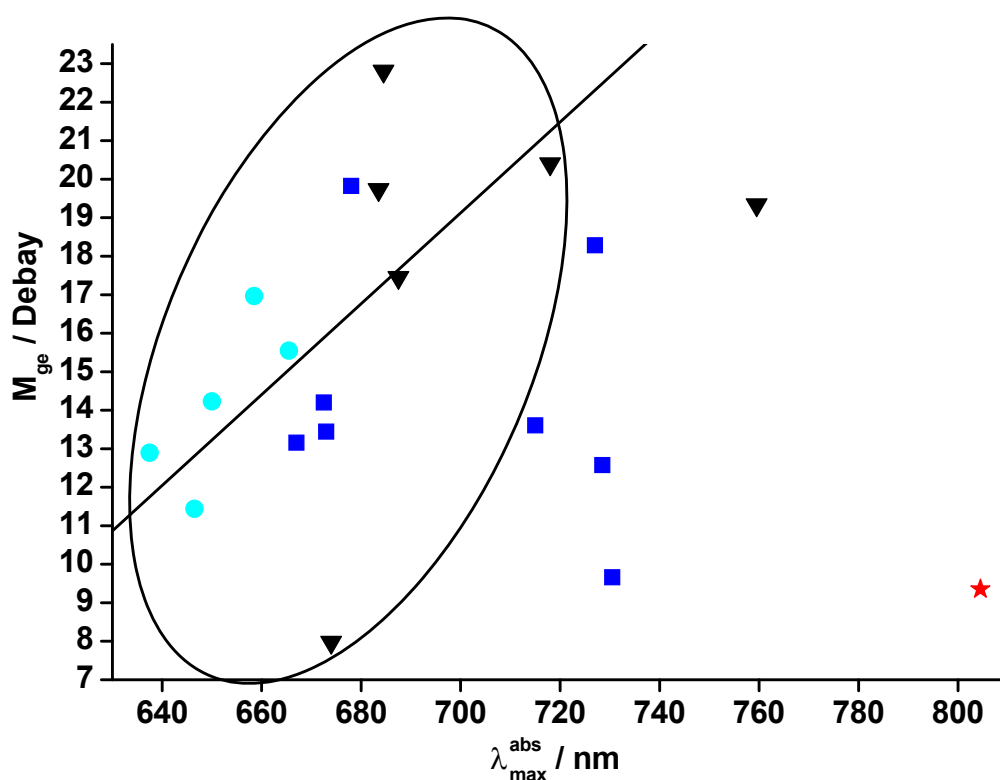


Figure 2.33: Plot of $|\vec{M}_{ge}|$ versus λ_{max}^{abs} from chloroform solution of the MSQs **8**, **9**, **10**, **11** and **12** (●), BSQs **13**, **15**, **20**, **19**, **17**, **14**, **16** and **18** (■), TSQs **21**, **22**, **23**, **24**, **25** and **26** (▼) and the special BSQ **27** (★). Data points in the oval were MSQs and BSQs and TSQs with tilted bridges. Linear fit relies on the data in the oval with $R^2 = 0.59$. Outside the oval were BSQs and TSQs with planar bridges.

BSQs and all tilted bridged TSQs were fitted linearly with $R^2 = 0.59$ (data points in the oval). Those values followed the theory of Kiprianov, since as a basic rule the higher the λ_{max}^{abs} value the higher the $|\vec{M}_{ge}|$ value was. However, the other dyes outside the oval were BSQs and TSQs with planar bridges, which seemed to disagree with the linear fitted tendency. Also the position of the super flat BSQ **27** (★) was unexpected. Since the calculation of the $|\vec{M}_{ge}|$ values depended on the weighting of the sample of the dyes, their errors also depended on each other. It was estimated that the error for $|\vec{M}_{ge}|$ is 25% which explains the variance of the data points in the oval. However, it is not sufficient to explain the rather low $|\vec{M}_{ge}|$ values for the data points outside the oval. Therefore, it is postulated, that in the planar bridged squaraines an additional parameter of electronic nature influences the dye-dye interaction. Furthermore, it is postulated that the planar bridged squaraines with more than one chromophore have a decreased transition moment because the coupling is so intense, that the chromophore

units were somehow fused and thereby a new single dye unit emerged. This postulate can be confirmed or contradicted by the calculation of the molecular orbitals, which will be discussed in section 2.2.4. To verify the relative position of the data points in figure 2.33, the $|\vec{M}_{ge}|$ values were calculated with equation 1.10 on page 3 with the help of the λ_{max}^{abs} and λ_{max}^{em} in different solvents, which is discussed in the next section.

2.2.2 Solvatochromy

Solvatochromy describes the slightly different absorption behavior of a homogeneously dissolved molecule in different solvents, due to the solute-solvent interaction based on polar attraction. For the determination of the relation how the solvent polarity is linked to the polarity of the solute several different correlations were found and published. Tatikolov et al. summarized some of them with the help of the structure homologue reference squaraine dye **8** [62]. He found that the Dimroth-Richardt's E_T value and also the solvent parameter π^* by Kamlet-Taft plotted versus the maximal absorption wavenumber $\tilde{\nu}_{max}^{abs}$ in 22 different solvents gave $R^2 < 0.3$ [62]. In conclusion, both solvent parameters were determined with a set of uncharged dyes whereas squaraines were permanently charged. Therefore, the solute-solvent interaction did not only consist of polar attractions and so the simple linear correlation based on the two named parameters was invalid. Tatikolov et al. also mentioned two refractive index (n_D^{20}) based functions for the correlation with $\tilde{\nu}_{max}^{abs}$. One was the Bayliss function 2.21:

$$f_{Bayliss}(n_D^{20}) = \frac{(n_D^{20})^2 - 1}{2 \cdot (n_D^{20})^2 + 1} \quad (2.21)$$

and the second one was similar to it, called the Lorentz-Lorenz function 2.22:

$$f_{Lorentz-Lorenz}(n_D^{20}) = \frac{(n_D^{20})^2 - 1}{(n_D^{20})^2 + 2} \quad (2.22)$$

Both functions gave a reasonable correlation coefficient of about 0.89 [62]. Also the corresponding functions where $(n_D^{20})^2$ is replaced by the dielectric constant (ϵ_s) of the solvent gave R^2 values in the same range [62]. A better correlation of 0.93 was achieved with the Lippert parameter (Δf , eq. 2.23) in terms of the Bayliss-Ooshika-McRae theory which he used in the argumentation of the postulated quadrupole moment in squaraines

in different mixtures of dioxane and water [62].

$$\Delta f = \frac{\epsilon_s - 1}{2 \cdot \epsilon_s + 1} - \frac{(n_D^{20})^2 - 1}{2 \cdot (n_D^{20})^2 + 1} \quad (2.23)$$

Albeit Tatikolov et al. even made more different plots for the correlation of the squaraine dye with the solvent. They ignored the fact that one cannot treat all solvents in the same manner [62].

In this work the solvatochromic effect was determined with ten solvents: decaline, dichloromethane, chloroform, toluene, chlorbenzene, 1,2-dichlorbenzene, acetone, ethanol, *N,N*-dimethylformamide and dimethylsulfoxide. For this solvents Δf was calculated and plotted versus the measured $\tilde{\nu}_{max}^{abs}(\Delta f)$ of the dyes. This function correlated for the data of the reference dye **8** with R^2 of 0.26. But this moderate value was dramatically improved by subdividing the solvents into three groups:

- Group A, solvents with an aromatic system as toluene, chlorbenzene and 1,2-dichlorbenzene.
- Group B, solvents containing an oxygen atom as acetone, ethanol, *N,N*-diemthylformamide and dimethylsulfoxide.
- Group C, consisting neither of an aromatic system nor of an oxygen atom as decaline, dichloromethane and chloroform.

This segmentation was justified by the following arguments: π - π interactions occur between aromatic solvents and the dye system, which is a stronger interaction than the Van-der-Waals interaction of the dye system with apolar solvents. The oxygen atom containing solvents were grouped according to the behavior of iodine. Iodine solutions are violet in solvents without any oxygen atoms and brown when the solvent contains them, due to the coordination of the iodine to the electron pairs of the oxygen atom. In figure 2.34 the function $\tilde{\nu}_{max}^{abs}(\Delta f)$ of MSQ **8** for each group and their linear fit were displayed. R^2 from group A in black was 0.87, group B in red and C in green were both 0.98. Indeed, after the novel segmentation three very nice linear relations between the solute property $\tilde{\nu}_{max}^{abs}$ and the solvent Lippert paramtert Δf were found. This was proven for all target dyes (data not shown).

The parameter Δf was actually used in the Ooshika-Lippert-Mataga-Equation 2.24 as a factor to connect the Stoke's shift (in wave numbers) with the difference of the

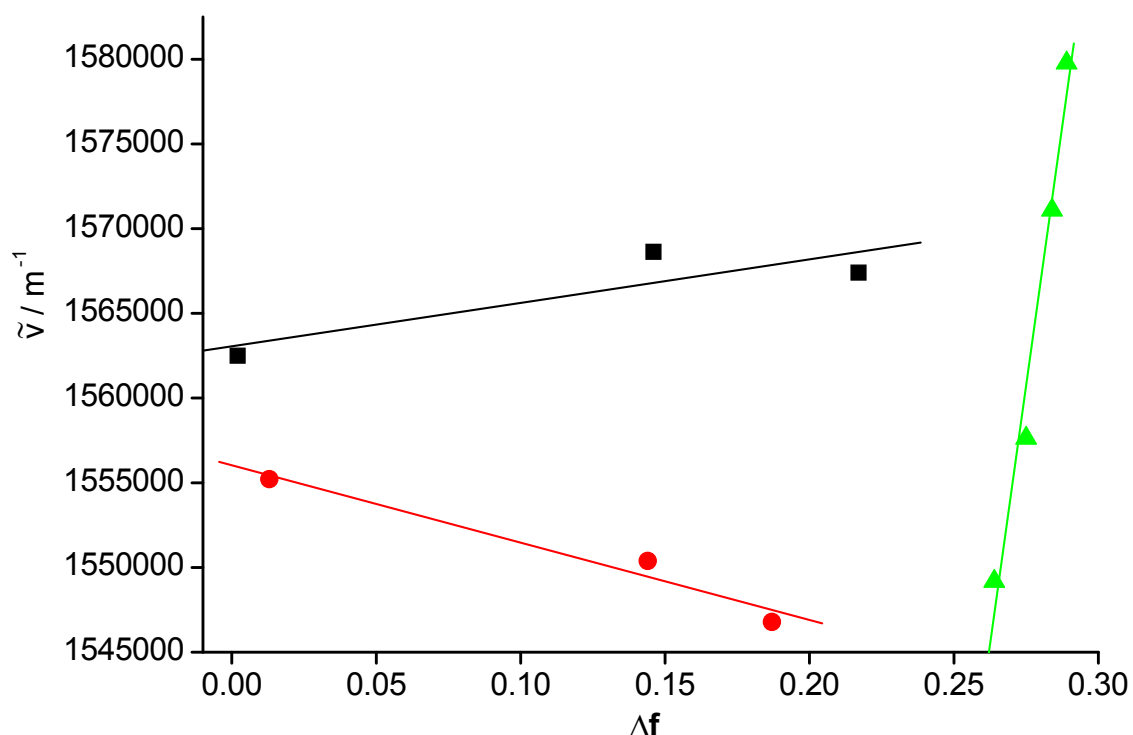


Figure 2.34: $\tilde{\nu}_{max}^{abs}(\Delta f)$ of MSQ 8, group A (■), group B (●) and group C (▼) and their linear fit.

static electric dipole moments of the ground state and the excited state $\mu_{el,g}$ and $\mu_{el,e}$ [66, 67, 8].

$$\Delta\tilde{\nu} = \tilde{\nu}_{max}^{abs} - \tilde{\nu}_{max}^{em} = \frac{2 \cdot \Delta f}{h \cdot c \cdot a_r^3} \cdot (\mu_{el,e} - \mu_{el,g})^2 \quad [m^{-1}] \quad (2.24)$$

a_r refers to the Onsager active radius which is defined in equation 2.25 as the spherical radius with the same volume and mass of one molecule, M_R refers to the molar mass of the dye and ρ to the estimated density of the dye crystal (1 g/mL). a_r of all the dyes were listed in table 2.8.

$$a_r = \sqrt[3]{\frac{3 \cdot M_R}{4 \cdot \pi \cdot \rho \cdot N_A}} \quad [m] \quad (2.25)$$

Furthermore, Ooshika-Lippert-Mataga-Equation 2.24 was split in order to determine $\tilde{\nu}_{max}^{abs}$ (eq. 2.26) and $\tilde{\nu}_{max}^{em}$ (eq. 2.27) separately [68, 8]. The splitting of the formula was possible because some factors as the effective reaction field and the dispersion force

could be neglected.

$$\tilde{\nu}_{max}^{abs} = \frac{2\mu_{el,g}(\mu_{el,g} - \mu_{el,e})}{h \cdot c \cdot a_r^3} \cdot \Delta f + C \quad [m^{-1}] \quad (2.26)$$

$$\tilde{\nu}_{max}^{em} = \frac{2\mu_{el,e}(\mu_{el,e} - \mu_{el,g})}{h \cdot c \cdot a_r^3} \cdot \Delta f + C \quad [m^{-1}] \quad (2.27)$$

Herewith $\mu_{el,g}$ and $\mu_{el,e}$ can be calculated by the slope p of group C in the plot $\tilde{\nu}_{max}^{abs}(\Delta f)$ and the slope q of group C in the plot $\tilde{\nu}_{max}^{em}(\Delta f)$ according to the following formulas [68,8]:

$$\mu_{el,g} = -\frac{p}{q} \cdot a_r^{3/2} \cdot \sqrt{\frac{q^2 \cdot h \cdot c}{2 \cdot (p - q)}} \quad [C \cdot m] \quad (2.28)$$

$$\mu_{el,e} = a_r^{3/2} \cdot \sqrt{\frac{q^2 \cdot h \cdot c}{2 \cdot (p - q)}} \quad [C \cdot m] \quad (2.29)$$

In fact, only the data from group C were used, because several effects could be neglected and the lowest distortion of the solute-solvent interaction was in group C. $\mu_{el,g}$ and $\mu_{el,e}$ were calculated for all dyes and listed in table 2.8.

As already indicated in equation 1.10 in the introduction, the weighted sample based $|\vec{M}_{ge}|$ can be compared with the UV/vis spectrum based values of $\mu_{el,g}$ and $\mu_{el,e}$. Therefore the linear combination coefficients a_g and a_e were estimated. Since a quantum leap is much faster than the life time of the excited state, a step function from the ground state $|g\rangle$ to the excited state $|e\rangle$ was assumed for the observable moment of absorption. Furthermore, in the moment of absorption the molecule is 50% in $|g\rangle$ and 50% in $|e\rangle$. Consequently, a_g and a_e were both set to 0.5. So the transition moment calculated over the solvatochromic effect was named μ_{total} . Because of the made simplification in the equation leading to the values of $\mu_{el,g}$ and $\mu_{el,e}$ an empirical constant summand was introduced for every dye which was actually the averaged difference of μ_{total} and $|\vec{M}_{ge}|$ and amounted 13.7 D. The corrected $\mu_{total,corrected}$ was determined by the equation 2.30:

$$\mu_{total,corrected} = \mu_{total} + 13.7 = 0.5 \cdot \mu_{el,g} + 0.5 \cdot \mu_{el,e} + 13.7 \quad [Debye] \quad (2.30)$$

For a better comparison the $|\vec{M}_{ge}|$ values were also listed next to the $\mu_{total,corrected}$ values of the dyes in the table 2.8 and the $|\vec{M}_{ge}|$ appear as \times in the figure 2.35. In this figure the data points of the squaraine dyes with tilted bridges and the MSQs (■) were surrounded

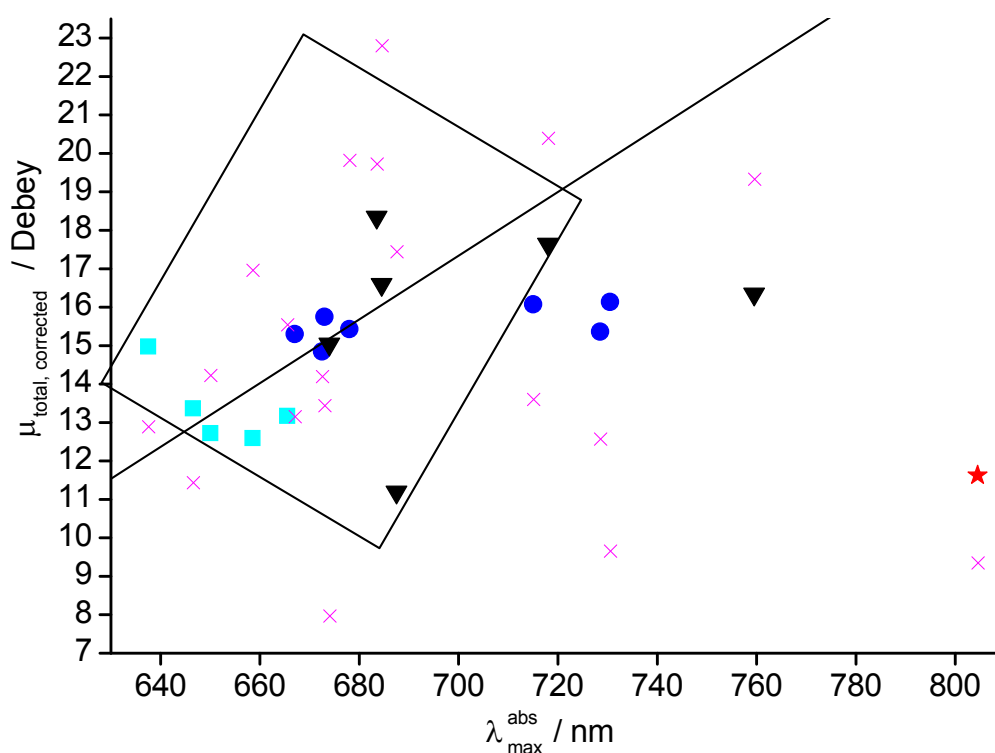


Figure 2.35: Plot of $\mu_{total,corrected}$ calculated from the solvatochromic effect versus λ_{max}^{abs} in chloroform of the MSQs **8**, **9**, **10**, **11** and **12** (■), BSQs **13**, **15**, **20**, **19**, **17**, **14** and **16** (●), TSQs **21**, **22**, **23**, **24**, **25** and **26** (▼) and the special BSQ **27** (★). Data points in the quad were MSQs and BSQs and TSQs with tilted bridges. Linear fit relays on the data in the oval with $R^2 = 0.490$. Outside the quad were BSQs and TSQs with planar bridges.

by the quad. These data were fitted linearly so that in general with increasing λ_{max}^{abs} also $\mu_{total,corrected}$ increases which is according to the Kiprianov theory and very similar to $|\vec{M}_{ge}|$. The data points of all BSQs and TSQs with a planar linking synthon were outside the quad. Moreover, these data showed a largely reduced transition moment compared to their absorption maximum, which proved the correct tendency of the $|\vec{M}_{ge}|$ values and underlined the thereby derived postulate.

2.2.3 Electrochemical Properties

Cyclic voltammetry was performed to determine the electrochemical properties in order to find the answers to the following questions whether the electrochemical band gap

Table 2.8: The Onsager radius a_r and the determination the static electric dipole moments of the ground and excited state and the corrected transition dipole moment $\mu_{total,corrected}$ by the Ooshika-Lippert-Mataga-Equation in comparison with the transition moment $|\vec{M}_{ge}|$ calculated over the peak area.

dye	a_r	$\mu_{el,g}$	$\mu_{el,e}$	$\mu_{total,corrected}$	$ \vec{M}_{ge} $
MSQ 8	$6.3 \cdot 10^{-10}$	2.5	0.1	15	13
MSQ 9	$6.3 \cdot 10^{-10}$	-9.9	9.3	13	11
MSQ 10	$6.8 \cdot 10^{-10}$	-3.6	1.4	13	17
MSQ 11	$5.9 \cdot 10^{-10}$	-2.2	0.3	13	14
MSQ 12	$6.1 \cdot 10^{-10}$	-4.8	3.7	13	16
BSQ 13	$7.9 \cdot 10^{-10}$	-0.5	4.0	15	20
BSQ 15	$8.5 \cdot 10^{-10}$	0.8	3.4	16	13
BSQ 19	$8.4 \cdot 10^{-10}$	-3.5	5.8	15	14
BSQ 20	$8.1 \cdot 10^{-10}$	-3.7	7.0	15	13
BSQ 17	$7.4 \cdot 10^{-10}$	-0.8	5.5	16	14
BSQ 14	$7.7 \cdot 10^{-10}$	-1.2	4.5	15	13
BSQ 16	$7.8 \cdot 10^{-10}$	-1.4	6.3	16	10
BSQ 27	$7.5 \cdot 10^{-10}$	-12.8	8.6	12	9
TSQ 21	$9.6 \cdot 10^{-10}$	-9.5	4.5	11	17
TSQ 22	$1.1 \cdot 10^{-9}$	5.4	3.9	18	20
TSQ 23	$1.2 \cdot 10^{-9}$	-2.2	8.0	17	23
TSQ 24	$6.5 \cdot 10^{-10}$	-1.8	4.5	15	8
TSQ 25	$9.3 \cdot 10^{-10}$	-4.7	12.6	18	20
TSQ 26	$8.5 \cdot 10^{-10}$	-0.4	5.7	16	19

ΔE_{el} is interrelated with the optical band gap ΔE_{opt} , whether the values of the oscillator strength f_{ge} are comparable with the values of the number of transferred electrons in the reduction and oxidation process ($Z_{red/ox}$) and whether the redox potentials are individually affected by the dye-dye interaction. As hitherto the analysis procedure was explained with the help of the reference dye **8**. In figure 2.36 the cyclic voltammogram of the neat solvent *N,N*-dimethylformamide (—) and the reference dye **8** (—) are displayed. The electrochemical band gap ΔE_{el} was determined by the difference of the values of the first reduction and oxidation potential (E_{red}^1 respectively E_{ox}^1). For the reference dye **8** E_{ox}^1 was 0.75 V and E_{red}^1 was -0.87 V under applied conditions and after calibration versus normal hydrogen electrode (NHE) [69]. The first redox potentials ($E_{red/ox}^1$) were defined as the average of their cathodic and anodic peak potentials

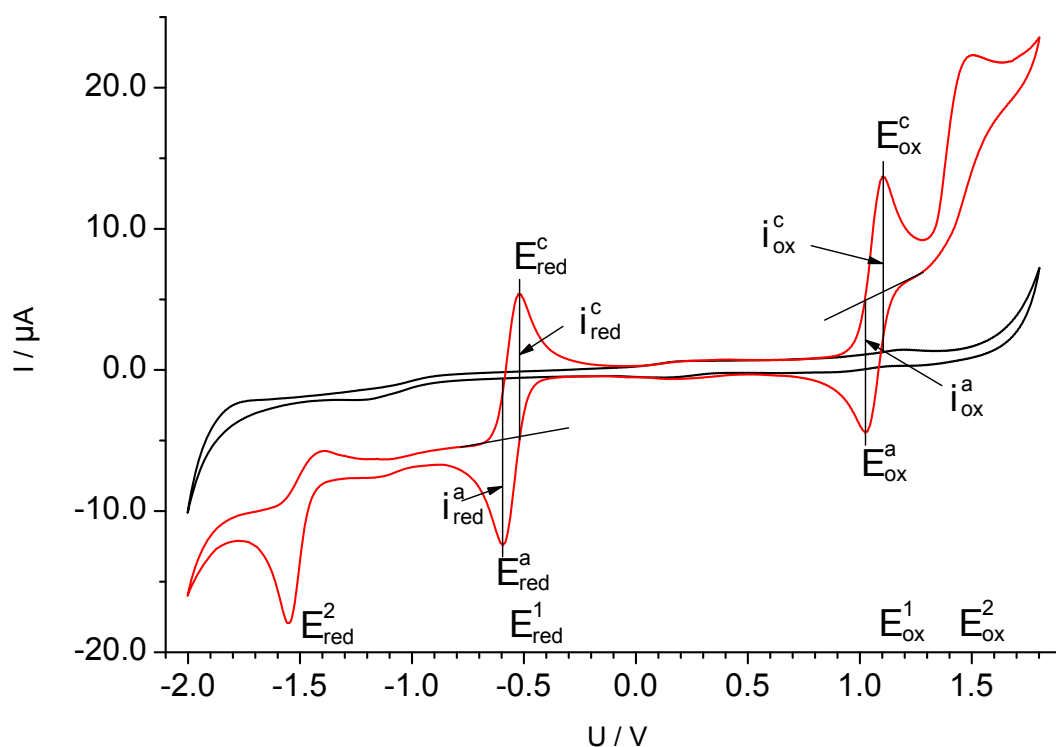


Figure 2.36: Cyclic voltammogram of the reference dye **8** (—) and neat (—). Conditions: $c(\mathbf{8})$: 1.16 mM, in *N,N*-dimethylformamide with 0.10 M tetrabutylammonium perchlorate, Au rotating disc working electrode with 50 rpm, Pt counter electrode and Ag/AgCl reference electrode in 0.10 M tetrabutylammonium chlorid in *N,N*-dimethylformamide, scanning rate was 100 mV/s.

($E_{red/ox}^c$ and $E_{red/ox}^a$) as shown in equation 2.31 [69].

$$E_{red/ox}^1 = \frac{E_{red/ox}^c + E_{red/ox}^a}{2} \quad [V] \quad (2.31)$$

The electrochemical band gap ΔE_{el} of the reference dye **8** was 1.62 V, which was about 260 mV smaller than the optical band gap ΔE_{opt} of 1.88 V measured in *N,N*-dimethylformamide (1.92 V in chloroform table 2.2). Additionally, the number of transferred electrons for the reduction z_{red} and the oxidation z_{ox} were calculated by the modified Nernst equation 2.32 [69] where R is the universal gas constant, T the absolute temperature and F the Faraday constant with a scanning rate of 100 mV/s. An approximation was made for room temperature of 25 °C.

$$z_{red/ox} = \frac{R \cdot T}{F \cdot (|E_{red/ox}^c - E_{red/ox}^a|)} \approx \frac{59.2 \text{ mV}}{|E_{red/ox}^c - E_{red/ox}^a|} \quad [-] \quad (2.32)$$

The values of z_{ox} and z_{red} for MSQ **8** were about 0.8, indicating a not complete reduction and oxidation process. Furthermore, the quotient of the cathodic and anodic peak height $i_{red/ox}^a/i_{red/ox}^c$ per redox step was measured (Equation 2.33 [69]). If the quotient reaches unity then the process is reversible. If the quotient is close to unity the process is called quasi reversible, because of the diffusion of reduced or oxidized dye from the boundary layer into the bulk solution. The process is irreversible if the quotient is much different from unity, which is caused by reactions with the solvent, decomposition or elimination of the reduced and oxidized dye species.

$$\frac{i_{red/ox}^a}{i_{red/ox}^c} \begin{cases} = 1 & \text{reversible process} \\ \approx 1 & \text{quasi reversible process} \\ \ll 1 & \text{irreversible process} \end{cases} \quad (2.33)$$

For the reference dye **8** the quotient was calculated to be 0.77 for the oxidation and 0.89 for the reduction, indicating quasi reversible processes.

The dyes were measured in *N,N*-dimethylformamide (DMF) because DMF is electrochemically stable in a very wide potential range (−2.0 to +1.8 V) and the reported value of the ferrozene calibration versus NHE was measured therein [69]. For some dyes the solvent was changed to chloroform due to their poor solubility (<1 mM) in *N,N*-dimethylformamide. The data of the cyclic voltammogram were analysed having a scanning rate of 100 mV/s and they were tabulated in table 2.9. A linear relationship of the optical band gap ΔE_{opt} and the electrochemical band gap ΔE_{el} was reported for over fifty cyanine dyes by Loutfy et al. (eq. 2.34 [70]):

$$\Delta E_{opt} = \Delta E_{el} + C_{Loutfy} \quad (2.34)$$

Loutfy et al. determined the averaged constant \overline{C}_{Loutfy} to be +0.35 V [70]. Here, for the squaraine dyes measured in *N,N*-dimethylformamide the correction constant C_{opt-el} was determined by the individual difference of ΔE_{opt} and ΔE_{el} . The averaged constant \overline{C}_{Loutfy} for the squaraines was calculated to be +0.20 V with a variance of ± 0.056 V. This relation connects the optical property with the electrochemical one.

In order to study the influence of the dye-dye interaction, the first reduction potential E_{red}^1 and the first oxidation potential E_{ox}^1 of the in *N,N*-dimethylformamide measured dyes (Table 2.9) were plotted versus their electrochemical band gap ΔE_{el} (Figure 2.37). The data points for the first oxidation potential E_{ox}^1 in Volt (black) and the one for the first reduction potential E_{red}^1 in Volt (red) were linearly fitted resulting in function 2.35

Table 2.9: Summary of the electrochemical data of the squaraines and the comparison with the optical band gap.

entry	solv.	E_{ox}^1 [V]	Z_{ox} [-]	$\frac{i_{ox}^a}{i_{ox}^c}$ [-]	E_{red}^1 [V]	Z_{red} [-]	$\frac{i_{red}^a}{i_{red}^c}$ [-]	ΔE_{el} [V]	ΔE_{opt} [V]	C_{opt-el} [mV]
MSQ 8	DMF	0.75	0.78	0.77	-0.87	0.81	0.89	1.62	1.88	0.26
MSQ 9	DMF	0.75	0.81	0.83	-0.86	0.79	0.87	1.61	1.84	0.24
MSQ 10	CHCl ₃	0.75	0.07	0.46	-	-	-	-	-	-
MSQ 11	DMF	0.74	0.83	0.90	-0.86	0.83	0.90	1.59	1.84	0.25
MSQ 12	DMF	0.73	0.79	0.83	-0.85	0.87	0.88	1.58	1.80	0.23
BSQ 13	DMF	0.73	0.76	0.84	-0.85	0.74	0.91	1.57	1.76	0.19
BSQ 15	DMF	0.73	0.71	0.74	-0.84	0.75	0.99	1.57	1.78	0.21
BSQ 19	DMF	0.74	0.76	0.75	-0.84	0.81	0.99	1.58	1.77	0.19
BSQ 20	DMF	0.77	0.74	0.86	-0.81	0.76	0.99	1.58	1.79	0.21
BSQ 17	CHCl ₃	0.85	0.20	0.81	-0.98	0.20	0.89	1.84	1.68	-0.16
BSQ 14	DMF	0.71	0.97	0.97	-0.82	0.58	0.92	1.53	1.63	0.10
BSQ 16	DMF	0.72	0.54	0.66	-0.82	0.67	0.85	1.54	1.63	0.09
BSQ 27	DMF	0.59	0.71	0.84	-0.72	0.97	0.63	1.31	1.49	0.18
BSQ 18	DMF	0.73	-	-	-0.73	-	-	1.47	1.65	0.18
TSQ 21	CHCl ₃	0.80	0.42	0.93	-1.05	0.37	0.69	1.85	1.74	-0.10
TSQ 24	CHCl ₃	0.92	0.53	0.64	-0.92	0.45	0.87	1.84	1.76	-0.08
TSQ 22	CHCl ₃	0.78	0.50	0.68	-1.06	0.41	0.38	1.84	1.76	-0.08
TSQ 23	CHCl ₃	0.79	0.48	0.56	-1.05	0.39	0.59	1.84	1.78	-0.06
TSQ 25	CHCl ₃	0.82	0.29	0.70	-1.03	0.30	0.53	1.85	1.64	-0.21
TSQ 26	CHCl ₃	0.80	0.70	0.72	-	-	-	-	-	-

for the oxidation with $R^2 = 0.814$ and function 2.36 for the reduction with $R^2 = 0.826$. Furthermore, according to the linear correlation of the optical and electrochemical band gap in equation 2.34 the energy of the redox potentials can be expressed by the optical band gap ΔE_{opt} .

$$E_{ox}^1 = 0.49 \cdot \Delta E_{el} - 0.033 \approx 0.49 \cdot \Delta E_{opt} - 0.131 \quad [V] \quad (2.35)$$

$$E_{red}^1 = -0.51 \cdot \Delta E_{el} - 0.033 \approx 0.51 \cdot \Delta E_{opt} + 0.069 \quad [V] \quad (2.36)$$

Conspicuously, the absolute values of functions 2.35 and 2.36 were similar. The slope of the reduction potential was a bit steeper than the one of the oxidation potential, evidencing that the influence of the aromatic π -systems and the dye-dye interactions affected the reduction slightly more than the oxidation potentials of squaraine dyes. Assuming that the size of the electric band gap ΔE_{el} in these kind of dyes can be

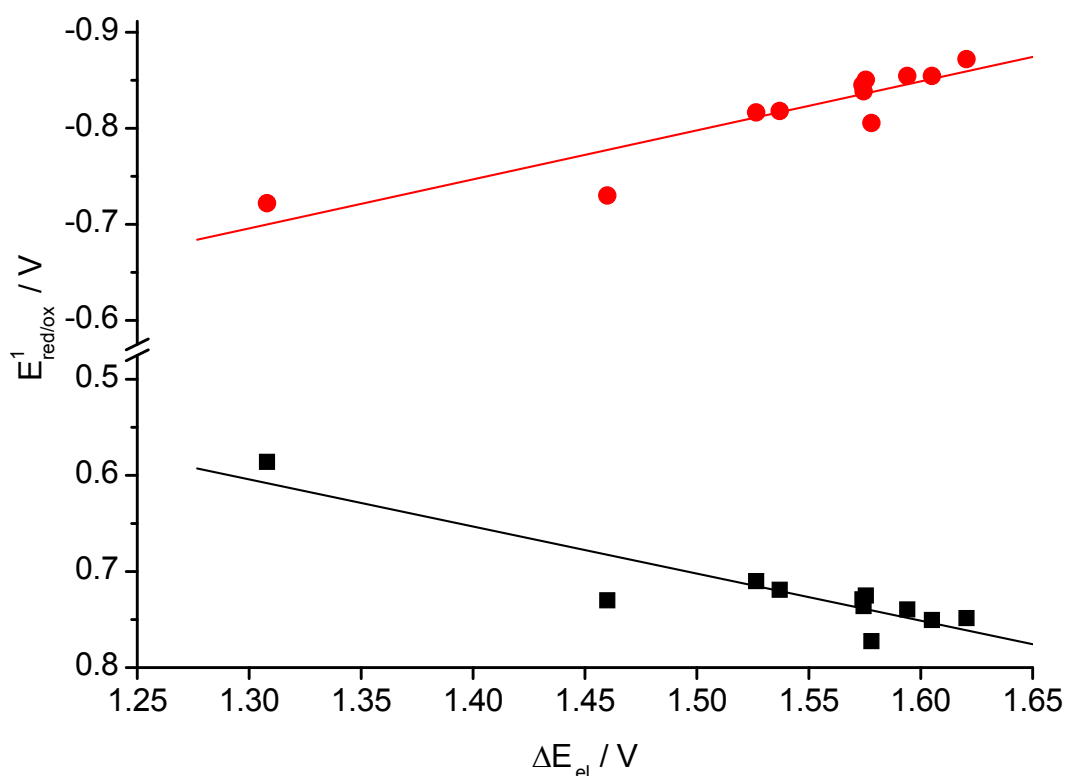


Figure 2.37: Comparison of the first oxidation potential E_{ox}^1 (■, $R^2 = 0.814$) and the first reduction potential E_{red}^1 (●, $R^2 = 0.826$) versus the electrochemical band gap ΔE_{el} of the in *N,N*-dimethylformamide measured dyes (table 2.9).

reduced to zero, the resulting Fermi energy level of a kind of metallic material would be -33 mV. This value implies a electrono-ambident property of squaraine dye radicals with a slight tendency towards the electrono-dative property [11], meaning those dyes have no preference for either being an oxidized or a reduced radical. In fact, radicals of the cyanine dyes with *3H*-indole aromatic end groups were also electrono-ambident materials [11].

The link between the electrochemical redox levels, the optical transition and the molecular orbital was explicitly explained by Loutfy et al. for the cyanine dyes [70]. The energy of the first oxidation potential E_{ox}^1 defined the energy of the ground state $|g\rangle$ and was also set as the energy level of the HOMO. To obtain the energy of the LUMO level of the ground state $|g\rangle$ three values were available: the energy of the first reduction potential E_{red}^1 , the optically excited singlet state $|e_S\rangle$ and the optically excited triplet state $|e_T\rangle$. According to Loutfy et al. the optically excited triplet state $|e_T\rangle$ was equalized identical with the calculated LUMO level, but unfortunately this energy level could not be measured. However, the energy of the first reduction potential E_{red}^1 is more

likely the one of $|e_T\rangle$ than the energy of the $|e_S\rangle$ [70]. And so it was assumed that the energy of the calculated LUMO level corresponded to the first reduction potential E_{red}^1 . In table 2.9 also the number of involved electrons during a redox process ($Z_{red/ox}$) was listed. Comparing these $Z_{red/ox}$ -values with the optical oscillator strength f_{ge} in table 2.7 on page 61 a fundamental difference was observed. The f_{ge} -values corresponded to the number of involved electrons during the optical transition and for the MSQs and the BSQs with tilted bridges at least the f_{ge} -values could be correlated with the number of chromophore units. This pointed towards nearly degenerated frontier orbitals due to the weak chromophore-chromophore coupling. In contrast, none of the dyes showed $Z_{red/ox}$ -values bigger than one. With the help of a simple model of frontier orbital levels (Figure 2.38) this apparent contradiction was explained. Firstly, the MSQs with one chromophore unit behaved as expected. Upon photon excitation one electron from the HOMO of the ground state $|g\rangle$ moved to the LUMO resulting in the singlet excited state $|e_S\rangle$. And in the case of the electrochemical reduction the additional electron was added into the LUMO level of $|g\rangle$ resulting in the reduced state $|red\rangle$ of the dye. Secondly, if the BSQs showed a small dye-dye interaction as it is the case for the tilted bridges then linear combination of the two chromophores resulted in nearly degenerated molecular orbitals. Therefore, upon photon excitation both chromophores can be excited individually by roughly the same energy, resulting in a higher value of the oscillator strength f_{ge} . However, each chromophore in the BSQs with small dye-dye interaction was reduced individually and step wise, resulting in a single electron reduction at the first reduction potential. This explanation was also valid for the TSQs with tilted bridges. Thirdly, BSQs with planar bridges showed a larger coupling which led to the creation of a single dye system with a reduced band gap. This new dye system behaved as the one of the MSQs, which explained the reduced values of the oscillator strength f_{ge} for these kind of dyes. Since the new dye system was a linear combination of the squaraine chromophore units, its frontier orbitals should be distributed over the entire molecule with a certain electron density distribution on the bridge which was investigated and reported in the next section.

2.2.4 Analysis of the dye structure - molecular modeling

As a result of the optical and electrochemical analysis it was assumed that the BSQs with a tilted linker inbetween the two chromophore units have nearly degenerated

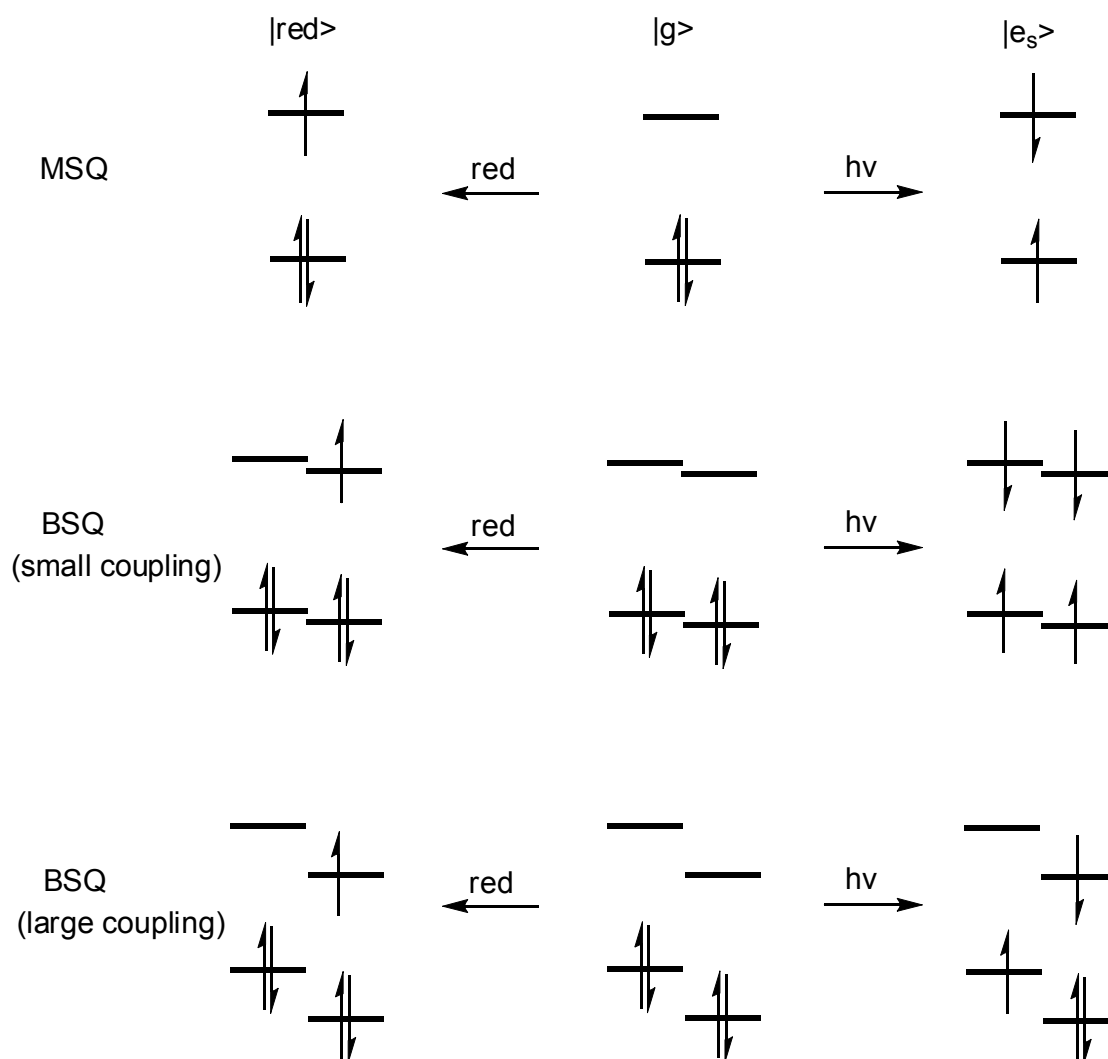


Figure 2.38: Model of the electron distribution of the frontier orbitals upon electrochemical reduction and photon excitation from the ground state.

energy levels with a small coupling. Due to the more intense dye-dye coupling in the planar linked BSQs a new single dye system was expected, which is visible in a different constellation of the frontier orbital density. So as to prove that, molecular modeling of the structure of the dyes was performed in order to investigate the distribution of the frontier orbitals in the molecule. For simplification of the calculations the alkyl chains were reduced to methyl synthons. The drawn molecules were then pre-optimization with the help of the molecular mechanics force field method MM2 using the program package ChemBioOffice 2008. Subsequently, a list of the Cartesian coordinates of the atoms served as the input for the geometry optimization of the molecular structure in

the parallelized NWChem 5.1 program [71, 72] on Ipazia – the Linux computing cluster at Empa [41]. According to literature [32] the reported calculation settings used Density Functional Theory (DFT, [73]) with B3LYP functional and 6-31G* as the basis set. In an additional calculation step, the energy of the geometry optimized molecular structure was calculated using the same settings in the NWChem 5.1 program. The programming and monitoring of the calculations on Ipazia as well as the analysis of the NWChem output files were performed by Dr. Thomas Geiger. For the illustration of the molecular structure and the calculated frontier orbitals the program Jmol open-source Java viewer for chemical structures was used [74]. With the help of the jmol-program also the torsion angle ϕ between the chromophore unit and the tilted bridge in the phenylene bridged BSQ **13**, fluorene bridged BSQ **15**, alkoxy phenylene bridged BSQ **19** and tetra fluoro phenylene bridged BSQ **20** were measured and listed in table 2.10. These ϕ values were different from the prior assumed value of 44.4° from the diphenyl molecule which was expected since the calculation was performed in vacuum. However, the larger torsion angle in the alkoxy phenylene bridged BSQ **19** and the tetrafluoro phenylene bridged BSQ **20** compared to the plain phenylene bridged BSQ **13** explained the lower values of the absorption maximum for these dyes according to the structure-property relation formula 2.20 on page 59. This evidence implied that the electronic structure of a tilted bridge might have a smaller impact than the torsion angle.

For a better illustration the frontier orbitals cut off was set to 2% for all dyes. In figure 2.39 the plain optimized structure (top), the LUMO (middle) and the HOMO (bottom) were grouped for the phenylene bridged BSQ **13** (top left), the fluorene bridged BSQ **15** (top right), the alkoxy phenylene bridged BSQ **19** (bottom left) and the tetrafluoro phenylene bridged BSQ **20** (bottom right). For these four BSQs the weight of the orbital clouds in the frontier orbitals were always equally distributed among the two chromophore units. The measurable impact of the aromatic end group indole derivatives was evidenced by the small electron density contributions in their HOMO and LUMO. However, the electron probability density in the frontier orbitals located on the linker

Table 2.10: Measured torsion angle ϕ between the chromophore unit and the tilted bridge in the geometry optimized structure of the BSQs.

BSQ	ϕ	$\cos^2(\phi)$
13	36°	0.655
15	37°	0.638
19	41°	0.570
20	41°	0.570

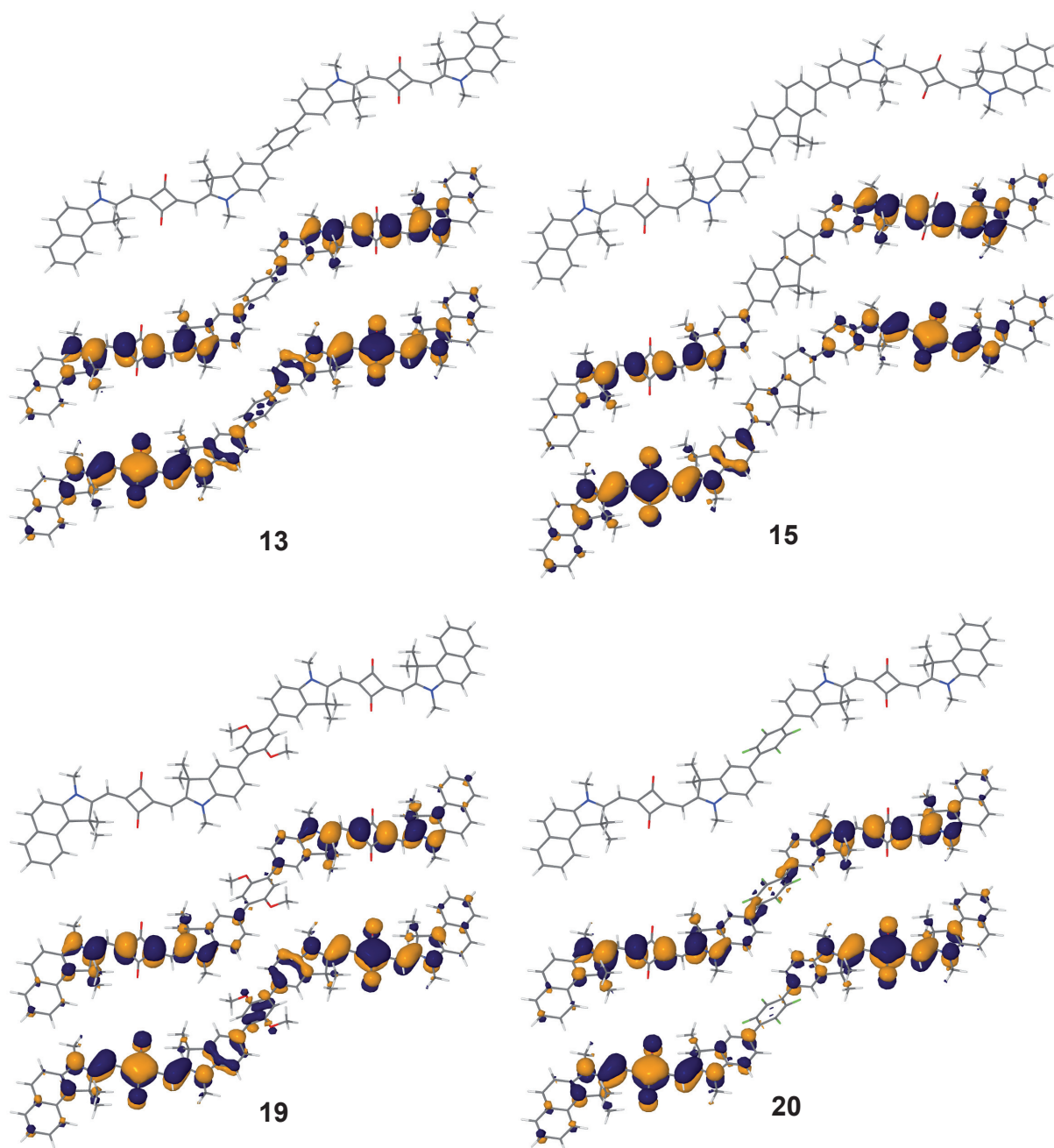


Figure 2.39: The optimized dye structure (top), the LUMO (middle) and the HOMO (bottom) were grouped for the phenylene bridged BSQ **13** (top left), the fluorene bridged BSQ **15** (top right), the alkoxy phenylene bridged BSQ **19** (bottom left) and the tetrafluoro phenylene bridged BSQ **20** (bottom right).

synthon is barely measurable, except in the HOMO of the alkoxy bridged BSQ **19** and

the LUMO of the tetrafluoro phenylene bridged BSQ **20**. The constellation of the frontier orbital electron probability density in the BSQs with tilted linkers underlined the priorly made educated guess that in these dyes the chromophores were nearly individual and showed quite degenerated energy states.

The more interesting question to be answered was whether the planar linked BSQs had a different constellation of the frontier orbital electron probability density. Therefore, the plain optimized structure (top), the LUMO (middle) and the HOMO (bottom) were grouped for the naphthalene bridged BSQ **17** with indole end groups (top left), the naphthalene bridged BSQ **14** (top right), the anthracene bridged BSQ **16** (bottom left) and the flat bridged BSQ **27** (bottom right) were displayed in figure 2.40. Indeed, the frontier orbitals of the naphthalene and anthracene bridged BSQs indicated a fusion of the two chromophore systems. However, the biggest part of the electron probability density was still at the center of each chromophore. So one can describe these three BSQs as the two strongly coupled but individual chromophores or as an incomplete fusion of the two squaraine dye units. Remarkably, the characteristics of the nodal planes through the LUMO of the planar linked BSQs implicated an over all conjugated system, especially over the five membered ring systems next to the center part. The HOMO of the flat bridged BSQ **27** showed a similar orbital cloud distribution as the naphthalene and anthracene bridged BSQs. However, its LUMO suggested that a new dye system was created since the centroid of the spacial distribution of the electron probability density was calculated to be in the center of the molecule, on the bridge! It is assumed that this complete fusion of the chromophore units accounted for the reduction of the band gap according to the model in the figure 2.38 on page 74 which thereby resulted in the giant bathochromic shift of the absorption maximum.

Finally, the effect on the frontier orbitals of BSQ **18** with the slightly unsymmetrical structure was investigated. One end group was a benzo[e]indole derivative and the other one a carboxy indole. Since both end groups have the same number of π -electron pairs in line with the chromophore it was not expected that the difference between the two dye systems would be noticeable. But in fact, roughly 75% of the total spacial orbital cloud distribution of the HOMO lay on the chromophore with the benzo[e]indole end group whereas the remaining 25% were on the other side as shown in figure 2.41. Interestingly, in the LUMO the spacial distribution was exactly the opposite, which suggested an electron transfer from the HOMO of the chromophore at the benzo[e]indole end group to the LUMO of the other chromophore upon photon excitation. This transfer can be seen as intra molecular charge separation resulting

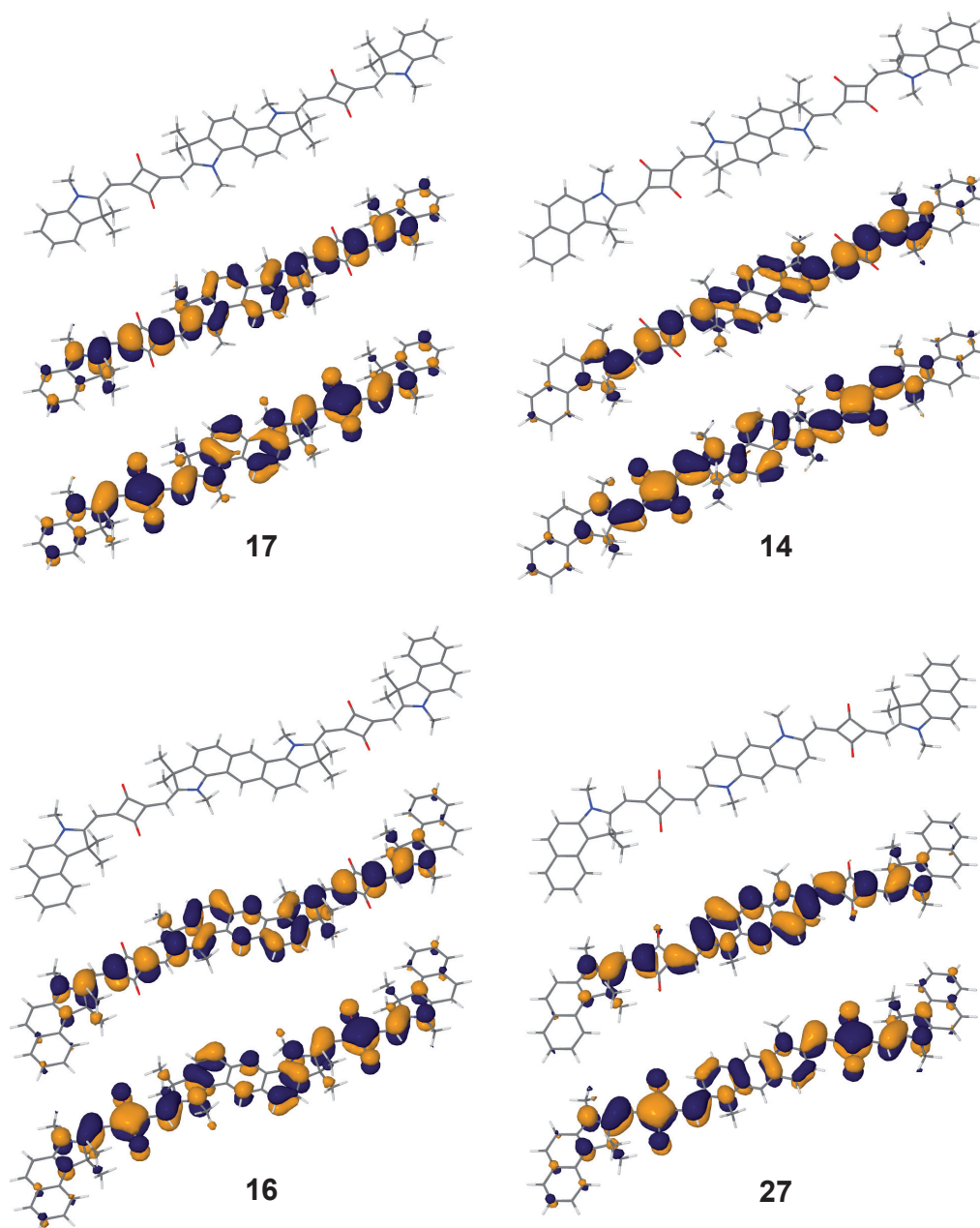


Figure 2.40: Per dye the optimized structure (top), the LUMO (middle) and the HOMO (bottom) were grouped for the naphthalene bridged BSQ with indole end groups **17** (top left), the naphthalene bridged BSQ **14** (top right), the anthracene bridged BSQ **16** (bottom left) and the flat bridged BSQ **27** (bottom right).

in a reduced dye unit at the carboxy indole end and an oxidized dye unit at the benzo[e]indole end of the molecule.

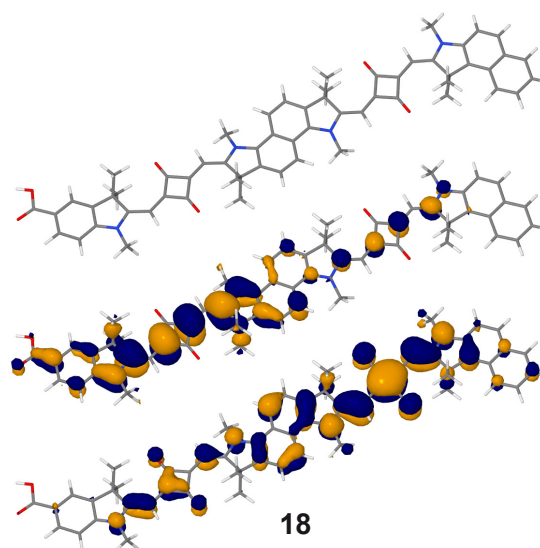


Figure 2.41: *The optimized structure (top), the LUMO (middle) and the HOMO (bottom) of the unsymmetric BSQ 18.*

2.2.5 Proof-of-concept in a dye sensitized solar cell

The calculated vectorial electron transfer, the fact that BSQ **18** possesses a carboxylic acid group and the broad and highly intense absorption band were three basic requirements for the use of this dye as a sensitizer in a dye sensitized solar cell (DSC). Therefore, a collaboration with the research group of Prof. Dr. Michael Grätzel at EPFL was intended in order to answer the question whether BSQ **18** shows the vectorial electron transfer and if this dye could be used as a NIR sensitizer for the DSC application. Next to the just mentioned three basic requirements for the use of an unsymmetric dye as a sensitizer additional conditions must be fulfilled. The fourth requirement is that after dye excitation the electron injection into the wide band gap semiconductor should be fast and efficient which requires specific electronic properties. This was proven for the squaraine dye class with **SQ01** and **SQ02** (Figure 2.42) [31,32]. Fifthly, the reduction potential of the dye has to match the titanium dioxide conduction band edge and finally the oxidation potential must be high enough to provide the necessary driving force for a fast dye regeneration by the electrolyte redox system. The latter two conditions were verified with cyclic voltammetry and is reported in section 2.2.3. Furthermore, BSQ **18** is a Ruthenium-free dye. Since ruthenium is a rather rare and expensive element any alternatives are of special interest [75, 30, 76].

The DSC device was prepared in the Grätzel group at the EPFL by Dr. Frédéric

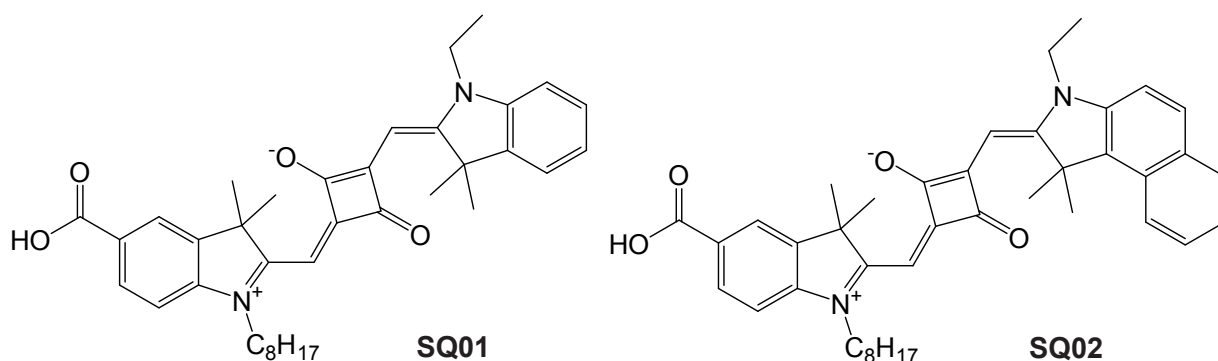


Figure 2.42: Molecular structure from **SQ01** and **SQ02** [31, 32].

Sauvage. He used their standard procedure for the cell preparation. According to it a screen-printed double layer thick film of interconnected titanium dioxide (TiO₂) particles was used as photo-anode upon NSG10 TCO glass (Nippon Sheet Glass). The first layer of 8 μm thickness and optically transparent, was composed of 20 nm particles of anatase TiO₂. A second 5 μm thick layer, based on 400 nm size particles, was used to backscatter the unabsorbed photons towards the dye. The cells were sensitized in a 10^{-5} mol·L⁻¹ solution of BSQ **18** in chloroform overnight. 3 α ,7 α -Dihydroxy-5 β -cholanic acid (CDCA) was used as de-aggregating agent in different proportions from 0 to 40 mol·mol⁻¹ during cell optimization. After being washed with acetonitrile and dried in a water free air box, the sensitized electrodes were separated by a 25 μm thick Surlyn gasket melt by heating with the Pt-modified TEC15 TCO. This Platinum latter was prepared by spreading out a drop of 5 mmol·L⁻¹ H₂PtCl₆ in ethanol solution prior to heating the counter electrode at 400°C for 15 min under air. The internal space between the two electrodes was filled via a hole with electrolyte (called: M1, see section 4.1) using a vacuum back filling system. The hole, priorly made by sand-blasting, was clogged-up with a melted Bynel sheet. One of these cells is shown in figure 2.43. Then, the prepared DSC was characterized. The evolution of the "incident photon conversion efficiency" (IPCE) curve as a function of the molar ratio of CDCA rising from 0 to 40 mol/mol was investigated where the best performance was obtained at the highest CDCA ratio. The current-voltage J-V curve is displayed in figure 2.44. The insert in this figure shows the wavelength dependent IPCE of the working DSC device. The cell showed a short circuit current density (J_{sc}) of 3.11 mA·cm⁻², an open circuit voltage (V_{oc}) of 545 mV and a fill factor (ff) of 0.76 leading to the photon-to-electron conversion efficiency (η) of 1.3% obtained under 100 mW·cm⁻² illumination intensity. It was clearly

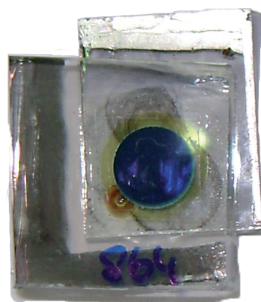


Figure 2.43: Picture of a working DSC of 6 mm in diameter coated with BSQ **18** by courtesy of Dr. Frédéric Sauvage.

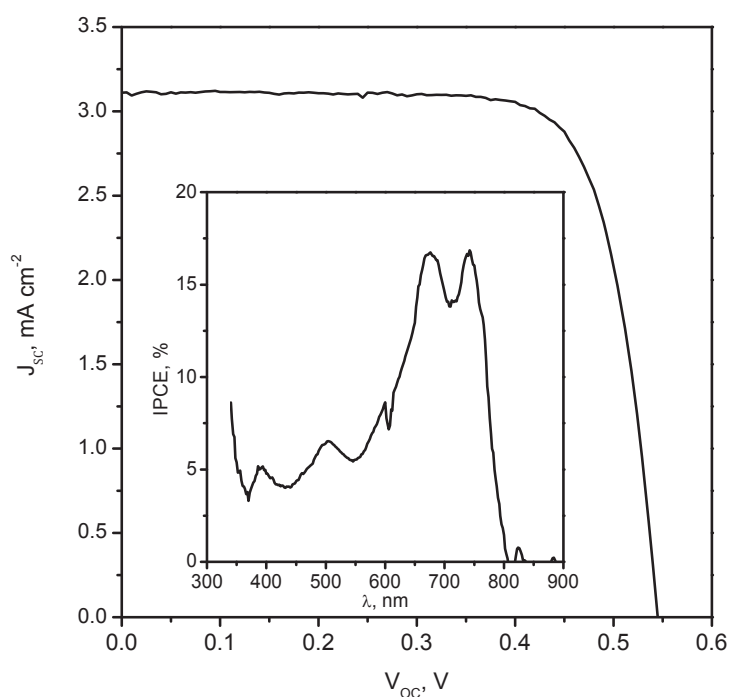


Figure 2.44: Graph: current-voltage (J - V) characteristics of a BSQ **18** sensitized solar cell; insert: wavelength dependent incident photon conversion efficiency (IPCE) of the working solar cell.

demonstrated that photo-current is produced from 550 nm up to 800 nm where BSQ **18** absorbs. This verified the calculated vectorial electron transfer. Furthermore, it was proven that NIR photons were converted to electricity by this dye.

The UV/vis spectrum in the homogeneous chloroform solution (Figure 2.27, page 52) looks different from the IPCE spectrum. The IPCE curve has mainly two bands situated at 675 nm and 742 nm whereas the solvent spectrum showed only one main transition

band at 727 nm in chloroform. It was assumed that this discrepancy might either derive from the presence of electrochemical decomposition products or from the formation of aggregates on the TiO_2 surface. The former argument was disproved by a long-term electrochemical stress experiment of BSQ **18** measured by cyclic voltammetry in *N,N*-dimethylformamide. The long-term measurement was performed by accomplishing 3500 full cycles up to 1.15 V and down to -0.85 V within 24 hours. The first and last scan of the series is shown in figure 2.45. Importantly, the electrochemical band gap of BSQ

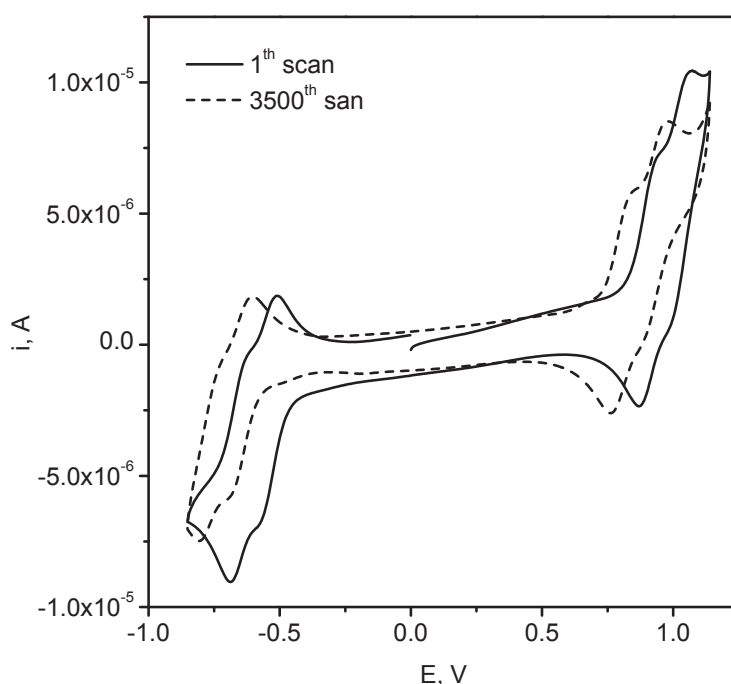


Figure 2.45: Long-term electrochemical stress experiment of dimer BSQ **18** measured in DMF. Cyclic voltammograms of the first and the 3500th scan after 24 h are provided.

18 remained unchanged after 3500 scans. All potentials were shifted towards lower voltage because the diffusion processes of chloride ions out of the reference electrode occurred. Also during the one day measurement neither an additional oxidation nor reduction peak appeared implying that the dye is indeed electrochemically stable under applied experimental conditions.

Aggregate formation was the second argument describing the discrepancy. Thus, aggregates from BSQ **18** were induced by successive change of the solvent polarity from a homogeneous dimethylsulfoxide solution to water [77, 78, 79]. The normalized spectra of this series were summarized in figure 2.46. Indeed, the induced aggregates

in the 40:60 dimethylsulfoxide-water mixture looked like the recorded IPCE spectrum. It was assumed that these aggregates were *H*-aggregates [79, 80] and they were known as one of the reasons for a bad solar cell performance. It was concluded that

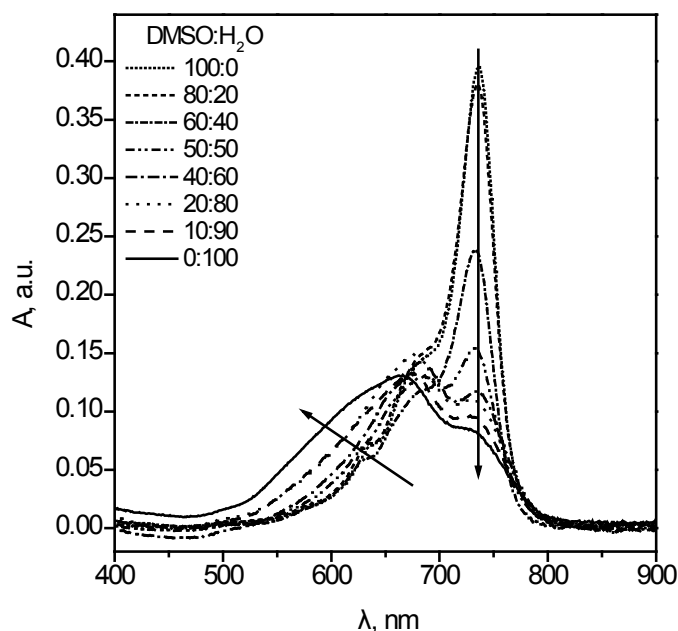


Figure 2.46: Normalized UV/vis absorption spectrum of BSQ **18** in DMSO-water mixtures. The arrows indicate the spectrum development with increasing water content.

although the anti-aggregation agent CDCA was used, aggregates were formed in the DSC device.

Furthermore, it was investigated in which production step towards the DSC device the aggregation of the well solubilized dye occurred. So BSQ **18** in chloroform (10^{-5} M) without anti-aggregation agent was absorbed on the surface of sintered TiO₂ nano particles. The UV/vis spectrum of this half-cell was recorded against air and is displayed in figure 2.47 together with the normalized spectrum of the chloroform solution. The spectrum of the absorbed dye was more similar to the spectrum of the chloroform solution than to the IPCE curve. Therefore, the aggregation of BSQ **18** might take place when it gets in contact with the very polar electrolyte. Measures to prevent this dye from aggregating were on the one hand the change of the electrolyte system and on the other hand the introduction of much longer alkyl side chains into the molecular structure. As already mentioned, if the aggregation of BSQ **18** could be avoided then the DSC performance will be better.

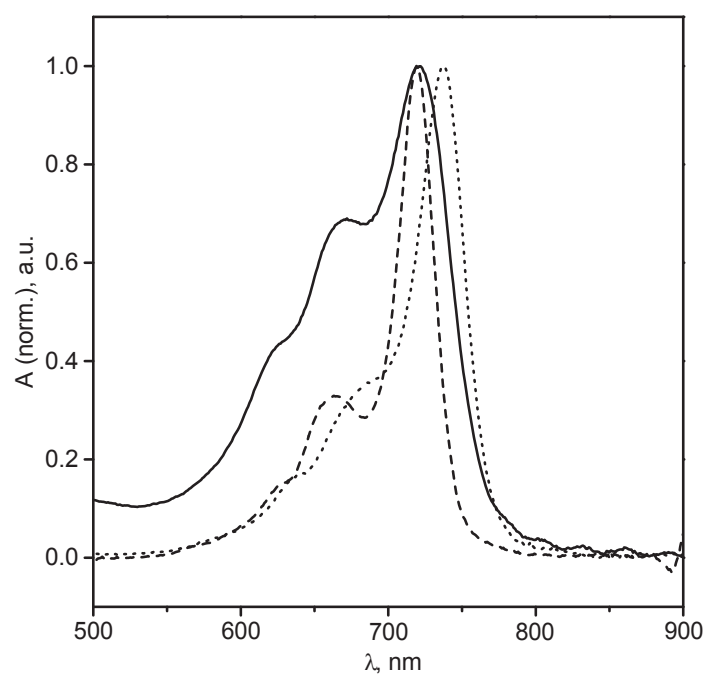


Figure 2.47: *BSQ 18 immobilized on TiO_2 surface against air (solid line), dissolved in MTBE (dashed line) and dissolved in DMSO (dotted line).*

Chapter 3

Conclusions and outlook

3.1 Conclusions

For the synthesis of the MSQs the strategy of Treibs and Jacob [45] for the symmetrical squaraines and the one of Terpetschnig et al. [48] for the unsymmetrical squaraines were followed. Their processes were adopted and modified. Mentionable is the alkylation with alkyl iodides and indole derivatives where the solvent was optimized. Using acetonitrile instead of 1-butanol gave 10 – 20% more total yield in half the time. Furthermore, the pathways for the modification of the end groups were optimized. It was shown that the only way to transform the aryl bromide at the indole derivative via Miyaura Borylation Reaction and Suzuki cross coupling was either before the nitrogen atom in the indole system had been alkylated or after the squaraine dye had been built up. Regarding the introduction of alkyl side chains, the longer the chain the better soluble the dyes were. Here, a maximal chain length of eight carbon atoms were introduced which was suitable for the MSQs, BSQs and TSQs in respect of the solubility. However, for a larger number of repeating units longer alkyl side chains would be needed as it was recently indicated by Völker et al. [60]. The last point concerning the alkylations, dealt with the double methylation of the bridging moieties. Although, tosylates are really strong alkylation agents, only methyl tosylates worked sufficiently under harsh conditions. Nevertheless, it was possible to prepare, purify and isolate all target molecules individually by multi step synthesis and optimized unit operations of chemical engineering. The experimental details were reported in chapter 4. The characterization of the optical property of the prepared dyes were determined

with UV/vis spectroscopy in diluted solution of various solvents. In the case of the five MSQs, their absorption maximum (λ_{max}^{abs}) were in the range of 637.5 to 665.5 nm in chloroform solution. The correlation of these λ_{max}^{abs} values with the number of the π -electron pairs outside the chromophore unit corrected by the torsion angle resulted in a linear structure-property relation. With this formula it was possible to prove the chromophore-chromophore interaction in the prepared BSQ molecules. The λ_{max}^{abs} values of those BSQs together with the ones of the corresponding MSQs and TSQs were the basic values for the determination of the saturation curves according to Meier [12]. Concluding, the here presented bridged squaraine dyes reach a saturation of the optical properties after five to eight repeating units and are in the range between 700 and 800 nm. These saturation curves were further analyzed resulting in a multi dimensional formula in which the parameters only consisted of structural information. Firstly, the structural information which influenced the optical properties were the number of π -electron pairs of the bridge corrected by the torsion angle. The more π -electron pairs and the more in-plan the bridge is, the more red shifted the λ_{max}^{abs} value was. Secondly, the distance (d) in-between the two chromophore units was also taken into account which showed that $1/d^2$ is proportional with the bathochromic shift. Thirdly, since the conjugation was also studied in tilted, biphenyl like bridges the number of tilts (m) between the two chromophores is also relevant. The more tilts the bridge has, the smaller the coupling of the chromophores is. Finally, the number of chromophore units (n) had a strong influence on the red shift when the value of n is between one and eight; above saturation is reached.

Also solvatochromic effects were studied by using various solvents to measure UV/vis spectroscopy of the prepared dyes. Concluding, three solvent groups were found which showed a linear behavior in a plot where the absorption wavenumber maximum of the dye is a function of the dielectric constant of the solvent. The solvents were subdivided into those who contain either an oxygen atom, an aromatic moiety or non of the two.

The electrochemical properties of the prepared dyes were determined by cyclic voltammetry in N,N-dimethylformamide or in chloroform. It was found, that the change of the molecular structure effected the first reduction and the first oxidation potential in a similar way and its influence on the electrochemical properties was linearly correlated with its impact on the optical properties. Furthermore, a direct relation between the individual reduction or oxidation potentials and the optical band gap (ΔE_{opt}) was found which allows the estimation of these electrochemical properties for any structure related squaraine dye when ΔE_{opt} is known.

This study indicated that the stronger the coupling in between two dye systems, the bigger the transition dipole moment is, as predicted by Kiprianov [19]. However, after a certain coupling strength, visible by the determined red shift, the transition dipole moment decreased. This contradicting behavior was explained with the increasing probability to form a fused, single dye system. This process was pictured by molecular modeling. Deducing, the BSQs showing a bigger bathochromic shifted λ_{max}^{abs} value had a bigger weight of probability density of the electrons in the frontier orbitals located on the bridging moiety. Furthermore, in the special case of the BSQ **27** the said probability density was actually predominant on the bridge in the LUMO.

Additionally, the molecular modeling showed that an unsymmetrically constructed, naphthalene bridged dimeric squaraine dye shows a directional charge transfer during optical excitation. This unsymmetric BSQ was synthesized, immobilized on titanium dioxide nano-particles and to get a proof-of-concept a first dye sensitized solar cell (DSC) was made therewith having an energy conversion efficiency (η) of 1.3%.

3.2 Outlook

In this thesis the indole based squaraine dyes with one, two and more dye units were studied. Though, a 1,5-diaza anthrazene bridged dye (BSQ **27**) was synthesized and characterized which showed outstanding optical properties. Therefore, a further study in the field with this type of bridges would open a new and interesting research area because they will have huge bathochromically shifted λ_{max}^{abs} values. Their polymeric variation might show the postulated electroconductivity and the broad absorption range of these type of dyes might be of special interest for the possible use in solar cell devices. As an outlook of this thesis, it is suggested that the series of similar flat conjugated bridges, as shown in figure 3.1, shall be synthesized. Additionally, trimers, oligomers and polymers with the said bridges would be interesting target molecules. And also the herein developed unsymmetric synthesis method for the BSQ **18** could be adopted in order to produce new NIR absorbers for solar cell applications. All these synthetic efforts should create a good basis for a similar structure-property relation study and also pave the way towards improved materials in optical applications.

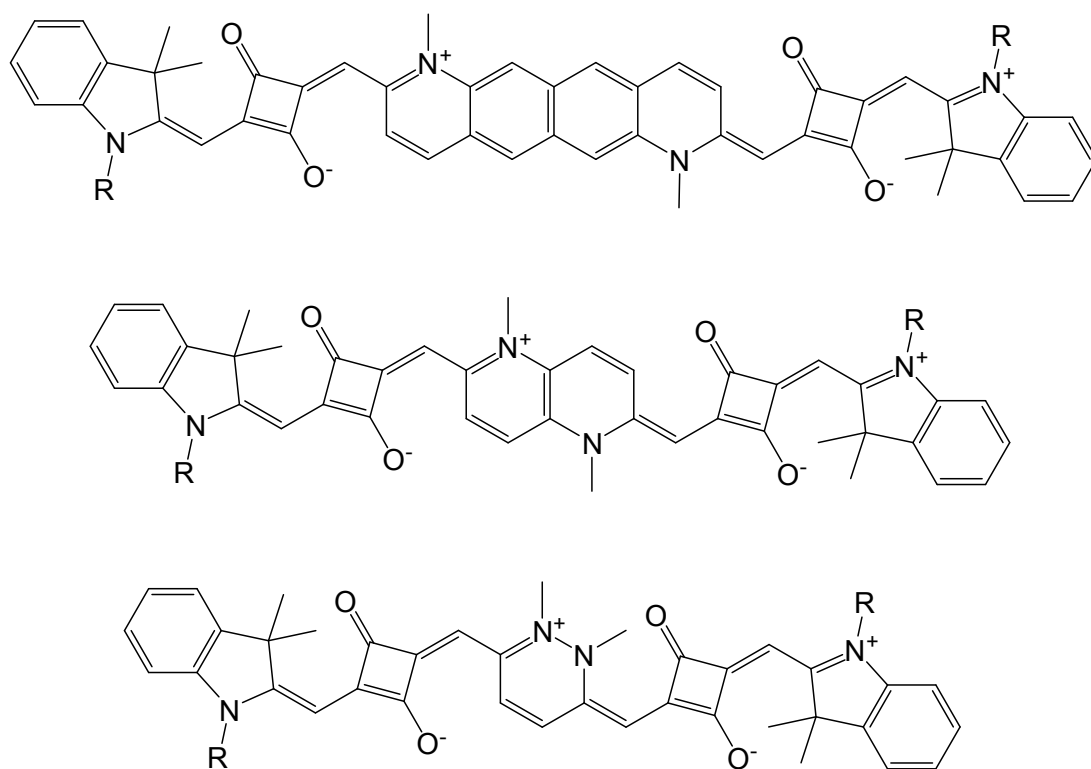


Figure 3.1: Suggested squaraines with new flat bridging synthons.

Chapter 4

Experimental Descriptions

4.1 General Information and Procedures

If not specially indicated, all chemicals were purchased either from Aldrich, Fluka or VWR with the appropriate purity and used unmodified. Room temperature (rt) refers to 23 °C. Unless otherwise stated, the reactions were run in a (three necked) round bottom flask under an argon atmosphere. The reaction mixtures and the apparatuses were evacuated (200 mbar) and flushed with argon several times before the reactions were started. Where indicated the reactor content was degassed using freeze-pump-thaw cycling thrice, utilizing liquid nitrogen, a high vacuum pump (down to 10^{-2} mbar) and thawing in argon atmosphere.

Reactions were monitored by analytical thin-layer chromatography (TLC) using silica gel baked on glass, on aluminium-foil or on PET-foil with a fluorescent indicator 254 nm from RediSepTM, Fluka or Merck. In order to visualize the TLC's by UV (254 and/or 365 nm) they were developed with either aqueous cobalt thiocyanate, aqueous alkaline potassium permanganate solution or silver nitrate in concentrated ammonium hydroxide solution.

Water free sodium sulphate powder (Na_2SO_4) was used for drying the organic layers after extraction. Subsequent evaporation of the solvent was performed in a Heidolph Laborota 4000 rotary evaporator with a bath temperature of 60 °C and an appropriate pressure.

For individual purification flash chromatography was performed with the CombyFlash TeledyneISCO system from Companion using RediSepTM Normal Phase Disposable

Columns (various sizes). To increase the separation performance, 0.1% of 1,1,1,3,3,3-hexafluoro isopropanol (ABCR) was added to the eluent. Isocratic flows as well as gradients were used.

Where stated the isolated compounds were dried in the Salvislab vacuum oven at 40 °C and 1 mbar overnight or for three days in special cases.

The yield is defined as the purified, dried and isolated material given in mass. The weighed starting materials are reported with three valid digits and the weigh-out quantity is given with two valid digits due to the accuracy of the purity calculation via NMR of 1%.

The averaged number of repeating units (\bar{X}_n) in the filtration residue of the oligomeric materials was determined by three methods:

- Carother's equation (eq. 4.1) where $\bar{X}_n^{Carother}$ is calculated over the conversion to the polymer (U). U was defined as the isolated mass yield.

$$\bar{X}_n^{Carother} = \frac{1}{1 - U} \quad [-] \quad (4.1)$$

- Medial allegation of the MALDI-TOF measurement results in $\bar{X}_n^{MALDI-TOF}$ according to equation 4.2, where M_R^{unit} is the molar mass of the repeating unit, m_i^{ion} the mass of ion i and S_i^{ion} is the signal intensity of ion i . For this equation it is assumed, that all ions have the same flying ability.

$$\bar{X}_n^{MALDI-TOF} = \frac{1}{M_R^{unit}} \cdot \frac{\sum_{i=1}^n (m_i^{ion} \cdot S_i^{ion})}{\sum_{i=1}^n S_i^{ion}} \quad [-] \quad (4.2)$$

- End group determination by NMR gives \bar{X}_n^{NMR} with the equation 4.3. Protons which were nearby the coupling side show a different shifted signal if they were in the bulk polymer or at the end of it. Their integrals per proton were entered into the equation only if both signals were identified.

$$\bar{X}_n^{NMR} = \frac{1}{n} \cdot \sum_{i=1}^n \frac{I_{bulk}}{I_{end}} \quad [-] \quad (4.3)$$

The microscopic pictures from crystalline material were taken on a Research High-Class Stereo-Microscope Olympus SZX16 with SDF PLAPO lenses with a κ DX 40

camera and appropriate software.

For the definition of the melting and freezing points but also for the verification of decomposition differential scanning calorimetry (DSC) was performed on a Perkin Elmer, DSC-7 in nitrogen atmosphere at various temperature ranges with a scanning speed of 5 or 20 °C per minute.

Thermogravimetric analysis (TGA) was performed on a NETZSCH, TG 209 F1 in nitrogen atmosphere. In the thermogramm the onset was used to calculate the boiling, sublimating or decomposition points. For this analysis, one to five milligrams of compound were weighed in a ceramic crucible and heated from room temperature to 600 °C with a heating rate of 20 °C per minute. In addition, the ash residue at 600 °C is reported in percent. "Spontaneous decomposition" marks compounds which deflagrated at their decomposition point. Caution: This mini-explosion might crack the ceramic crucible.

Nuclear magnetic resonance (NMR) spectra were recorded at 297 K in a 5 mm broadband inverse probe on a Bruker 400 MHz spectrometer operating at 400 MHz for ¹H-NMR, 100 MHz for ¹³C-NMR, 376 MHz for ¹⁹F-NMR and 162 MHz for ³¹P-NMR. Unless otherwise stated deuterated chloroform was used as solvent. All NMR spectra were referenced to residual proto-deutero solvent signals in the solvent indicated according to Gottlieb et al. [81] (see below).

Solvent	δ /ppm (¹ H-NMR)	δ /ppm (¹³ C-NMR)
CDCl ₃	7.26	77.00
DMSO-d ₆	2.50	39.52
C ₆ D ₆	7.16	128.06

Data were reported as follows: chemical shifts (δ) in parts per million (ppm), if possible identification according to the numeration in the drawn molecular structure, corresponding signal integral, multiplicity abbreviation (s = singlet, d = doublet, t = triplet, q = quartet, p = pentet, hex = hexet, hep = heptet, m = multiplet, br = broad) and if possible coupling constant in Herz (Hz).

Mass spectra were recorded on a Bruker maXis-ESI-Q-TOF mass spectrometer (ESI-QTOF) or on a HiRes-ESI IonSpec Varian Ultima-ESI FTICR-MS spectrometer (IonSpec, Lake Forest, CA, USA). ESI spectra of small organic molecules were measured in methanol or dichloromethane if not otherwise stated. For the electron ionization mass spectrometry a Micromass (Waters) AutoSpec Ultima-EI-EBE-MS (EI) was used without any solvents or matrices. Matrix-assisted laser desorption/ionization

(MALDI) spectra were performed on an IonSpec Varian Ultima–MALDI-FTICR-MS or on a Bruker UltraFlex II - MALDI-TOF (MALDI-TOF). MALDI spectra of small organic molecules were usually measured in a matrix of 3-hydroxypicolinic acid (3-HPA). MALDI-TOF was measured in a matrix of 2-[(2*E*)-3-(4-*tert*-butylphenyl)-2-methylprop-2-enylidene]malononitrile sodium salt (DCTB+Na). Calculated masses were based on average isotope composition or on single isotope masses for high resolution spectra. Unless otherwise indicated MALDI was used for mass spectroscopy and HR-MALDI for exact mass determination. Data are reported as follows: isotopic mass in atomic mass units, relative intensity in percent written in in parenthesis and if possible the identification is given in squared brackets. If special isotopic constellations were visible, like two bromine atoms, some of the isotopic distribution signals were also described as A, A+1, A+2 and so on.

Elemental analysis for C, H, N and O was measured by an apparatus from LECO. The elements F, Cl, Br, I were measured by titration or with an ion chromatograph after a Schöniger-pulping. Due to solvent incorporation into the product crystals of most of the target compounds those elemental analysis results were outside the tolerance of 0.5%. Data were reported as follows: chemical element symbol with its per cent content of the molecular formula.

Ultraviolet and visible (UV/vis) spectra were recorded on a Varian Cary 50 Scan spectrometer in a 1.000 cm optical glass or quartz cuvette. The spectra were recorded in the absorption versus wavelength mode with a linear sweep of monochromatic light starting from the lower energy end of the spectra in 0.5 nm steps. All spectra were base line corrected before they were analyzed.

Fluorescence spectroscopy was carried out on a Fluorolog from Horbia Jobin Yvon with a UV/vis detector. The detection mode was front face because of the big re-absorption of the emitted light due to the very small Stock's shift. The excitation wavelength was normally set 50 nm below the absorption maximum, because the machine had a light diffusion of ± 25 nm and squaraine dyes generally have a very small Stock's shift.

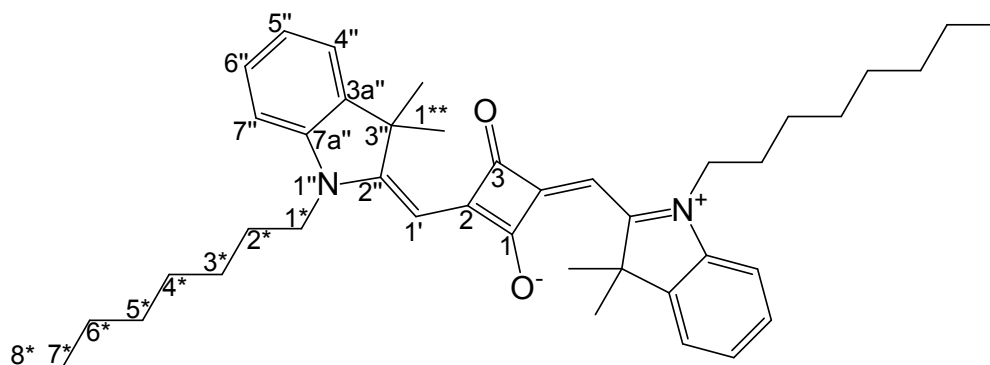
Cyclic voltammetry measurements were recorded on a PGStat 30 potentiostat (Autolab) using a three cell electrode system consisting of a rotating gold or glassy carbon working electrode, a platinum counter electrode and a Ag/AgCl (0.1 M tetrabutyl ammonium chloride in water free solvent) reference electrode. As a non-aqueous supporting electrolyte 0.1 M tetrabutyl ammonium perchlorate (TBAP) in *N,N*-dimethylformamide or chloroform were used. All solvents were deoxygenated with argon prior to electrochemical measurements. The ferrocene/ferrocenium couple

(Fc/Fc⁺) was used as an internal reference. The scanning rate was varied from 10–2000 mVs⁻¹ and the rotation speed of the working electrode was set to 50 rpm. For comparability with the published literature, all potentials were referenced to normal hydrogen electrode (NHE), by adopting a potential for Fc/Fc⁺ to +0.72 V vs. NHE in *N,N*-dimethylformamide [69] and +0.25 V vs. NHE in chloroform.

The DSC was prepared as described in section 2.2.5 with the volatile M1 electrolyte. This electrolyte is composed by 0.6 mol·L⁻¹ 1-butyl-3-methylimidazolium iodide (BMII), 50 mmol·L⁻¹ LiI, 40 mmol·L⁻¹ I₂, 0.275 mol·L⁻¹ tert-butylpyridine and 0.05 mol·L⁻¹ GuNCS in a solvent mixture of 85% acetonitrile with 15% valeronitrile by volume. The prepared DSC was then characterized as follows: A 450 W xenon light source (Oriel, USA) was used to provide an incident irradiance of 100 mW·cm⁻² at the surface of the solar cells. The spectral output of the lamp was filtered using Schott K113 Tempax sunlight filter (Präzisions Glas & Optik GmbH, Germany) to reduce light mismatch between real solar illumination and the simulated one to less than 2%. Light intensities were regulated with wire mesh attenuators. The J-V measurements were performed using a Keithley model 2400 digital source meter (Keithley, USA) by applying independently external voltage to the cell and by measuring the photo-generated current out from the cell. Incident photon-to-current conversion efficiency (IPCE) measurements were realized using a 300 W xenon light source (ILC Technology, USA). A Gemini-180 double monochromator Jobin Yvon Ltd. (UK), was used to select and increment wavelength irradiation to the cell.

4.2 Synthesis: Prescription and Characterization

4-((3,3-Dimethyl-1-octyl-3*H*-indolium-2-yl)methylene)-2-((3,3-dimethyl-1-octylindolin-2-ylidene)methyl)-3-oxocyclobut-1-enolate (**8**)



In a Dean-Stark apparatus **28** (15.0 g, 40.3 mmol, page 126), squaric acid (2.24 g, 19.7 mmol, OChem Inc.), toluene (60 mL), 1-butanol (120 mL) and quinoline (10 mL) were combined and boiled under reflux overnight. The next morning the reaction mixture was concentrated under reduced pressure to the half of its volume. The ensuing residue was poured while stirring into an aqueous citric acid solution (1.5 L, 5%). The stirring was prolonged until the copper shiny oil transformed to a golden-green solid. The precipitate was filtered and the residue was recrystallized from boiling ethanol (500 mL) to yield **8** (9.4 g, 15 mmol, 76%).

Melting point: 155–160 °C.

Decomposition onset: 290 °C. Residue: 16%.

¹H-NMR: 7.34 (C(4'')H, 2H, d, ³J(4''-5'')=7.4Hz), 7.29 (C(6'')H, 2H, ddd, ³J(6''-7'')=7.8Hz, ³J(6''-5'')=7.6Hz, ⁴J(6''-4'')=1.0Hz), 7.12 (C(5'')H, 2H, dd, ³J(5''-4'')=7.4Hz, ³J(5''-6'')=7.6Hz), 6.96 (C(7'')H, 2H, d, ³J(7''-6'')=7.8Hz), 5.95 (C(1')H, 2H, s), 4.1-3.8 (C(1'')H₂, 4H, br), 1.8-1.7 (C(1*)H₃, C(2'')H₂, 16H, m), 1.4-1.2 (C(3'')H₂, C(4'')H₂, C(5'')H₂, C(6'')H₂, C(7'')H₂, 10H, m), 0.86 (C(8'')H₃, 6H, t, ³J(8''-7'')=6.9Hz).

¹³C-NMR: 182.25, 179.42, 169.92, 142.41, 142.17, 127.66, 123.55, 122.20, 109.27, 86.48, 49.20, 43.66, 31.66, 29.25, 29.08, 27.01, 26.98, 22.52, 14.00.

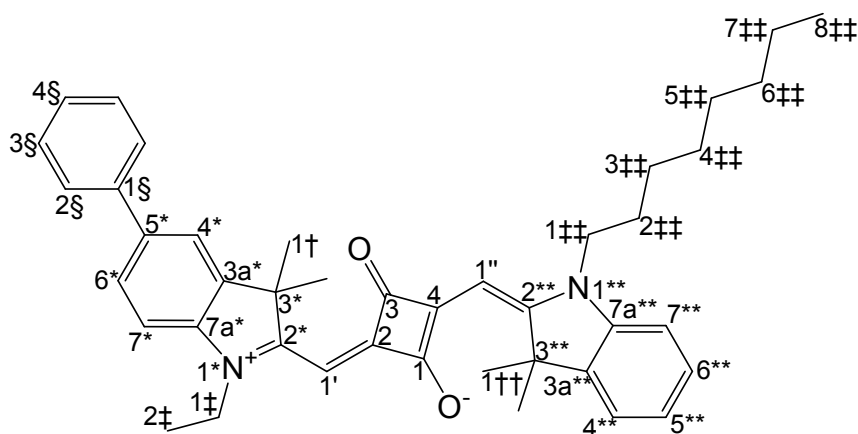
MS: 621 (100) [M+H]⁺, 620 (100) [M]⁺, 605 (7) [M-CH₃]⁺, 364 (7) [C₂₄H₃₀NO₂]⁺, 310.7

(5) $[M+H]^{++}$, 310.2 (4) $[M]^{++}$, 207.1 (1) $[M+H]^{3+}$, 155.4 (2) $[M+H]^{4+}$, 103.6 (1) $[M+H]^{6+}$, 88.8 (1) $[M+H]^{7+}$, 77.7 (0.4) $[M+H]^{8+}$, 69.1 (0.4) $[M+H]^{9+}$.

HR-MS: calculated for $C_{42}H_{56}N_2O_2$ $[M]^+$: 620.4336. Found: 620.4410.

Elemental analysis: calculated for $C_{42}H_{56}N_2O_2$: C, 81.24; H, 9.09; N, 4.51; O, 5.15. Found: C, 81.14; H, 9.10; N, 4.50; O, 5.23.

4-((3,3-Dimethyl-1-octyl-3*H*-indolium-2-yl)methylene)-2-((1-ethyl-3,3-dimethyl-5-phenylindolin-2-ylidene)methyl)-3-oxocyclobut-1-enolate (9)



In a 50 mL Schlenk tube **36** (1.00 g, 1.51 mmol, page 138), bromobenzene (0.355 g, 2.26 mmol), potassium acetate (0.445 g, 4.53 mmol), dichloro[1,1'-bis(diphenylphosphino)-ferrocen]-palladium(II) (50 mg, 56 μ mol, CombiPhos Catalysts Inc.) and dioxane (20 mL) were mixed and stirred at 80°C for 4 d. The solvent was then evaporated under vacuum and the residue was dissolved in chloroform (50 mL). The suspension was filtered through a silica gel bed (3 cm) and the residue was washed with chloroform (2x40 mL). The solvent of the filtrate was removed under reduced pressure. The purification of the crude product by column chromatography (chloroform) yielded **9** (0.42 g, 0.60 mmol, 40%) as a golden crystalline powder.

Decomposition onset: 283°C. Residue: 17%.

1 H-NMR (DMSO- d_6): 7.85 (C(4*)H, 1H, d, $^4J(4^*-6^*)=1.7$ Hz), 7.71 (C(2§)H, 2H, dd,

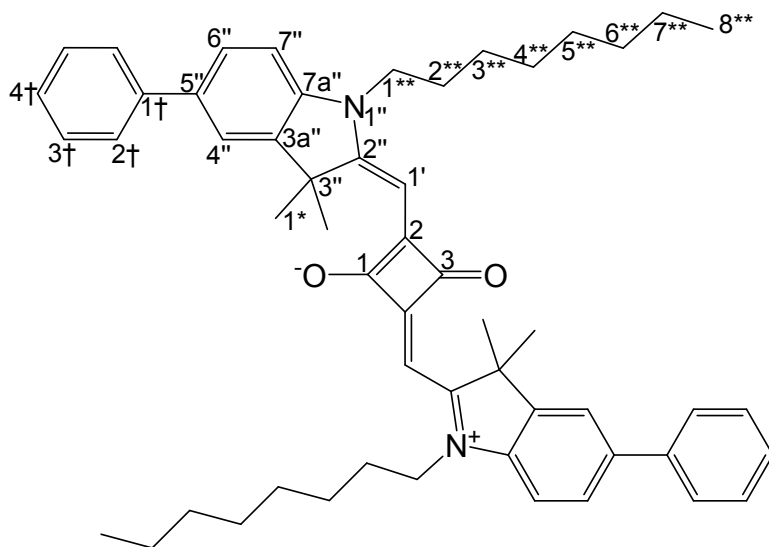
$^3J(2\text{\S}-3\text{\S})=7.4\text{Hz}$, $^4J(2\text{\S}-4\text{\S})=1.2\text{Hz}$, 7.64 (C(6^{*})H, 1H, dd, $^3J(6^*-5^*)=8.3\text{Hz}$, $^4J(4^*-6^*)=1.8\text{Hz}$), 7.51 (C(4^{**})H, 1H, d, $^3J(4^{**}-5^{**})=7.3\text{Hz}$), 7.46 (C(3\text{\S})H, 2H, dd, $^3J(3\text{\S}-4\text{\S})=7.9\text{Hz}$, $^3J(3\text{\S}-2\text{\S})=7.4\text{Hz}$), 7.39 (C(7^{*})H, 1H, d, $^3J(7^*-6^*)=8.4\text{Hz}$), 7.37-7.29 (C(6^{**})H, C(7^{**})H, C(4\text{\S})H, 3H, m), 7.16 (C(5^{**})H, 1H, ddd, $^3J(5^{**}-6^{**})=8.2\text{Hz}$, $^3J(5^{**}-4^{**})=7.3\text{Hz}$, $^4J(5^{**}-7^{**})=1.8\text{Hz}$), 5.80 (C(1')H, C(1'')H, 2H, m), 4.15 (C(1‡)H₂, 2H, q, $^3J(1‡-2‡)=6.7\text{Hz}$), 4.07 (C(1‡‡)H₂, 2H, t, $^3J(1‡‡-2‡‡)=6.2\text{Hz}$), 1.77-1.65 (C(1†)H₃, C(1††)H₃, C(2‡‡)H₂, 14H, m), 1.4-1.2 (C(3‡‡)H₂, C(4‡‡)H₂, C(5‡‡)H₂, C(6‡‡)H₂, C(7‡‡)H₂, C(2‡)H₃, 13H, m), 0.81 (C(8‡‡)H₃, 3H, t, $^3J(8‡‡-7‡‡)=6.8\text{Hz}$).

$^{13}\text{C-NMR}$ (DMSO-*d*₆): 180.65, 178.90, 178.45, 169.11, 168.34, 142.38, 142.21, 141.43, 141.30, 139.93, 135.89, 128.89, 127.96, 127.10, 126.59, 126.52, 123.69, 122.25, 120.76, 110.34, 86.15, 86.02, 48.80, 48.73, 42.92, 38.06, 31.14, 28.66, 28.58, 26.51, 26.50, 26.47, 26.19, 25.49, 22.04, 13.93, 11.78.

MS: 613 (99) [M+H]⁺, 612 (100) [M]⁺, 597 (21) [M-CH₃]⁺, 583 (2) [M-C₂H₅]⁺, 499 (1) [M-C₈H₁₇]⁺, 364 (11) [C₂₄H₃₀NO₂]⁺, 356 (13) [C₂₄H₂₂NO₂]⁺, 306 (9) [M]⁺⁺, 153 (2) [M]⁴⁺.

HR-MS: calculated for C₄₂H₄₈N₂O₂ [M]⁺: 612.3710. Found: 612.3589.

4-((3,3-Dimethyl-1-octyl-5-phenyl-3*H*-indolium-2-yl)methylene)-2-((3,3-dimethyl-1-octyl-5-phenylindolin-2-ylidene)methyl)-3-oxocyclobut-1-enolate (10)



38 (3.00 g, 3.44 mmol, page 140), bromobenzene (1.62 g, 10.32 mmol), potassium acetate (2.02 g, 20.6 mmol), dichloro[1,1'-bis(diphenylphosphino)-ferrocen]-palladium(II) (200 mg, 250 μ mol, CombiPhos Catalysts Inc.) and dioxane (50 mL) were combined in a 100 mL Schlenk tube and heated to 80 °C for 4 d. The product precipitated during the reaction. After reaction, the reactor content was cooled to rt and the crude product was filtered. The filtration residue was recrystallized from hot dimethyl sulfoxide (600 mL at 120 °C). The crystals were filtered and washed with cold ethanol (3x10 mL) and dried to yield **10** (1.9 g, 2.5 mmol, 71%) as golden needle like crystals (Figure 4.1).



Figure 4.1: Isolated **10** as golden needle like crystals.

Due to insolubility in common organic solvents and aggregation formation in chloroform, NMR analysis was performed in dimethylsulfoxide in low concentration (< 1 mg / mL) causing the inability to measure ^{13}C -NMR.

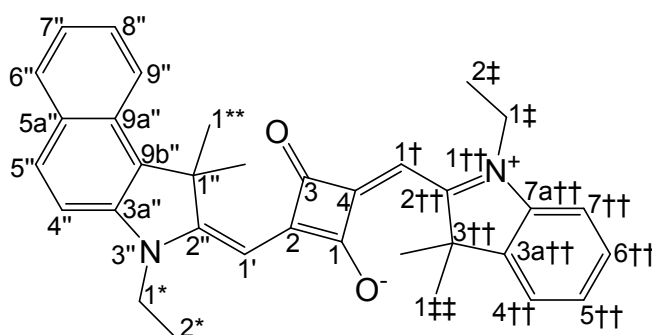
Decomposition onset: 304 °C. Residue: 25%.

^1H -NMR (DMSO- d_6): 7.86 (C(4'')H, 2H, d, $^4\text{J}(4''-6'')=1.5\text{Hz}$), 7.72 (C(2†)H, 4H, d, $^3\text{J}(2†-3†)=7.7\text{Hz}$), 7.66 (C(6'')H, 2H, dd, $^3\text{J}(6''-7'')=8.4\text{Hz}$, $^4\text{J}(6''-4'')=1.5\text{Hz}$), 7.47 (C(3†)H, 4H, dd, $^3\text{J}(3†-2†)=7.7\text{Hz}$, $^3\text{J}(3†-4†)=7.5\text{Hz}$), 7.41 (C(7'')H, 2H, d, $^3\text{J}(7''-6'')=8.4\text{Hz}$), 7.35 (C(4†)H, 2H, t, $^3\text{J}(4†-3†)=7.5\text{Hz}$), 5.83 (C(1')H, 2H, s), 4.12 (C(1'')H₂, 4H, br), 1.8-1.6 (C(1*)H₃, C(2'')H₂, 16H, m), 1.5-1.2 (C(3'')H₂, C(4'')H₂, C(5'')H₂, C(6'')H₂, C(7'')H₂, 20H, m), 0.85 (C(8'')H₃, 6H, t, $^3\text{J}(8''-7'')=6.8\text{Hz}$).

MS: 774 (100) $[M+H]^+$, 772 (97) $[M]^+$, 757 (21) $[M-CH_3]^+$, 660 (2) $[M+H-C_8H_{17}]^+$, 440 (10) $[C_{30}H_{34}NO_2]^+$, 386 (3) $[M]^{2+}$, 193 (1) $[M]^{4+}$.

HR-MS: calculated for $C_{54}H_{64}N_2O_2$ $[M]^+$: 772.4962. Found: 772.4974.

2-((3-Ethyl-1,1-dimethyl-1*H*-benzo[*e*]indol-2(3*H*)-ylidene)methyl)-4-((1-ethyl-3,3-dimethyl-3*H*-indolium-2-yl)methylene)-3-oxocyclobut-1-enolate (11)



42 (6.85 g, 20.5 mmol, page 145), **39** (6.80 g, 21.6 mmol, page 141), toluene (50 mL), 1-butanol (100 mL) and quinoline (10 mL) were mixed in a Dean-Stark apparatus. The condensation proceeded for 15 h at reflux temperature. Then the reaction mixture was concentrated under vacuum and the bluish-black oily residue was diluted in ethanol (50 mL). While stirring vigorously the solution was poured in an aqueous citric acid solution (800 mL, 5%). The green precipitate was filtered off and the ensuing residue was recrystallized from boiling methanol (120 mL) to yield **11** (3.8 g, 7.6 mmol, 37%) as golden crystals.

Decomposition onset: 288 °C. Residue: 28%.

¹H-NMR (DMSO-*d*₆): 8.23 (C(9'')H, 1H, dd, ³J(9''-8'')=8.4Hz, ⁴J(9''-7'')=0.8Hz), 8.03 (C(5'')H, 1H, d, ³J(5''-4'')=8.8Hz), 8.01 (C(6'')H, 1H, dd, ³J(6''-7'')=8.0Hz, ⁴J(6''-8'')=1.3Hz), 7.71 (C(4'')H, 1H, d, ³J(4''-5'')=8.8Hz), 7.62 (C(8'')H, 1H, ddd, ³J(8''-9'')=8.4Hz, ³J(8''-7'')=7.0Hz, ⁴J(8''-6'')=1.3Hz), 7.53 (C(7††)H, 1H, dd, ³J(7††-6††)=7.2Hz, ⁴J(7††-5††)=1.3Hz), 7.45 (C(7'')H, 1H, ddd, ³J(7''-6'')=8.0Hz, ³J(7''-8'')=7.0Hz, ⁴J(7''-9'')=0.8Hz), 7.35 (C(6††)H, 1H, dd, ³J(6††-5††)=7.2Hz, ³J(6††-7††)=7.2Hz, ⁴J(6††-4††)=0.8Hz), 7.31 (C(4††)H, 1H, dd, ³J(4††-5††)=7.2Hz, ⁴J(4††-

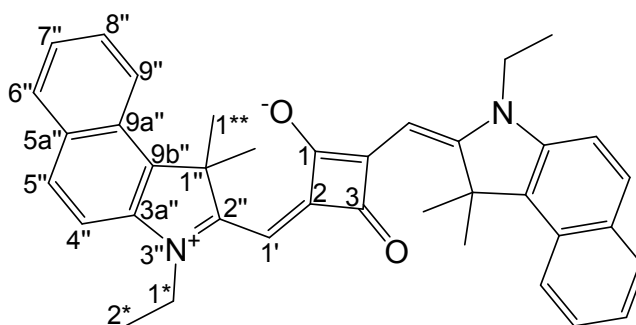
6††)=0.8Hz), 7.16 (C(5††)H, 1H, dd, $^3J(5††-6††)=7.2\text{Hz}$, $^3J(5††-4††)=7.2\text{Hz}$, $^4J(5††-7††)=1.3\text{Hz}$), 5.86 (C(1')H, 1H, s), 5.80 (C(1†)H, 1H, s), 4.27 (C(1**)H₂, 2H, q, $^3J(1**-2**) = 7.1\text{Hz}$), 4.12 (C(1‡)H₂, 2H, q, $^3J(1‡-2‡) = 6.9\text{Hz}$), 1.95 (C(1*)H₃, 6H, s), 1.70 (C(1‡‡)H₃, 6H, s), 1.34 (C(2**)H₃, 3H, t, $^3J(2**-1**) = 7.1\text{Hz}$). 1.29 (C(2†)H₃, 3H, t, $^3J(2†-1†) = 6.9\text{Hz}$).

$^{13}\text{C-NMR}$ (DMSO-d₆): 180.72, 178.36, 177.91, 170.24, 168.18, 141.77, 141.51, 139.24, 133.31, 130.91, 129.83, 129.73, 127.99, 127.95, 127.44, 124.22, 123.53, 122.29, 122.25, 111.15, 109.96, 85.66, 85.58, 50.62, 48.63, 38.22, 37.89, 26.50, 26.10, 12.09, 11.72.

MS: 525 (2) [M+Na]⁺, 503 (100) [M+H]⁺, 502 (97) [M]⁺, 487 (5) [M-CH₃]⁺, 473 (1) [M-C₂H₅]⁺, 330 (6) [C₂₂H₂₀NO₂]⁺, 280 (8) [C₁₈H₁₈NO₂]⁺, 276 (7) [C₁₉H₁₈NO]⁺, 252 (7) [M+H]²⁺, 251 (7) [M]²⁺, 168 (1) [M+H]³⁺, 126 (3) [M+H]⁴⁺, 101 (1) [M+H]⁵⁺, 84 (1) [M+H]⁶⁺, 72 (1) [M+H]⁷⁺, 63 (1) [M+H]⁸⁺.

HR-MS: calculated for C₃₄H₃₅N₂O₂ [M+H]⁺: 503.2693. Found: 503.2696.

2-((3-Ethyl-1,1-dimethyl-1*H*-benzo[*e*]indol-2(3*H*)-ylidene)methyl)-4-((3-ethyl-1,1-dimethyl-1*H*-benzo[*e*]indolium-2-yl)methylene)-3-oxocyclobut-1-enolate (12)



In a Dean-Stark apparatus **40** (15.4 g, 42.1 mmol, page 142), squaric acid (2.34 g, 20.5 mmol, OChem Inc.), toluene (50 mL), 1-butanol (100 mL) and quinoline (10 mL) were mixed and heated to reflux for 36 h. Thereafter, the reaction mixture was concentrated under reduced pressure and the oily residue was dissolved in ethanol (100 mL). While stirring, the solution was added dropwise to an aqueous citric acid solution (1 L, 5%).

After 30 min the precipitate was filtered and subsequent recrystallization of the remnant from boiling chloroform (750 mL) yielded **12** as copper-red shiny crystals (Figure 4.2 right hand side). After drying in the vacuum oven, NMR analysis showed that two mol chloroform per one mol **12** were present which was also verified by TGA analytics. Chloroform was incorporated into the crystal structure, since chloroform is only released above 130°C. These reddish crystals were then recrystallized from boiling methanol to yield chloroform- and methanol-free, golden-green shiny crystalline **12** (6.6 g, 12 mmol, 58%, Figure 4.2 left hand side). Interestingly this transformation is reversible.



Figure 4.2: *Picture of the solvent-free, golden-green crystals (left hand side) and the copper-red chloroform adduct of **12**.*

TGA of the copper-red coloured shiny crystal modification: onset(1): 130°C Δm : 30% (corresponds to two mol chloroform per mol **12**; decomposition onset(2): 323°C. Residue: 18%.

DSC of the copper-red coloured shiny crystal modification: no melting point before decomposition. Release of Chloroform visible from 130 – 200°C.

TGA of the golden-green shiny crystal modification: decomposition onset: 318°C. Residue: 26%. No release of methanol visible.

DSC of the golden-green shiny crystal modification: no melting point before decomposition. No release of methanol visible.

¹H-NMR (DMSO- d_6): (8.31 (chloroform, 2H, s, only in reddish crystal modification),) 8.23 (C(9'')H, 2H, dd, $^3J(9''-8'')$ =8.3Hz, $^4J(9''-7'')$ =0.9Hz), 8.03 (C(5'')H, 2H, d, $^3J(5''-$

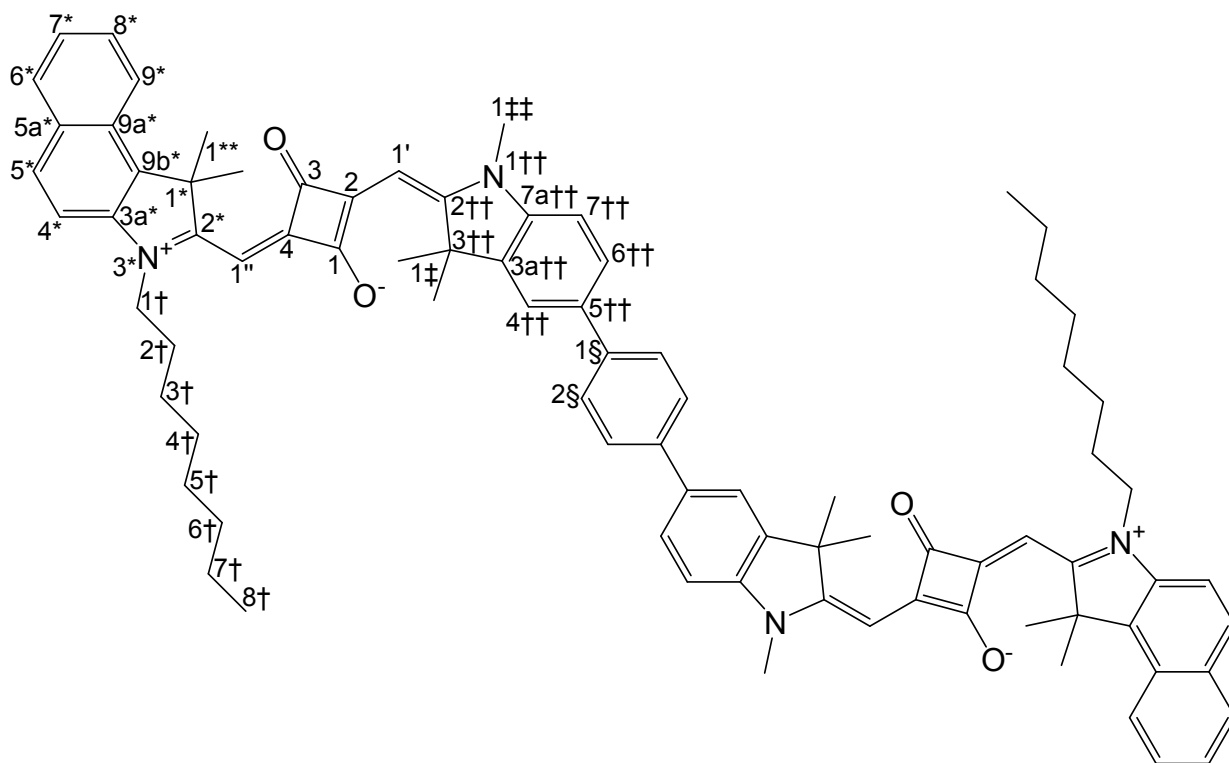
$^1\text{H-NMR}$ (DMSO- d_6): 8.02 (C(6'')H, 2H, dd, $^3J(6''-7'')=7.9\text{Hz}$, $^4J(6''-8'')=1.4\text{Hz}$), 7.71 (C(4'')H, 2H, d, $^3J(4''-5'')=8.9\text{Hz}$), 7.62 (C(8'')H, 2H, ddd, $^3J(8''-9'')=8.3\text{Hz}$, $^3J(8''-7'')=6.9\text{Hz}$, $^4J(8''-6'')=1.4\text{Hz}$), 7.45 (C(7'')H, 2H, ddd, $^3J(7''-6'')=7.9\text{Hz}$, $^3J(7''-8'')=6.9\text{Hz}$, $^4J(7''-9'')=0.9\text{Hz}$), 5.87 (C(1')H, 2H, s), 4.27 (C(1'')H₂, 4H, q, $^3J(1''-2'')=7.1\text{Hz}$), 1.97 (C(1*)H₃, 12H, s), 1.35 (C(2'')H₃, 6H, t, $^3J(2''-1'')=7.1\text{Hz}$).

$^{13}\text{C-NMR}$ (DMSO- d_6): 184.74, 177.51, 169.85, 138.91, 133.18, 130.86, 129.82, 129.75, 127.99, 127.45, 124.18, 122.24, 111.12, 85.54, 50.55, 38.18, 26.16, 12.08.

MS: 575 (2) $[\text{M}+\text{Na}]^+$, 552 (100) $[\text{M}]^+$, 537 (5) $[\text{M}-\text{CH}_3]^+$, 523 (2) $[\text{M}-\text{C}_2\text{H}_5]^+$, 330 (18) $[\text{C}_{22}\text{H}_{20}\text{NO}_2]^+$, 276 (7) $[\text{M}]^{2+}$, 184 (1) $[\text{M}]^{3+}$, 138 (1) $[\text{M}]^{4+}$, 110 (1) $[\text{M}]^{5+}$, 92 (1) $[\text{M}]^{6+}$, 79 (1) $[\text{M}]^{7+}$.

HR-MS: calculated for $\text{C}_{38}\text{H}_{36}\text{N}_2\text{O}_2$ $[\text{M}]^+$: 552.2771. Found: 552.2779.

2,2'-(5,5'-(1,4-Phenylene)bis(1,3,3-trimethylindoline-5-yl-2-ylidene))bis(methan-1-yl-1-ylidene)bis(4-((1,1-dimethyl-3-octyl-1*H*-benzo[*e*]indolium-2-yl)methylene)-3-oxocyclobut-1-enolate) (13)



43 (1.36 g, 3.27 mmol, page 146), **47** (1.00 g, 1.31 mmol, page 151), toluene (10 mL), 1-butanol (20 mL) and quinoline (5 mL) were combined and boiled for 60 h in a Dean-Stark apparatus. Afterwards, the reaction mixture was concentrated *in vacuo*. The residue was diluted with ethanol (50 mL) and added dropwise to cold aqueous citric acid solution (600 mL, 10% w/v) as it was stirred vigorously for 15 min. The suspension was filtered and the residue was digested in saturated potassium carbonate solution (100 mL) and, afterwards, washed with water thrice. Subsequent purification by column chromatography (chloroform) yielded **13** (1.1 g, 0.85 mmol, 65%).

Decomposition onset: 300 °C. Residue: 44%.

¹H-NMR: 8.18 (C(9*)H, 2H, d, ³J(9*-8*)=8.5Hz), 7.86 (C(6*)H, 2H, d, ³J(6*-7*)=8.1Hz), 8.84 (C(5*)H, 2H, d, ³J(5*-4*)=8.8Hz), 7.66 (C(2§)H, 4H, s), 7.6-7.5 (C(8*)H, C(4††)H,

C(6††)H, 6H, m), 7.38 (C(7*)H, 2H, dd, $^3J(7^*-6^*)=8.1\text{Hz}$, $^3J(7^*-8^*)=7.5\text{Hz}$), 7.27 (C(4*)H, 2H, d, $^3J(4^*-5^*)=8.8\text{Hz}$), 7.03 (C(7††)H, 2H, d, $^3J(7††-6††)=8.2\text{Hz}$), 6.04 (C(1'')H, 2H, s), 5.95 (C(1')H, 2H, s), 4.10 (C(1†)H₂, 4H, br), 3.52 (C(1‡‡)H₃, 6H, br), 2.06 (C(1**)H₃, 12H, s), 2.0-1.8 (C(1‡)H₃, C(2†)H₂, 16H, m), 1.5-1.2 (C(3†)H₂, C(4†)H₂, C(5†)H₂, C(6†)H₂, C(7†)H₂, 20H, m), 0.84 (C(8†)H₃, 6H, t, $^3J(8†-7†)=6.8\text{Hz}$).

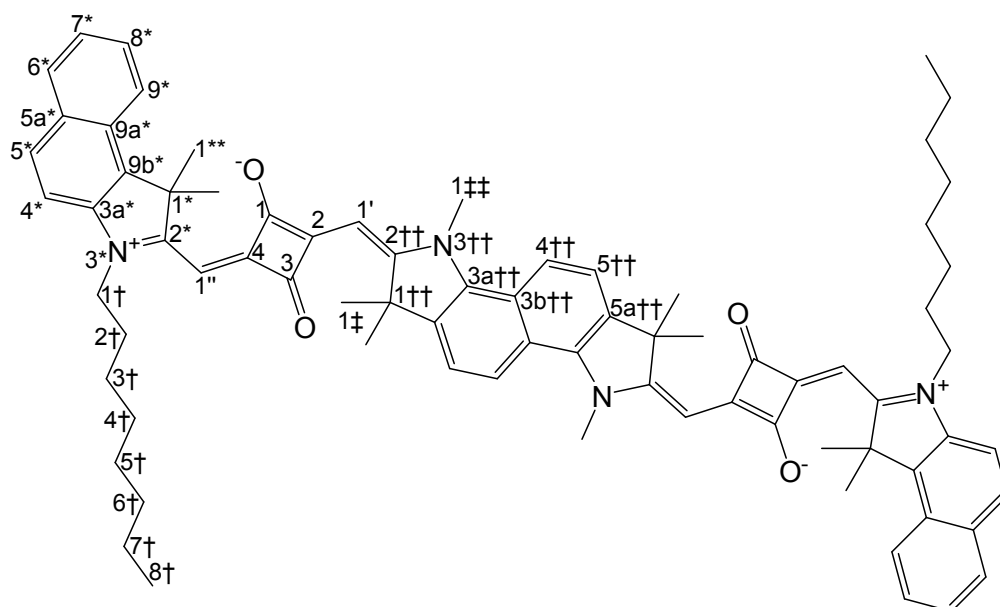
¹³C-NMR: 182.27, 179.74, 177.49, 172.13, 169.24, 142.55, 142.45, 139.26, 135.93, 134.50, 131.15, 129.53, 128.41, 127.18, 127.14, 126.43, 124.29, 122.40, 120.59, 110.05, 109.04, 86.84, 86.48, 51.22, 48.79, 43.78, 31.51, 29.12, 28.94, 27.25, 27.14, 26.83, 26.50, 22.39, 13.90.

MS: 1220 (100) [M+H]⁺, 1219 (82) [M]⁺, 1205 (24) [M+H-CH₃]⁺, 1190 (10) [M+H-2·CH₃]⁺, 912 (16) [C₆₂H₆₂N₃O₄]⁺, 805 (11) [C₅₆H₅₉N₃O₂]⁺, 790 (6) [C₅₅H₅₆N₃O₂]⁺, 609.8 (4) [M+H]⁺⁺, 609.3 (3) [M]⁺⁺, 414 (12) [C₂₈H₃₂NO₂]⁺.

HR-MS: calculated for C₈₄H₉₀N₄O₄ [M]⁺: 1218.6957. Found: 1218.6980.

Elemental analysis: calculated for C₈₄H₉₀N₄O₄: C, 82.72; H, 7.44; N, 4.59; O, 5.25. Found: C, 82.45; H, 7.50; N, 4.65; O, 5.45.

2,2'-(1,1,3,6,6,8-Hexamethylindolo[7,6-g]indole-2,7(1*H*,3*H*,6*H*,8*H*)-diylidene)bis(methan-1-yl-1-ylidene)bis(4-((1,1-dimethyl-3-octyl-1*H*-benzo[*e*]indolium-2-yl)methylene)-3-oxocyclobut-1-enolate) (14)



43 (1.36 g, 3.27 mmol, page 146), **57** (1.00 g, 1.31 mmol, Thomas Geiger [23]), toluene (10 mL), 1-butanol (20 mL) and quinoline (5 mL) were combined in a Dean-Stark apparatus and boiled for 60 h. Subsequently, the reaction mixture was concentrated *in vacuo*. The residue was dissolved in ethanol (50 mL) and added dropwise to cold aqueous citric acid solution (600 mL, 10% w/v) as it was stirred vigorously for 15 min. The suspension was filtered and the residue was digested in saturated potassium carbonate solution (100 mL) and, afterwards, washed with water four times. Subsequent purification by column chromatography (chloroform) yielded **14** (1.1 g, 0.85 mmol, 65%) and in an earlier fraction the mono Knoevenagel condensation product **58** (0.12 g, 0.14 mmol) was verified by UV/Vis spectroscopy ($\lambda_{max} = 687$ nm in chloroform, same λ_{max} as the compound **68** with ethylated benzo[*e*]indole synthon) which was then used without further characterization in the preparation of **26** (page 123).

Decomposition onset: 317 °C. Residue: 28%.

¹H-NMR: 8.25-8.15 (C(4††)H, 2H, m), 8.21 (C(9*)H, 2H, dd, ³J(9*-8*)=8.6Hz, ⁴J(9*-7*)=0.8Hz), 7.90 (C(6*)H, 2H, dd, ³J(6*-7*)=7.8Hz, ⁴J(6*-8*)=1.1Hz), 7.88 (C(5*)H, 2H,

d, $^3J(5^*-4^*)=8.7\text{Hz}$, 7.58 (C(8^{*})H, 2H, ddd, $^3J(8^*-9^*)=8.6\text{Hz}$, $^3J(8^*-7^*)=7.0\text{Hz}$, $^4J(8^*-6^*)=1.1\text{Hz}$), 7.55-7.45 (C(5††)H, 2H, m), 7.43 (C(7^{*})H, 2H, ddd, $^3J(7^*-6^*)=7.8\text{Hz}$, $^3J(7^*-8^*)=7.0\text{Hz}$, $^4J(7^*-9^*)=0.8\text{Hz}$), 7.31 (C(4^{*})H, 2H, d, $^3J(4^*-5^*)=8.7\text{Hz}$), 6.2-6.0 (C(1')H, C(1'')H, 4H, m), 4.5-4.0 (C(1†)H₂, C(1‡‡)H₃, 10H, m), 2.08 (C(1**)H₃, 12H, s), 1.95-1.15 (C(1‡)H₃, C(2†)H₂, C(3†)H₂, C(4†)H₂, C(5†)H₂, C(6†)H₂, C(7†)H₂, 36H, m), 0.86 (C(8†)H₃, 6H, t, $^3J(8†-7†)=6.9\text{Hz}$).

¹³C-NMR: 182.43, 180.19, 177.13 (2C), 172.72, 171.12, 139.31, 138.93, 138.42, 134.86, 131.39, 129.72, 129.67, 128.54, 127.36, 124.54, 122.60, 122.33, 119.43, 117.89, 110.21, 88.08, 86.87, 51.50, 49.35, 48.62, 44.03, 31.66, 29.64, 29.28, 29.08, 27.45, 26.98, 26.59, 22.53, 14.01.

MS: 1140 (2) [M+Na]⁺, 1118 (100) [M+H]⁺, 1117 (65) [M]⁺, 1103 (17) [M+H-CH₃]⁺, 1088 (7) [M+H-2·CH₃]⁺, 1062 (2) [C₇₂H₇₇N₄O₄]⁺, 1006 (4) [C₆₈H₆₉N₄O₄]⁺, 810 (5) [C₅₄H₅₆N₃O₄]⁺, 718 (10) [C₄₉H₅₆N₃O₂]⁺, 704 (6) [C₄₈H₅₄N₃O₂]⁺, 558.8 (4) [M+H]²⁺, 414 (3) [C₂₈H₃₂NO₂]⁺, 279 (2) [M+H]⁴⁺.

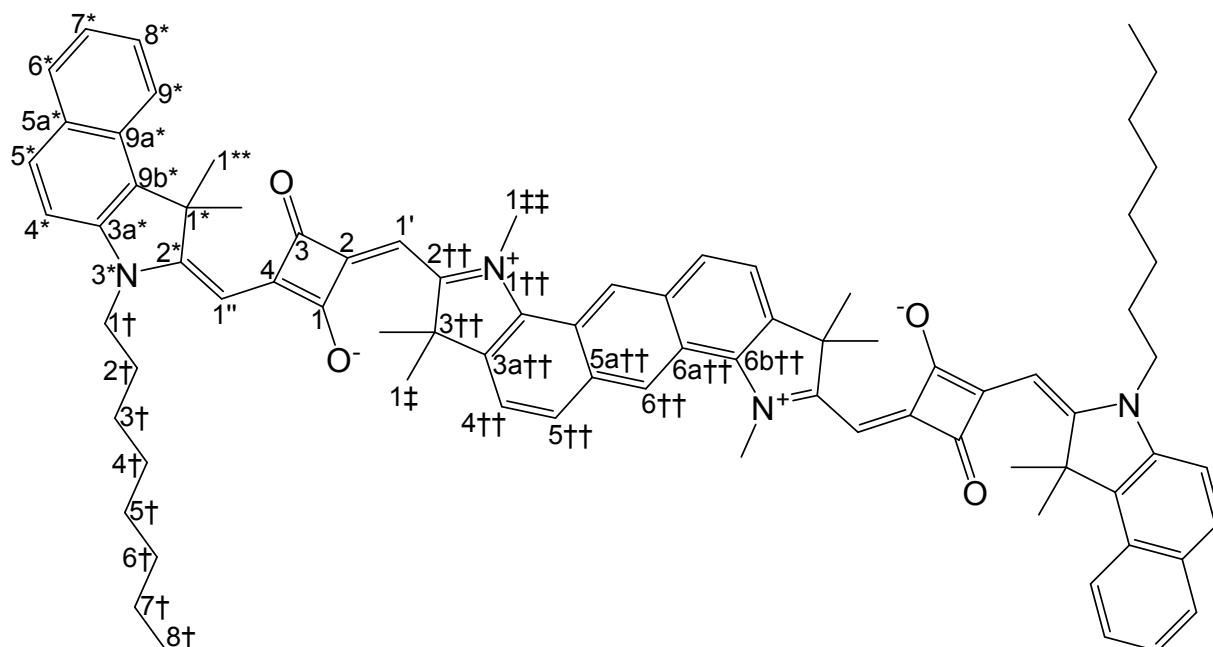
HR-MS: calculated for C₇₆H₈₅N₄O₄ [M+H]⁺: 1117.6565. Found: 1117.6590.

(C(8*)H, C(4††)H, C(6††)H, C(1§)H, C(3§)H, 10H, m), 7.43 (C(7*)H, 2H, ddd, $^3J(7^*-6^*)=8.0\text{Hz}$, $^3J(7^*-8^*)=7.0\text{Hz}$, $^4J(7^*-9^*)=0.8\text{Hz}$), 7.31 (C(4*)H, 2H, d, $^3J(4^*-5^*)=9.2\text{Hz}$), 7.05 (C(7††)H, 2H, d, $^3J(7††-6††)=8.5\text{Hz}$), 6.15-5.9 (C(1')H, C(1'')H, 4H, m), 4.2-4.0 (C(1†)H₂, 4H, m), 3.7-3.5 (C(1‡‡)H₃, 6H, br), 2.2-2.0 (C(1§§)H₂, C(1**)H₃, 16H, m), 2.0-1.7 (C(1‡)H₃, C(2†)H₂, 16H, m), 1.5-1.2 (alkyl chain, 24H, m), 1.0-0.7 (alkyl chain, 20H, m), 0.65-0.5 (alkyl chain, 10H, m).

MS: 1532 (100) [M+H]⁺, 1517 (14) [M+H-CH₃]⁺, 1225 (4) [C₈₅H₉₉N₃O₄]⁺, 1118 (2) [C₇₉H₉₅N₃O₂]⁺, 766 (1) [M+H]⁺⁺.

HR-MS: calculated for C₁₀₇H₁₂₇N₄O₄ [M+H]⁺: 1531.9852. Found: 1531.9823.

4-((1,1-Dimethyl-3-octyl-1*H*-benzo[*e*]indolium-2-yl)methylene)-2-((8-((3-((1,1-dimethyl-3-octyl-1*H*-benzo[*e*]indolium-2-yl)methylene)-2-oxido-4-oxocyclobut-1-enyl)methylene)-1,3,3,7,9,9-hexamethyl-8,9-dihydro-1,7-diaza-dicyclopenta[*a,h*]anthracen-2(3*H*)-ylidene)methyl)-3-oxocyclobut-1-enolate (16)



To transform **63** (3.00 g, 5.27 mmol, page 168) into the deprotonated reactive species, it was suspended in a mixture of toluene (30 mL) and aqueous sodium hydroxide solution (10 mL, 40% w/w) at rt in the dark while stirring for 30 min. The product containing organic layer was separated, dried with sodium sulphate and placed in a new reactor in which **43** (8.80 g, 21.1 mmol, page 146), 1-butanol (70 mL) and quinoline (10 mL) were also added. The reaction mixture was then heated to reflux for 3 d. Thereafter, the solvent was evaporated under reduced pressure and the remainder was dissolved in ethanol (50 mL). This solution was then added dropwise into ice-water (1 L) and stirred for 1 h. The precipitate was filtered and subsequent purification of the residue by column chromatography (chloroform) yielded **16** (0.46 g, 0.39 mmol, 7%) as a gold shimmering crystalline powder.

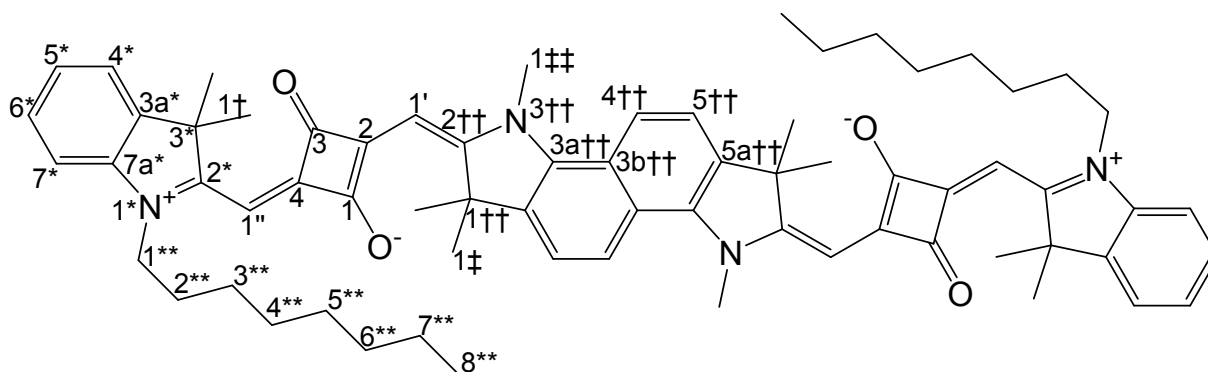
Decomposition onset: 293 °C. Residue: 34%.

¹H-NMR: 9.05 (C(6††)H, 2H, s), 8.22 (C(9*)H, 2H, d, ³J(9*-8*)=8.6Hz), 7.9-7.8 (C(5*)H, C(6*)H, C(4††)H, 6H, m), 7.59 (C(8*)H, 2H, ddd, ³J(8*-9*)=8.6Hz, ³J(8*-7*)=6.8Hz, ⁴J(8*-6*)=1.3Hz), 7.5 (C(5††)H, 2H, m), 7.44 (C(7*)H, 2H, ddd, ³J(7*-6*)=7.0Hz, ³J(7*-8*)=6.8Hz, ⁴J(7*-9*)=0.8Hz), 6.3-6.0 (C(1')H, C(1'')H, 4H, m), 4.29 (C(1†)H₂, 4H, m), 4.15 (C(1††)H₃, 6H, m), 2.09 (C(1**)H₃, 12H, s), 2.0-1.2 (C(1‡)H₃, C(2†)H₂, C(3†)H₂, C(4†)H₂, C(5†)H₂, C(6†)H₂, C(7†)H₂, 36H, m), 0.87 (C(8†)H₂, 6H, t, ³J(8†-7†)=7.0Hz).

MS: 1190 (4) [M+Na]⁺, 1168 (100) [M+H]⁺, 1153 (22) [M+H-CH₃]⁺, 1138 (8) [M+H-2·CH₃]⁺, 1123 (3) [M+H-3·CH₃]⁺, 1056 (4) [C₇₂H₇₁N₄O₄]⁺, 999 (10) [C₆₈H₆₃N₄O₄]⁺, 860 (8) [C₅₈H₅₈N₃O₄]⁺, 754 (6) [C₅₂H₅₆N₃O₂]⁺, 584 (4) [M+H]⁺⁺, 414 (3) [C₂₈H₃₂NO₂]⁺.

HR-MS: calculated for C₈₀H₈₇N₄O₄ [M+H]⁺: 1167.6722. Found: 1167.6728.

2,2'-(1,1,3,6,6,8-Hexamethylindolo[7,6-g]indole-2,7(1H,3H,6H,8H)-diylidene)bis(methan-1-yl-1-ylidene)bis(4-((3,3-dimethyl-1-octyl-3H-indolium-2-yl)methylene)-3-oxocyclobut-1-enolate) (17)



The condensation reaction was performed in a Dean-Stark apparatus with **34** (1.50 g, 3.59 mmol, page 135) and **57** (630 mg, 1.44 mmol, Thomas Geiger [23]) in the solvent mixture of toluene (10 mL), 1-butanol (20 mL) and quinoline (5 mL) at reflux temperature for 5 d. Afterwards, the solvent was evaporated *in vacuo*. The remainder was dissolved in ethanol (100 mL) and added dropwise into cold aqueous citric acid solution (800 mL, 10% w/w) while stirring. After 15 min the suspension was filtered and the residue was suspended in saturated potassium carbonate solution (100 mL) filtered and washed with water several times. Subsequent purification by column chromatography (chloroform:ethanol = 95:5) yielded **17** (0.93 g, 0.89 mmol, 62%).

Decomposition onset: 304 °C. Residue: 34%.

¹H-NMR: 8.18 (C(4††)H, 2H, d, ³J(4††-5††)=8.2Hz), 7.47 (C(5††)H, 2H, d, ³J(5††-4††)=8.2Hz), 7.37 (C(7*)H, 2H, dd, ³J(7*-6*)=7.3Hz, ⁴J(7*-5*)=0.9Hz), 7.32 (C(5*)H, 2H, ddd, ³J(5*-4*)=7.8Hz, ³J(5*-6*)=7.7Hz, ⁴J(5*-7*)=0.9Hz), 7.17 (C(6*)H, 2H, ddd, ³J(6*-5*)=7.7Hz, ³J(6*-7*)=7.3Hz, ⁴J(6*-4*)=0.6Hz), 7.01 (C(4*)H, 2H, dd, ³J(4*-5*)=7.8Hz, ⁴J(4*-6*)=0.6Hz), 6.2-5.9 (C(1')H, C(1'')H, 4H, m), 4.5-3.9 (C(1**)H₂, C(1††)H₃, 10H, m), 2.0-1.5 (C(1‡)H₃, C(1†)H₃, C(2**)H₂, 28H, m), 1.5-1.2 (C(3**)H₂, C(4**)H₂, C(5**)H₂, C(6**)H₂, C(7**)H₂, 20H, m), 0.86 (C(8**)H₃, 6H, t, ³J(8**-7**) = 6.9Hz).

¹³C-NMR: 182.35, 181.07, 178.27, 171.52, 171.03 (2C), 142.33, 142.24, 138.90,

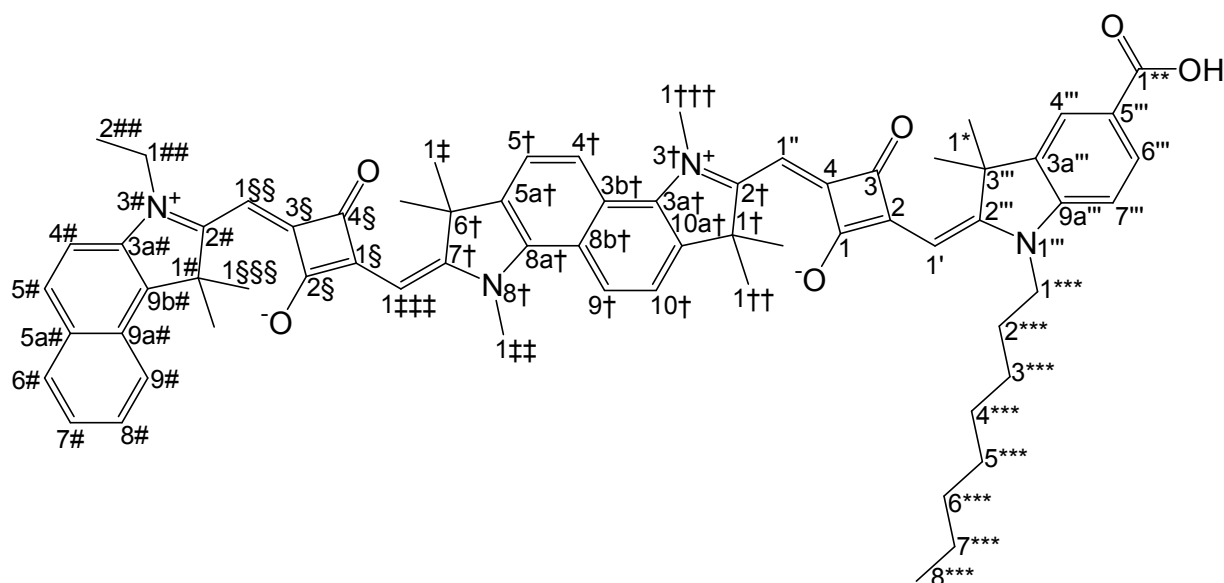
138.56, 127.79, 124.07, 122.37, 122.30, 119.47, 118.14, 109.66, 88.09, 87.11, 49.55, 48.73, 43.87, 36.71, 31.67, 29.26, 29.08, 27.23, 27.10, 27.01, 26.85, 22.53, 14.02.

MS: 1040 (3) $[M+Na]^+$, 1018 (100) $[M+H]^+$, 1017 (58) $[M]^+$, 1003 (12) $[M+H-CH_3]^+$, 988 (3) $[M+H-2\cdot CH_3]^+$, 654 (4) $[C_{44}H_{52}N_3O_2]^+$, 508.8 (4) $[M+H]^{++}$.

HR-MS: calculated for $C_{68}H_{80}N_4O_4$ $[M]^+$: 1016.6174. Found: 1016.6180.

Elemental analysis: calculated for $C_{68}H_{80}N_4O_4$: C, 80.28; H, 7.93; N, 5.51; O, 6.29. Found: C, 80.00; H, 7.94; N, 5.28; O, 6.37.

2-((5-Carboxy-3,3-dimethyl-1-octylindolin-2-ylidene)methyl)-4-((7-((3-((3-ethyl-1,1-dimethyl-1*H*-benzo[*e*]indol-2(3*H*)-ylidene)methyl)-2-oxido-4-oxocyclobut-2-enylidene)methyl)-1,1,3,6,6,8-hexamethyl-1,6-dihydroindolo[7,6-*g*]indol-3,8-diium-2-yl)methylene)-3-oxocyclobut-1-enolate (18)



68 (1.50 g, 1.77 mmol, page 172), **64** (1.29 g, 1.84 mmol, page 169), toluene (15 mL), 1-butanol (30 mL) and quinoline (1 mL) were combined and were brought to reaction for 3 d at reflux temperature. After this time the reaction mixture was cooled to rt

and poured in ice (1 L). The precipitation was filtered and subsequently dissolved in chloroform (200 mL) which was then extracted with water (3x200 mL) and saturated aqueous potassium carbonate solution (200 mL). Unfortunately, the potassium salt of the product precipitated as a gel between the two phases. It could be separated by centrifugation. The gel-like residue was washed several times with water until the consistency of the residue changed to a powder like shape. The wet centrifugation residue was filtered through a 0.45 μm cellulose membrane filter. The fine powder was acidified with saturated citric acid (25 mL), extracted with chloroform (250 mL) and the organic layer was concentrated under vacuum to yield **18** (0.36 g, 0.35 mmol, 19%) as dark blue powder. The below presented picture shows the absorbed dye **18** on titanium dioxide nano particles (20nm) which were sintered to a homogeneous 8 μm thick layer on a glass plate (Figure 4.3).

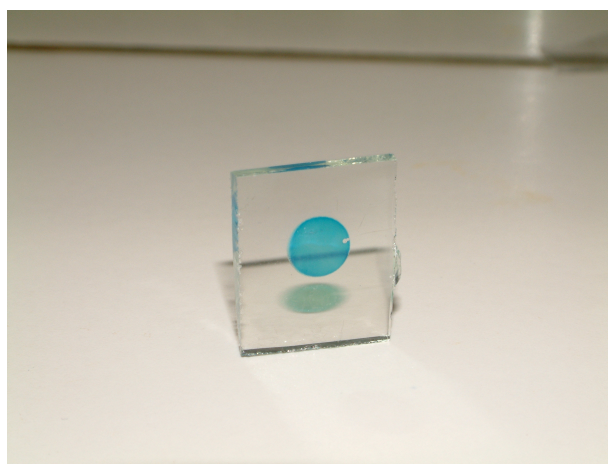


Figure 4.3: Picture of **64** absorbed from a 10^{-5} M chloroform solution on sintered titanium dioxide nano particle spot of 6 mm in diameter on a glass plate.

Decomposition onset: 273 °C. Residue: 45%.

$^1\text{H-NMR}$ (DMSO- d_6): 8.39 (C(4 \dagger)H, 1H, d, $^3\text{J}(4\ddagger-5\ddagger)=9.2\text{Hz}$), 8.34 (C(9 \dagger)H, 1H, d, $^3\text{J}(9\ddagger-10\ddagger)=8.8\text{Hz}$), 8.26 (C(9 $\#$)H, 1H, d, $^3\text{J}(9\#-8\#)=8.2\text{Hz}$), 8.05 (C(5 $\#$)H, 1H, d, $^3\text{J}(5\#-4\#)=9.0\text{Hz}$), 8.03 (C(6 $\#$)H, 1H, d, $^3\text{J}(6\#-7\#)=7.2\text{Hz}$), 8.00 (C(4 $'''$)H, 1H, d, $^4\text{J}(4'''-6''')=1.4\text{Hz}$), 7.94 (C(6 $'''$)H, 1H, d, $^3\text{J}(6'''-7''')=8.6\text{Hz}$, $^4\text{J}(6'''-4''')=1.4\text{Hz}$), 7.78 (C(10 \dagger)H, 1H, d, $^3\text{J}(10\ddagger-9\ddagger)=8.8\text{Hz}$), 7.77 (C(5 \dagger)H, 1H, d, $^3\text{J}(5\ddagger-7)=9.4\text{Hz}$), 7.75 (C(4 $\#$)H, 1H, d, $^3\text{J}(4\#-5\#)=9.0\text{Hz}$), 7.63 (C(8 $\#$)H, 1H, d, $^3\text{J}(8\#-9\#)=8.2\text{Hz}$, $^3\text{J}(8\#-7\#)=7.6\text{Hz}$), 7.47 (C(7 $\#$)H, 1H, d, $^3\text{J}(7\#-8\#)=7.6\text{Hz}$, $^3\text{J}(7\#-6\#)=7.2\text{Hz}$), 7.36 (C(7 $'''$)H, 1H, d, $^3\text{J}(7'''-$

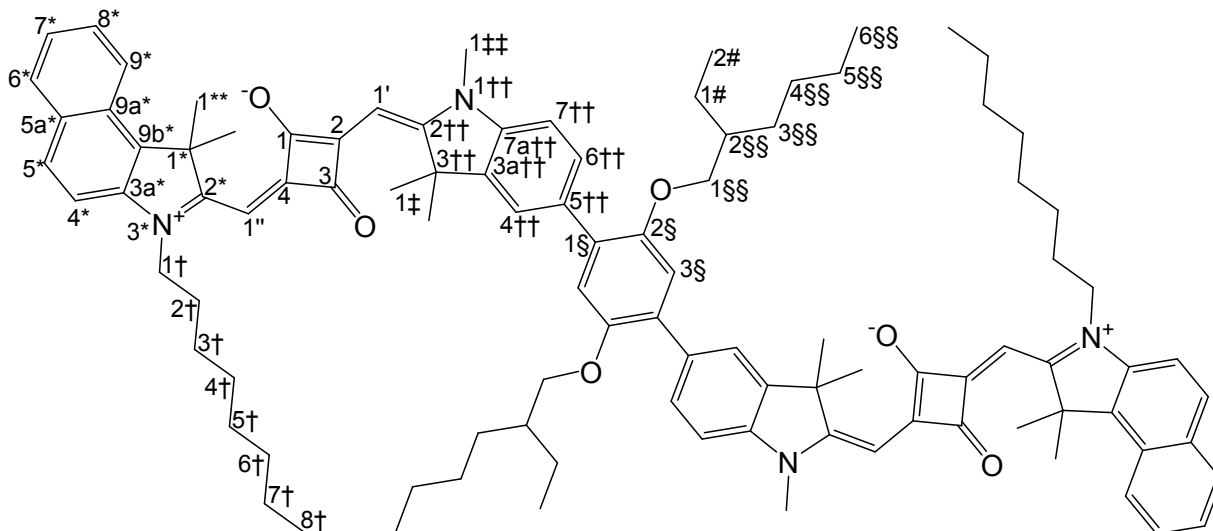
6^{'''})=8.6Hz), 6.0-5.85 (C(1')H, C(1'')H, C(1‡‡‡)H, C(1§§)H, 4H, m), 4.31 (C(1##)H₂, 2H, q, ³J(1##-2##)=6.8Hz), 4.15-4.05 (C(1†††)H₃, C(1‡‡)H₃, C(1***H₂, 8H, m), 1.96 (C(1§§§)H₃, 6H, s), 1.74 (C(1††)H₃, C(1‡)H₃, 12H, s), 1.70 (C(1*)H₃, 6H, s), 1.74-1.70 (C(2***H₂, 2H, m), 1.40-1.20 (C(2##)H₃, C(3***H₂, C(4***H₂, C(5***H₂, C(6***H₂, C(7***H₂, 13H, m), 0.85 (C(8***H₃, 3H, t, ³J(8***-7***)=6.4Hz).

¹³C-NMR (DMSO-d₆): 181.10, 181.02, 180.89, 180.76, 177.70, 176.72, 173.17, 171.15, 167.86, 167.12, 146.24, 141.26, 139.12, 138.91, 138.71, 138.31, 133.76, 131.09, 130.28, 129.93, 129.76, 127.90, 127.53, 125.22, 124.47, 123.13, 122.38, 122.08, 121.78, 120.16, 119.64, 118.26, 111.30, 109.67, 104.58, 88.10, 87.56, 87.28, 86.16, 50.91, 48.89, 48.17, 48.10, 42.98, 40.19, 38.48, 37.50, 31.15, 28.67, 28.59, 26.67, 26.66, 26.44, 26.43, 26.19, 26.17, 26.00, 22.06, 13.96, 12.21.

MS: 1050 (3) [M+Na]⁺, 1028 (100) [M+H]⁺, 1027 (64) [M]⁺, 1012 (16) [M-CH₃]⁺, 997 (5) [M-CH₂CH₃]⁺, 983 (1) [M-CO₂]⁺, 915 (1) [C₅₉H₅₅N₄O₆]⁺, 804 (2) [C₅₁H₅₄N₃O₆]⁺, 726 (1) [C₄₈H₄₄N₃O₄]⁺, 709 (3) [C₄₆H₅₁N₃O₄]⁺, 697 (2) [C₄₅H₅₁N₃O₄]⁺, 619 (1) [C₄₂H₄₁N₃O₂]⁺, 514 (4) [M+H]⁺⁺, 408 (1) [C₂₅H₃₀NO₄]⁺, 330 (2) [C₂₂H₂₀NO₂]⁺, 257 (1) [M+H]⁴⁺.

HR-MS: calculated for C₆₇H₇₁N₄O₆ [M+H]⁺: 1027.5368. Found: 1027.5386.

2,2'-(5,5'-(2,5-Bis(2-ethylhexyloxy)-1,4-phenylene)bis(1,3,3-trimethylindoline-5-yl-2-ylidene))bis(methan-1-yl-1-ylidene)bis(4-((1,1-dimethyl-3-octyl-1*H*-benzo[*e*]indolium-2-yl)methylene)-3-oxocyclobut-1-enolate) (19)



In a Dean-Stark apparatus **43** (1.25 g, 2.85 mmol, page 146), **54** (1.00 g, 1.14 mmol, page 160), toluene (5 mL), 1-butanol (5 mL) and 1-methyl-2-pyrrolidinone (5 mL) were mixed and heated to reflux for 2 d. According to UV/Vis measurements the reaction proceeded slowly and the pH changed from 6 to 7.5. In order to acidify the reaction mixture, aqueous hydrochloric acid (2 mL, 1 N) was added. The reaction was completed by refluxing for an additional day. Afterwards, the solvent was removed under reduced pressure. The concentrate was diluted with ethanol (10 mL) and poured in water (250 mL). The suspension was stirred for 30 min and the precipitate was filtered. The residue was digested with diethyl ether several times. Subsequent purification by column chromatography (chloroform) yielded **19** (0.48 g, 0.33 mmol, 29%).

Decomposition onset: 287 °C. Residue: 35%.

¹H-NMR: 8.21 (C(9*)H, 2H, dd, ³J(9*-8*)=8.4Hz, ⁴J(9*-7*)=1.0Hz), 7.90 (C(6*)H, 2H, dd, ³J(6*-7*)=8.0Hz, ⁴J(6*-8*)=1.2Hz), 7.88 (C(5*)H, 2H, d, ³J(5*-4*)=9.0Hz), 7.66 (C(4††)H, 2H, d, ⁴J(4††-6††)=1.5Hz), 7.58 (C(8*)H, 2H, ddd, ³J(8*-9*)=8.4Hz,

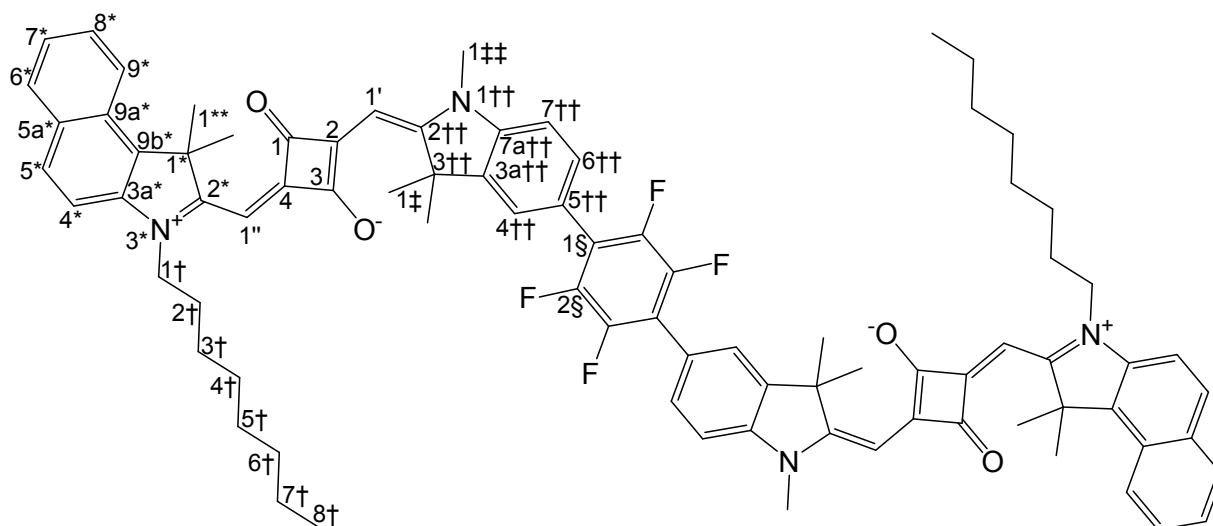
$^3J(8^*-7^*)=7.0\text{Hz}$, $^4J(8^*-6^*)=1.2\text{Hz}$, 7.51 (C(6††)H, 2H, dd, $^3J(6††-7††)=8.2\text{Hz}$, $^4J(6††-5††)=1.5\text{Hz}$), 7.42 (C(7*)H, 2H, ddd, $^3J(7^*-6^*)=8.0\text{Hz}$, $^3J(7^*-8^*)=7.0\text{Hz}$, $^4J(7^*-9^*)=1.0\text{Hz}$), 7.31 (C(4*)H, 2H, d, $^3J(4^*-5^*)=9.0\text{Hz}$), 7.05 (C(7††)H, 2H, d, $^3J(7††-6††)=8.2\text{Hz}$), 6.99 (C(3§)H, 2H, s), 6.1-5.8 (C(1')H, C(1'')H, 4H, m), 4.2-4.0 (C(1†)H₂, 4H, m), 4.0-3.7 (C(1§§)H₂, 4H, m), 3.7-3.5 (C(1‡‡)H₃, 6H, br), 2.07 (C(1**)H₃, 12H, s), 2.0-1.7 (C(1‡)H₃, C(2†)H₂, 16H, m), 1.7-1.5 (C(2§§)H₂, 4H, m), 1.5-1.1 (C(3†)H₂, C(4†)H₂, C(5†)H₂, C(6†)H₂, C(7†)H₂, C(3§§)H₂, C(4§§)H₂, C(5§§)H₂, C(1#)H₂, 36H, m), 0.86 (C(8†)H₃, C(6§§)H₂, C(2#)H₂, 18H, m).

$^{13}\text{C-NMR}$: 182.43, 178.68, 177.47, 172.13, 170.04, 166.59, 150.35, 141.45, 139.46, 134.63, 134.07, 131.28, 130.14, 129.67, 129.65, 128.86, 128.60, 127.31, 124.39, 123.86, 122.59, 120.27, 115.54, 110.18, 108.47, 86.88, 86.54, 71.61, 51.32, 49.06, 43.95, 39.59, 31.72, 31.69, 30.40, 29.30, 29.11, 28.97, 27.40, 27.21, 27.01, 26.66, 23.88, 22.95, 22.55, 14.03, 11.01.

MS: 1498 (3) [M+Na]⁺, 1476 (100) [M+H]⁺, 1475 (55) [M]⁺, 1461 (11) [M+H-CH₃]⁺, 1446 (2) [M-C₂H₅]⁺, 1169 (6) [C₇₈H₉₄N₃O₆]⁺, 1077 (12) [C₇₃H₉₄N₃O₄]⁺, 1062 (7) [C₇₂H₉₁N₃O₄]⁺, 738 (1) [M+H]⁺⁺.

HR-MS: calculated for C₁₀₀H₁₂₃O₆N₄ [M+H]⁺: 1475.9437. Found: 1475.9468.

2,2'-(5,5'-(Perfluoro-1,4-phenylene)bis(1,3,3-trimethylindoline-5-yl-2-ylidene))bis(methan-1-yl-1-ylidene)bis(4-((1,1-dimethyl-3-octyl-1*H*-benzo[*e*]indolium-2-yl)methylene)-3-oxocyclobut-1-enolate) (20)



In a Dean-Stark apparatus **43** (474 mg, 1.08 mmol, page 146), **56** (300 mg, 0.433 mmol, page 162), toluene (5 mL), 1-butanol (5 mL) and 1-methyl-2-pyrrolidinone (5 mL) were combined to generate **20** within 7 d at 120 °C. Due to a change of the pH value to about 7.5 the reaction proceeded very slowly which was visualized by UV/Vis measurements. Therefore aqueous hydrochloric acid (2 mL, 1 N) was added and the reaction mixture was heated for an additional 2 d. Then the reaction mixture was concentrated *in vacuo* and the remnant was dissolved in ethanol (10 mL). This solution was added dropwise into water (1 L). After stirring for 30 min the suspension was filtered and the residue was digested in diethyl ether several times to yield **20** (0.39 g, 0.30 mmol, 69%).

Decomposition onset: 283 °C. Residue: 37%.

¹H-NMR: 8.21 (C(9*)H, 2H, d, ³J(9*-8*)=8.5Hz), 7.91 (C(6*)H, 2H, d, ³J(6*-7*)=8.3Hz), 7.89 (C(5*)H, 2H, d, ³J(5*-4*)=8.6Hz), 7.59 (C(8*)H, 2H, dd, ³J(8*-9*)=8.5Hz, ³J(8*-7*)=7.0Hz), 7.5-7.4 (C(4††)H, C(6††)H, C(7*)H, 6H, m), 7.32 (C(4*)H, 2H, d, ³J(4*-5*)=8.6Hz), 7.05 (C(7††)H, 2H, d, ³J(7††-6††)=8.4Hz), 6.12 (C(1'')H, 2H, br), 6.00 (C(1')H, 2H, br), 4.18 (C(1†)H₂, 4H, m), 3.56 (C(1‡‡)H₃, 6H, br), 2.07 (C(1***)H₃, 12H, s), 2.0-1.7 (C(1‡)H₃, C(2†)H₂, 16H, m), 1.5-1.2 (C(3†)H₂, C(4†)H₂, C(5†)H₂, C(6†)H₂,

$C(7\uparrow)H_2$, 20H, m), 0.87 ($C(8\uparrow)H_3$, 6H, $^3J(8\uparrow-7\uparrow)=6.5\text{Hz}$).

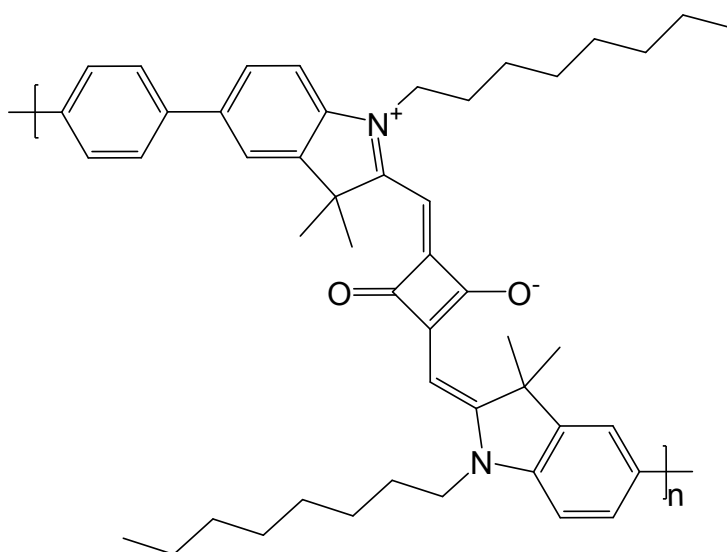
$^{13}\text{C-NMR}$: 182.44, 178.68, 177.47, 173.36, 170.04, 168.89, 145.49, 143.84, 142.86, 142.25, 139.23, 135.10, 131.51, 130.70, 130.02, 129.80, 129.70, 128.53, 127.44, 124.70, 124.05, 122.66, 121.99, 110.28, 108.71, 87.32, 87.07, 51.64, 48.69, 44.18, 31.69, 30.43, 29.29, 29.10, 27.51, 27.22, 27.00, 26.56, 22.55, 14.03.

$^{19}\text{F-NMR}$: -144.4 ($C(2\text{§})F$, 4F, s).

MS: 1314 (2) $[M+Na]^+$, 1292 (100) $[M+H]^+$, 1277 (16) $[M+H-CH_3]^+$, 1262 (7) $[M-C_2H_5]^+$, 984 (5) $[C_{62}H_{58}F_4N_3O_4]^+$, 877 (4) $[C_{56}H_{55}F_4N_3O_2]^+$, 720 (8) $[C_{45}H_{44}F_4N_2O_2]^+$, 646 (4) $[M+H]^{++}$, 414 (4) $[C_{28}H_{32}NO_2]^+$.

HR-MS: calculated for $C_{84}H_{87}F_4N_4O_4$ $[M+H]^+$: 1291.6658. Found: 1291.6634.

(*para*-phenylene-(4-((3,3-dimethyl-1-octyl-3*H*-indolium-2,5-diyl)methylene)-2-((3,3-dimethyl-1-octylindolin-2-ylidene-5-yl)methyl)-3-oxocyclobut-1-enolate))₃₋₄ (21)



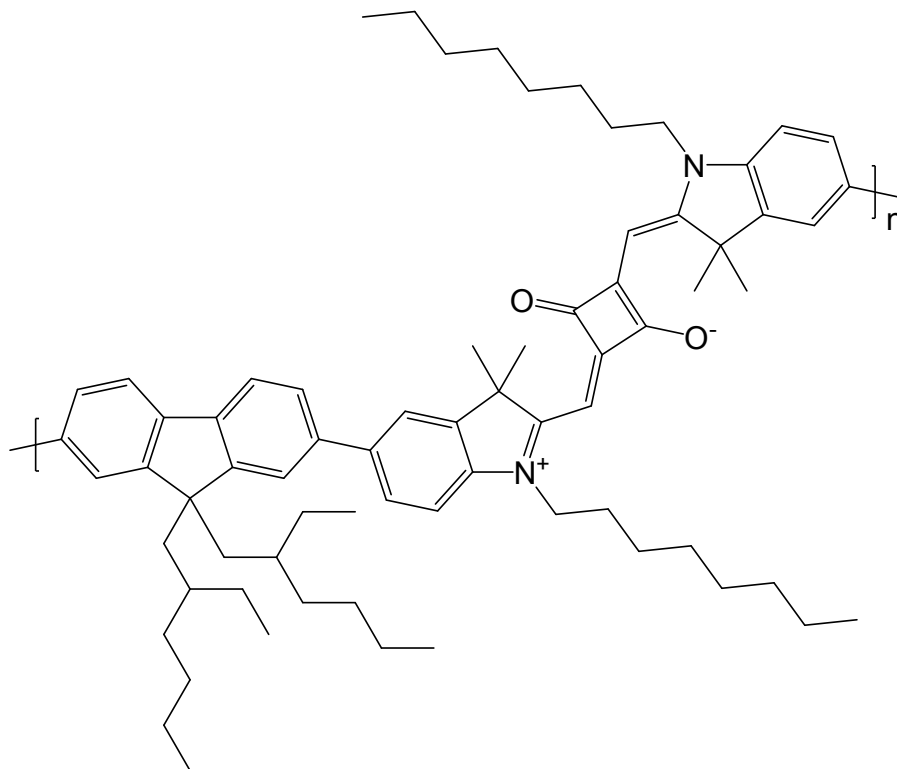
All solvents and solutions were degassed by freeze-pump-thaw cycles. **29** (200 mg, 257 μmol , page 128), **37** (63.2 mg, 257 μmol , page 139) and the catalyst **71** (2.0 mg, 1.8 μmol , page 175) were placed in a 25 mL round bottom flask and fitted with a septum. Then 1-methyl-2-pyrrolidone (5 mL), tetrahydrofuran (3 mL) and an aqueous saturated

sodium hydrogen carbonate solution (2 mL) were added via syringe. The reaction mixture was heated to 80°C for 7 d, while a very dark powder started to precipitate. After reaction, the solvent was completely removed under vacuum and the residue was dissolved in chloroform (100 mL). This organic layer was washed with water (2x50 mL) and brine (50 mL). The dried organic layer was concentrated under reduced pressure to about 2 – 5 mL which was then dripped into ethanol (250 mL) under vigorously stirring. A very fine dark powder precipitated and was filtered. According to UV/Vis measurements the residue showed an more red shifted λ_{max} then the filtrate, therefore it was assumed that some of the lower molecular weight component could be washed out by this precipitation. **21** (0.12 g, 0.17 mmol per formal unit, 67%, \bar{X}_n : 3) was obtained by drying the filtration residue in a vacuum oven.

Decomposition onset: 288°C. Residue: 52%.

MS (MALDI-TOF): 4254 (2) [6 dye units and 5 bridges], 3559 (10) [5 dye units and 5 bridges], 3132 (4) [4 dye units and 5 bridges], 2864 (42) [4 dye units and 3 bridges], 2437 (13) [3 dye units and 4 bridges], 2168 (100) [3 dye units and 2 bridges], 1742 (10) [2 dye units and 3 bridges], 1047 (7) [1 dye unit and 2 bridges].

(9,9-bis(2-ethylhexyl)-9*H*-2,7-fluorenylene-(4-((3,3-dimethyl-1-octyl-3*H*-indolium-2,5-diyl)methylene)-2-((3,3-dimethyl-1-octylindolin-2-ylidene-5-yl)methyl)-3-oxocyclobut-1-enolate))₃₋₄ (22)



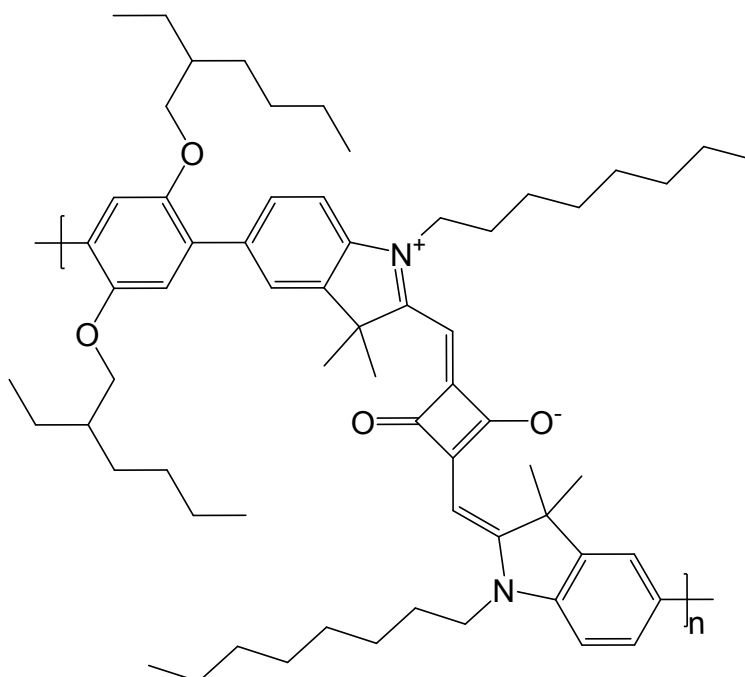
All solvents and solutions were degassed by freeze-pump-thaw cycles. **38** (200 mg, 229 μmol , page 140), 2,7-dibromo-9,9-bis(2-ethylhexyl)-9*H*-fluorene (126 mg, 229 μmol) and the catalyst **71** (1.9 mg, 1.6 μmol , page 175) were placed in a 25 mL round bottom flask and fitted with a septum. Then 1-methyl-2-pyrrolidone (5 mL), tetrahydrofuran (3 mL) and an aqueous saturated sodium hydrogen carbonate solution (2 mL) were added via syringe. The reaction mixture was heated to 80°C for 7 d, while a very dark powder started to precipitate. After reaction, the solvent was completely removed under vacuum and the residue was dissolved in chloroform (100 mL). This organic layer was washed with water (2x50 mL) and brine (50 mL). The dried organic layer was concentrated under reduced pressure to about 2 – 5 mL which was then dripped into ethanol (250 mL) under vigorously stirring. A very fine dark powder precipitated and was filtered. According to UV/Vis measurements the residue showed an more red

shifted λ_{max} then the filtrate, therefore it was assumed that some of the lower molecular weight component could be washed out by this precipitation. **22** (150 mg, 0.15 mmol per formal unit, 64%, \bar{X}_n : 3) was obtained by drying the filtration residue in a vacuum oven.

Decomposition onset: 296 °C. Residue: 49%.

MS (MALDI-TOF): 6595 (3) [6 dye units and 7 bridges], 5587 (10) [5 dye units and 6 bridges], 4578 (34) [4 dye units and 5 bridges], 4186 (8) [4 dye units and 4 bridges], 3764 (15) [4 dye units and 3 bridges], 3571 (77) [3 dye units and 4 bridges], 3180 (11) [3 dye units and 3 bridges], 2756 (21) [3 dye units and 2 bridges], 2563 (24) [2 dye units and 3 bridges], 1748 (41) [2 dye units and 1 bridge], 933 (55).

(2,5-bis(2-ethylhexyloxy)-*para*-phenylene-(4-((3,3-dimethyl-1-octyl-3*H*-indolium-2,5-diyl)methylene)-2-((3,3-dimethyl-1-octylindolin-2-ylidene-5-yl)methyl)-3-oxocyclobut-1-enolate))₃₋₅(23)



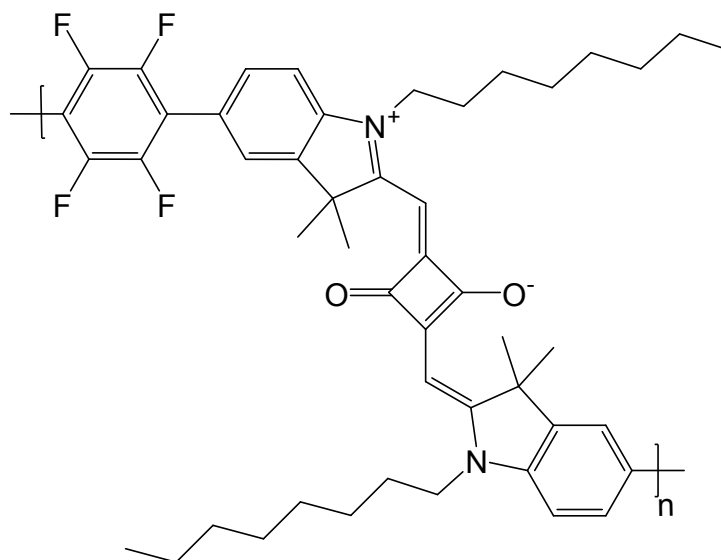
All solvents and solutions were degassed by freeze-pump-thaw cycles. **38** (200 mg, 229 μ mol, page 140), **52** (113 mg, 229 μ mol, page 157) and the catalyst **71** (1.9 mg, 1.6

μmol , page 175) were placed in a 25 mL round bottom flask and fitted with a septum. Then 1-methyl-2-pyrrolidone (5 mL), tetrahydrofuran (3 mL) and an aqueous saturated sodium hydrogen carbonate solution (2 mL) were added via syringe. The reaction mixture was heated to 80°C for 7 d, while a very dark powder started to precipitate. After reaction, the solvent was completely removed under vacuum and the residue was dissolved in chloroform (100 mL). This organic layer was washed with water (2x50 mL) and brine (50 mL). The dried organic layer was concentrated under reduced pressure to about 2 – 5 mL which was then dripped into ethanol (250 mL) under vigorously stirring. A very fine dark powder precipitated and was filtered. According to UV/Vis measurements the residue showed an more red shifted λ_{max} then the filtrate, therefore it was assumed that some of the lower molecular weight component could be washed out by this precipitation. **23** (80 mg, 84 μmol per formal unit, 37%, \bar{X}_n : 2) was obtained by drying the filtration residue in a vacuum oven.

Decomposition onset: 344 °C. Residue: 44%.

MS (MALDI-TOF): 8106 (2) [8 dye units and 9 bridges], 7153 (3) [7 dye units and 8 bridges], 6202 (12) [6 dye units and 7 bridges], 5250 (34) [5 dye units and 6 bridges], 4854 (9) [5 dye units and 5 bridges], 4298 (100) [4 dye units and 5 bridges], 3903 (23) [4 dye units and 4 bridges], 3347 (80) [3 dye units and 4 bridges], 2588 (8) [3 dye units and 2 bridges], 1636 (16) [2 dye units and 1 bridge].

(*para*-2,3,5,6-tetra fluoro phenylene-(4-((3,3-dimethyl-1-octyl-3*H*-indolium-2,5-diyl)methylene)-2-((3,3-dimethyl-1-octylindolin-2-ylidene-5-yl)methyl)-3-oxocyclobut-1-enolate))₃₋₄ (**24**)

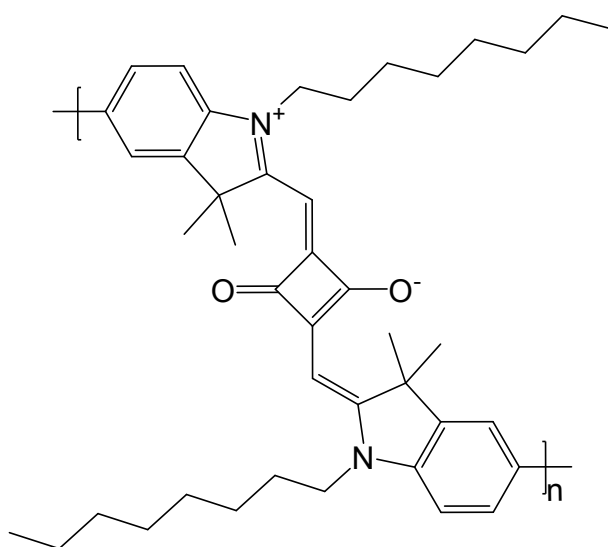


All solvents and solutions were degassed by freeze-pump-thaw cycles. **38** (200 mg, 229 μmol , page 140), 1,4-dibromotetrafluorobenzene (70.5 mg, 229 μmol , ABCR) and the catalyst **71** (1.9 mg, 1.6 μmol , page 175) were placed in a 25 mL round bottom flask and fitted with a septum. Then 1-methyl-2-pyrrolidone (5 mL), tetrahydrofuran (3 mL) and an aqueous saturated sodium hydrogen carbonate solution (2 mL) were added via syringe. The reaction mixture was heated to 80 °C for 7 d, while a very dark powder started to precipitate. After reaction, the solvent was completely removed under vacuum and the residue was dissolved in chloroform (100 mL). This organic layer was washed with water (2x50 mL) and brine (50 mL). The dried organic layer was concentrated under reduced pressure to about 2 – 5 mL which was then dripped into ethanol (250 mL) under vigorously stirring. A very fine dark powder precipitated and was filtered. According to UV/Vis measurements the residue showed an more red shifted λ_{max} then the filtrate, therefore it was assumed that some of the lower molecular weight component could be washed out by this precipitation. **24** (70 mg, 91 μmol per formal unit, 40%, \bar{X}_n : 2) was obtained by drying the filtration residue in a vacuum oven.

Decomposition onset: 345 °C. Residue: 52%.

MS (MALDI-TOF): 4682 (1) [6 dye units and 5 bridges], 4064 (4) [5 dye units and 5 bridges], 3837 (3) [5 dye units and 4 bridges], 3297 (8) [4 dye units and 4 bridges], 832 (13) [1 dye unit].

(4-((3,3-dimethyl-1-octyl-3*H*-indolium-2,5-diyl)methylene)-2-((3,3-dimethyl-1-octylindolin-2-ylidene-5-yl)methyl)-3-oxocyclobut-1-enolate))₃₋₄ (25)



All solvents and solutions were degassed by freeze-pump-thaw cycles. **38** (200 mg, 229 μmol , page 140), **29** (178 mg, 229 μmol , page 128) and the catalyst **71** (1.9 mg, 1.6 μmol , page 175) were placed in a 25 mL round bottom flask and fitted with a septum. Then 1-methyl-2-pyrrolidone (5 mL), tetrahydrofuran (3 mL) and an aqueous saturated sodium hydrogen carbonate solution (2 mL) were added via syringe. The reaction mixture was heated to 80°C for 7 d, while a very dark powder started to precipitate. After reaction, the solvent was completely removed under vacuum and the residue was dissolved in chloroform (100 mL). This organic layer was washed with water (2x50 mL) and brine (50 mL). The dried organic layer was concentrated under reduced pressure to about 2 – 5 mL which was then dripped into ethanol (250 mL) under vigorously stirring. A very fine dark powder precipitated and was filtered. According to UV/Vis measurements the residue showed an more red shifted λ_{max} then the filtrate, therefore

58 (115 mg, 141 μmol , page 104) and squaric acid (7 mg, 61 μmol , OChem Inc.) were mixed with benzene (5 mL), 1-butanol (5 mL), 1-methyl-2-pyrrolidinone (5 mL) and quinoline (0.1 mL) in Dean-Stark apparatus. The reaction mixture was heated to reflux for 7 d before it was poured on ice-cold aqueous citric acid solution (5%, 250 mL). The precipitate was filtered, then dissolved in chloroform (250 mL) which was subsequently washed with water (4x200 mL) and brine (2x200 mL). The dried organic layer was concentrated under reduced pressure to a few milliliters which was then cooled to room temperature. Meanwhile the product precipitated, it was filtered and dried in the vacuum oven (30 $^{\circ}\text{C}$, 1 mbar) to yield **26** (48 mg, 32 μmol , 52%) as golden shiny crystalline powder.

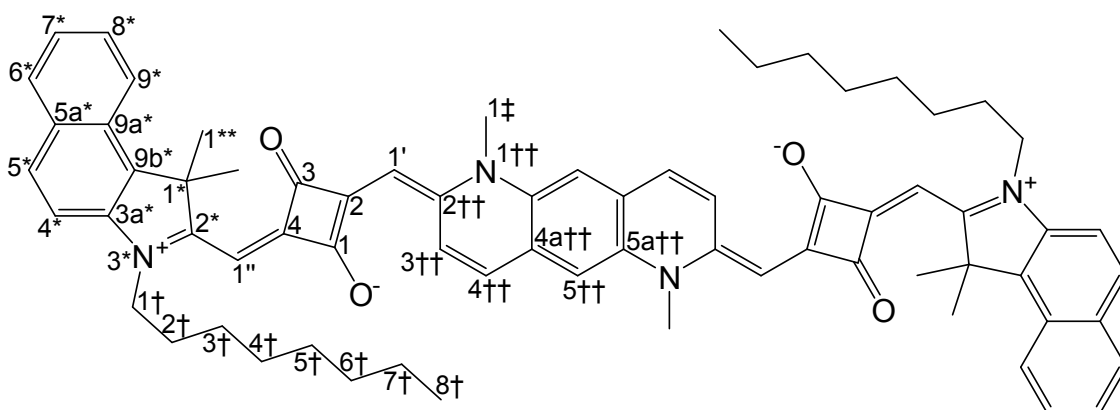
Decomposition onset: 302 $^{\circ}\text{C}$. Residue: 44%.

$^1\text{H-NMR}$: 8.3-8.2 (C(4'')H, C(9'')H, 4H, m), 8.21 (C(9§§)H, 2H, d, $^3\text{J}(9§§-8§§)=8.3\text{Hz}$), 7.94 (C(6§§)H, 2H, d, $^3\text{J}(6§§-7§§)=7.9\text{Hz}$), 7.92 (C(5§§)H, 2H, d, $^3\text{J}(5§§-4§§)=8.5\text{Hz}$), 7.62 (C(8§§)H, 2H, dd, $^3\text{J}(8§§-9§§)=8.3\text{Hz}$, $^3\text{J}(8§§-7§§)=7.1\text{Hz}$), 7.55-7.5 (C(5'')H, C(10'')H, 4H, m), 7.48 (C(7§§)H, 2H, dd, $^3\text{J}(7§§-6§§)=7.9\text{Hz}$, $^3\text{J}(7§§-8§§)=7.1\text{Hz}$), 7.36 (C(4§§)H, 2H, d, $^3\text{J}(4§§-5§§)=8.5\text{Hz}$), 6.6-6.0 (C(1')H, C(1‡)H, C(1§)H, 6H, m), 4.4-4.0 (C(1##)H₂, C(1††)H₃, C(1**)H₃, 16H, m), 2.1-2.0 (C(1#)H₃, C(2##)H₂, 16H, m), 2.0-1.7 (C(1*)H₃, C(1†)H₃, C(3##)H₂, 28H, m), 1.55-1.2 (C(4##)H₂, C(5##)H₂, C(6##)H₂, C(7##)H₂, 16H, m), 0.87 (C(8##)H₃, 6H, t, $^3\text{J}(8##-7##)=6.8\text{Hz}$).

MS: 1514 (100) [M+H]⁺, 1513 (56) [M]⁺, 1499 (14) [M+H-CH₃]⁺, 1484 (4) [M+H-2·CH₃]⁺, 1100 (10) [C₇₄H₇₇N₅O₄]⁺, 414 (6) [C₂₈H₃₂NO₂]⁺.

HR-MS: calculated for C₁₀₂H₁₀₈N₆O₆ [M]⁺: 1512.8325. Found: 1512.8291.

2,2'-(1,6-Dimethylpyrido[2,3-*g*]quinoline-2,7(1*H*,6*H*)-diylidene)bis(methan-1-yl-1-ylidene)bis(4-((1,1-dimethyl-3-octyl-1*H*-benzo[*e*]indolium-2-yl)methylene)-3-oxocyclobut-1-enolate) (27)



The condensation reaction was performed in a Dean-Stark apparatus with **43** (670 mg, 1.60 mmol, page 146) and **70** (280 mg, 0.64 mmol, page 174) as reactants in a solvent mixture of toluene (20 mL), 1-butanol (10 mL) and quinoline (5 mL). The light yellow solution was heated to reflux for 4 d. The solvent was then evaporated under vacuum and the green-black remainder was dissolved in ethanol (40 mL). To precipitate the crude product this solution was dripped in ice cold aqueous citric acid solution (600 mL, 5%) while stirring vigorously for 30 min and then filtered. The ensuing residue was purified with column chromatography (chloroform) to yield **27** (0.25 g, 0.24 mmol, 38%) as an blue-black coloured powder.

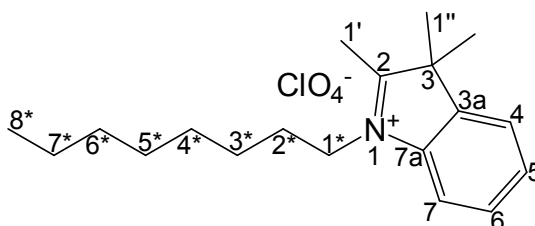
Decomposition onset: 277 °C. Residue: 33%.

¹H-NMR (DMSO-*d*₆, T: 313 K): 9.55 (C(3††)H, 2H, d, ³J(3††-4††)=9.7Hz), 8.53 (C(4††)H, 2H, d, ³J(4††-3††)=9.7Hz), 8.17 (C(9*)H, 2H, d, ³J(9*-8*)=8.5Hz), 8.08 (C(5††)H, 2H, s), 7.93 (C(5*)H, C(6*)H, 4H, m), 7.58 (C(8*)H, 2H, dd, ³J(8*-9*)=8.5Hz, ³J(8*-7*)=7.2Hz), 7.50 (C(4*)H, 2H, d, ³J(4*-5*)=8.7Hz), 7.37 (C(7*)H, 2H, dd, ³J(7*-6*)=8.0Hz, ³J(7*-8*)=7.2Hz), 6.0-5.6 (C(1')H, C(1'')H, 4H, br), 4.1 (C(1†)H₂, 4H, br), 4.0 (C(1‡)H₃, 6H, br), 1.97 (C(1**)H₃, 12H, s), 1.8 (C(2†)H₂, 4H, m), 1.5-1.2 (C(3†)H₂, C(4†)H₂, C(5†)H₂, C(6†)H₂, C(7†)H₂, 20H, m), 0.9-0.8 (C(8†)H₃, 6H, m). Due to aggregate formation in CDCl₃ and critical solubility in other deuterated solvents no ¹³C-NMR could be measured.

MS: 1036 (100) $[M+H]^+$, 1035 (75) $[M]^+$, 1021 (24) $[M+H-CH_3]^+$, 1006 (7) $[M+H-2\cdot CH_3]^+$, 922 (5) $[M+H-C_8H_{17}]^+$, 728 (17) $[C_{48}H_{46}N_3O_4]^+$, 659 (17) $[C_{45}H_{44}N_3O_2]^+$, 517.8 (4) $[M+H]^{++}$.

HR-MS: calculated for $C_{70}H_{74}N_4O_4$ $[M]^+$: 1034.5705. Found: 1034.5671.

2,3,3-Trimethyl-1-octyl-3*H*-indolium perchlorate (**28**)



1,1,2-Trimethyl-1*H*-indole (45.9 g, 288 mmol, FEW Chemicals), 1-iodooctane (100 g, 416 mmol, ABCR) and 1-butanol (60 mL) were mixed and heated to 120 °C for 36 h. After that the reaction mixture was chilled to rt and subsequently poured into hexane (1 L). A light brown coloured oil precipitated. The oil was emulsified in fresh hexane (400 mL), the supernatant was decanted and the remnant was dissolved in ethanol (200 mL). In order to precipitate the product, this solution was dripped in diethyl ether (1.2 L) under vigorously stirring, but 2,3,3-trimethyl-1-octyl-3*H*-indolium *iodide* had a honey like consistence of a transparent red colour (Figure 4.4 left hand side). An aliquot was taken for the analysis. For further purification a crystallization step was induced by anion exchange. Thereto, the rest was dissolved in hot ethanol (600 mL), then saturated sodium perchlorate solution (100 mL) was added and finally the mixture was cooled down slowly to rt while the white crystalline product precipitated. **28** (73 g, 0.20 mol, 68%, Figure 4.4 right hand side) was obtained by filtration and subsequent drying.

Melting point (Iodide): 5–10 °C (Phase transition), 60–75 °C (melting).

Melting point (Perchlorate): 117–119 °C (melting).

Decomposition onset (Iodide): 208 °C. Residue: 4%.

Decomposition onset (Perchlorate): 287 °C. Residue: 28%.

¹H-NMR: 7.6-7.45 (C(4)H, C(5)H, C(6)H, C(7)H, 4H, m), 4.40 (C(1*)H₂, 2H, t, ³J(1*-



Figure 4.4: The red transparent **28** as iodide in a beaker with the molecular structure on paper underneath (left hand side) and the isolated and dried white crystals of **28** as perchlorate (right hand side).

$^1\text{H-NMR}$ (CDCl_3): 7.51 (C(1')H₃, 2H, s), 2.76 (C(1'')H₃, 6H, s), 1.86 (C(2*)H₂, 2H, m), 1.51 (C(3*)H₂, C(4*)H₂, C(5*)H₂, C(6*)H₂, C(7*)H₂, 10H, m), 0.81 (C(8*)H₃, 3H, t, $^3\text{J}(8^*-7^*)=6.9\text{Hz}$).

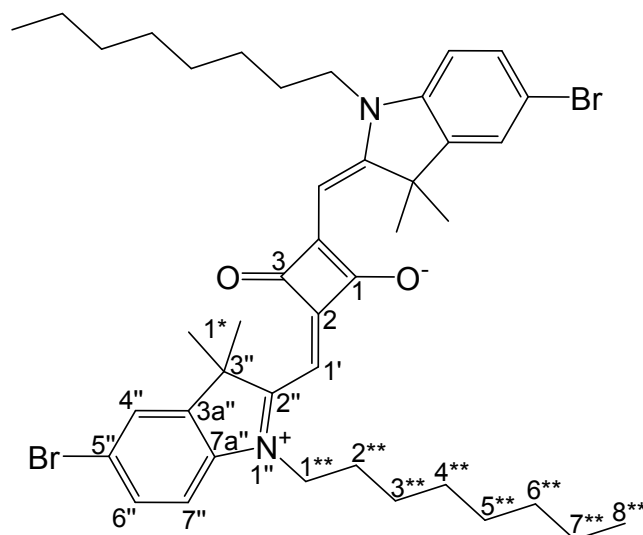
$^{13}\text{C-NMR}$: 195.65, 141.51, 140.67, 129.87, 129.19, 123.17, 114.87, 54.46, 48.37, 31.40, 28.73, 27.58, 26.48, 22.50, 22.31, 14.03, 13.84.

MS (ESI-QTOF+): 272 (100) [M-CIO₄]⁺.

HR-MS (ESI-QTOF+): calculated for C₁₉H₃₀N [M-CIO₄]⁺: 272.2373. Found: 272.2370.

Elemental analysis: calculated for C₁₉H₃₀NCIO₄: C, 61.36; H, 8.13; N, 3.77; O, 17.21; Cl, 9.53. Found: C, 61.20; H, 8.05; N, 3.77; O, 17.11; Cl, 9.63.

4-((5-Bromo-3,3-dimethyl-1-octyl-3*H*-indolium-2-yl)methylene)-2-((5-bromo-3,3-dimethyl-1-octylindolin-2-ylidene)methyl)-3-oxocyclobut-1-enolate (29)



In a Dean-Stark apparatus **72** (40.0 g, 83.6 mmol, page 176), squaric acid (4.65 g, 40.8 mmol, OChem Inc.), toluene (150 mL), 1-butanol (300 mL) and quinoline (50 mL) were combined and heated to reflux for 2 d. Then the reaction mixture was concentrated *in vacuo*. To remove the quinoline, the oily residue was dissolved in ethanol (200 mL) and poured on aqueous citric acid solution (1 L, 5%). After stirring for 30 min, the precipitation was filtered, dissolved in chloroform (350 mL) and extracted with aqueous citric acid solution (600 mL, 10%), water (4x600 mL), aqueous potassium carbonate solution (600 mL, 10%) and anew with water (3x600 mL). The solvent was removed under vacuum and the raw product was recrystallized from boiling ethanol (450 mL) to yield **29** (21 g, 27 mmol, 66%) as golden crystals (Figure 4.5).

Melting point: 205 – 215 °C.

Decomposition onset: 310 °C. Residue: 18%.

¹H-NMR: 7.44 (C(4'')H, d, ⁴J(4''-6'')=1.9Hz), 7.41 (C(6'')H, dd, ³J(6''-7'')=8.3Hz, ⁴J(4''-6'')=1.9Hz), 6.83 (C(7'')H, d, ³J(7''-6'')=8.3Hz), 5.95 (C(1')H, s), 3.93 (C(1'')H₂, br), 1.8-1.71 (C(2'')H₂, m), 1.77 (C(1*)H₃, s), 1.45-1.18 (C(3'')H₂, C(4'')H₂, C(5'')H₂, C(6'')H₂, C(7'')H₂, m), 0.87 (C(8'')H₃, t, ³J(8''-7'')=6.9Hz).



Figure 4.5: Picture of the crystal hedgehog of **29**.

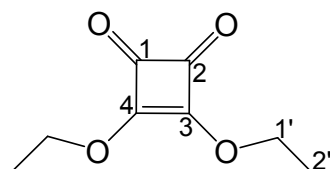
¹³C-NMR: 182.04, 180.11, 169.41, 144.16, 141.49, 130.62, 125.65, 116.53, 110.64, 87.04, 49.29, 43.82, 31.65, 29.23, 29.06, 26.98, 26.91, 22.52, 14.01.

MS: 783 (4) [M]⁺ (A+7) and [M+H]⁺ (A+6), 782 (19) [M]⁺ (A+6) and [M+H]⁺ (A+5), 781 (58) [M]⁺ (A+5) and [M+H]⁺ (A+4), 780 (80) [M]⁺ (A+4) and [M+H]⁺ (A+3), 779 (95) [M]⁺ (A+3) and [M+H]⁺ (A+2), 778 (100) [M]⁺ (A+2) and [M+H]⁺ (A+1), 777 (44) [M]⁺ (A+1) and [M+H]⁺ (A), 776 (41) [M]⁺ (A), 763 (7) [M-CH₃]⁺ (A+2) and [M+H-CH₃]⁺ (A+1), 761 (3) [M-CH₃]⁺ (A), 723 (3) [M-C₄H₈]⁺ (A+3) and [M+H-C₄H₈]⁺ (A+2), 722 (4) [M-C₄H₈]⁺ (A+2) and [M+H-C₄H₈]⁺ (A+1), 720 (2) [M-C₄H₈]⁺ (A), 700 (2) [C₄₂H₅₅⁸¹BrN₂O₂]⁺, 698 (2) [C₄₂H₅₅⁷⁹BrN₂O₂]⁺, 444 (8) [C₂₄H₂₉⁸¹BrNO₂]⁺, 442 (8) [C₂₄H₂₉⁷⁹BrNO₂]⁺, 390.6 (3) [M]⁺⁺ (A+5) and [M+H]⁺⁺ (A+4), 390.1 (3) [M]⁺⁺ (A+4) and [M+H]⁺⁺ (A+3), 389.6 (4) [M]⁺⁺ (A+3) and [M+H]⁺⁺ (A+2), 389.1 (4) [M]⁺⁺ (A+2) and [M+H]⁺⁺ (A+1), 388.6 (2) [M]⁺⁺ (A+1) and [M+H]⁺ (A), 388.1 (3) [M]⁺⁺ (A).

HR-MS: calculated for C₄₂H₅₄Br₂N₂O₂ [M]⁺: 776.2546. Found: 776.2552.

Elemental analysis: calculated for C₄₂H₅₄N₂O₂Br₂: C, 64.78; H, 6.99; N, 3.60; O, 4.11; Br, 20.52. Found: C, 64.72; H, 7.02; N, 3.60; O, 4.18; Br, 20.47.

3,4-Diethoxycyclobut-3-ene-1,2-dione (30)



The reaction was performed analogue to Liu et al. [49] with some adjustments of the work-up method. In a 2 L round bottom flask first squaric acid (100 g, 0.877 mol, OChem Inc.) and ethanol (1.2 L) then triethyl orthoformate (325 g, 2.19 mol) were combined in order to generate **30** at boiling temperature within 20 h. The solvent was evaporated under reduced pressure. The remnant was distilled in high vacuum (0.03 mbar) which resulted in a yellowish main fraction which was distilled a second time to yield **30** (0.13 kg, 0.75 mol, 86%) as a colourless liquid.

Caution: This compound and some derivatives are used in medicinal applications as sensibilisers. Milligram quantities can amplify allergic reactions to such an extent that it can cause serious health problems.

Melting point: +13 to +18 °C. Freezing point –5 to –7 °C.

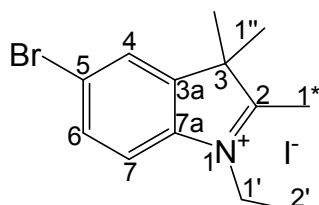
Boiling point: 245 °C (ambient pressure). Residue: 0%. Head temperatur in the distillation: 82 °C at 0.03 mbar.

¹H-NMR: 4.69 (C(1')H₂, q, ³J(1'-2')=7.11Hz), 1.43 (C(2')H₂, t, ³J(2'-1')=7.11Hz).

¹³C-NMR: 189.08 (C(1), C(2)), 184.04 (C(3), C(4)), 70.37 C(1'), 15.40 C(2').

MS (Magnet EI+): 170 (77) [M]⁺, 142 (11) [C₆H₆O₄]⁺, 113 (50) [C₄HO₄]⁺, 84 (8) [C₃HO₃]⁺, 57 (17) [C₂HO₂]⁺, 29 (100) [C₂H₅]⁺.

HR-MS (Magnet EI+): calculated for C₈H₁₀O₄ [M]⁺: 170.0574. Found: 170.0572.

5-Bromo-1-ethyl-2,3,3-trimethyl-3*H*-indolium iodide (31)

The alkylation of **32** (20.0 g, 84.0 mmol, page 132) with iodoethane (20.0 mL, 169 mmol, Merck) in 1-butanol (20 mL) was performed in a 100 mL Schlenk tube at reflux temperature. Due to the instability of iodoethane a second portion (5.0 mL, 42.3 mmol) was added after 18 h. The orange-brown product started to precipitate after 24 h. After 40 h the reaction mixture was allowed to cool to rt before it was poured in diethyl ether (1 L) and stirred for 1 h. The precipitate was filtered and washed with diethyl ether (3x25 mL). The filtration residue was recrystallized from boiling chloroform (2 L) to yield **31** (22 g, 54 mmol, 64%).

Decomposition onset: 227 °C. Residue: 14%.

¹H-NMR (DMSO-*d*₆): 8.19 (C(4)H, 1H, d, ⁴J(4-6)=1.8Hz), 7.95 (C(7)H, 1H, d, ³J(7-6)=8.6Hz), 7.85 (C(6)H, 1H, dd, ³J(6-7)=8.6Hz, ⁴J(6-4)=1.8Hz), 4.48 (C(1')H₂, 2H, q, ³J(1'-2')=7.3Hz), 2.82 (C(1*)H₃, 3H, s), 1.55 (C(1'')H₃, 6H, s), 1.42 (C(2')H₃, 3H, t, ³J(1'-2')=7.3Hz).

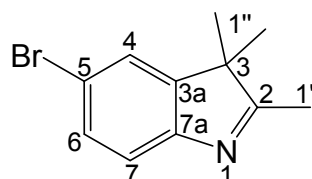
¹³C-NMR: (DMSO-*d*₆): 196.62, 144.23, 140.07, 131.85, 126.93, 122.74, 117.27, 54.38, 43.30, 21.67, 14.00, 12.59.

MS (ESI-QTOF+): 392 (0.3) [M-H]⁺, 266 (100) [M-I]⁺.

HR-MS (ESI-QTOF+): calculated for C₁₃H₁₇BrN [M-I]⁺: 266.0539. Found: 266.0542.

Elemental analysis: calculated for C₁₃H₁₇NBrI: C, 39.62; H, 4.35; N, 3.55; Br, 20.28; I, 32.20. Found: C, 39.48; H, 4.49; N, 3.50; Br, 20.16; I, 32.43.

5-Bromo-2,3,3-trimethyl-3H-indole (32)



32 was produced differently by Moreau et al. [44]. The method analogue to Kim et al. [43] was used with necessary changes. Ethanol (460 mL) was placed in a 2 L three necked round bottom flask and cooled to $\sim 0^{\circ}\text{C}$ in an ice bath. Then sulphuric acid (45.0 mL, 0.84 mol, 98% pure) was added slowly at 0°C . Subsequently, 4-bromophenylhydrazine hydrochloride (100 g, 447 mmol) and 3-methyl-2-butanone (47.0 g, 546 mmol) were added and the brownish suspension was heated to reflux at 82°C for 24 h. During the reaction the side product ammonium hydrogensulphate precipitated. After removal of the solvent *in vacuo* the residue was suspended in methyl *tert*-butyl ether (500 mL) and extracted with aqueous sodium hydroxide solution (600 mL, 30% w/w), followed by aqueous sodium chloride solution (5x250 mL, 10% w/w) and brine (3x250 mL). The solvent of the combined dried organic layer was evaporated under reduced pressure. The product was purified by distillation to yield **32** (53 g, 0.22 mol, 49%) in the main fraction.

Melting point: $43 - 47^{\circ}\text{C}$ (DSC).

Boiling point: 232°C (onset in TGA) and 77°C at 0.04 mbar (head temperature during distillation).

$^1\text{H-NMR}$: 7.42-7.34 (C(4)H, C(6)H, C(7)H, 3H, m), 2.23 (C(1')H₃, 3H, s), 1.27 (C(1'')H₃, 6H, s).

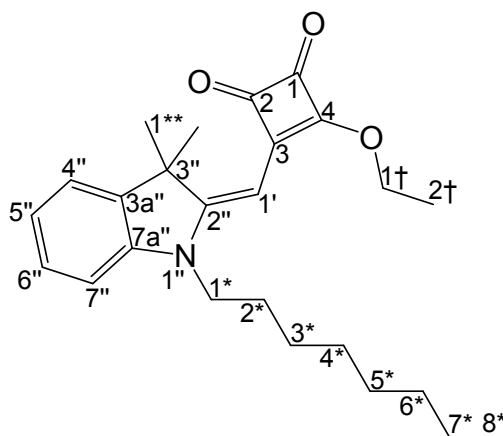
$^{13}\text{C-NMR}$: 188.32 C(2), 152.65 C(3a), 147.75 C(7a), 130.55 C(4), 124.75 C(6), 121.19 C(7), 118.74 C(5), 54.04 C(3), 22.85 C(1''), 15.34 C(1').

MS (Magnet EI+): 237 (100) [M]⁺, 224 (55) [C₁₀H₉N⁸¹Br]⁺, 222 (57) [C₁₀H₉N⁷⁹Br]⁺, 198 (6) [C₈H₇N⁸¹Br]⁺, 196 (7) [C₈H₇N⁷⁹Br]⁺, 158 (27) [C₁₁H₁₂N]⁺, 143 (31) [C₁₀H₉N]⁺, 118.5 (1) [M]⁺⁺, 117 (46) [C₈H₇N]⁺, 116 (17) [C₈H₆N]⁺, 115 (54) [C₈H₅N]⁺, 102 (30) [C₇H₄N]⁺, 75 (18) [C₆H₃]⁺, 51 (15) [C₄H₃]⁺, 39 (17) [C₃H₃]⁺, 27 (8) [C₂H₃]⁺.

HR-MS (Magnet EI+): calculated for C₁₁H₁₂N⁷⁹Br [M]⁺: 237.0148. Found: 237.0147.

Elemental analysis: calculated for C₁₁H₁₂NBr: C, 55.48; H, 5.08; N, 5.88; Br, 33.56. Found: C, 55.21; H, 5.27; N, 5.92; Br, 33.74.

3-((3,3-Dimethyl-1-octylindolin-2-ylidene)methyl)-4-ethoxycyclobut-3-ene-1,2-dione (**33**)



In a 250 mL Schlenk tube **28** (15.0 g, 40.3 mmol, page 126) was suspended in ethanol (150 mL) at rt before triethylamine (8.57 g, 84.7 mmol, distilled over KOH) was added dropwise. While heating to reflux the starting material deprotonated to the soluble en-amine form. At that point the reaction mixture was cooled to rt and **30** (7.55 g, 44.4 mmol, page 130) was added via syringe. The reaction mixture was heated to reflux overnight and the next morning the solvent was evaporated under vacuum. The remainder was diluted in ethyl acetate (300 mL), extracted with water (3x200 mL) and the residue of the organic layer was purified via column chromatography (hexane:ethyl acetate = 8:2→5:5) to yield **33** (10 g, 25 mmol, 62%) as a bright yellow crystals (Figure 4.6).

Melting point: 71 – 77 °C.

Decomposition onset: 275 °C. Residue: 16%.

¹H-NMR: 7.29-7.24 (C(4'')H, C(6'')H, 2H, m), 7.06 (C(5'')H, 1H, ddd, ³J(5''-4'')=7.5Hz, ³J(5''-6'')=7.4Hz, ⁴J(5''-7'')=0.9Hz), 6.87 (C(7'')H, 1H, d, ³J(7''-6'')=7.9Hz), 5.40 (C(1')H, 1H, s), 4.89 (C(1†)H₂, 2H, q, ³J(1†-2†)=7.1Hz), 3.80 (C(1*)H₂, 2H, t, ³J(1*-2*)=7.6Hz),

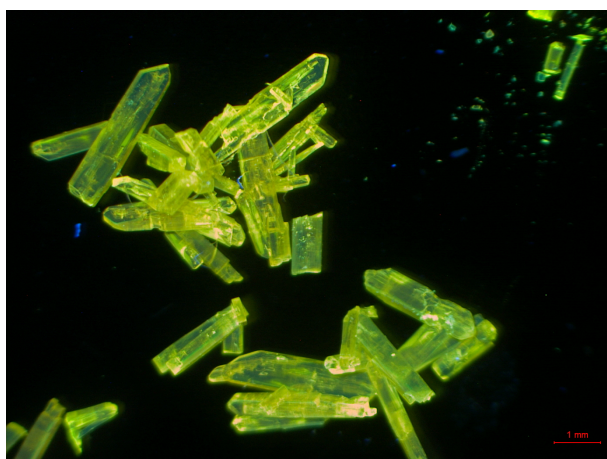


Figure 4.6: Microscopic picture of **33** lightened with incident UV light.

1.80-1.68 (C(2^{**})H₂, 2H, m), 1.62 (C(1^{**})H₃, 6H, s), 1.53 (C(2†)H₂, 3H, t, ³J(2†-1†)=7.1Hz), 1.46-1.20 (C(3^{*})H₂, C(4^{*})H₂, C(5^{*})H₂, C(6^{*})H₂, C(7^{*})H₂, 10H, m), 0.87 (C(8^{*})H₃, 3H, t, ³J(8^{*}-7^{*})=6.9Hz).

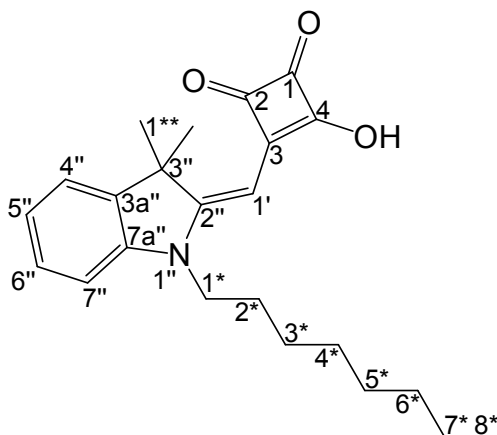
¹³C-NMR: 192.39, 187.31, 173.65, 168.26, 142.55, 140.83, 127.61, 122.52 (2C), 121.84, 108.28, 81.15, 69.74, 47.83, 42.87, 31.61, 29.11, 28.98, 26.86, 26.82, 26.21, 22.46, 15.80, 13.94.

MS: 434 (7) [M+K]⁺, 418 (17) [M+Na]⁺, 396 (100) [M+H]⁺, 368 (2) [C₂₃H₃₀NO₃]⁺, 340 (6) [C₂₂H₃₀NO₂]⁺, 310 (5) [C₂₁H₂₈NO]⁺, 257 (8) [C₁₈H₂₇N]⁺, 198 (6) [M+H]⁺⁺, 132 (1) [M+H]³⁺, 99 (2) [M+H]⁴⁺, 79 (0.5) [M+H]⁵⁺, 66 (0.6) [M+H]⁶⁺.

HR-MS: calculated for C₂₅H₃₄O₃N [M+H]⁺: 396.2533. Found: 396.2526.

Elemental analysis: calculated for C₂₅H₃₃NO₃: C, 75.92; H, 8.41; N, 3.54; O, 12.13. Found: C, 75.86; H, 8.31; N, 3.55; O, 12.08.

3-((3,3-Dimethyl-1-octylindolin-2-ylidene)methyl)-4-hydroxycyclobut-3-ene-1,2-dione (34)



33 (17.7 g, 44.7 mmol, page 133) was dissolved in ethanol (180 mL) and heated to reflux. Then aqueous sodium hydroxide solution (10.4 mL, 40% w/w) was dripped in. After 10 min the hot reactor content was poured into an ethanol-water (100:500 mL) mixture under vigorous stirring. The protonated product precipitated after the addition of concentrated hydrochloric acid (30 mL) and the brick stone coloured powder was filtered and washed with cold water. **34** was yielded by drying the residue in the vacuum oven (16 g, 43 mmol, 93%).

Decomposition onset: 195 °C. Residue: 22%.

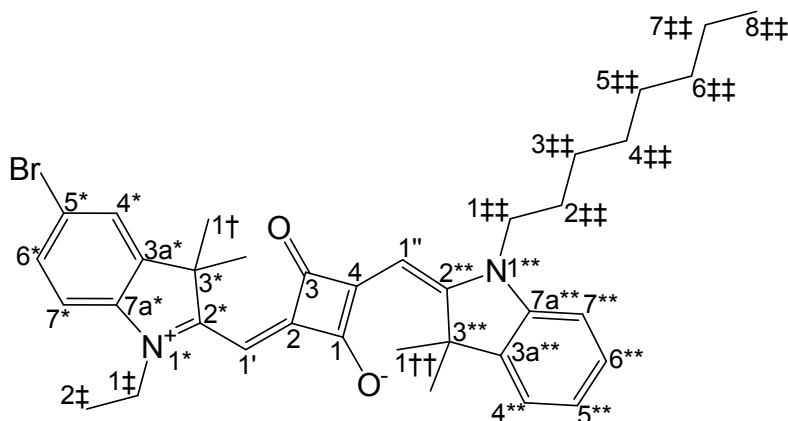
¹H-NMR (DMSO-*d*₆): 7.38 (C(4'')H, 1H, dd, ³J(4''-5'')=7.4Hz, ⁴J(4''-6'')=0.8Hz), 7.25 (C(6'')H, 1H, ddd, ³J(6''-7'')=7.9Hz, ³J(6''-5'')=7.6Hz, ⁴J(6''-4'')=0.8Hz), 7.08 (C(7'')H, 1H, d, ³J(7''-6'')=7.9Hz), 7.00 (C(5'')H, 1H, dd, ³J(5''-6'')=7.6Hz, ³J(5''-4'')=7.4Hz), 5.51 (C(1')H, 1H, s), 3.84 (C(1*)H₂, 2H, t, ³J(1*-2*)=7.3Hz), 1.7-1.6 (C(2*)H₂, 2H, m), 1.54 (C(1'')H₃, 6H, s), 1.4-1.1 (C(3*)H₂, C(4*)H₂, C(5*)H₂, C(6*)H₂, C(7*)H₂, 10H, m), 0.82 (C(8*)H₃, 3H, t, ³J(8*-7*)=6.8Hz).

¹³C-NMR (DMSO-*d*₆): 191.88 (2C), 190.87, 173.92, 165.71, 142.77, 140.16, 127.73, 121.87, 121.82, 108.61, 81.35, 47.00, 42.02, 31.15, 28.68, 28.58, 26.74, 26.20, 25.75, 22.04, 13.93.

MS (ESI-QTOF+): 390 (9) [M+Na]⁺, 386 (17) [M+H₃O]⁺, 368 (100) [M+H]⁺, 330 (30).

HR-MS (ESI-QTOF+): calculated for C₂₃H₃₀NO₃ [M+H]⁺: 368.2220. Found: 368.2208.

5-Bromo-2-((3-((3,3-dimethyl-1-octylindolin-2-ylidene)methyl)-2-hydroxy-4-oxocyclobut-2-enylidene)methyl)-1-ethyl-3,3-dimethyl-3*H*-indolium (35)



34 (12.5 g, 34.0 mmol, page 135), **31** (16.8 g, 42.5 mmol, page 131), 1-butanol (200 mL), toluene (100 mL) and quinoline (50 mL) were combined in a Dean-Stark apparatus. The yellow mixture was heated to reflux for 2 d before the dark blue reaction mixture was concentrated under reduced pressure. The concentrate was dissolved in ethanol (75 mL) and the solution was poured into ice cold aqueous citric acid solution (1 L, 5%) while stirring. The ensuing precipitate was isolated by filtration. Subsequent purification with column chromatography (chloroform) yielded **35** (15 g, 24 mmol, 70%) as a copper shiny amorphous powder (Figure 4.7).

Decomposition onset: 282 °C. Residue: 19%.

¹H-NMR: 7.41 (C(4*)H, 1H, d, ⁴J(4*-6*)=1.9Hz), 7.38 (C(6*)H, 1H, dd, ³J(6*-5*)=8.3Hz, ⁴J(4*-6*)=1.9Hz), 7.34 (C(4**)H, 1H, dd, ³J(4**-5**) =7.4Hz, ⁴J(4**-6**) =1.2Hz), 7.30 (C(6**)H, 1H, ddd, ³J(6**-7**) =7.8Hz, ³J(6**-5**) =7.6Hz, ⁴J(6**-4**) =1.2Hz), 7.15 (C(5**)H, 1H, ddd, ³J(5**-6**) =7.6Hz, ³J(5**-4**) =7.4Hz, ⁴J(5**-7**) =0.8Hz), 6.99 (C(7**)H, 1H, d, ³J(7**-6**) =7.8Hz), 6.80 (C(7*)H, 1H, d, ³J(7*-6*) =8.3Hz), 5.98 (C(1'')H, 1H, s), 5.90 (C(1')H, 1H, s), 4.1-3.9 (C(1†)H₂, C(1††)H₂, 4H, m), 1.8-1.7 (C(1†)H₃, C(1††)H₃, C(2††)H₂, 14H, m), 1.4-1.2 (C(3††)H₂, C(4††)H₂, C(5††)H₂, C(6††)H₂, C(7††)H₂, C(2†)H₃, 13H, m), 0.85 (C(8††)H₃, 3H, t, ³J(8††-7††) =6.9Hz).

¹³C-NMR: 182.20, 180.96, 178.42, 171.01, 167.83, 144.14, 142.25, 142.18, 141.10,



Figure 4.7: Isolated **35** after drying overnight in the vacuum oven.

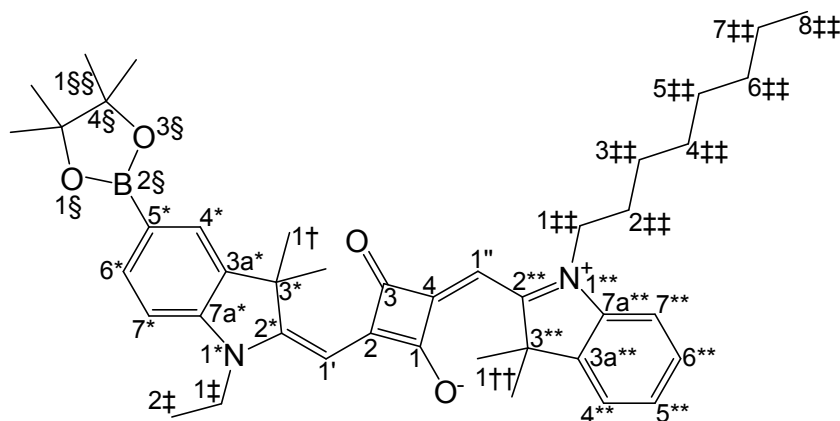
130.53, 127.73, 125.60, 124.00, 122.24, 115.99, 110.01, 109.59, 86.84, 86.36, 49.47, 48.98, 43.81, 38.23, 31.62, 29.20, 29.03, 27.03, 27.01, 26.96, 26.82, 22.49, 13.98, 11.71.

MS: 616 (100) $[M]^+$ (A+2), 615 (85) $[M]^+$ (A+1), 614 (86) $[M]^+$ (A), 599 (6) $[M-CH_3]^+$, 364 (6) $[C_{24}H_{30}NO_2]^+$, 360 (4) $[C_{18}H_{17}^{81}BrNO_2]^+$, 358 (4) $[C_{18}H_{17}^{79}BrNO_2]^+$, 307 (4) $[M]^{++}$, 153.6 (2) $[M]^{4+}$.

HR-MS: calculated for $C_{36}H_{43}BrN_2O_2$ $[M]^+$: 614.2502. Found: 614.2506.

Elemental analysis: calculated for $C_{36}H_{43}N_2O_2Br$: C, 70.23; H, 7.04; N, 4.55; O, 5.20; Br, 12.98. Found: C, 70.29; H, 7.08; N, 4.60; O, 5.34; Br, 12.86.

4-((3,3-Dimethyl-1-octyl-3*H*-indolium-2-yl)methylene)-2-((1-ethyl-3,3-dimethyl-5-(4,4,5,5-tetramethyl-1,3,2-dioxaborolan-2-yl)indolin-2-ylidene)methyl)-3-oxocyclobut-1-enolate (36)



The Miyaura borylation reaction was performed in a 2 L round bottom flask using **35** (10.0 g, 15.9 mmol, page 136), bis(pinacolato)diboron (6.00 g, 23.8 mmol, CombiPhos Catalysts Inc.) and potassium acetate (15.3 g, 156 mmol) as reactants, dichloro-[1,1'-bis(diphenylphosphino)-ferrocen]-palladium(II) (490 mg, 0.600 mmol, CombiPhos Catalysts Inc.) as catalyst and dioxane (1 L) as solvent. The reaction proceeded at an elevated temperature of 85 – 90 °C for 14 h. In the next step, the solvent was removed at reduced pressure and the remnant was suspended in chloroform (100 mL). The suspension was filtered through a silica gel bed (5 cm) and the residue was washed with chloroform (2x30 mL). The solvent of the filtrate was evaporated under reduced pressure and the remainder was purified with column chromatography (chloroform). Subsequent sublimation (145 °C, 0.02 mbar) of the inseparable excess of bis(pinacolato)diboron out of the crude product yielded **36** (6.9 g, 10 mmol, 65%) as greenish-blue powder.

Decomposition onset: 286 °C. Residue: 29%.

¹H-NMR: 7.78 (C(6*)H, 1H, dd, ³J(6*-7*)=8.0Hz, ⁴J(6*-4*)=1.0Hz), 7.75 (C(4*)H, 1H, d, ⁴J(4*-6*)=1.0Hz), 7.35 (C(4**)H, 1H, dd, ³J(4**-5**) =7.4Hz, ⁴J(4**-6**) =1.1Hz), 7.31 (C(6**)H, 1H, ddd, ³J(6**-7**) =7.8Hz, ³J(6**-5**) =7.6Hz, ⁴J(6**-5**) =1.1Hz), 7.15 (C(5**)H, 1H, ddd, ³J(5**-6**) =7.6Hz, ³J(5**-4**) =7.4Hz, ⁴J(5**-7**) =0.6Hz), 6.99 (C(7**)H, 1H, dd, ³J(7**-6**) =7.8Hz, ⁴J(7**-5**) =0.6Hz), 6.96 (C(7*)H, 1H, d, ³J(7*-

$6^*)=8.0\text{Hz}$), 5.99 (C(1')H, 1H, br), 5.97 (C(1'')H, 1H, br), 4.1-3.9 (C(1‡)H₂, C(1‡‡)H₂, 4H, m), 1.9-1.7 (C(1†)H₃, C(1††)H₃, C(2‡‡)H₂, 14H, m), 1.5-1.2 (C(3‡‡)H₂, C(4‡‡)H₂, C(5‡‡)H₂, C(6‡‡)H₂, C(7‡‡)H₂, C(1§§)H₃, C(2‡)H₃, 22H, m), 0.86 (C(8‡‡)H₃, 3H, t, $^3J(8‡‡-7‡‡)=6.9\text{Hz}$).

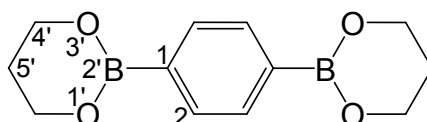
$^{13}\text{C-NMR}$: 182.29 (2C), 180.35, 178.78, 170.72, 169.26, 144.61, 142.32, 141.50, 135.10, 128.26, 127.75, 123.90, 123.66, 122.28, 109.53, 108.34, 86.79, 86.61, 83.81, 49.43, 48.96, 43.83, 38.28, 31.70, 29.28, 29.10, 27.07, 27.03, 27.02, 26.91, 24.82, 22.55, 14.04, 11.96. C(5*) signal is not visible, since the $^{13}\text{C-}^{11}\text{B}$ and $^{13}\text{C-}^{10}\text{B}$ couplings split the signal to zero.

MS: 662 (100) [M]⁺, 647 (2) [M-CH₃]⁺, 406 (3) [C₂₄H₂₉BNO₄]⁺, 364 (4) [C₂₄H₃₀NO₂]⁺, 331 (4) [M]⁺⁺, 165.6 (2) [M]⁴⁺.

HR-MS: calculated for C₄₂H₅₅BN₂O₄ [M]⁺: 662.4255. Found: 662.4254.

Elemental analysis: calculated for C₄₂H₅₅N₂O₄B: C, 76.12; H, 8.36; N, 4.23; O, 9.66; B, 1.63. Found: C, 75.19; H, 8.37; N, 4.17. Boron disturbs the oxygen measurement.

1,4-Di-(1,3,2-dioxaborinan-2-yl)benzene (37)



Benzene-1,4-diboronic acid (2.50 g, 15.1 mmol, ABCR), 1,3-propanediol (8.15 g, 107 mmol) and toluene (50 mL) were mixed and headed to reflux for 16 h. After the reaction, the solvent was removed under reduced pressure and the remnant was dried in high vacuum (10^{-3} mbar) overnight before it was recrystallized from boiling cyclohexane (250 mL) to yield **37** (3.3 g, 14 mmol, 89%) as white crystals.

Melting point: 103 – 110 °C.

Decomposition onset: 222 °C. Residue: 0%.

$^1\text{H-NMR}$: 7.74 (C(2)H, 4H, s), 4.16 (C(4')H₂, 8H, t, $^3J(4'-5')=5.5\text{Hz}$), 2.05 (C(5')H₂, 4H, p, $^3J(5'-4')=5.5\text{Hz}$).

$^{13}\text{C-NMR}$: 132.70 C(2), 61.94 C(4'), 27.40 C(5'). C(1) signal is not visible, since the

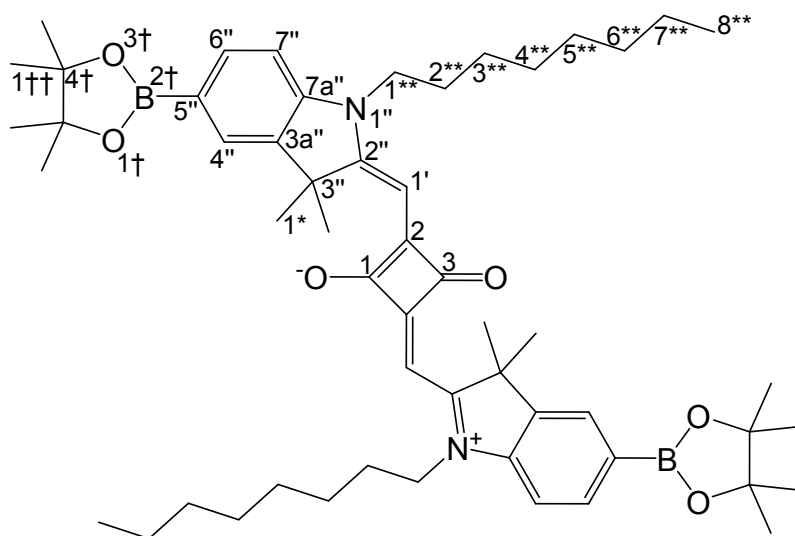
^{13}C - ^{11}B and ^{13}C - ^{10}B couplings split the signal to zero.

MS (Magnet EI+): 246 (100) $[\text{M}]^+$, 188 (54) $[\text{C}_9\text{H}_{10}\text{B}_2\text{O}_3]^+$, 130 (30) $[\text{C}_6\text{H}_4\text{B}_2\text{O}_2]^+$, 117 (6) $[\text{C}_5\text{H}_3\text{B}_2\text{O}_2]^+$, 103 (4) $[\text{C}_6\text{H}_4\text{BO}]^+$, 90 (5) $[\text{C}_5\text{H}_3\text{BO}]^+$, 77 (5) $[\text{C}_4\text{H}_2\text{BO}]^+$, 57 (4) $[\text{C}_3\text{H}_5\text{O}]^+$, 41 (15) $[\text{C}_3\text{H}_5]^+$, 28 (15) $[\text{C}_2\text{H}_4]^+$.

HR-MS (Magnet EI+): calculated for $\text{C}_{12}\text{H}_{16}\text{B}_2\text{O}_4$ $[\text{M}]^+$: 246.1229. Found: 246.1227.

Elemental analysis: calculated for $\text{C}_{12}\text{H}_{16}\text{O}_4\text{B}_2$: C, 58.62; H, 6.56; O, 26.03; B, 8.79. Found: C, 58.34; H, 6.65. Boron disturbs the oxygen measurement.

4-((3,3-Dimethyl-1-octyl-5-(4,4,5,5-tetramethyl-1,3,2-dioxaborolan-2-yl)-3*H*-indolium-2-yl)methylene)-2-((3,3-dimethyl-1-octyl-5-(4,4,5,5-tetramethyl-1,3,2-dioxaborolan-2-yl)indolin-2-ylidene)methyl)-3-oxocyclobut-1-enolate (38)



29 (15.0 g, 19.3 mmol, page 128), bis(pinacolato)diboron (19.6 g, 77.1 mmol, CombiPhos Catalysts Inc.), potassium acetate (11.4 g, 116 mmol), dioxane (1.5 L) and dichloro[1,1'-bis(diphenylphosphino)-ferrocene]-palladium(II) (310 mg, 0.385 mmol, CombiPhos Catalysts Inc.) were mixed and the suspension was heated to 80 °C for 16 h before it was concentrated *in vacuo* to about 350 mL. The concentrate was filtered and the solvent of the filtrate was evaporated under reduced pressure. The

remainder was suspended in boiling tetrahydrofuran (150 mL) and filtered hot. Ethanol (500 mL) was added to the filtrate and while cooling to rt the product precipitated to yield **38** (13 g, 15 mmol, 77%).

Decomposition onset: 318 °C. Residue: 22%.

¹H-NMR: 7.71 (C(6'')H, 2H, dd, ³J(6''-7'')=7.9Hz, ⁴J(4''-6'')=0.9Hz), 7.70 (C(4'')H, 2H, d, ⁴J(4''-6'')=0.9Hz), 6.90 (C(7'')H, 2H, d, ³J(7''-6'')=7.9Hz), 5.93 (C(1')H, 2H, s), 3.91 (C(1'')H₂, 4H, br), 1.8-1.65 (C(2'')H₂, 4H, m), 1.73 (C(1*)H₃, 6H, s), 1.39-1.10 (C(3'')H₂, C(4'')H₂, C(5'')H₂, C(6'')H₂, C(7'')H₂, 20H, m), 1.26 (C(1††)H₃, 24H, s), 0.78 (C(8'')H₃, 6H, t, ³J(8''-7'')=6.9Hz).

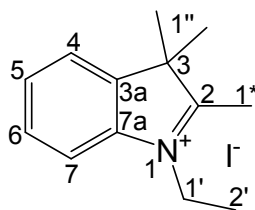
¹³C-NMR: 181.97, 179.98, 170.00, 144.79, 141.22, 134.86, 128.01, 123.66, 108.57, 86.91, 83.56, 48.87, 43.46, 31.45, 29.05, 28.85, 26.82, 26.76, 24.61, 22.32, 13.83.

MS: 872 (100) [M]⁺, 857 (10) [M-CH₃]⁺, 490 (17) [C₃₀H₄₁BNO₄]⁺, 436 (3) [M]⁺⁺, 218 (1) [M]⁴⁺, 145 (1) [M]⁶⁺.

HR-MS: calculated for C₅₄H₇₈O₆N²B₂ [M]⁺ (A+2): 872.6056. Found: 872.6058.

Elemental analysis: calculated for C₅₄H₇₈N₂O₆B₂I: C, 74.31; H, 9.01; N, 3.21; O, 11.00; B, 2.48. Found: C, 74.24; H, 9.08; N, 3.07.

1-Ethyl-2,3,3-trimethyl-3H-indolium iodide (39)



2,3,3-Trimethyl-3H-indole (100 g, 628 mmol, FEW Chemicals), 1-butanol (100 mL) and 1-iodoethane (75 mL, 942 mmol, Merck) were suspended and heated to reflux (82 °C) for 18 h. A second portion of 1-iodoethane (25 mL, 314 mmol) was added and the mixture was heated to reflux for additional 18 h. The green reaction mixture was cooled to rt and poured into diethyl ether (500 mL) under vigorous stirring. The dark precipitate was filtered and then dissolved in boiling chloroform (400 mL). By the addition of acetone (800 mL) the precipitation was started and continued until rt was reached.

The light yellow crystals were filtered off and washed with acetone. The evaporated remainder of the mother liquid was recrystallized accordingly to yield in total **39** (170 g, 510 mmol, 81%).

Decomposition onset: 229°C. Residue: 1%.

¹H-NMR (DMSO-*d*₆): 8.03 (C(7)H, 1H, m), 7.89 (C(6)H, 1H, m), 7.63-7.56 (C(4)H, C(5)H, 2H, m), 4.53 (C(1')H₂, 2H, q, ³J(1'-2')=7.3Hz), 2.91 (C(1*)H₃, 3H, s), 1.55 (C(1'')H₃, 6H, s), 1.45 (C(2')H₃, 3H, q, ³J(2'-1')=7.3Hz).

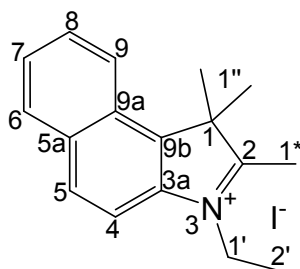
¹³C-NMR (DMSO-*d*₆): 195.88 C(2), 141.79 C(3a), 140.52 C(7a), 129.20 C(6), 128.79 C(5), 123.53 C(4), 115.28 C(7), 54.04 C(1'), 43.28 C(3), 21.85 C(1''), 14.56 C(2'), 12.81 C(1*).

MS (ESI-QTOF+): 188 (100) [M-I]⁺, 173 (3) [C₁₂H₁₅N]⁺, 158 (2) [C₁₁H₁₂N]⁺.

HR-MS (ESI-QTOF+): calculated for C₁₃H₁₈N [M-I]⁺: 188.1434. Found: 188.1437.

Elemental analysis: calculated for C₁₃H₁₈NI: C, 49.54; H, 5.76; N, 4.44; I, 40.26. Found: C, 49.44; H, 5.81; N, 4.67; I, 39.98.

3-Ethyl-1,1,2-trimethyl-1*H*-benzo[*e*]indolium iodide (40)



1,1,2-Trimethyl-1*H*-benzo[*e*]indole (100 g, 0.478 mol, FEW Chemicals), iodoethane (100 g, 0.641 mol, Merck) and 1-butanol (100 mL) were mixed in a 250 mL Schlenk tube and brought to react at 80°C for 8 h. Subsequently, another portion of iodoethane (40 g, 0.257 mol) was added. After prolonged stirring at 80°C for 16 h the reaction mixture was chilled below 40°C when it was poured into diethyl ether (1 L). The precipitate was filtered and washed with cold diethyl ether several times. The residue was dissolved in boiling chloroform (450 mL) and crystallized by the addition of acetone (2 L). After

cooling to rt the white needle like crystalline **40** were filtered and dried (130 g, 0.35 mol, 73%).

Decomposition onset: 228 °C. Residue: 6%.

¹H-NMR (DMSO-*d*₆): 8.37 (C(9)H, 1H, d, ³J(9-8)=8.3Hz), 8.30 (C(5)H, 1H, d, ³J(5-4)=8.9Hz), 8.22 (C(6)H, 1H, d, ³J(6-7)=8.0Hz), 8.17 (C(4)H, 1H, d, ³J(4-5)=8.9Hz), 7.79 (C(8)H, 1H, dd, ³J(8-7)=7.2Hz, ³J(8-9)=8.3Hz), 7.72 (C(7)H, 1H, dd, ³J(7-6)=8.0Hz, ³J(7-8)=7.2Hz), 4.64 (C(1')H₂, 2H, q, ³J(1'-2')=7.2Hz), 2.97 (C(1*)H₃, 3H, s), 1.76 (C(1'')H₃, 6H, s), 1.51 (C(2')H₃, 3H, t, ³J(2'-1')=7.2Hz).

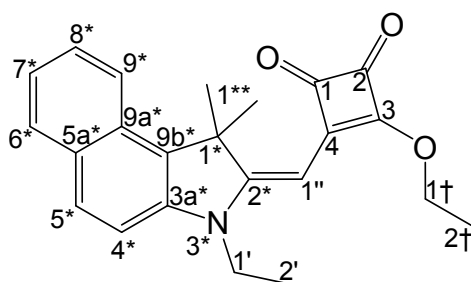
¹³C-NMR (DMSO-*d*₆): 195.87, 138.13, 136.95, 132.96, 130.65, 129.65, 128.34, 127.20, 127.16, 123.36, 113.17, 55.40, 43.39, 21.44, 13.84, 12.90.

MS (ESI-QTOF+): 364 (0.5) [M-H]⁺, 238 (100) [M-I]⁺, 223 (1) [C₁₆H₁₇N]⁺.

HR-MS (ESI-QTOF+): calculated for C₁₇H₂₀N [M-I]⁺: 238.1590. Found: 238.1601.

Elemental analysis: calculated for C₁₇H₂₀Nl: C, 55.90; H, 5.52; N, 3.83; l, 34.74. Found: C, 55.75; H, 5.72; N, 3.83; l, 34.96.

3-Ethoxy-4-((3-ethyl-1,1-dimethyl-1*H*-benzo[*e*]indol-2(3*H*)-ylidene)methyl)cyclobut-3-ene-1,2-dione (41)



40 (50.0 g, 137 mmol, page 142), ethanol (150 mL) and triethylamine (22.8 mL, 164 mmol, distilled over potassium hydroxide) were suspended and heating to reflux for 30 min until the entire starting material was converted to the soluble iminium salt by deprotonation. At that moment the solution was cooled to rt when **30** (25.6 g, 151 mmol, page 130) was dripped in via a syringe. The reaction proceeded at 60 °C for 30 min before the solvent was evaporated under reduced pressure. To get rid of the excess

triethylamine, the residue was dried in high vacuum overnight. Afterwards to remove the unreacted starting materials, the rest was digested in ethanol (50 mL) for 1 h and then cooled to -5°C , filtered and washed with cold ethanol (2x10 mL). The ensuing residue was dissolved in chloroform (100 mL) at rt which was subsequently poured into toluene (500 mL). The white precipitate presumably triethylamine hydroiodide was filtered and the product containing filtrate was concentrated *in vacuo*. The last remaining, blue side product was separated by digesting the greenish concentrate in ethyl acetate (50 mL) and subsequent filtration resulted in an orange residue which was crystallized after 3 h from a hot chloroform solution by adding ethanol and cooling the mixture slowly down to yield in **41** (44 g, 0.12 mol, 88%) as orange hexagonal plates (Figure 4.8).

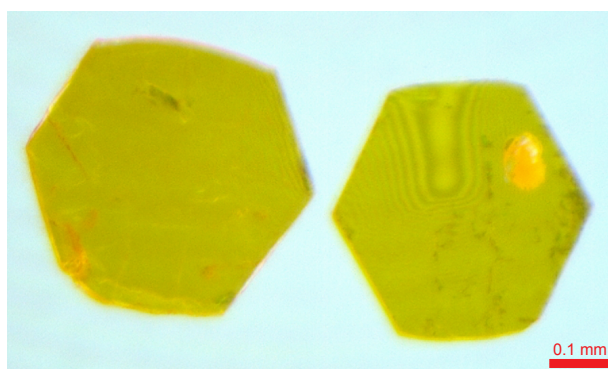


Figure 4.8: Microscopic picture of the hexagonal plates of **41**.

Melting point: 182–184 $^{\circ}\text{C}$.

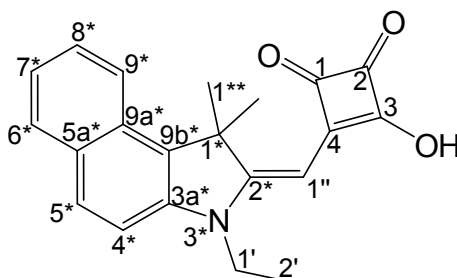
Decomposition onset: 265 $^{\circ}\text{C}$. Residue: 27%.

$^1\text{H-NMR}$: 8.10 (C(9 *)H, 1H, d, $^3\text{J}(9^*-8^*)=8.8\text{Hz}$), 7.87 (C(6 *)H, 1H, d, $^3\text{J}(6^*-7^*)=8.4\text{Hz}$), 7.85 (C(5 *)H, 1H, d, $^3\text{J}(5^*-4^*)=8.8\text{Hz}$), 7.53 (C(8 *)H, 1H, ddd, $^3\text{J}(8^*-9^*)=8.8\text{Hz}$, $^3\text{J}(8^*-7^*)=7.0\text{Hz}$, $^4\text{J}(8^*-7^*)=1.4\text{Hz}$), 7.37 (C(7 *)H, 1H, ddd, $^3\text{J}(7^*-6^*)=8.4\text{Hz}$, $^3\text{J}(7^*-8^*)=7.0\text{Hz}$, $^4\text{J}(7^*-9^*)=1.2\text{Hz}$), 7.9 * (C(4 *)H, 1H, d, $^3\text{J}(4^*-5^*)=8.8\text{Hz}$), 5.45 (C(1 $''$)H, 1H, s), 4.93 (C(1 $'$)H₂, 2H, q, $^3\text{J}(1'-2')=7.0\text{Hz}$), 4.01 (C(1 \dagger)H₂, 2H, q, $^3\text{J}(1\dagger-2\dagger)=7.2\text{Hz}$), 1.90 (C(1 **)H₃, 6H, s), 1.56 (C(2 $'$)H₃, 3H, t, $^3\text{J}(2'-1')=7.0\text{Hz}$), 1.39 (C(2 \dagger)H₃, 3H, t, $^3\text{J}(2\dagger-1\dagger)=7.2\text{Hz}$).

$^{13}\text{C-NMR}$: 192.70, 187.14, 187.03, 173.26, 169.86, 139.22, 132.58, 130.79, 129.79, 129.60, 128.58, 127.15, 123.73, 122.16, 109.45, 80.48, 69.85, 49.82, 37.80, 26.58, 15.96, 11.68.

HR-MS: calculated for $C_{23}H_{24}NO_3^+$ $[M+H]^+$: 362.1751. Found: 362.1753.

3-((3-Ethyl-1,1-dimethyl-1*H*-benzo[*e*]indol-2(3*H*)-ylidene)methyl)-4-hydroxycyclobut-3-ene-1,2-dione (**42**)



41 (10.0 g, 27.7 mmol, page 143) was dissolved in a mixture of chloroform (100 mL) and ethanol (100 mL) and then heated to reflux when an aqueous sodium hydroxide solution (10 mL, 40%, w/w) was dripped in via syringe. After 20 min the solvent was evaporated under reduced pressure. The residue was suspended in ethanol (40 mL), cooled to 0°C, filtered and washed with cold ethanol (2x10 mL). The yellow filtration residue was dissolved in water (500 mL) and acidified with aqueous saturated citric acid (50 mL) which precipitated the product. To obtain **42** (5.9 g, 17 mmol, 61%) as an intensive yellow powder the residue was filtered, washed with water (3x15 mL) and dried in the vacuum oven.

Decomposition onset: 92°C. Residue: 30%.

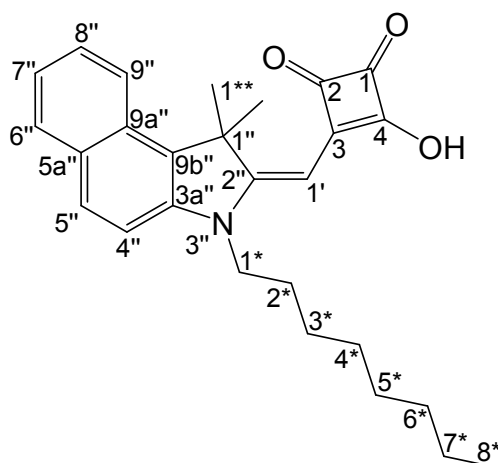
¹H-NMR: 8.12 (C(9*)H, 1H, d, $^3J(9^*-8^*)=7.9\text{Hz}$), 7.88 (C(6*)H+C(5*)H, 2H, m), 7.54 (C(8*)H, 1H, dd, $^3J(8^*-9^*)=7.9\text{Hz}$, $^3J(8^*-7^*)=7.4\text{Hz}$), 7.41 (C(7*)H, 1H, dd, $^3J(7^*-6^*)=8.1\text{Hz}$, $^3J(7^*-8^*)=7.4\text{Hz}$), 7.27 (C(4*)H, 1H, d, $^3J(4^*-5^*)=8.0\text{Hz}$), 5.72 (C(1'')H, 1H, s), 4.10 (C(1')H₂, 2H, q, $^3J(1'-2')=7.1\text{Hz}$), 1.94 (C(1**)H₃, 6H, s), 1.42 (C(2')H₃, 3H, t, $^3J(2'-1')=7.1\text{Hz}$).

¹³C-NMR: 189.92, 188.01, 187.99, 176.16, 171.65, 139.01, 133.37, 131.10, 129.73, 129.71, 128.55, 127.33, 124.21, 122.33, 109.68, 81.56, 50.43, 38.28, 26.60, 11.90.

MS (ESI-QTOF+): 356 (14) $[M+Na]^+$, 334 (100) $[M+H]^+$, 296 (31), 266 (20), 238 (42), 194 (14) $[C_{14}H_{12}N]^+$.

HR-MS (ESI-QTOF+): calculated for $C_{21}H_{19}NO_3Na$ $[M+Na]^+$: 356.1257. Found: 356.1256.

3-((1,1-Dimethyl-3-octyl-1*H*-benzo[*e*]indol-2(3*H*)-ylidene)methyl)-4-hydroxycyclobut-3-ene-1,2-dione (43**)**



45 (4.00 g, 8.98 mmol, page 148) was dissolved in ethanol (40 mL) in a 100 mL Schlenk tube and heated to reflux. Then an aqueous sodium hydroxide solution (2.20 mL, 40% w/w) was added via syringe. After boiling for 15 min, the solvent was evaporated under reduced pressure. Due to crystallization problems of the crude product in a small amount of ethanol the residue was dissolved in ethanol (300 mL) and water (500 mL). Upon acidification with concentrated hydrochloric acid (10 mL) of the basic solution the protonated product precipitated and was filtered. The brick stone coloured residue was dissolved in boiling ethyl acetate (70 mL) and precipitated by the addition of hexane (150 mL) to yield **43** (2.6 g, 5.9 mmol, 66%).

Decomposition onset: 177 °C. Residue: 34%.

1H -NMR: 8.12 (C(9'')H, 1H, d, $^3J(9''-8'')$ =8.4Hz), 7.92 (C(6'')H, 1H, d, $^3J(6''-7'')$ =8.0Hz), 7.90 (C(5'')H, 1H, d, $^3J(5''-4'')$ =8.8Hz), 7.51 (C(8'')H, 1H, m), 7.49 (C(4'')H, 1H, d, $^3J(4''-5'')$ =8.8Hz), 7.34 (C(7'')H, 1H, dd, $^3J(7''-6'')$ =8.0Hz, $^3J(7''-8'')$ =7.5Hz), 5.57 (C(1')H, 1H, s), 3.96 (C(1*)H₂, 2H, t, $^3J(1*-2^*)$ =6.9Hz), 1.82 (C(1**)H₃, 6H, s), 1.7-1.6 (C(2*)H₂, 2H, m), 1.4-1.1 (C(3*)H₂, C(4*)H₂, C(5*)H₂, C(6*)H₂, C(7*)H₂, 10H, m), 0.78 (C(8*)H₃, 3H,

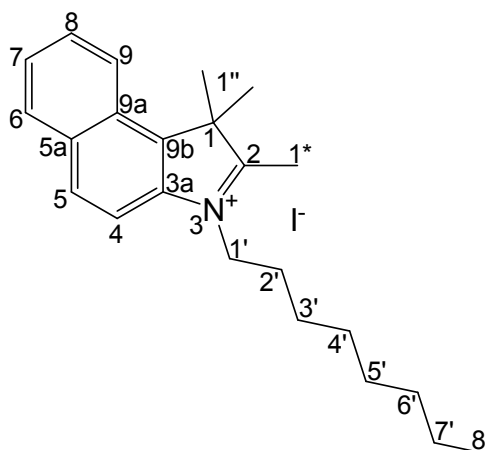
t, $^3J(8^*-7^*)=6.5\text{Hz}$).

$^{13}\text{C-NMR}$: 191.86, 190.75, 173.54, 167.39, 140.29, 130.82, 130.08, 129.62, 129.42, 128.07, 127.12, 123.20, 121.88, 110.58, 81.15, 48.83, 42.12, 31.14, 28.70, 28.58, 26.38, 26.17, 26.05, 22.02, 13.90.

MS (ESI-QTOF+): 440 (8) $[\text{M}+\text{Na}]^+$, 418 (100) $[\text{M}+\text{H}]^+$, 380 (46), 279 (20).

HR-MS (ESI-QTOF+): calculated for $\text{C}_{27}\text{H}_{32}\text{NO}_3$ $[\text{M}]^+$: 418.2377. Found: 418.2374.

1,1,2-Trimethyl-3-octyl-1*H*-benzo[*e*]indolium iodide (**44**)



1,1,2-Trimethyl-1*H*-benzo[*e*]indole (60.3 g, 288 mmol, FEW Chemicals), 1-iodooctane (100 mL, 416 mmol, ABCR) and 1-butanol (60 mL) were combined in a 250 mL Schlenk tube in which the suspension was heated to reflux (120 °C) for 18 h. Subsequently, the reaction mixture was chilled just below 40 °C and then poured into diethyl ether (1.2 L). The precipitate was filtered and washed with cold diethyl ether. Recrystallization from boiling acetone (800 mL) and subsequent recrystallization of the distillation residue of the mother liquid yielded in total **44** (86 g, 0.19 mol, 65%) as ecru crystals.

Decomposition onset: 194 °C. Residue: 4%.

$^1\text{H-NMR}$ (DMSO-d_6): 8.37 (C(9)H, 1H, d, $^3J(9-8)=8.5\text{Hz}$), 8.30 (C(5)H, 1H, d, $^3J(5-4)=9.0\text{Hz}$), 8.21 (C(6)H, C(4)H, 2H, m), 7.78 (C(8)H, 1H, ddd, $^3J(8-9)=8.5\text{Hz}$, $^3J(8-7)=7.3\text{Hz}$, $^4J(8-6)=1.0\text{Hz}$), 7.70 (C(7)H, 1H, ddd, $^3J(7-6)=8.3\text{Hz}$, $^3J(7-8)=7.3\text{Hz}$, $^4J(7-9)=0.7\text{Hz}$), 4.63 (C(1')H₂, 2H, t, $^3J(1'-2')=7.8\text{Hz}$), 3.02 (C(1')H₃, 3H, s), 2.0-1.8 (C(2')H₂,

2H, m), 1.77 (C(1'')H₃, 6H, s), 1.5-1.4 (C(3')H₂, 2H, m), 1.35-1.1 (C(4')H₂, C(5')H₂, C(6')H₂, C(7')H₂, 8H, m), 0.8-0.7 (C(8')H₃, 3H, t, ³J(8'-7')=6.8Hz).

¹³C-NMR (DMSO-d₆): 196.03, 138.33, 136.77, 132.87, 130.53, 129.53, 128.25, 127.05 (2xC), 123.30, 113.32, 55.35, 47.99, 30.98, 28.45, 28.30, 27.38, 25.75, 21.86, 21.54, 14.41, 13.75.

MS (ESI-QTOF+): 448 (0.4) [M-H]⁺, 322 (100) [M-I]⁺, 224 (1) [C₁₆H₁₈N]⁺.

HR-MS (ESI-QTOF+): calculated for C₂₃H₃₂N [M-I]⁺: 322.2529. Found: 322.2508.

Elemental analysis: calculated for C₂₃H₃₀Nl: C, 61.75; H, 6.76; N, 3.13; l, 28.36. Found: C, 61.20; H, 6.34; N, 3.10; l, 28.16.

3-((1,1-Dimethyl-3-octyl-1*H*-benzo[*e*]indol-2(3*H*)-ylidene)methyl)-4-ethoxycyclobut-3-ene-1,2-dione (45)



Figure 4.9: Molecular structure of **44** and picture of the isolated product after drying.

44 (14.4 g, 32.0 mmol, page 147), freshly distilled **30** (4.00 g, 23.5 mmol, page 130) and ethanol (32 mL) were combined heated to reflux until the starting materials dissolved. Then the reaction mixture was allowed to cool to 55°C when triethylamine (3.90 mL, 28.2 mmol) was added via syringe. The colour changed immediately from light yellow to brown and then to dark green. The reaction mixture was heated to reflux overnight. The solvent was removed under reduced pressure followed by the purification of the

crude product with column chromatography (ethyl acetate:hexane = 1:9→5:5) to yield in **45** (7.2 g, 16 mmol, 69%) as an orange crystalline powder (Figure 4.9).

Melting point: 72 – 76 °C.

Decomposition onset: 276 °C. Residue: 17%.

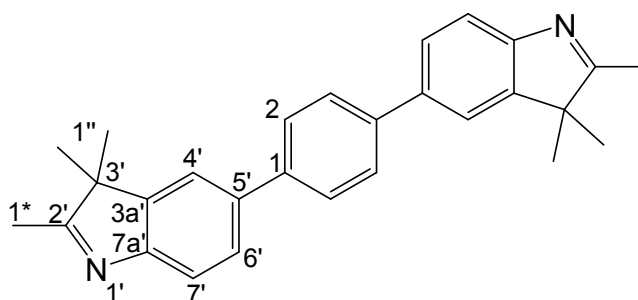
¹H-NMR: 8.09 (C(9'')H, 1H, d, ³J(9''-8'')=8.3Hz), 7.87 (C(6'')H, 1H, d, ³J(6''-7'')=8.1Hz), 7.83 (C(5'')H, 1H, d, ³J(5''-4'')=8.8Hz), 7.52 (C(8'')H, 1H, ddd, ³J(8''-9'')=8.3Hz, ³J(8''-7'')=7.0Hz, ⁴J(8''-6'')=1.0Hz), 7.37 (C(7'')H, 1H, ddd, ³J(7''-6'')=8.1Hz, ³J(7''-8'')=7.0Hz, ⁴J(7''-9'')=0.7Hz), 7.21 (C(4'')H, 1H, d, ³J(4''-5'')=8.8Hz), 5.45 (C(1')H, 1H, s), 4.92 (C(1†)H₂, 2H, q, ³J(1†-2†)=7.1Hz), 3.94 (C(1*)H₂, 2H, t, ³J(1*-2*)=6.3Hz), 1.90 (C(1**)H₃, 6H, s), 1.85-1.75 (C(2*)H₂, 2H, m), 1.56 (C(2†)H₃, 3H, t, ³J(2†-1†)=7.1Hz), 1.5-1.2 (C(3*)H₂, C(4*)H₂, C(5*)H₂, C(6*)H₂, C(7*)H₂, 10H, m), 0.87 (C(8*)H₃, 3H, t, ³J(8*-7*)=6.8Hz).

¹³C-NMR: 192.63, 187.03, 173.21, 170.23, 139.76, 132.34, 130.71, 129.64, 129.48, 128.49, 127.08, 123.67, 122.10, 109.74, 80.74, 69.77, 49.77, 43.06, 31.64, 29.16, 29.02, 26.86, 26.64, 26.59, 22.49, 15.90, 13.99.

MS: 484 (2) [M+K]⁺, 468 (5) [M+Na]⁺, 446 (100) [M+H]⁺, 390 (5) [C₂₆H₃₂NO₂]⁺, 360 (6) [C₂₅H₃₀NO]⁺, 307 (5) [C₂₂H₉₉N]⁺, 262 (3) [C₁₈H₁₆NO]⁺, 223 (2) [M+H]⁺⁺, 148.8 (1) [M+H]³⁺, 111.6 (3) [M+H]⁴⁺, 89.3 (0.4) [M+H]⁵⁺, 74.4 (0.8) [M+H]⁶⁺, 63.8 (0.7) [M+H]⁷⁺, 55.8 (0.4) [M+H]⁸⁺.

HR-MS: calculated for C₂₉H₃₆NO₃ [M+H]⁺: 446.2690. Found: 446.2684.

1,4-Bis(2,3,3-trimethyl-3H-indol-5-yl)benzene (46)



Benzene-1,4-diboronic acid (4.00 g, 24.1 mmol, ABCR), **32** (15.5 g, 65.1 mmol, page 132), tetrahydrofuran (200 mL) and water (50 mL) were combined in a 500 mL Schlenk tube and degassed by freeze-pump-thaw cycles. After that, tetrakis(triphenylphosphine)-palladium(0) (1.25 g, 1.08 mmol, Merck) was added and the solution was heated to reflux for 60 h. The reaction mixture was then cooled to rt and quenched by the addition of dichloromethane (200 mL). The ensuing emulsion was stirred for 30 min. The organic layer was separated and washed with water (5x200 mL) and brine (2x150 mL). After drying and filtering through a silica gel bed (5 cm), the filtrate was concentrated under reduced pressure. The remainder solely contained **46** (6.2 g, 15 mmol, 62%), which was used without further purification.

Decomposition onset: 239 °C. Residue: 29%.

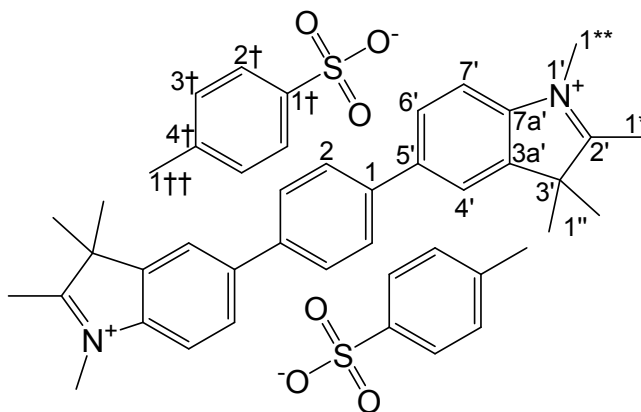
¹H-NMR: 7.68 (C(2)H, 4H, s), 7.61 (C(7')H, 2H, d, ³J(7'-6')=8.0Hz), 7.58 (C(6')H, 2H, dd, ³J(6'-7')=8.0Hz, ⁴J(6'-4')=1.6Hz), 7.53 (C(4')H, 2H, d, ⁴J(4'-6')=1.6Hz), 2.31 (C(1*)H₃, 6H, s), 1.37 (C(1'')H₃, 12H, s).

¹³C-NMR: 188.30 C(2'), 153.26 C(7a'), 146.34 C(3a'), 140.07 C(5'), 137.86 C(1), 127.50 C(2), 126.58 C(6'), 120.06 C(4'), 120.02 C(7'), 53.73 C(3'), 23.16 C(1''), 15.50 C(1*).

MS: 393 (87) [M+H]⁺, 378 (100) [C₂₇H₂₆N₂]⁺, 361 (46) [C₂₆H₂₁N₂]⁺, 196.6 (6) [M+H]⁺⁺, 189.1 (7) [C₂₇H₂₆N₂]⁺⁺.

HR-MS: calculated for C₂₈H₂₉N₂ [M+H]⁺: 393.2325. Found: 393.2330.

Elemental analysis: calculated for C₂₈H₂₈N₂: C, 85.67; H, 7.19; N, 7.14. Found: C, 85.39; H, 7.12; N, 6.99.

**5,5'-(1,4-Phenylene)bis(1,2,3,3-tetramethyl-3*H*-indolium)
bis(4-methylbenzenesulfonate) (47)**

46 (4.50 g, 11.5 mmol, page 149) and methyl *p*-toluenesulfonate (50.0 g, 268 mmol) were added to a 100 mL Schlenk tube. The reaction mixture was heated to 130 °C for 60 h. Then the brown suspension was cooled to rt, filtered and the residue was washed several times with cyclohexane. To yield **47** (7.7 g, 9.1 mmol, 79%) as a light brown coloured powder the filtration residue was dried in the vacuum oven.

Decomposition onset: 85 °C. Residue: 40%. (Decomposition above 85 °C was also proven by DSC).

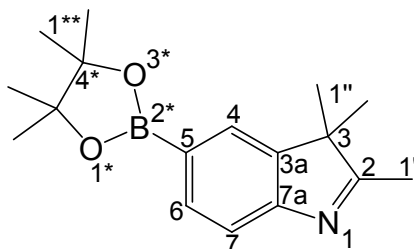
¹H-NMR (DMSO-*d*₆): 8.26 (C(7')H, 2H, m), 8.00 (C(4')H, C(6')H, 4H, m), 7.95 (C(2)H, 4H, s), 7.46 (C(2†)H, 4H, d, ³J(2†-3†)=7.9Hz), 7.09 (C(3†)H, 4H, d, ³J(3†-2†)=7.9Hz), 4.01 (C(1**)H₃, 6H, s), 2.79 (C(1*)H₃, 6H, s), 2.27 (C(1††)H₃, 6H, s), 1.60 (C(1'')H₃, 12H, s).

¹³C-NMR (DMSO-*d*₆): 196.17, 145.76, 142.58, 141.74, 140.58, 138.55, 137.63, 128.07, 127.84, 127.24, 125.51, 121.62, 115.63, 54.14, 34.74, 21.78, 20.81, 14.08.

MS (ESI-TOF+): 421 (100) [M-TsOH-TsO⁻]⁺, 407 (8) [M-TsOH-TsO⁻-CH₃]⁺, 326 (4) [C₂₄H₂₄N]⁺, 250 (4) [C₁₈H₂₀N]⁺, 211.6 (68) [M+H-2·TsO⁻]⁺⁺, 211.1 (100) [M-2·TsO⁻]⁺⁺, 203.6 (73) [M-2·TsO⁻-CH₃]⁺⁺.

HR-MS (ESI-TOF+): calculated for C₃₀H₃₃N₂ [M-TsOH-TsO⁻]⁺: 421.2638. Found: 421.2641.

2,3,3-Trimethyl-5-(4,4,5,5-tetramethyl-1,3,2-dioxaborolan-2-yl)-3H-indole (48)



Water free potassium acetate (31.3 g, 0.319 mol), bis(pinacolato)diborone (40.0 g, 0.158 mol, CombiPhos Catalysts Inc.), **32** (25.0 g, 0.105 mol, page 132), dioxane (2 L) and dichloro[1,1'-bis(diphenylphosphino)-ferrocen]-palladium(II) (3.19 g, 3.91 mmol, CombiPhos Catalysts Inc.) were added to a 3 L round bottom flask, which was then connected to the rotary evaporator apparatus. During slow rotation the reaction proceeded at a bath temperature of 85 – 90°C and a pressure of 850 mbar. As the mixture was heated the colour changed from red to orange and finally to dark brown. After 2.5 h the reaction mixture was concentrated *in vacuo* to 500 mL, filtrated through a silica gel bed (12 cm) and the solvent of the filtrate was removed completely at rotary evaporator. The orange residue was purified by column chromatography (hexane:acetone, 100:0→90:10). For further purification the product was sublimated at high vacuum (145°C, 0.02 mbar) to yield **48** (24 g, 85 mmol, 81%) as light pink crystals.

Melting point: 125 – 135°C.

Decomposition onset: 243°C. Residue: 0%.

¹H-NMR: 7.79 (C(6)H, 1H, dd, ³J(6-7)=7.7Hz, ⁴J(6-4)=1.1Hz), 7.72 (C(4)H, 1H, dd, ⁴J(4-6)=1.1Hz, ⁵J(4-7)=0.6Hz), 7.52 (C(7)H, 1H, dd, ³J(7-6)=7.7Hz, ⁵J(7-4)=0.6Hz), 2.28 (C(1')H₃, 3H, s), 1.35 (C(1**)H₃, 12H, s), 1.30 (C(1'')H₃, 6H, s).

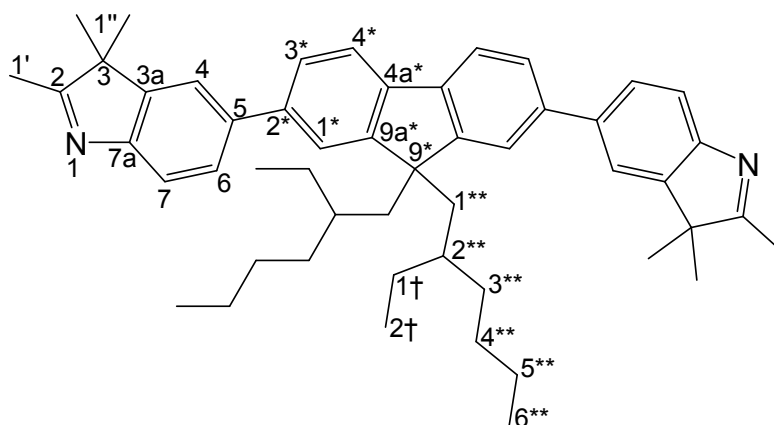
¹³C-NMR: 189.37, 156.25, 144.70, 134.68, 127.19, 119.13, 83.46, 53.27, 24.67, 22.81, 15.30. C(5) signal is not visible, since the ¹³C-¹¹B and ¹³C-¹⁰B couplings split the signal to zero.

MS: 286.2 (100) [M+H]⁺, 235 (15), 143 (2) [M+H]⁺⁺.

HR-MS: calculated for C₁₇H₂₅O₂BN [M+H]⁺: 286.1973. Found: 286.1969.

Elemental analysis: calculated for $C_{17}H_{24}NO_2B$: C, 71.60; H, 8.48; N, 4.91; O, 11.22; B, 3.79. Found: C, 71.45; H, 8.25; N, 4.87. Boron disturbs the oxygen measurement.

5,5'-(9,9-Bis(2-ethylhexyl)-9*H*-fluorene-2,7-diyl)bis(2,3,3-trimethyl-3*H*-indole) (49)



48 (8.80 g, 30.9 mmol, page 152), 2,7-dibromo-9,9-bis-(2-ethyl-hexyl)-9*H*-fluorene (6.81 g, 12.4 mmol, racemate) and tetrahydrofuran (250 mL) were placed in a 500 mL Schlenk tube. All solutions and solvents were degassed by freeze-pump-thaw cycles. An aqueous potassium carbonate solution (4.30 g, 31.1 mmol in 50 mL) was prepared in a separate 100 mL Schlenk tube and transferred via syringe into previous reaction mixture. Next, tetrakis(triphenylphosphine)palladium(0) (1.18 g, 1.02 mmol) was added and then the reaction mixture was heated to reflux for 48 h. After that the suspension was cooled to rt and quenched with dichloromethane (100 mL) under vigorous stirring for 30 min. The organic layer was diluted with dichloromethane (400 mL) and washed with water (10x500 mL) and brine (2x500 mL). The solvent of the combined and dried organic layers was distilled under reduced pressure. The residue was purified by column chromatography (hexane:methyl *tert*-butyl ether, 50:50→0:100) to yield **49** (6.3 g, 8.5 mmol, 69%) as a light yellow powder.

Decomposition onset: 123 °C. Residue: 15%. (Decomposition above 125 °C was also proven by DSC).

¹H-NMR: 7.77 (C(7)H, 2H, d, ³J(7-6)=8.0Hz), 7.6-7.5 (C(4)H, C(6)H, C(1*)H, C(3*)H,

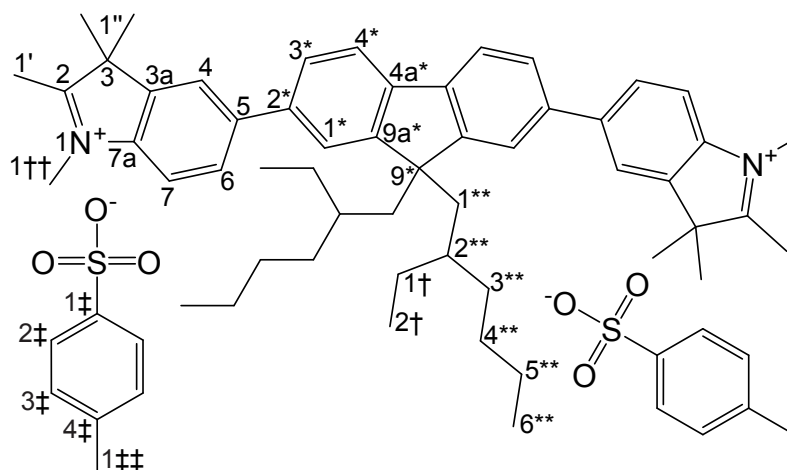
C(4*)H, 10H, m), 2.33 (C(1')H₃, 6H, s), 2.10 (C(1**)H₂, 4H, m), 1.40 (C(1'')H₃, 12H, s), 1.0-0.7 (C(3**)H₂, C(4**)H₂, C(5**)H₂, C(1†)H₂, 16H, m), 0.65-0.5 (C(2**)H, C(2†)H₃, C(6**)H₃, 14H, m).

¹³C-NMR: [189.13, 189.09, 189.07], [151.78, 151.75, 151.71], [151.34, 151.30, 151.27], [145.92, 145.89, 145.86], [140.22, 140.18, 140.15], [139.70, 139.64, 139.57], [139.66, 139.56, 139.43], [126.95, 126.89, 126.82], [126.25, 129.24, 126.22], [123.06, 122.91, 122.73], [120.29, 120.28, 120.25], [119.93, 119.91, 119.89], [119.63, 119.59, 119.55], [55.09], [53.80], [44.50], [34.74], [33.83, 33.81], [28.20, 28.16], [27.19, 27.17], [23.20, 23.17, 23.14], [22.74], [15.13, 15.12, 15.11], [13.98], [10.43, 10.41]. The chemical shifts are expected to be different in a racemic diastereomeric mixture. In this particular case three stereoisomers are present: an enantiomeric pair (*R,R* and *S,S*) and the *meso-R,S* form. The probability that two ¹³C are present in the same molecule is very low, let alone for them to be in mirror position to each other. This results in a symmetry reduction and the stereoisomeric (*R,R*) and (*S,S*) pair is no longer enantiomeric. The theoretical frequency of (*R,R*)*:(*meso-R,S*)*:(*S,S*)* is therefore 1:2:1, except for those carbons located on the σ plain as well as those with increased flexibility.

MS: 706 (100) [M+H]⁺, 690 (25) [M-CH₃]⁺, 493 (10) [C₃₅H₃₃N₂]⁺, 479 (8) [C₃₅H₃₁N₂]⁺, 478 (8) [C₃₅H₃₀N₂]⁺, 464 (3) [C₃₄H₂₈N₂]⁺, 463 (3) [C₃₄H₂₇N₂]⁺, 353 (5) [M+H]⁺⁺, 235 (1) [M+H]³⁺, 176 (2) [M+H]⁴⁺.

HR-MS: calculated for C₅₁H₆₅N₂ [M+H]⁺: 705.5142. Found: 705.5154.

5,5'-(9,9-Bis(2-ethylhexyl)-9*H*-fluorene-2,7-diyl)bis(1,2,3,3-tetramethyl-3*H*-indolium) bis(4-methylbenzenesulfonate) (50)



49 (6.30 g, 8.94 mmol, page 153) and methyl *p*-toluenesulfonate (33.5 g, 180 mmol) were placed in a 100 mL Schlenk tube. The reaction mixture was heated to 110°C overnight and then to for 3 h to 130°C. The dark blue reaction mixture was cooled to 50°C prior to pouring into cyclohexane (700 mL) under vigorous stirring. The dark oil was separated from cyclohexane and extracted again with cyclohexane (500 mL). The oily residue was dissolved in ethanol (200 mL) and added dropwise to fresh cyclohexane (600 mL). The very light blue precipitated product **50** was filtered and dried (5.62g, 5.0 mmol, 55%).

Decomposition onset: 305°C. Residue: 37%. (Decomposition was also proven by DSC).

¹H-NMR: 8.22 (C(7)H, 2H, d, ³J(7-6)=4.5Hz), 8.05 (C(6)H, 2H, d, ³J(7-6)=4.5Hz), 8.03-7.95 (C(1*)H, C(3*)H, C(4)H, 6H, m), 7.83 (C(4*)H, 2H, d, ³J(4*-3*)=7.8Hz), 7.45 (C(2†)H, 4H, d, ³J(2†-3†)=7.8Hz), 7.09 (C(3†)H, 4H, d, ³J(3†-2†)=7.8Hz), 4.01 (C(1††)H₃, 6H, s), 2.79 (C(1')H₃, 6H, s), 2.27 (C(1††)H₃, 6H, s), 2.22 (C(1**)H₂, 4H, m), 1.60 (C(1'')H₃, 12H, s), 1.0-0.6 (C(3**)H₂, C(4**)H₂, C(5**)H₂, C(1†)H₂, 16H, m), 0.6-0.4 (C(2**)H, C(2†)H₃, C(6**)H₃, 14H, m).

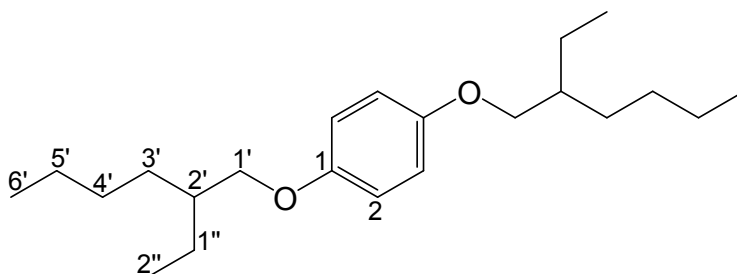
¹³C-NMR: [195.75, 195.72, 195.70], [151.43, 151.38, 151.32], [145.84], [142.48, 142.43, 142.40], [141.68, 141.63, 141.56], [141.39, 141.36, 141.33], [140.52, 140.48, 140.44], [137.49], [137.17, 137.11, 137.01], [128.00], [126.87], [126.26, 126.17,

126.07], [125.47], [122.88, 122.75, 122.63], [121.32, 121.30, 121.26], [120.63, 120.61, 121.60], [115.57, 115.50, 115.44], [55.01, 55.00], [54.03, 54.01, 53.99], [43.03], [34.68], [34.31], [33.26, 33.18], [27.40, 27.33], [26.86, 26.83], [22.14], [21.82, 21.79, 21.76], [20.76], [13.99], [13.77], [10.36, 10.32]. The chemical shifts are expected to be different in a racemic diastereomeric mixture. In this particular case three stereoisomers are present: an enantiomeric pair (*R,R* and *S,S*) and the *meso-R,S* form. The probability that two ^{13}C are present in the same molecule is very low, let alone for them to be in mirror position to each other. This results in a symmetry reduction and the stereoisomeric (*R,R*) and (*S,S*) pair is no longer enantiomeric. The theoretical frequency of (*R,R*)*:(*meso-R,S*)*:(*S,S*)* is therefore 1:2:1, except for those carbons located on the σ plain as well as those with increased flexibility.

MS (ESI-QTOF+): 734 (38) $[\text{M}-\text{TsOH}-\text{TsO}^-]^+$, 368 (69) $[\text{M}+\text{H}-2\cdot\text{TSO}^-]^{++}$, 367 (100) $[\text{M}-2\cdot\text{TSO}^-]^{++}$.

HR-MS (ESI-QTOF+): calculated for $\text{C}_{53}\text{H}_{69}\text{N}_2$ $[\text{M}-\text{TsOH}-\text{TsO}^-]^+$: 733.5455. Found: 733.5442.

1,4-Bis(2-ethylhexyloxy)benzene (51)



Hydroquinone (11.0 g, 99.9 mmol), potassium hydroxide (12.1 g, 215 mmol), potassium iodide (3.50 g, 20 mmol), 2-ethylhexyl bromide (39.65 g, 205 mmol) and ethanol (100 mL) were suspended and heated to reflux for 4 d. After the reaction the ethanol was distilled under reduced pressure. The residue was dissolved in dichloromethane (500 mL) and extracted with an aqueous sodium hydroxide solution (6x250 mL, 15% w/w), water (4x250 mL) and brine (250 mL). The product **51** (20.0 g, 45 mmol, 45%) was isolated by distilling the chloroform.

Melting point: 2–5 °C.

Boiling point: 317 °C. Residue: 0%.

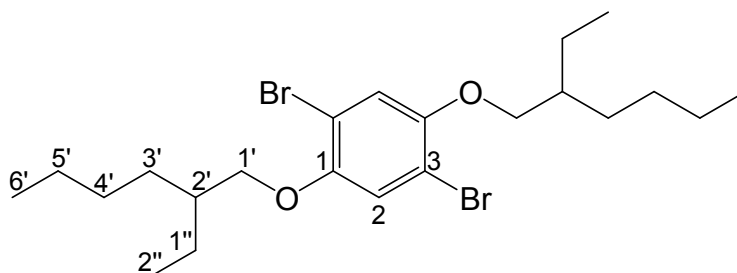
¹H-NMR: 6.83 (C(2)H, 4H, s), 3.8-3.7 (C(1')H_a, C(1')H_b, 4H, m), 1.75-1.65 (C(2')H, 2H, m), 1.55-1.2 (C(3')H₂, C(4')H₂, C(5')H₂, C(1'')H₂, 16H, m), 0.95-0.85 (C(6')H₃, C(2'')H₃, 12H, m).

¹³C-NMR: 153.42 C(1), 115.34 C(2), 71.18 C(1'), 39.45 C(2'), 30.52 C(3'), 29.08 C(4'), 23.84 C(1''), 23.06 C(5'), 14.08 C(6'), 11.09 C(2'').

MS (EI+): 334 (10) [M]⁺, 222 (6) [C₁₄H₂₂O₂]⁺, 110 (100) [C₆H₆O₂]⁺, 71 (8) [C₅H₁₁]⁺, 57 (15) [C₄H₉]⁺, 55 (7) [C₄H₇]⁺, 43 (15) [C₃H₇]⁺, 41 (11) [C₃H₅]⁺, 29 (7) [C₂H₅]⁺.

HR-MS (EI+): calculated for C₂₂H₃₈O₂ [M]⁺: 334.2867. Found: 334.2866.

1,4-Dibromo-2,5-bis(2-ethylhexyloxy)benzene (**52**)



51 (18.00 g, 53.8 mmol, page 156) was dissolved in dichloromethane (150 mL) and glacial acetic acid (150 mL). To the yellowish solution, *N*-bromosuccinimide (20.1 g, 113 mmol) was added and the suspension was boiled for 36 h. The colour of the solution changed to dark red. The reaction was quenched by pouring it on ice (2 L). The organic layer was separated and additionally the water layer was extracted with dichloromethane (2x200 mL). The combined organic layers were extracted with aqueous sodium thiosulphate solution (4x350 mL, 5% w/v), water (4x500 mL) and brine (3x250 mL). The separated dark brown organic layer was filtrated through a silica gel bed (8 cm) before distilling the solvent *in vacuo*. The light yellow residue was then purified by column chromatography (hexane) to yield **52** (14 g, 25 mmol, 45%) as a colourless oil.

Melting point: -70 to -65 °C.

Decomposition onset: 336 °C. Residue: 0%.

$^1\text{H-NMR}$: 7.08 (C(2)H, 4H, s), 3.9-3.8 (C(1')H_a, C(1')H_b, 4H, m), 1.8-1.7 (C(2')H, 2H, m), 1.6-1.25 (C(3')H₂, C(4')H₂, C(5')H₂, C(1'')H₂, 16H, m), 1.0-0.8 (C(6')H₃, C(2'')H₃, 12H, m).

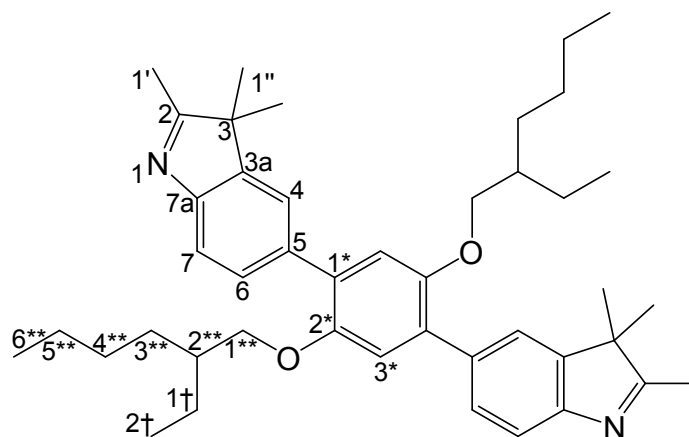
$^{13}\text{C-NMR}$: 150.17 C(1), 118.17 C(2), 111.05 C(3), 72.52 C(1'), 39.42 C(2'), 30.44 C(3'), 29.02 C(4'), 23.86 C(1''), 23.01 C(5'), 14.07 C(6'), 11.14 C(2'').

MS (Magnet EI+): 494 (17) [M]⁺ (A+4), 492 (33) [M]⁺ (A+2), 490 (17) [M]⁺ (A), 382 (2) [C₁₄H₁₉O₂^{81,81}Br₂]⁺, 380 (4) [C₁₄H₁₉O₂^{79,81}Br⁸¹Br]⁺, 378 (2) [C₁₄H₁₉O₂^{79,79}Br₂]⁺, 270 (49) [C₆H₂O₂^{81,81}Br₂]⁺, 268 (100) [C₆H₂O₂⁸¹Br⁷⁹Br]⁺, 266 (49) [C₆H₂O₂^{79,79}Br₂]⁺, 113 (18) [C₈H₁₇]⁺, 83 (6) [C₆H₁₁]⁺, 71 (45) [C₅H₁₁]⁺, 69 (16) [C₅H₉]⁺, 57 (70) [C₄H₉]⁺, 55 (28) [C₄H₇]⁺, 43 (61) [C₃H₇]⁺, 41 (42) [C₃H₅]⁺, 29 (27) [C₂H₅]⁺, 27 (8) [C₂H₃]⁺.

HR-MS (Magnet EI+): calculated for C₂₂H₃₆O₂Br₂ [M]⁺: 490.1077. Found: 490.1080.

Elemental analysis: calculated for C₂₂H₃₆O₂Br₂: C, 53.67; H, 7.37; O, 6.50; Br, 32.46. Found: C, 53.61; H, 7.19; O, 6.48; Br, 32.21.

5,5'-(2,5-Bis(2-ethylhexyloxy)-1,4-phenylene)bis(2,3,3-trimethyl-3H-indole) (53)



In this reaction all solvents and solutions were degassed by freeze-pump-thaw cycles. **48** (8.80 g, 30.9 mmol, page 152), **52** (6.11 g, 12.4 mmol, page 157) and tetrahydrofuran

(250 mL) were combined in a 500 mL Schlenk tube. An aqueous potassium carbonate (4.30 g, 31.1 mmol in 50 mL) was transferred via a syringe into the tetrahydrofuran solution. After that, tetrakis(triphenylphosphine)palladium(0) (1.03 g, 0.891 mmol, Merck) was added before heating the reaction mixture to reflux for 56 h. The reaction was quenched by the addition of dichloromethane (100 mL) at rt. This was stirred for 30 min vigorously. The organic layer was diluted with dichloromethane (500 mL) and washed with water (4x500 mL) and brine (1x500 mL). The solvent of the combined and dried organic layers was distilled under reduced pressure. **48** and **53** have very similar elution properties on silica gel. In order to remove the residual **48** the orange residue was dissolved in a suspension of ethanol:water (1000:350 mL) and silica gel (15 g). The suspension was stirred overnight at rt. After filtration, the filtrate was concentrated to the half its volume under vacuum and then cooled to 4 °C overnight. Orange 0.3 – 1 cm long needle like crystals precipitated, were filtered and dried to yield **53** (4.8 g, 7.4 mmol, 60%).

Decomposition onset: 373 °C. Residue: 32%. (Decomposition was also proven in DSC).

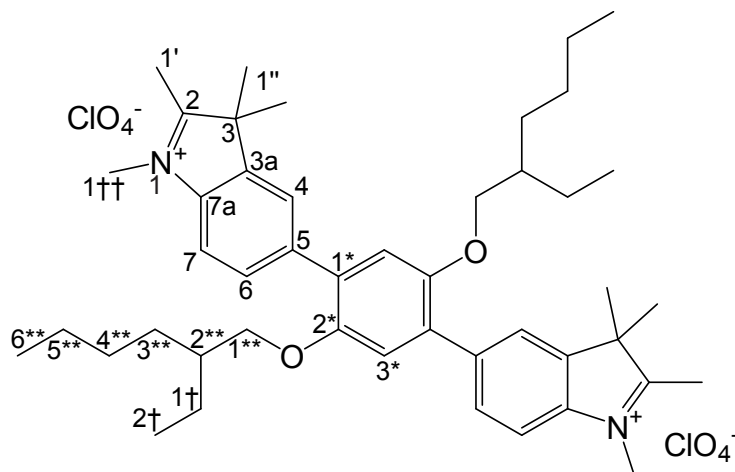
¹H-NMR: 7.60 (C(4)H, 2H, d, ⁴J(4-6)=1.6Hz), 7.57 (C(7)H, 2H, d, ³J(7-6)=8.0Hz), 7.49 (C(6)H, 2H, d, ³J(6-7)=8.0Hz, ⁴J(6-4)=1.6Hz), 7.02 (C(3*)H, 2H, s), 3.84 (C(1**)H₂, 4H, m), 2.32 (C(1')H₃, 6H, s), 1.7-1.5 (C(2**)H₂, 2H, m), 1.45-1.1 (C(3**)H₂, C(4**)H₂, C(5**)H₂, C(1†)H₂, C(1'')H₃, 28H, m), 0.9-0.75 (C(6**)H₃, C(2†)H₃, 12H, m).

¹³C-NMR: 188.57, 151.93, 150.30, 144.72, 135.70, 130.67, 128.83, 123.07, 119.03, 115.90, 71.65, 53.63, 39.58, 30.43, 28.93, 23.82, 23.10, 23.08, 22.92, 15.17, 13.95, 10.97.

MS: 649 (100) [M+H]⁺, 634 (3) [M-CH₃]⁺, 536 (4) [C₃₆H₄₄N₂O₂]⁺, 424 (4) [C₂₈H₂₈N₂O₂]⁺, 325 (5) [M+H]⁺⁺, 217 (1) [M+H]³⁺, 162 (2) [M+H]⁴⁺, 108 (1) [M+H]⁶⁺, 93 (1) [M+H]⁷⁺.

HR-MS: calculated for C₄₄H₆₁N₂O₂ [M+H]⁺: 649.4728. Found: 649.4724.

5,5'-(2,5-Bis(2-ethylhexyloxy)-1,4-phenylene)bis(1,2,3,3-tetramethyl-3*H*-indolium) bis perchlorate (54**)**



In a 50 mL Schlenk tube **53** (1.22 g, 1.88 mmol, page 158) was dissolved in melted methyl *p*-toluenesulfonate (7.08 g, 38.0 mmol) at 120 °C. The solution was stirred for 3 d before chilled and poured as lukewarm black oil into cyclohexane (250 mL). The oily phase was separated and washed with cyclohexane (300 mL). The supernatant was decanted and the residue was dissolved in hot ethanol (200 mL, 60 °C). To induce the precipitation the product was converted to the bis perchlorated derivative by adding to this solution a saturated ethanolic sodium perchlorate solution (50 mL). The mixture was cooled to rt and **54** (1.4 g, 1.6 mmol, 83%) was harvested by filtration and subsequent drying in a vacuum oven.

Decomposition onset: 286 °C. Spontaneous decomposition. Residue: 27%.

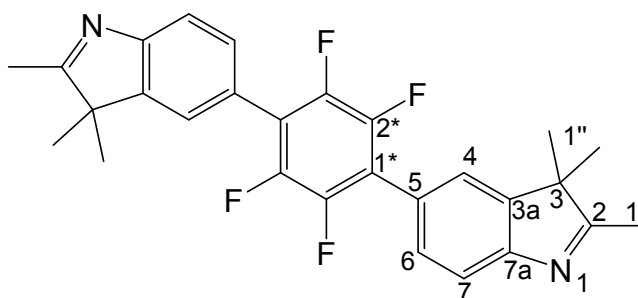
¹H-NMR (DMSO-*d*₆): 7.99 (C(4)H, 2H, d, ⁴J(4-6)=0.7Hz), 7.97 (C(7)H, 2H, d, ³J(7-6)=8.3Hz), 7.81 (C(6)H, 2H, dd, ³J(6-7)=8.3Hz, ⁴J(6-4)=0.7Hz), 7.16 (C(3*)H, 2H, s), 4.02 C(1††)H₃, 6H, s), 4.0-3.8 (C(1**)H₂, 4H, m), 2.79 (C(1')H₃, 6H, s), 1.7-1.5 (C(1'')H₃, C(2**)H, 14H, m), 1.4-1.1 (C(3**)H₂, C(4**)H₂, C(5**)H₂, C(1†)H₂, 16H, m), 0.9-0.7 (C(6**)H₃, C(2†)H₃, 12H, m).

¹³C-NMR (DMSO-*d*₆): 195.91, 149.77, 141.08, 141.06, 138.91, 129.81, 129.08, 124.26, 115.46, 114.64, 70.83, 53.91, 38.90, 34.66, 29.96, 28.39, 23.39, 22.45, 21.78, 14.01, 13.91, 10.90.

MS (ESI-QTOF+): 678 (15) $[M-H-2\cdot ClO_4^-]^+$, 340 (100) $[M+H-2\cdot ClO_4^-]^{++}$, 339 (100) $[M-2\cdot ClO_4^-]^{++}$.

HR-MS (ESI-QTOF+): calculated for $C_{46}H_{65}N_2O_2$ $[M-H-2\cdot ClO_4^-]^+$: 677.5041. Found: 677.5042.

5,5'-(Perfluoro-1,4-phenylene)bis(2,3,3-trimethyl-3H-indole) (55)

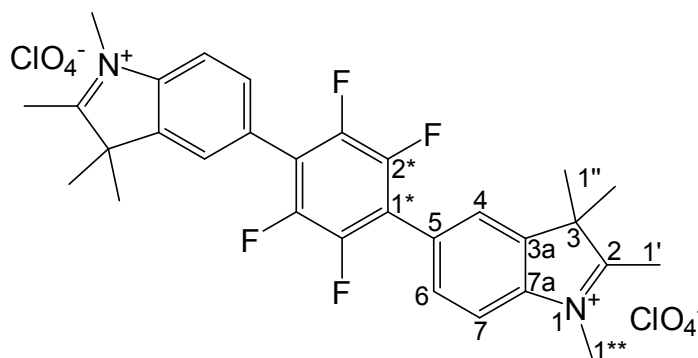


48 (8.80 g, 30.9 mmol, page 152), 1,4-dibromotetrafluorobenzene (freshly sublimated at 140 °C and 0.02 mbar, 3.82 g, 12.4 mmol, ABCR) and tetrahydrofuran (250 mL) were placed in a 500 mL Schlenk tube and degassed by freeze-pump-thaw cycles. In a separate 100 mL Schlenk tube an aqueous solution of potassium carbonate (4.30 g, 31.1 mmol in 50 mL) was prepared and degassed by freeze-pump-thaw cycles which was then dripped into the tetrahydrofuran solution. In order to start the reaction, tetrakis(triphenylphosphine)palladium(0) (1.03 g, 0.891 mmol, Merck) was added and the reaction mixture was heated to reflux for 72 h. The reaction was quenched by cooling to rt and adding dichloromethane (100 mL) while stirring vigorously for 30 min. The organic layer was diluted in dichloromethane (500 mL) and washed with water (5x500 mL) and brine (2x300 mL). After removal of the solvent under vacuum, the raw product was purified by column chromatography (chloroform) to yield **55** (0.50 g, 1.0 mmol, 8%) as an orange powder, which was immediately used in the next reaction. Unfortunately the aliquot was evidently wasted before the analysis could be completed.

¹H-NMR: 7.8-7.6 (C(7)H, 2H, m), 7.5-7.3 (C(4)H, C(6)H, 4H, m), 2.3 (C(1')H₃, 6H, br), 1.4 (C(1'')₃, 12H, br).

¹⁹F-NMR: -139.16 (C(2')F, 4F, m).

5,5'-(Perfluoro-1,4-phenylene)bis(1,2,3,3-tetramethyl-3*H*-indolium) bis perchlorate (**56**)



In a 50 mL Schlenk tube **55** (400 mg, 0.861 mmol, page 161) was dissolved in melted methyl *p*-toluenesulfonate (10.0 g, 53.7 mmol) at 120 °C. The solution was stirred for 3 d before cooling and the lukewarm dark oily reaction mixture was poured into cyclohexane (250 mL). The oily phase separated which was washed with fresh cyclohexane (300 mL). The supernatant was decanted and the residue was dissolved in hot ethanol (100 mL, 60 °C). To induce the precipitation the product was converted to the bis perchlorated derivative by adding to this solution a saturated ethanolic sodium perchlorate solution (25 mL). The mixture was cooled to rt and **56** (0.45 g, 0.65 mmol, 75%) filtered and dried in a vacuum oven.

Decomposition onset: 304 °C. Spontaneous decomposition. Residue: 2%.

¹H-NMR (DMSO-*d*₆): 8.13 (C(7)H, 2H, d, ³J(7-6)=8.4Hz), 8.10 (C(4)H, 2H, s), 7.78 (C(6)H, 2H, d, ³J(6-7)=8.4Hz), 4.03 (C(1^{**})H₃, 6H, s), 2.82 (C(1')H₃, 6H, s), 1.59 (C(1'')H₃, 12H, s).

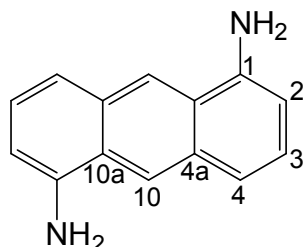
¹³C-NMR (DMSO-*d*₆): 197.89, 145.12, 143.39, 142.59, 131.31, 127.80, 125.44, 119.25, 116.17, 54.66, 35.18, 22.00, 14.57.

¹⁹F-NMR (DMSO-*d*₆): -143.5 (C(2^{*})F, 4F, s).

MS (ESI-QTOF⁺): 495 (7) [M+H-2·ClO₄⁻]⁺, 494 (41) [M-2·ClO₄⁻]⁺, 493 (100) [M-H-2·ClO₄⁻]⁺, 398 (3) [C₂₄H₂₀F₄N]⁺, 322 (14) [C₁₈H₁₆F₄N]⁺, 248 (47) [M+H-2·ClO₄⁻]⁺⁺, 247 (100) [M-2·ClO₄⁻]⁺⁺.

HR-MS (ESI-QTOF⁺): calculated for C₃₀H₂₉F₄N₂ [M-H-2·ClO₄⁻]⁺: 493.2261. Found:

493.2284.

Anthracene-1,5-diamine (59)

In a 250 mL beaker, copper(II) sulfate pentahydrate (4.00 g, 16.0 mmol) was dissolved in water (100 mL). Thereupon, zinc dust (200 g, 3.06 mol, ABCR) was added, the water was decanted and the zinc-copper-alloy was dispersed with water (2x200 mL). This activated zinc powder was then placed in a 3 L flask together with 1,5-diamino anthraquinone (60.0 g, 252 mmol, ABCR) and an aqueous sodium hydroxide solution (1.8 L, 4 N). While heating the reaction mixture to reflux for 48 h under a continuous argon stream, the red starting material turned into a highly yellow-greenish fluorescent product (Figure 4.10). Thereafter, the reaction mixture was cooled to rt, carefully filtered, washed with a sodium hydroxide solution (200 mL, 10 N) and the residue was immediately suspended in dimethyl sulfoxide (600 mL).

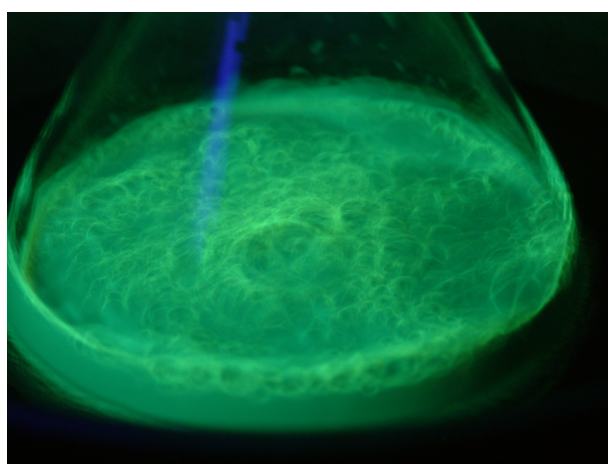


Figure 4.10: Picture of the reaction mixture lightened with an UV-lamp (356 nm).

To separate the product from the excess of zinc the suspension was filtered. Most of the side products present in this reaction stuck to the silica when TLC was performed. Therefore the dark brown dimethyl sulfoxide filtrate was filtered through a silica gel bed (12 cm). The filtrate was concentrated under vacuum (90 °C, 10 mbar) to 100 mL. This concentrate was added dropwise to water (2 L) while stirring. The precipitate was filtered and dried in a vacuum oven to yield **59** (45 g, 0.22 mol, 87%) as a yellow powder.

Caution: Firstly, during the reaction hydrogen gas is evolved! Risk of explosion if heated under confinement! The reaction mixture has to be flushed continuously with an argon stream.

Secondly, after the reaction, the zinc dust is highly reactive. Specially, the filtration residue after the first filtration with dimethyl sulfoxide is critical which must be immediately added to water to prevent auto-ignition.

Thirdly, due to the light sensitivity of the anthracene derivate the reaction was performed with dimmed light and the product was stored in darkness.

Decomposition onset: 325 °C. Residue: 16%.

¹H-NMR (DMSO-*d*₆): 8.54 (C(10)H, 2H, s), 7.25 (C(4)H, 2H, dd, ³J(4-3)=8.3Hz, ⁴J(4-2)=0.8Hz), 7.17 (C(3)H, 2H, dd, ³J(3-4)=8.3Hz, ³J(3-2)=7.1Hz), 6.60 (C(2)H, 2H, dd, ³J(2-3)=7.1Hz, ⁴J(2-4)=0.8Hz), 5.78 (C(1)NH₂, C(5)NH₂, 4H, br).

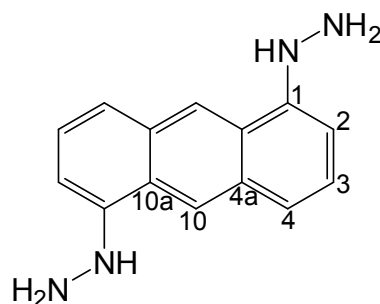
¹³C-NMR (DMSO-*d*₆): 144.39 C(1), 131.62 C(4a), 126.15 C(3), 123.25 C(10a), 120.81 C(10), 116.40 C(4), 105.61 C(2).

MS (ESI-QTOF+): 273 (8) [M+H+Zn]⁺, 209 (100) [M+H]⁺, 195 (4) [C₁₄H₁₃N]⁺.

HR-MS (ESI-QTOF+): calculated for C₁₄H₁₃N₂ [M+H]⁺: 209.1073. Found: 209.1073.

Elemental analysis: calculated for C₁₄H₁₂N₂: C, 80.74; H, 5.81; N, 13.45. Found: C, 79.25; H, 5.60; N, 12.93; rest is Zn salt.

1,5-Dihydrazinylanthracene (60)



In a beaker at rt, **59** (21.8 g, 105 mmol, page 163) was mixed with hydrochloric acid (800 mL, 32% w/w) and stirred for 1 h. The grey suspension was cooled in a 3 L glass reactor with jacked cooling to -15°C . Over a time period of 3 h a cold solution of sodium nitrite (16.0 g, 232 mmol) in water (70 mL) was dripped in. Afterwards, the brown-yellow solution was allowed to warm to -5°C while stirring for 2 h. To eliminate the excess of nitrite a cold solution of urea (45.0 g, 750 mmol) in water (100 mL) was added at once, causing a very vigorous gas evolving. The reaction mixture was stirred at -5°C for 2 h and subsequently cooled to -15°C . At this temperature, a cold solution of tin(II) chloride dihydrate (100 g, 441 mmol) in water (150 mL) was put in at once. The consequent exothermal reaction heated the reactor content up to -8°C . The brown suspension was stirred at -15°C overnight, then kept for 2 h at -5°C and finally allow to warm to $+1^{\circ}\text{C}$ within 2 h. Thereupon, the entire reactor content was centrifuged. The supernatant was decanted and the remnant was washed with hydrochloric acid (3x2.5 L, 16%) and centrifuged anew. The brown residue was then dissolved in water (6 L) and filtered before basified with aqueous sodium hydroxide solution (32%) to pH 12 - 13. The precipitate was centrifuged, washed with water (4x2 L) and finally dried in a vacuum oven to yield **60** (15 g, 59 mmol, 56%) as a brown powder.

Decomposition onset: 155°C . Residue: 52%.

$^1\text{H-NMR}$ (DMSO- d_6): 8.50 (C(10), 2H, s), 7.45 (C(1)NH, 2H, s) 7.3-7.2 (C(4)H, C(3)H, 4H, m), 6.85 (C(2)H, 2H, dd, $^3\text{J}(2-3)=6.3\text{Hz}$, $^3\text{J}(2-4)=2.0\text{Hz}$).

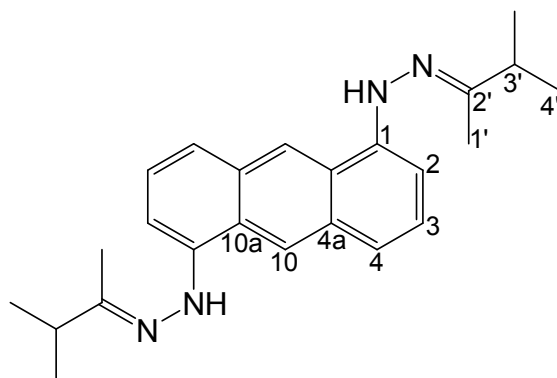
$^{13}\text{C-NMR}$ (DMSO- d_6): 146.85 C(1), 131.28 C(4a), 126.19 C(3), 122.11 C(10a), 119.86 C(10), 117.51 C(4), 101.89 C(2).

MS (ESI-QTOF+): 239 (11) $[\text{M}+\text{H}]^+$, 222 (100) $[\text{C}_{14}\text{H}_{12}\text{N}_3]^+$, 209 (17) $[\text{C}_{14}\text{H}_{13}\text{N}_2]^+$, 207

(7) $[C_{14}H_{11}N_2]^+$, 194 (50) $[C_{14}H_{12}N]^+$.

HR-MS (ESI-QTOF+): calculated for $C_{14}H_{15}N_4$ $[M+H]^+$: 239.1291. Found: 239.1304.

1,5-Bis(2-(3-methylbutan-2-ylidene)hydrazinyl)anthracene (61)

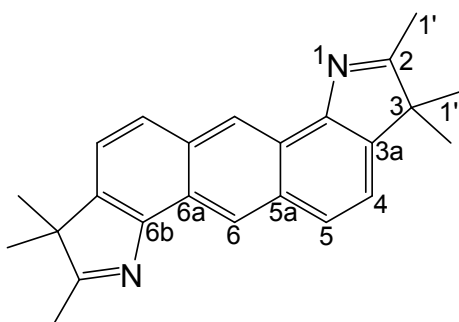


In the dark **60** (12.0 g, 50.4 mmol, page 165) was mixed with 3-methyl-2-butanone (1 L) and heated to 65 °C overnight. Afterwards, the excess of 3-methyl-2-butanone was evaporated under reduced pressure. The concentrate was dried in the vacuum oven overnight at rt. An aliquot was taken for analysis and the rest of the crude product was immediately used without further purification. According to NMR the residue was still wet, so no yield is stated at this point.

$^1\text{H-NMR}$ (DMSO- d_6): 8.73 (C(10)H, 2H, s), 8.66 (C(1)NH, 2H, s), 7.51 (C(4)H, 2H, dd, $^3J(4-3)=7.9\text{Hz}$, $^4J(4-2)=1.4\text{Hz}$), 7.35 (C(3)H, 2H, dd, $^3J(3-4)=7.9\text{Hz}$, $^3J(3-2)=7.4\text{Hz}$), 7.33 (C(2)H, 2H, dd, $^3J(2-3)=7.4\text{Hz}$, $^4J(2-4)=1.4\text{Hz}$), 2.61 (C(3')H, 2H, h, $^3J(3'-4')=6.9\text{Hz}$), 2.12 (C(1')H₃, 6H, s), 1.17 (C(4')H₃, 12H, d, $^3J(3'-4')=6.9\text{Hz}$).

$^{13}\text{C-NMR}$ (DMSO- d_6): 155.32 C(2''), 141.72 C(1), 131.45 C(4a), 126.09 C(3), 122.26 C(10a), 120.46 C(10), 119.17 C(4), 105.73 C(2), 36.89 C(3'), 20.45 C(4'), 14.12 C(1').

MS (ESI-QTOF+): 290 (76) $[C_{19}H_{20}N_3]^+$, 222 (100) $[C_{14}H_{12}N_3]^+$, 209 (7) $[C_{14}H_{13}N_2]^+$, 207 (26) $[C_{14}H_{11}N_2]^+$, 194 (19) $[C_{14}H_{12}N]^+$ (No M^+ detected. Cleavage of one hydrazone unit yields in the 290 m/z fragment).

2,3,3,8,9,9-Hexamethyl-3,9-dihydro-1,7-diazadicyclopenta[*a,h*]anthracene (62)

In the dark **61** (entire residue, page 166) was intermixed with glacial acetic acid (350 mL). The Fischer Indole Synthesis was performed at reflux temperature (118 °C) for 12 h before the acetic acid was distilled under reduced pressure. The residue was basified with ammonium hydroxide solution (100 mL) and filtered. The remnant was elutriated in boiling acetonitrile (300 mL) and filtered hot. The filtration residue was dried and yielded **62** (8.5 g, 25 mmol, 50% calculated from the used hydrazine **60**) as yellow-brown powder.

Decomposition onset: 282 °C. Residue: 42%.

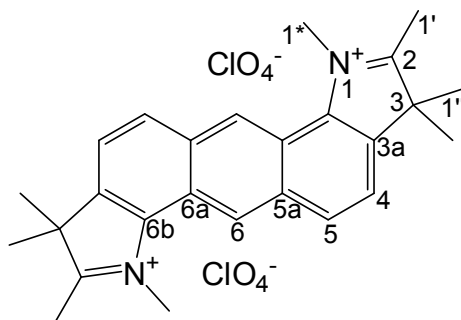
¹H-NMR (DMSO-*d*₆): 9.10 (C(6)H, 2H, s), 8.07 (C(4)H, 2H, d, ³J(4-3)=8.5Hz), 7.67 (C(3)H, 2H, d, ³J(3-4)=8.5Hz), 2.38 (C(1')H₃, 6H, s), 1.36 (C(1'')H₃, 12H, s).

¹³C-NMR (DMSO-*d*₆): 188.58 C(2), 148.07 C(6b), 140.90 C(5a), 131.76 C(3a), 125.75 C(4), 124.87 C(6), 121.59 C(5), 120.16 C(6a), 54.95 C(3), 21.88 C(1''), 15.38 C(1').

MS (ESI-QTOF+): 358 (39) [M+NH₄]⁺, 341 (100) [M+H]⁺.

HR-MS (ESI-QTOF+): calculated for C₂₄H₂₅N₂ [M+H]⁺: 341.2012. Found: 341.2011.

1,2,3,3,7,8,9,9-Octamethyl-3,9-dihydro-1,7-diazadicyclopenta[*a,h*]anthracene-dium bis(perchlorate) (63)



In the dark **62** (2.50 g, 7.34 mmol, page 167) was intermixed with methyl *p*-toluenesulfonate (20.0 g, 107 mmol) and heated to 120 °C for 48 h. The reaction mixture was then cooled to rt and poured in cyclohexane (300 mL). A black oil precipitated which was emulsified with cyclohexane (2x150 mL) under stirring vigorously. The supernatant was decanted. The dark brown residue was then dissolved in hot ethanol (200 mL) and a saturated solution of sodium perchlorate was added dropwise which resulted in the anion exchange to the better crystallisable bis(perchlorate). In order to isolate the crude product the gel like precipitation was centrifuged. The remnant was elutriated in boiling water (100 mL), filtered and washed with cold ethanol (2x15 mL) to yield **63** (3.1 g, 4.9 mmol, 67%) as a brown powder.

Decomposition onset: 297 °C. Residue: 0%.

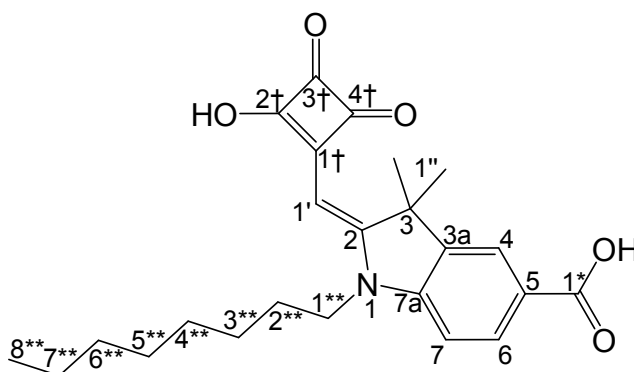
¹H-NMR (DMSO-*d*₆): 9.65 (C(6)H, 2H, s), 8.70 (C(5)H, 2H, d, ³J(5-4)=8.7Hz), 8.10 (C(4)H, 2H, d, ³J(4-5)=8.7Hz), 4.62 (C(1*)H₃, 6H, s), 2.91 (C(1')H₃, 6H, s), 1.64 (C(1'')H₃, 12H, s).

¹³C-NMR (DMSO-*d*₆): 196.18, 143.01, 135.86, 132.75, 132.42, 122.65, 120.34, 99.54, 54.26, 40.20, 20.82, 14.26.

MS (ESI-QTOF+): 369 (100) [M-HClO₄-ClO₄⁻]⁺, 355 (14) [C₂₅H₂₇N₂]⁺, 341 (3) [C₂₄H₂₅N₂]⁺, 186 (1) [M+H-2·ClO₄⁻]⁺⁺, 185 (4) [M-2·ClO₄⁻]⁺⁺.

HR-MS (ESI-QTOF+): calculated for C₂₆H₂₉N₂ [M-HClO₄-ClO₄⁻]⁺: 369.2325. Found: 369.2326.

2-((2-Hydroxy-3,4-dioxocyclobut-1-enyl)methylene)-3,3-dimethyl-1-octylindoline-5-carboxylic acid (**64**)



In a 500 mL three neck round bottom flask **66** (10.0 g, 22.8 mmol, page 171), chloroform (100 mL) and ethanol (100 mL) were mixed and heated to reflux before an aqueous sodium hydroxide solution (5 mL, 40% w/w) was added dropwise via syringe. Immediately, the colour changed from orange to dark brown and after 5 min the reaction mixture was concentrated *in vacuo*. The black oily residue was dissolved in chloroform (200 mL) and extracted with saturated aqueous citric acid (200 mL). The protonated product precipitated between the layers of the organic and the aqueous phase and was filtered. Owing to the good water solubility of the product the residue was not washed with pure water; hence, the dried product contained 33% citric acid. **64** (5.50 g, 8.7 mmol, 38%) was isolated as orange powder and was immediately used in the next reaction.

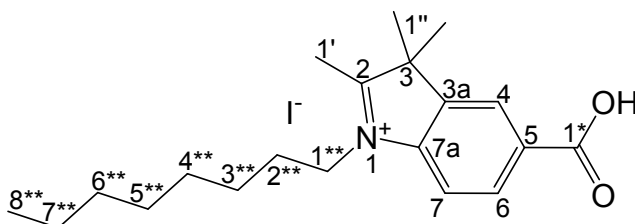
Decomposition onset: 142 °C. Residue: 24%.

¹H-NMR (DMSO-*d*₆): 7.86 (C(4)H+C(6)H, 2H, m), 7.10 (C(7)H, 1H, d, ³J(7-6)=8.8Hz), 5.59 (C(1')H, 1H, s), 3.84 (C(1**)H₂, 2H, t, ³J(1**-2**) = 6.0Hz), 2.76 (citric acid C(α)H_a, 2.1H, d, ²J(a-b)=15.4Hz), 2.65 (citric acid C(α)H_b, 2.1H, d, ²J(b-a)=15.4Hz), 1.61 (C(2**)H₂, 2H, m), 1.56 (C(1'')H₃, 6H, s), 1.4-1.1 (C(3**)H₂, C(4**)H₂, C(5**)H₂, C(6**)H₂, C(7**)H₂, 10H, br), 0.80 (C(8**)H₃, 3H, t, ³J(8**-7**) = 6.2Hz).

MS (ESI-QTOF+): 412 (100) [M+H]⁺, 358 (82), 279 (72), 208 (39), 194 (65), 159 (83).

HR-MS (ESI-QTOF+): calculated for C₂₄H₃₀NO₅ [M+H]⁺: 412.2118. Found: 412.2111.

5-Carboxy-2,3,3-trimethyl-1-octyl-3*H*-indolium iodide (65)



2,3,3-Trimethyl-3*H*-indole-5-carboxylic acid (29.8 g, 147 mmol, Intatrade) were mixed with butanol (100 mL) and 1-iodooctane (67.2 g, 280 mmol) in a 500 mL round bottom flask. The reactor content was heated to reflux for 1 d before cooling to rt. In order to precipitate the product, the reaction mixture was subsequently dropped into diethyl ether (700 mL) while stirring. Compound **65** (43 g, 92 mmol, 69%) was harvested by filtration as a light brown coloured powder.

Decomposition onset: 201 °C. Residue: 6%.

¹H-NMR (DMSO-*d*₆): 8.39 (C(4)H, 1H, s), 8.17 (C(7)H, 1H, d, ³J(7-6)=8.0Hz), 8.10 (C(6)H, 1H, d, ³J(6-7)=8.0Hz), 4.48 (C(1**)H₂, 2H, q, ³J(1**-2**) = 6.8Hz), 2.90 (C(1')H₃, 3H, s), 1.83 (C(2**)H₂, 2H, m), 1.58 (C(1'')H₃, 6H, s), 1.5-1.2 (C(3**)H₂, C(4**)H₂, C(5**)H₂, C(6**)H₂, C(7**)H₂, 10H, m), 0.84 (C(8**)H₃, 3H, t, ³J(8**-7**) = 6.0Hz).

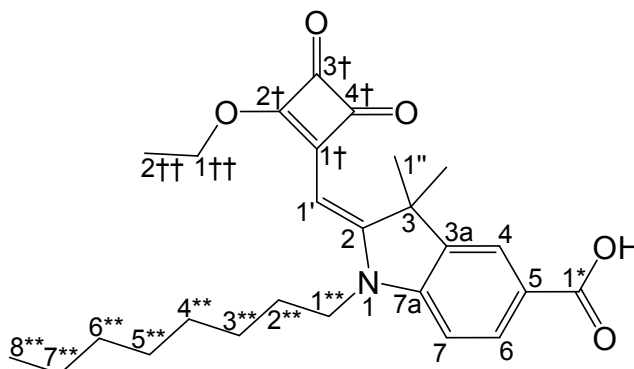
¹³C-NMR (DMSO-*d*₆): 199.43, 166.42, 144.23, 142.26, 131.68, 130.44, 124.42, 115.75, 54.49, 47.97, 31.15, 28.58, 28.47, 27.18, 25.90, 22.02, 21.84, 14.56, 13.94.

MS (ESI-QTOF+): 442 (2) [M-H]⁺, 338 (18) [M-H-I+Na]⁺, 316 (100) [M-I]⁺.

HR-MS (ESI-QTOF+): calculated for C₂₀H₃₀NO₂ [M-I]⁺: 316.2271. Found: 316.2271.

Elemental analysis: calculated for C₂₀H₃₀NO₂I: C, 54.18; H, 6.82; N, 3.16. Found: C, 53.09; H, 6.68; N, 3.17.

2-((2-Ethoxy-3,4-dioxocyclobut-1-enyl)methylene)-3,3-dimethyl-1-octylindoline-5-carboxylic acid (**66**)



65 (15.0 g, 33.8 mmol, page 170) and **30** (7.20 g, 42.3 mmol, page 130) were suspended in ethanol (40 mL) and heated to reflux for 15 min. After cooling to 55°C, triethylamine (11.7 mL, 84.6 mmol) was added. While boiling the solution for 15 h the colour changed from light yellow to brown and finally to dark green. The solvent was distilled under reduced pressure and the residue was dried in high vacuum overnight. For purification the crude product was dissolved in chloroform (200 mL), extracted with saturated citric acid (2x150 mL), washed with water (3x200 mL) and brine (150 mL). The solvent of the combined and dried organic layer was removed under vacuum. The crude product was recrystallized with a chloroform:toluene (50:200 mL) mixture to yield **66** (11 g, 25 mmol, 74%) as an bright orange solid.

Decomposition onset: 210°C. Residue: 31%. According to DSC **66** melts (186 – 192°C) just before decomposition.

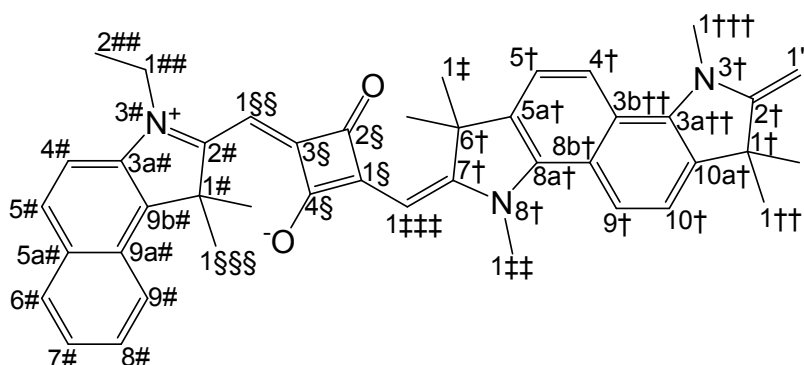
¹H-NMR: 8.09 (C(6)H, dd, ³J(6-7)=8.3Hz, ⁴J(6-4)=2.3Hz), 7.97 (C(4)H, d, ⁴J(4-6)=2.3Hz), 6.89 (C(7)H, d, ³J(7-6)=8.3Hz), 5.49 (C(1')H, s), 4.91 (C(1††)H₂, q, ³J(1††-2††)=7.2Hz), 3.83 (C(1**)H₂, t, ³J(1**-2**) =7.6Hz), 1.75 (C(2**)H₂, m), 1.65 (C(1'')H₃+C(12)H₃, s), 1.55 (C(2††)H₃, t, ³J(1**-2**) =7.2Hz), 1.5-1.2 (C(3**)H₂, C(4**)H₂, C(5**)H₂, C(6**)H₂, C(7**)H₂, m), 0.88 (C(8**)H₃, t, ³J(8**-7**) =6.8Hz).

¹³C-NMR: 192.1, 188.76, 188.47, 173.68, 171.23, 167.39, 147.52, 140.87, 131.47, 123.85, 122.93, 107.72, 83.27, 70.25, 47.30, 43.16, 31.71, 29.20, 29.09, 27.03, 26.96, 26.33, 22.57, 15.90, 14.06.

MS: 462 (31) $[M+Na]^+$, 440 (100) $[M+H]^+$, 422 (39) $[M+H-H_2O]^+$, 355 (16) $[C_{22}H_{29}NO_3]^+$, 256 (12) $[C_{18}H_{26}N]^+$.

HR-MS: calculated for $C_{26}H_{33}NO_5$ $[M+H]^+$: 440.2432. Found: 440.2427.

4-((3-Ethyl-1,1-dimethyl-1*H*-benzo[*e*]indolium-2-yl)methylene)-2-((1,1,3,6,6,8-hexamethyl-7-methylene-7,8-dihydroindolo[7,6-*g*]indol-2(1*H*,3*H*,6*H*)-ylidene)methyl)-3-oxocyclobut-1-enolate (68)



To generate the activated intermediate of **57** (3.40 g, 6.55 mmol, Thomas Geiger [23]), it was deprotonated in an emulsion of toluene (35 mL) and aqueous sodium hydroxide solution (10 mL, 40% w/w) at ambient temperature for 30 min under vigorously stirring. The organic layer containing the bis enamine **67** (figure 2.16 on page 37) was separated, dried with sodium sulfate and placed in a Dean-Stark apparatus. In this reactor **42** (2.20 g, 6.40 mmol, page 145), 1-butanol (70 mL) and quinoline (20 mL) were added and the mixture was heated to reflux overnight. The entire reactor content was poured on ice (1 L). The precipitation was filtered and the residue was purified by column chromatography (A: ethylacetate:triethylamine = 95:5; B: chloroform:triethylamine = 95:5; A:B = 100:0→25:75) to yield in **68** (1.9 g, 2.2 mmol, 35%). According to NMR the product contained about 15% of the eluent additive 1,1,1,3,3,3-hexafluoroisopropanol because of incorporation into the crystal structure.

Decomposition onset: 187°C. Residue: 28%. Release of incorporated solvent above 120°C.

¹H-NMR (DMSO-*d*₆): 8.24 (1H, d, ³J=8.8Hz), 8.17 (1H, d, ³J=8.8Hz), 8.03 (1H, d,

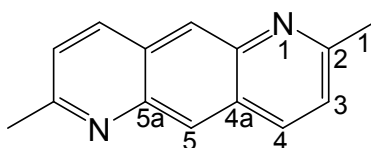
$^3J=8.8\text{Hz}$), 8.02 (1H, d, $^3J=8.0\text{Hz}$), 7.93 (1H, d, $^3J=8.8\text{Hz}$), 7.71 (1H, d, $^3J=8.8\text{Hz}$), 7.62 (1H, m), 7.56 (1H, d, $^3J=8.4\text{Hz}$), 7.46 (1H, t, $^3J=7.2\text{Hz}$), 7.45 (1H, d, $^3J=8.4\text{Hz}$), 5.88 (2H, br), 5.16 (1,1,1,3,3,3-hexafluoroisopropanol, C(2)H, 0.7H, hep, $^3J(\text{H-F})=6.8\text{Hz}$), 4.27 (2H, q, $^3J=7.2\text{Hz}$), 4.14 (1H, d, $^3J=2.0\text{Hz}$), 4.10 (1H, d, $^3J=2.0\text{Hz}$), 4.07 (3H, s), 1.96 (6H, s), 1.72 (6H, s), 1.35 (9H, m).

$^{13}\text{C-NMR}$ (DMSO- d_6): 180.90, 177.49, 170.17, 164.15, 142.33, 139.26, 133.34, 132.02, 130.92, 129.83, 129.74, 127.96, 127.45, 124.24, 122.28, 122.22, 120.80, 120.47, 119.39, 118.03, 113.26, 111.16, 104.57, 104.53, 87.17, 85.77, 77.21, 67.27, 66.90, 50.65, 48.35, 45.70, 43.58, 38.25, 35.71, 30.04, 26.53, 26.09, 12.12, 11.75.

MS: 634 (97) $[\text{M}+\text{H}]^+$, 633 (100) $[\text{M}]^+$, 619 (11) $[\text{C}_{42}\text{H}_{41}\text{N}_3\text{O}_2]^+$, 411 (6) $[\text{C}_{27}\text{H}_{26}\text{N}_2\text{O}_2]^+$, 317 (5) $[\text{M}+\text{H}]^{++}$.

HR-MS: calculated for $\text{C}_{43}\text{H}_{43}\text{N}_3\text{O}_2$ $[\text{M}]^+$: 633.3350. Found: 633.3351.

2,7-Dimethylpyrido[2,3-*g*]quinoline (69)



69 was prepared by the Doebner-Miller reaction, a Skraup Quinoline Synthesis variation, from 1,4-benzene-diamine (5.00 g, 46.2 mmol) which was dissolved in hydrochloric acid (450 mL, 6 N). The solution was heated to reflux where over a time period of 30 min cold crotonaldehyde (7.78 g, 111 mol) was added dropwise. In addition, the reaction mixture was refluxed for 4 h before the dark brown reaction mixture was allowed to cool to rt and it was filtered. To initiate the precipitation of the product the dark filtrate was basified with aqueous sodium hydroxide solution (350 mL, 32% w/w) and cooled to 4 °C overnight. Next morning the violet needles were filtered and yielded **69** (1.6 g, 7.6 mmol, 15%) after drying.

Decomposition onset: 263 °C. Residue: 9%.

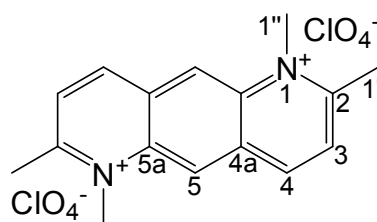
$^1\text{H-NMR}$ (DMSO- d_6): 9.09 (C(4)H, 2H, d, $^3J(4-3)=8.4\text{Hz}$), 8.06 (C(5)H, 2H, s), 7.61 (C(3)H, 2H, d, $^3J(3-4)=8.4\text{Hz}$), 2.70 (C(1')H₃, 6H, s).

$^{13}\text{C-NMR}$ (DMSO- d_6): 158.70 C(2), 146.19 C(5a), 131.60 C(4), 131.13 C(3), 122.51 C(5), 122.47 C(5a), 24.51 C(1').

MS (ESI-QTOF+): 209 (37) $[\text{M}+\text{H}]^+$, 172 (100), 159 (12), 122 (24).

HR-MS (ESI-QTOF+): calculated for $\text{C}_{14}\text{H}_{13}\text{N}_2$ $[\text{M}+\text{H}]^+$: 209.1073. Found: 209.1077.

1,2,6,7-Tetramethylpyrido[2,3-*g*]quinoline-1,6-dium bis(perchlorate) (**70**)



69 (250 mg, 1.20 mmol, page 173) and methyl *p*-toluenesulfonate (4.47 g, 24.0 mmol) were intermixed and heated to 130°C. The reaction was monitored by NMR. The first nitrogen atom was alkylated within hours but to methylate the second one took days. After heating for 60 h a ratio between **70** and mono alkylated intermediate of 9:1 was reached. At this point the reaction was terminated by cooling to room temperature and pouring the reactor content into cyclohexane (200 mL). The black oil was suspended in fresh cyclohexane (200 mL) and the supernatant was decanted. The remnant was dissolved in ethanol (100 mL) and heated in a beaker to 60°C before a saturated ethanolic sodium perchlorate solution (50 mL) was added. The product precipitated and after cooling to rt **70** (0.30 g, 0.69 mmol, 58%) was obtained by filtration and drying as a grey powder.

Decomposition onset: 329°C. Residue: 13%.

$^1\text{H-NMR}$ (DMSO- d_6): 10.07 (C(4)H, 2H, d, $^3\text{J}(4-3)=8.4\text{Hz}$), 9.19 (C(5)H, 2H, s), 8.57 (C(3)H, 2H, d, $^3\text{J}(3-4)=8.4\text{Hz}$), 4.63 (C(1'') H_3 , 6H, s), 3.19 (C(1') H_3 , 6H, s).

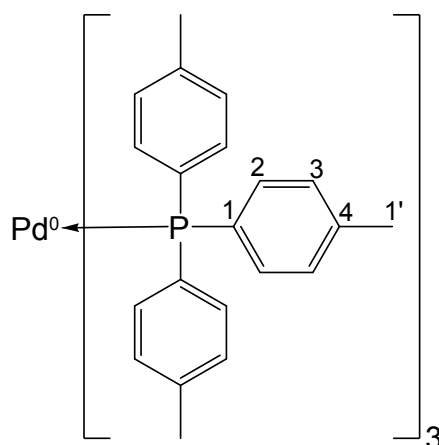
$^{13}\text{C-NMR}$ (DMSO- d_6): 162.32 C(2), 140.81 C(5a), 138.82 C(4), 128.08 C(5), 125.75 C(4a), 124.77 C(3), 40.97 C(1''), 23.04 C(1').

MS (ESI-QTOF+): 237 (25) $[\text{M}-\text{ClO}_4-\text{HClO}_4]^+$, 223 (100) $[\text{M}-\text{ClO}_4-\text{HClO}_4-\text{CH}_3]^+$, 119

(38) $[M-2\cdot ClO_4]^{++}$.

HR-MS (ESI-QTOF+): calculated for $C_{16}H_{18}N_2$ $[M-2\cdot ClO_4]^{++}$: 119.0730. Found: 119.0729.

Tris-(tri(*p*-tolyl)-phosphine)-palladium(0) (**71**)



Palladium(II) chloride (0.234 g, 1.32 mmol, Alfa Aesar), tri(*p*-tolyl)phosphine (2.00 g, 6.57 mmol) and dimethyl sulfoxide (12 mL) were placed in a Schlenk tube. The reaction mixture and all other solvents were degassed by freeze-pump-thaw cycles before used. The reaction mixture was then heated to reflux (135 °C). The initial colourless suspension turned to a light brick stone solution. It was then allowed to cool to 120 °C before hydrazine hydrate (0.28 mL, 5.75 mmol) was added via syringe. Immediately, the colour changed to light yellow and the product started to crystallize. After cooling to rt, the reaction mixture was filtered under argon atmosphere. The residue was washed with absolute ethanol (8 mL) followed by absolute methanol (25 mL) under argon. The ensuing residue was dried in high vacuum (10^{-3} mbar) for 1 h to yield **71** (1.0 g, 1.0 mmol, 76%).

Decomposition onset: 175 °C. Residue: 20%.

1H -NMR (C_6D_6): 7.56 (C(2)H, 18H, dd, $^3J(2-3)=7.8$ Hz, $^3J(C(2)H-P)=8.5$ Hz), 6.83 (C(3)H, 18H, dd, $^3J(3-2)=7.8$ Hz), 2.03 (C(1')H₃, 27H, s).

^{13}C -NMR (C_6D_6): 137.84 (C(4), s), 137.12 (C(1), d, $^1J(C(1)-P)=14.5$ Hz), 134.46 (C(2),

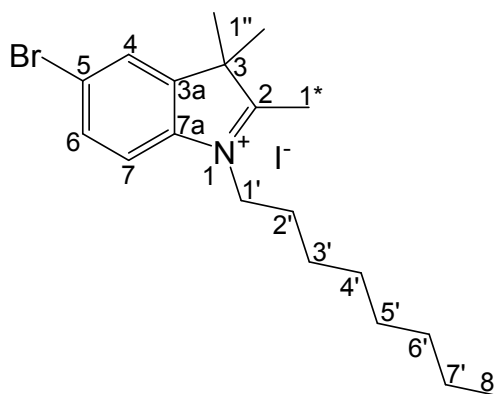
d, $^2J(\text{C}(2)\text{-P})=17.6\text{Hz}$, 129.03 (C(3), d, $^3J(\text{C}(3)\text{-P})=12.1\text{Hz}$), 21.20 (C(1'), s).

$^{31}\text{P-NMR}$ (C_6D_6): 19-15 (P, br).

MS (ESI-QTOF+): 1017 (2) $[\text{M-H}]^+$, 983 (11) $[\text{C}_{63}\text{H}_{65}\text{NaO}_3\text{P}_3]^+$, 759 (92) $[\text{Pd}(\text{H})(\text{P}(\text{p-tol})_2(\text{CO}_2))]^+$, 715 (80) $[\text{Pd}(\text{H})(\text{P}(\text{p-tol})_2)]^+$, 663 (59) $[\text{C}_{42}\text{H}_{42}\text{NaO}_2\text{P}_2]^+$, 395 (81) $[\text{P}(\text{p-tol})_4]^+$, 343 (100) $[\text{C}_{21}\text{H}_{21}\text{NaOP}]^+$, 321 (100) $[\text{C}_{21}\text{H}_{22}\text{OP}]^+$, 305 (74) $[\text{C}_{21}\text{H}_{22}\text{P}]^+$.

HR-MS (ESI-QTOF+): calculated for $\text{C}_{63}\text{H}_{62}\text{P}_3\text{Pd}$ $[\text{M-H}]^+$: 1017.3094. Found: 1017.3080.

5-Bromo-2,3,3-trimethyl-1-octyl-3*H*-indolium iodide (**72**)



Indole **32** (10.0 g, 42.0 mmol, page 132), 1-iodooctane (20.2 g, 84.0 mmol, ABCR) and 1-butanol (10 mL) were placed in a 50 mL Schlenk tube. The suspension was heated to 120 °C and stirred overnight. After cooling to rt the reaction mixture was poured into diethyl ether (600 mL) and stirred for 30 min. Subsequently, the brown precipitate was filtered. The ensuing residue was recrystallized from boiling chloroform (150 mL). The crystalline product was harvested by filtration. The evaporated remnant of the mother liquid was recrystallized accordingly to yield in total **72** (12 g, 21 mmol, 50%) as light brown crystalline powder.

Melting point: 160 – 167 °C.

Decomposition onset: 200 °C. Residue: 14%.

$^1\text{H-NMR}$: 8.19 (C(4)H, 1H, d, $^4J(4\text{-}6)=1.5\text{Hz}$), 7.97 (C(7)H, 1H, d, $^3J(7\text{-}6)=8.8\text{Hz}$), 7.83 (C(6)H, 1H, dd, $^3J(6\text{-}7)=8.8\text{Hz}$, $^4J(6\text{-}4)=1.5\text{Hz}$), 4.44 (C(1')H₂, 2H, t, $^3J(1'\text{-}2')=7.8\text{Hz}$),

2.85 (C(1^{*})H₃, 3H, s), 1.86-1.75 (C(2')H₂, 2H, m), 1.55 (C(1'')H₃, 6H, s), 1.46-1.18 (C(3')H₂, C(4')H₂, C(5')H₂, C(6')H₂, C(7')H₂, 10H, m), 0.84 (C(8')H₃, t, ³J(8'-7')=6.8Hz).

¹³C-NMR: 196.87, 144.12, 140.35, 131.80, 126.88, 122.76, 117.46, 54.39, 47.85, 31.11, 28.53, 28.41, 27.14, 25.82, 21.98, 21.79, 14.31, 13.90.

MS (ESI-QTOF+): 476 (1) [M-H]⁺, 350 (100) [M-I]⁺.

HR-MS (ESI-QTOF+): calculated for C₁₉H₂₉N⁷⁹Br [M-I]⁺: 350.1478. Found: 350.1481.

Elemental analysis: calculated for C₁₉H₂₉NBrI: C, 47.72; H, 6.11; N, 2.93; Br, 16.71; I, 26.54. Found: C, 47.16; H, 6.10; N, 2.91; Br, 16.69; I, 26.45.

References

- [1] P. A. Tipler. *Physik*. Spectrum Akademischer Verlag, Heidelberg, 2nd edition, 1998.
- [2] Heinrich Zollinger. *Color Chemistry: Syntheses, Properties, and Applications of Organic Dyes and Pigments*. Helvetica Chimica Acta, 3rd, revised edition, 2003.
- [3] Wikipedia. Dye. <http://en.wikipedia.org/wiki/Dye>, March 2010.
- [4] F. Merkt. Spectroscopy script for PC V. ETHZ at D-CHAB, SS 2005.
- [5] G. Herzberg. *Molecular Spectra and Molecular Structure*, volume I of *Spectra of Diatomic Molecules*. Krieger Publishing Company, Malabar, 1989.
- [6] G. Herzberg. *Molecular Spectra and Molecular Structure*, volume II of *Infrared and Raman Spectra of Polyatomic Molecules*. Krieger Publishing Company, Malabar, 1991.
- [7] G. Herzberg. *Molecular Spectra and Molecular Structure*, volume III of *Electronic Spectra and Electronic Structure of Polyatomic Molecules*. Krieger Publishing Company, Malabar, 1991.
- [8] T. Laurent. Aufbau einer Anlage zur Messung transients optischer Absorption und Test anhand einer Photodissoziationsreaktion. Master's thesis, Institut für Physikalische und Theoretische Chemie der Humboldt-Universität zu Berlin, 1998.
- [9] F. A. Khan and J. E. Hansen. The dirac (bracket) notation in the undergraduate physical chemistry curriculum: a pictorial introduction. *Chemical Educator*, 5:113–119, 2000.
- [10] F. P. Schäfer, H. Gerischer, F. Willig, H. Meier, H. Jahnke, M. Schönborn, and G. Zimmermann. *Physical and Chemical Applications of Dyestuffs*, volume 61 of *Topics in current chemistry*. Springer Berlin / Heidelberg, 1976.
- [11] N. Tyutyulkov, J. Fabian, A. Mehlhorn, F. Dietz, and Tadjer A. *Polymethine Dyes Structure and Properties*. St. Kliment Ohridski University Press, Sofia, 1991.

- [12] H. Meier. Conjugated oligomers with terminal donor-acceptor substitution. *Angewandte Chemie-International Edition*, 44(17):2482–2506, 2005.
- [13] In the review of meier [12] numbered compounds **5d** and **38b** were the same, except of an different alkyl chain outside the chromophore synthon. But λ_{max} of **5d** was 462 nm (CHCl₃) and the one of **38b** was 430 nm (CHCl₃). UV/vis spectra of **38b** were reported in the review's [12] cited primary literature [82, 83], which in my opinion looked like spectra of aggregates and not of nicely solvated single molecules. Aggregate formation is a known misleading fact which led to the misinterpretation in the review.
- [14] G. M. Shalhoub. Visible spectra of conjugated dyes: integrating quantum chemical concepts with experimental data. *Journal of Chemical Education*, 74(11):1317–1319, 1997.
- [15] H. Meier, U. Stalmach, and H. Kolshorn. Effective conjugation length and UV/vis spectra of oligomers. *Acta Polymerica*, 48(9):379–384, 1997.
- [16] P. Nayler and M. C. Whiting. Researches on polyenes. Part III: the synthesis and light absorption of dimethylpolyenes. *Journal of the Chemical Society*, pages 3037–3047, 1955.
- [17] R. E. Martin, U. Gubler, J. Cornil, M. Balakina, C. Boudon, C. Bosshard, J. P. Gisselbrecht, F. Diederich, P. Gunter, M. Gross, and J. L. Bredas. Monodisperse poly(triacetylene) oligomers extending from monomer to hexadecamer: joint experimental and theoretical investigation of physical properties. *Chemistry – A European Journal*, 6(19):3622–3635, 2000.
- [18] S. S. Malhotra and M. C. Whiting. Researches on polyenes. Part VII: the preparation and electronic absorption spectra of homologous series of simple cyanines, merocyanines, and oxonols. *Journal of the Chemical Society*, pages 3812–3822, 1960.
- [19] A.I. Kiprianov. Absorption spectra of organic dyes containing two chromophores. *Russian Chemical Reviews*, 40(7):594–607, 1971.
- [20] M. Pailer and E. Renner-Kuhn. Untersuchungen über polykondensierte Trimethinfarbstoffe. *Monatsheft für Chemie*, 85:601–606, 1954.
- [21] G. Kossmehl and P. Bocioneck. Syntheses and characterization of polymeric cyanine dyes. *Makromolekulare Chemie – Macromolecular Chemistry and Physics*, 182(12):3427–3444, 1981.
- [22] G. Kossmehl and P. Bocioneck. Darkconductivity and photoconductivity of polymeric cyanine dyes. *Makromolekulare Chemie – Macromolecular Chemistry and Physics*, 182(12):3445–3456, 1981.

- [23] T. Geiger, H. Benmansour, B. Fan, R. Hany, and F. A. Nüesch. Low-band gap polymeric cyanine dyes absorbing in the NIR region. *Macromolecular Rapid Communications*, 29(8):651–658, 2008.
- [24] C. A. T. Laia and S. M. B. Costa. Probing the interface polarity of AOT reversed micelles using centro-symmetrical squaraine molecules. *Physical Chemistry Chemical Physics*, 1(18):4409–4416, 1999.
- [25] J. Xu, H. Zhang, L. Wang, G. J. Liang, L. X. Wang, X. L. Shen, and W. L. Xu. DFT and TD-DFT studies on symmetrical squaraine dyes for nanocrystalline solar cells. *Monatshefte für Chemie*, 141(5):549–555, 2010.
- [26] G. J. Ashwell, G. Jefferies, D. G. Hamilton, D. E. Lynch, M. P. S. Roberts, G. S. Bahra, and C. R. Brown. Strong 2nd-harmonic generation from centrosymmetric dyes. *Nature*, 375(6530):385–388, 1995.
- [27] L. Beverina, M. Crippa, P. Salice, R. Ruffo, C. Ferrante, I. Fortunati, R. Signorini, C. M. Mari, R. Bozio, A. Facchetti, and G. A. Pagani. Indolic squaraines as two-photon absorbing dyes in the visible region: X-ray structure, electrochemical, and nonlinear optical characterization. *Chemistry of Materials*, 20(10):3242–3244, 2008.
- [28] S. Webster, S. A. Odom, L. A. Padilha, O. V. Przhonska, D. Peceli, H. H. Hu, G. Nootz, A. D. Kachkovski, J. Matichak, S. Barlow, H. L. Anderson, S. R. Marder, D. J. Hagan, and E. W. Van Stryland. Linear and nonlinear spectroscopy of a porphyrin-squaraine-porphyrin conjugated system. *Journal of Physical Chemistry B*, 113(45):14854–14867, 2009.
- [29] G. J. Ashwell, A. N. Dyer, and A. Green. Diminished second-harmonic generation from oligomeric squaraine derivatives of N-octadecylpyrrole relative to the intensity from films of the centric anilinosquaraines. *Langmuir*, 15(10):3627–3631, 1999.
- [30] A. Mishra, M. K. R. Fischer, and P. Bäuerle. Metal-free organic dyes for dye-sensitized solar cells: from structure: property relationships to design rules. *Angewandte Chemie-International Edition*, 48(14):2474–2499, 2009.
- [31] J. H. Yum, P. Walter, S. Huber, D. Rentsch, T. Geiger, F. A. Nüesch, F. De Angelis, M. Grätzel, and M. K. Nazeeruddin. Efficient far red sensitization of nanocrystalline TiO₂ films by an unsymmetrical squaraine dye. *Journal of the American Chemical Society*, 129(34):10320–10321, 2007.
- [32] T. Geiger, S. Kuster, J. H. Yum, S. J. Moon, M. K. Nazeeruddin, M. Grätzel, and F. A. Nüesch. Molecular design of unsymmetrical squaraine dyes for high efficiency conversion of low energy photons into electrons using TiO₂ nanocrystalline films. *Advanced Functional Materials*, 19(17):2720–2727, 2009.

- [33] S. Kuster, F. Sauvage, Md. K. Nazeeruddin, M. Grätzel, F. A. Nüesch, and T. Geiger. Unsymmetrical squaraine dimer with an extended π -electron framework: an approach in harvesting near infra-red photons for energy conversion. *Dyes and Pigments*, 87:30–38, 2010.
- [34] E. E. Havinga, W. Tenhoeve, and H. Wynberg. A new class of small band-gap organic polymer conductors. *Polymer Bulletin*, 29(1-2):119–126, 1992.
- [35] E. E. Havinga, W. Tenhoeve, and H. Wynberg. Alternate donor-acceptor small-band-gap semiconducting polymers - polysquaraines and polycroconaines. *Synthetic Metals*, 55(1):299–306, 1993.
- [36] E. E. Havinga, A. Pomp, W. Tenhoeve, and H. Wynberg. Water-soluble polysquaraines and polycroconaines. *Synthetic Metals*, 69(1-3):581–582, 1995.
- [37] G. Brocks and A. Tol. Small band gap semiconducting polymers made from dye molecules: polysquaraines. *Journal of Physical Chemistry*, 100(5):1838–1846, 1996.
- [38] J. Eldo and A. Ajayaghosh. New low band gap polymers: control of optical and electronic properties in near infrared absorbing π -conjugated polysquaraines. *Chemistry of Materials*, 14(1):410–418, 2002.
- [39] A. Ajayaghosh. Donor-acceptor type low band gap polymers: polysquaraines and related systems. *Chemical Society Reviews*, 32(4):181–191, 2003.
- [40] D. G. Devi, T. R. Cibir, D. Ramaiah, and A. Abraham. Bis(3,5-diiodo-2,4,6-trihydroxyphenyl)squaraine: a novel candidate in photodynamic therapy for skin cancer models in vivo. *Journal of Photochemistry and Photobiology B: Biology*, 92(3):153–159, 2008.
- [41] IPAZIA the Empa Linux Computing Cluster. <http://www.empa.ch/plugin/template/empa/1139>. March 2010.
- [42] A. C. Pardal, S. S. Ramos, P. F. Santos, L. V. Reis, and P. Almeida. Synthesis and spectroscopic characterisation of N-alkyl quaternary ammonium salts typical precursors of cyanines. *Molecules*, 7(3):320–330, 2002.
- [43] S. H. Kim and S. H. Hwang. Synthesis and photostability of functional squarylium dyes. *Dyes and Pigments*, 35(2):111–121, 1997.
- [44] M. F. Moreau, F. Laparlus, and G. Meyniel. Synthesis of indomonocarbocyanines producing selective biliar elimination - experimental study on animals. *European Journal of Medicinal Chemistry*, 9(3):274–280, 1974.
- [45] A. Treibs and K. Jacob. Cyclobutenderivate der Pyrrolreihe. II: Über Vierring-trimethin-Farbstoffe. *Justus Liebig's Annalen der Chemie*, 712:123–137, 1968.

- [46] Z. Y. Li, S. Xu, L. Huang, X. Huang, L. H. Niu, Z. H. Chen, Z. Zhang, F. S. Zhang, and K. Kasatani. Large third-order optical nonlinearities of centrosymmetric squaraines with heterocyclic donor groups measured by femtosecond degenerate four-wave mixing technique. *Chemical Physics Letters*, 441(1-3):123–126, 2007.
- [47] E. Terpetschnig, H. Szmecinski, and J. R. Lakowicz. Synthesis, spectral properties and photostabilities of symmetrical and unsymmetrical squaraines - a new class of fluorophores with long-wavelength excitation and emission. *Analytica Chimica Acta*, 282(3):633–641, 1993.
- [48] E. Terpetschnig and J. R. Lakowicz. Synthesis and characterization of unsymmetrical squaraines - a new class of cyanine dyes. *Dyes and Pigments*, 21(3):227–234, 1993.
- [49] H. Liu, C. S. Tomooka, and H. W. Moore. An efficient general synthesis of squarate esters. *Synthetic Communications*, 27(12):2177–2180, 1997.
- [50] M. V. Reddington. Synthesis and properties of phosphonic acid containing cyanine and squaraine dyes for use as fluorescent labels. *Bioconjugate Chemistry*, 18(6):2178–2190, 2007.
- [51] T. Ishiyama, M. Murata, and N. Miyaura. Palladium(0)-catalyzed cross-coupling reaction of alkoxydiboron with haloarenes - a direct procedure for arylboronic esters. *Journal of Organic Chemistry*, 60(23):7508–7510, 1995.
- [52] G. Sauter, H. J. Braun, and N. Reichlin. Preparation of 5-aryl-1,3,3-trimethyl-2-methylen-indoles and their iminium salts for the temporary dyeing of hair fibers (DE 10119204 A1 20021024). 2002.
- [53] However knowing that patent prescriptions were mostly problematic, Guido Sauter himself drew my attention on some of his prescriptions in the patent [52] and they worked.
- [54] P. H. Aubert, M. Knipper, L. Groenendaal, L. Lutsen, J. Manca, and D. Vanderzande. Copolymers of 3,4-ethylenedioxythiophene and of pyridine alternated with fluorene or phenylene units: synthesis, optical properties, and devices. *Macromolecules*, 37(11):4087–4098, 2004.
- [55] J. J. Li. *Name Reactions*. Springer Berlin / Heidelberg, 2002.
- [56] E. L. Martin. A modification of the clemmensen method of reduction. *Journal of the American Chemical Society*, 58:1438–1442, 1936.
- [57] R. M. Kandre, F. Kutzner, H. Schlaad, and A. D. Schlüter. Synthesis of high molecular weight amphiphilic polyphenylenes by suzuki polycondensation. *Macromolecular Chemistry and Physics*, 206(16):1610–1618, 2005.

- [58] Murage et al. [84] and Eddy et al. [85] reported a chloroform tolerant catalyst which was not considered for these reactions.
- [59] G. Sandford, A. Tadeusiak, D. S. Yufit, and J. A. K. Howard. Functional tetrahydroquinoxalines from perfluoroaromatic precursors. *Journal of Fluorine Chemistry*, 128(10):1216–1220, 2007.
- [60] S. F. Völker, S. Uemura, M. Limpinsel, M. Mingebach, C. Deibel, V. Dyakonov, and C. Lambert. Polymeric squaraine dyes as electron donors in bulk heterojunction solar cells. *Condensed Matter - Materials Science*, pages 1–10, 2010.
- [61] Origin. OriginLab Corporation, Northampton, MA 01060 USA, Version 7.0383. <http://www.OriginLab.com>.
- [62] A. S. Tatikolov and S. M. B. Costa. Photophysical and aggregation properties of a long-chain squarylium indocyanine dye. *Journal of Photochemistry and Photobiology A: Chemistry*, 140(2):147–156, 2001.
- [63] J. Fu, O. V. Przhonska, L. A. Padilha, D. J. Hagan, E. W. Van Stryland, M. V. Bondar, Y. L. Slominsky, and A. D. Kachkovski. Two-photon absorption studies of polymethine and squaraine dyes with analogous structures. In *Conference on Lasers & Electro-Optics/Quantum Electronics and Laser Science Conference (CLEO/QELS)*, page 2. IEEE, 2006.
- [64] D. Vonlanthen, A. Mishchenko, M. Elbing, M. Neuburger, T. Wandlowski, and M. Mayor. Chemically controlled conductivity: torsion-angle dependence in a single-molecule biphenyldithiol junction. *Angewandte Chemie-International Edition*, 48(47):8886–8890, 2009.
- [65] M. P. Johansson and J. Olsen. Torsional barriers and equilibrium angle of biphenyl: Reconciling theory with experiment. *Journal of Chemical Theory and Computation*, 4(9):1460–1471, September 2008.
- [66] C. A. T. Laia and S. M. B. Costa. Ground- and excited-state solvation of a squaraine dye by water in dioxane. *Chemical Physics Letters*, 285(5-6):385–390, 1998.
- [67] M. Y. Berezin, H. Lee, W. Akers, and S. Achilefu. Near infrared dyes as lifetime solvatochromic probes for micropolarity measurements of biological systems. *Biophysical Journal*, 93(8):2892–2899, 2007.
- [68] G. H. Morine and R. R. Kuntz. Spectral shifts of the p-aminophenylthiyl radical absorption and emission in solution. *Chemical Physics Letters*, 67(2-3):552–554, 1979.
- [69] A. J. Bard. *Electrochemical methods: fundamentals and applications*. Wiley New York, 2nd edition, 2001.

- [70] R. O. Loutfy and J. H. Sharp. Correlation between photographic properties of dyes and their electrochemical and spectroscopic parameters. *Photographic Science and Engineering*, 20(4):165–174, 1976.
- [71] T. P. Straatsma, E. Aprà, T. L. Windus, E. J. Bylaska, W. de Jong, S. Hirata, M. Valiev, Hackler M., L. Pollack, R. Harrison, M. Dupuis, D. M. A. Smith, J. Nieplocha, V. Tipparaju, M. Krishnan, A. A. Auer, E. Brown, G. Cisneros, G. Fann, H. Früchtl, J. Garza, K. Hirao, R. Kendall, J. Nichols, K. Tse-mekhman, K. Wolinski, J. Anchell, D. Bernholdt, P. Borowski, T. Clark, D. Clerc, H. Dachsel, M. Deegan, K. Dyall, D. Elwood, E. Glendening, M. Gutowski, A. Hess, J. Jaffe, B. Johnson, J. Ju, R. Kobayashi, R. Kutteh, Z. Lin, R. Littlefield, X. Long, B. Meng, T. Nakajima, S. Niu, M. Rosing, G. Sandrone, M. Stave, H. Taylor, G. Thomas, J. van, Lenthe, A. Wong, and Z. Zhang. Nwchem, a computational chemistry package for parallel computers, version 4.6. Pacific Northwest National Laboratory, Richland, Washington 99352-0999, USA, 2004.
- [72] R. A. Kendall, E. Aprà, D. E. Bernholdt, E. J. Bylaska, M. Dupuis, G. Fann, R. J. Harrison, J. Ju, J. A. Nichols, J. Nieplocha, T. P. Straatsma, T. L. Windus, and A. T. Wong. High performance computational chemistry: an overview of nwchem a distributed parallel application. *Computer Physics Communications*, 128:260–283, 2000.
- [73] Frank Jensen. *Introduction to computational chemistry*. Wiley (Chichester), 2nd edition, 2007.
- [74] Jmol. an open-source Java viewer for chemical structures in 3D: <http://www.jmol.org>. Version 11.7.34., March 2009.
- [75] T. Bessho, E. C. Constable, M. Grätzel, A. H. Redondo, C. E. Housecroft, W. Kylberg, M. K. Nazeeruddin, M. Neuburger, and S. Schaffner. An element of surprise - efficient copper-functionalized dye-sensitized solar cells. *Chemical Communications*, (32):3717–3719, 2008.
- [76] Y. Ooyama and Y. Harima. Molecular designs and syntheses of organic dyes for dye-sensitized solar cells. *European Journal of Organic Chemistry*, (18):2903–2934, 2009.
- [77] A. J. McKerrow, E. Buncel, and P. M. Kazmaier. Aggregation of squaraine dyes - structure-property relationships and solvent effects. *Canadian Journal of Chemistry-revue Canadienne De Chimie*, 73(10):1605–1615, 1995.
- [78] H. J. Chen, M. S. Farahat, K. Y. Law, and D. G. Whitten. Aggregation of surfactant squaraine dyes in aqueous solution and microheterogeneous media: Correlation of aggregation behavior with molecular structure. *Journal of the American Chemical Society*, 118(11):2584–2594, March 1996.

- [79] B. Neumann and P. Pollmann. Investigation of two cyanine dyes at normal and high pressure by UV/vis spectroscopy. *Physical Chemistry Chemical Physics*, 2(20):4784–4792, 2000.
- [80] S. H. Kim, J. H. Kim, J. Z. Cui, Y. S. Gal, S. H. Jin, and K. Koh. Absorption spectra, aggregation and photofading behaviour of near-infrared absorbing squarylium dyes containing perimidine moiety. *Dyes and Pigments*, 55(1):1–7, 2002.
- [81] H. E. Gottlieb, V. Kotlyar, and A. Nudelman. NMR chemical shifts of common laboratory solvents as trace impurities. *Journal of Organic Chemistry*, 62(21):7512–7515, 1997.
- [82] A. Slamaschwok, M. Blancharddesce, and J. M. Lehn. Intramolecular charge-transfer in donor-acceptor molecules. *Journal of Physical Chemistry*, 94(10):3894–3902, 1990.
- [83] D. M. Shin and D. G. Whitten. Solvatochromic behavior of intramolecular charge-transfer diphenylpolyenes in homogeneous solution and microheterogeneous media. *Journal of Physical Chemistry*, 92(10):2945–2956, 1988.
- [84] J. Murage, J. W. Eddy, J. R. Zimbalist, T. B. McIntyre, Z. R. Wagner, and F. E. Goodson. Effect of reaction parameters on the molecular weights of polymers formed in a suzuki polycondensation. *Macromolecules*, 41(20):7330–7338, 2008.
- [85] J. W. Eddy, E. A. Davey, R. D. Malsom, A. R. Ehle, S. Kassel, and F. E. Goodson. Palladium complexes with aqueous-partitioning dibenzylideneacetone ligands. a new strategy for catalyst design in suzuki polycondensation reactions. *Macromolecules*, 42(22):8611–8614, 2009.

Acknowledgments

Thank God! The thesis comes to an end.

Many very special thanks to Dr. Thomas Geiger for the creation of a friendly working atmosphere and his presumably endless patience but also for his advices, his guidance and friendship.

Also many special thanks to my wife Kirsten for her patience, comprehension and her help with the English correction.

Prof. A. Dieter Schlüter is acknowledged for being my sovereign professor.

A special thanks to the teammates, above all Simon Huber, Beatrice Fischer, Yulia Shcherbakova, Simone Hochleitner, Andrea Härer and Tohru Matsumura for their helping hands; and the others for the communicative atmosphere.

Swiss Federal Laboratories for Materials Testing and Research (Empa), Laboratory for Functional Polymers, Überlandstrasse 129, CH-8600 Dübendorf, Switzerland headed by Dr. Frank A. Nüesch is thankfully acknowledged for the funding of this thesis.

The MS service at the ETH, Swiss Federal Institute of Technology Zürich is thanked for all the MS measurements reported in this work.

Also the Mikro Elementar Analysis team at the ETH is acknowledged for the elemental analysis of my compounds.

Dr. Daniel Rentsch is also acknowledged for the help with the ^{19}F -NMR measurements.

The developers of the program TeXnicCenter and Rene Fehlmann for providing the Latex ETH PhD-thesis class (1996) are thankfully acknowledged.

A special thank to the collaborators at the EPFL Prof. Michael Grätzel, Dr. Mohammad Khaja Nazeeruddin and Dr. Frédéric Sauvage.

Finally, I also want to thank all those who read my thesis up to here.

Curriculum Vitae

Personal data

Name Kuster
First name Simon
Birthday 24th of December 1980
E-mail masterofscienceeth@gmx.ch

Further Education at the ETH Zurich

2007–2010 Dissertation at the ETH Zurich with Prof. Dr. A. Dieter Schlüter working at Empa Dübendorf with Dr. Thomas Geiger
2006 Master thesis with Prof. Dr. Donald Hilvert and Jörg Serafimov at the ETH Zurich
2005–2006 Semester thesis with Prof. Dr. François Diederich and Anna Vogt-Gehrig at the ETH Zurich
2005 Semester thesis with Prof. Dr. Peter Seeberger and Dr. Jerum Codée at the ETH Zurich
2005–2006 Master Study at the ETH in Zurich in D-CHAB
2004–2005 Bachelor Study at the ETH in Zurich in D-CHAB

Professional Occupation

2004 Assistant for Prof. Dr. Urs Michel, Prof. Dr. Gaston Wolf and Prof. Dr. Roger Marti at the Zürcher Fachhochschule Winterthur (ZHW)
2004 Responsible person for the NMR custom service
2004 Research project on amino acids in collaboration with Senn Chemicals AG, Dielsdorf
2002–2003 Teacher in the Berufsschule St. Gallen

Further Education as a Teacher

2004–2011 Study for the "Didaktischer Ausweis in Chemie"

Further Education at the Zürcher Fachhochschule Winterthur (ZHW)

- 2003 Winner of the Schweizerischer Verband diplomierter Chemiker (SVC) award for the best diploma thesis
- 2003 Diploma thesis with Prof. Dr. Urs Michel in organic Chemistry
- 2000–2003 Chemistry study at the ZHW with a major in organic chemistry and additional semester works in chemical engineering, biochemical engineering, industrial chemistry, physical chemistry and biochemistry

Education

- 1997–2000 Berufsmaturität at the Technische Berufsschule St. Gallen
- 1997–2000 Apprenticeship as Chemielaborant at the Kantonales Amt für Lebensmittelkontrolle St. Gallen (KAL)

Software Skills

Good knowledge in using MS-Office on a Windows system as well as using OpenOffice on OpenSUSE (Linux) systems. Off course, advanced user for LaTeX and also reasonable knowledge in the use of additional scientific and chemical programs as ChemDraw, IsisDraw, GAMESS, Hyperchem, Jmol, JabRef, POV-Ray, Adobe Acrobat, Distiller, Illustrator and Photoshop, Origin and Topspin.

Languages

Swiss German (native tongue)
German (quite well)
English (good)
French (basic)

References

on request